ANNÉE 2017

THÈSE / UNIVERSITÉ DE RENNES 1
sous le sceau de l'Université Bretagne Loire

pour le grade de

DOCTEUR DE L'UNIVERSITÉ DE RENNES 1
Mention : Sciences de la Terre

Ecole doctorale EGAAL

JOSEPH OFFEI THOMPSON

Préparée à l'unité de recherche UMR 6118 CNRS
Géosciences Rennes
UFR Sciences et Propriété de la Matière

The opening of the Indian Ocean: what is the impact on the East African, Madagascar and Antarctic margins, and what are the origins of the aseismic ridges?

Thèse soutenue à Brest
le 21 Novembre 2017

devant le jury composé de :

Professor Mohamed SAHABI
Professor Faculté des sciences d'El Jadida, Moroc/examinateur

Dr Stefane MAHAJANE
Geoscientist National Petroleum Institute Maputo/examinateur

Professor Maarten de WIT
Professor, Nelson Mandela University/ rapporteur

Dr Wilfred JOKAT
Researcher, Alfred Wegener Institute/ rapporteur

Dr Charlotte NIELSON
(Geological Engineer Total) – examinateur

Professor François GUILLOCHEAU
Professor Department of Geoscience,
Université de Rennes 1 / directeur de thèse

Dr Maryline MOULIN
(Researcher Ifremer) / co directeur de thèse

Dr Daniel ASLANIAN
(Researcher Ifremer) / co directeur de thèse

Philippe de Clarens
(Researcher Total) / co directeur de thèse

ANNÉE 2017

THÈSE / UNIVERSITÉ DE RENNES 1
sous le sceau de l'Université Bretagne Loire

pour le grade de

DOCTEUR DE L'UNIVERSITÉ DE RENNES 1
Mention : Sciences de la Terre

Ecole doctorale EGAAL

JOSEPH OFFEI THOMPSON

Préparée à l'unité de recherche UMR 6118 CNRS
Géosciences Rennes
UFR Sciences et Propriété de la Matière

The opening of the Indian Ocean: what is the impact on the East African, Madagascar and Antarctic margins, and what are the origins of the aseismic ridges?

Thèse soutenue à Brest
le 21 Novembre 2017

devant le jury composé de :

Professor Mohamed SAHABI
Professor Faculté des sciences d'El Jadida, Moroc/examinateur

Dr Stefane MAHAJANE
Geoscientist National Petroleum Institute Maputo/examinateur

Professor Maarten de WIT
Professor, Nelson Mandela University/ rapporteur

Dr Wilfred JOKAT
Researcher, Alfred Wegener Institute/ rapporteur

Dr Charlotte NIELSON
(Geological Engineer Total) – examinateur

Professor François GUILLOCHEAU
Professor Department of Geoscience,
Université de Rennes 1 / directeur de thèse

Dr Maryline MOULIN
(Researcher Ifremer) / co directeur de thèse

Dr Daniel ASLANIAN
(Researcher Ifremer) / co directeur de thèse

Philippe de Clarens
(Researcher Total) / co directeur de thèse

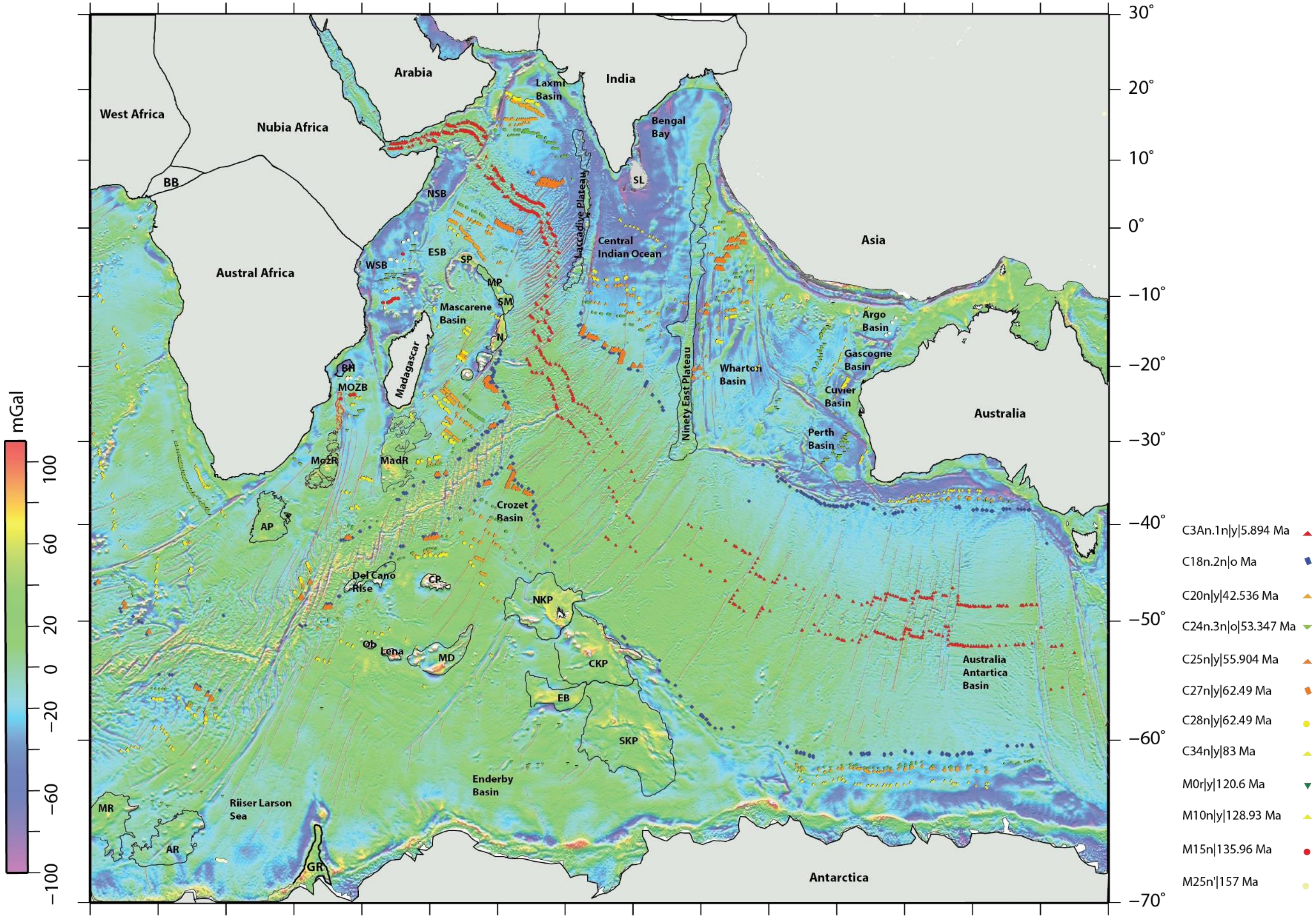

Figure 1: Sandwell et al., (2014) free-air satellite-derived gravity anomalies showing anomalous tectonic features on the seafloor of the Indian Ocean. The magnetic anomaly plots were derived from The Global Seafloor Fabric and Magnetic Lineation Data Base Project (GSFML). The ocean is the third largest of the world's oceans, covering approximately 20% of the earth surface with an average depth of 3.741m and a maximum depth of 7.906m. AP: Agulhas Plateau; AR: Astrid Ridge; BH: Beira High; CKP = Central Kerguelen Plateau; ESB: Eastern Somali Basin; EB: Elan Bank; LP: Laccadive Plateau; MadR: Madagascar Ridge; MR: Maud Rise; MOZB: Mozambique Basin; MadR: Madagascar Ridge; MP: Mascarene Plateua; MozR: Mozambique Ridge; N: Nazareth Plateau; NNV: Northern Natal Valley, NKP = N Kerguelen Plateau; SB: Saya de Malha Bank; SL is Sri Lanka and SKP = South Kerguelen Plateau; SNV: South Natal Valley; WSB: Western Somali Basin. Red lines: fracture zones. The North Mozambique Ridge (In red) was found during recent expedition in the Mozambique Basin of MOZ3-5 to consist mainly of sediments muscle on a thinned continental crust (Lepretre et al., 2017; Moulin et al., submitted). The Southern Mozambique Ridge maybe composed of volcanics (Gohl et al., 2011) probably emplaced at a triple junction. (*Mercator projection)*

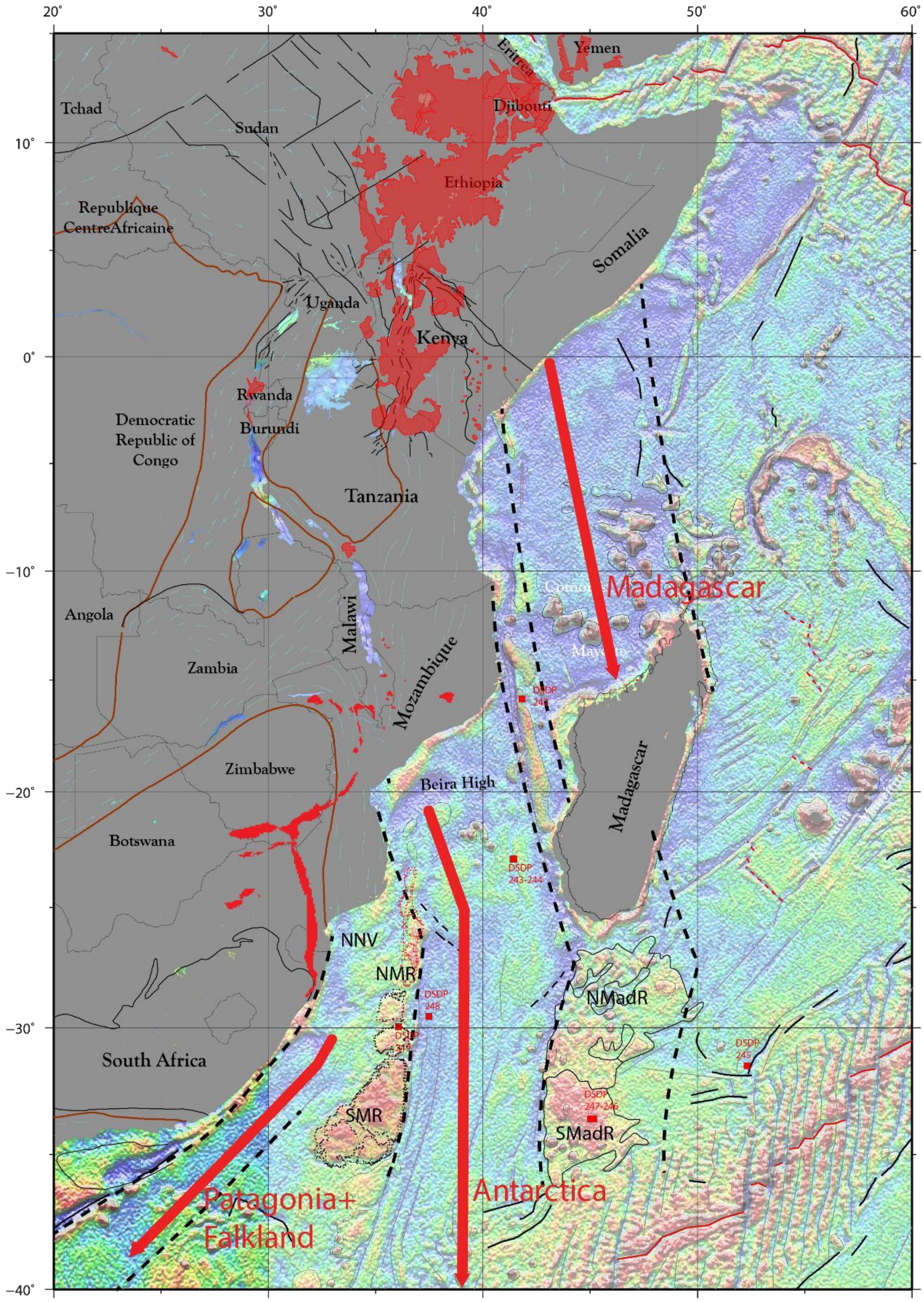

Figure 2: Gravity and bathymetry map of Mozambique Channel, showing the complexity and segmentation of the East African margin. The top and middle arrows corresponds to the movement of the Madagascar and Antarctica tectonic plates respectively, and the lower arrow corresponds to a later event involving the drifting of the Falkland and Patagonian plates. NNV= North Natal Valley; NMR= North Mozambique Ridge; SMR= South Mozambique Ridge; NMadR= North Madagascar Ridge; SMadR= South Madagascar Ridge. Notice the positions of DSDP 245, 246, 247, 248, 249. In red= Volcanism . (Mercator projection)

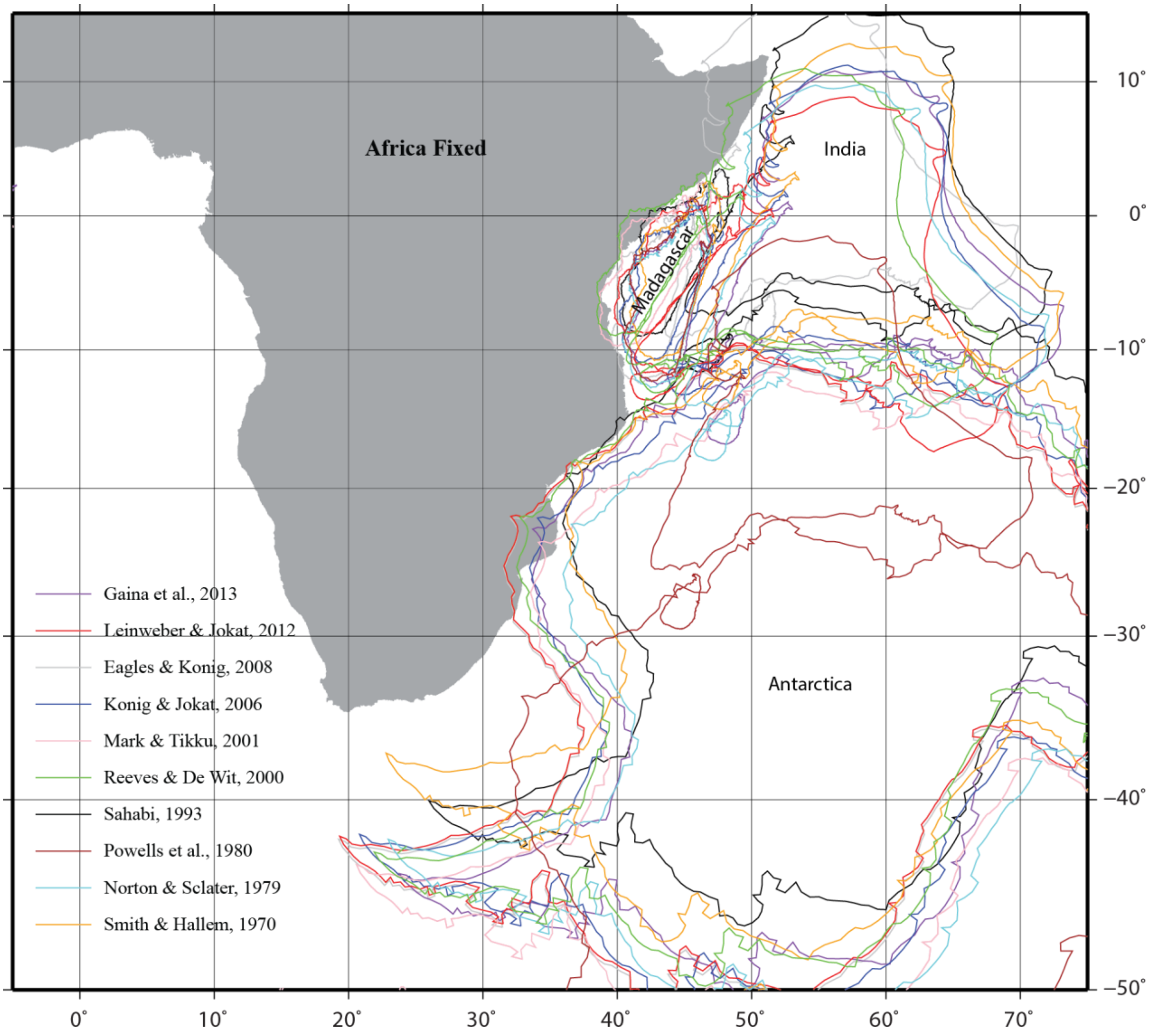

*Figure 3: Gondwana reconstructions models by (Smith and Hallem, 1970; Norton and Sclater, 1979; Sahabi, 1993; Reeves and de Wit, 2000; Marks and Tikku, 2001; Konig and Jokat, 2006; Eagles and Konig, 2008; Leinweber et al., 2012; Gaina et al., 2013). The models present different positions for the plates, and result in overlaps, gaps, latitudinal, and angular differences. (*Mercator projection).

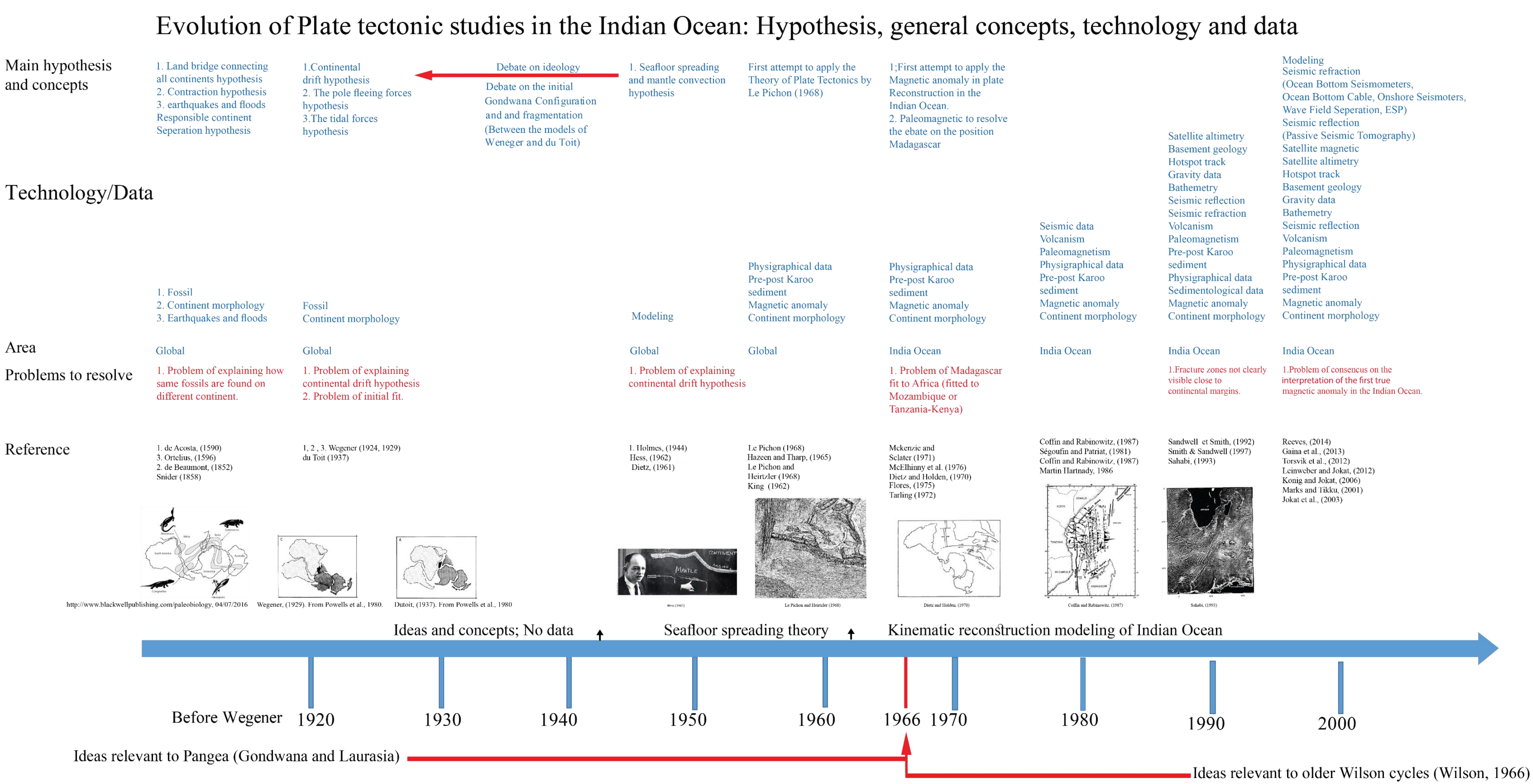

Figure 4: Evolution of plate tectonics studies in the Indian Ocean, from 1500s to present day. The land bridge theory and the compression theory were poposed in the1500s and 1800s, respectively. Wegener (1924) proposed the continental drift hypothesis, in which he stated that all the continents were once compressed together into a single super-continent which he called Pangaea. His ideals were not accepted until Holmes (1944), Harry Hess (1962) and Deitz (1961) elaborated on one of his idea, and showed that the mantle undergoes thermal convection. The initial reconstruction of the Indian Ocean was based on the shape of the continents (Wegener 1929 and duToit, 1937). Notices the rapid increase in data for the reconstruction from the 1970's to present age

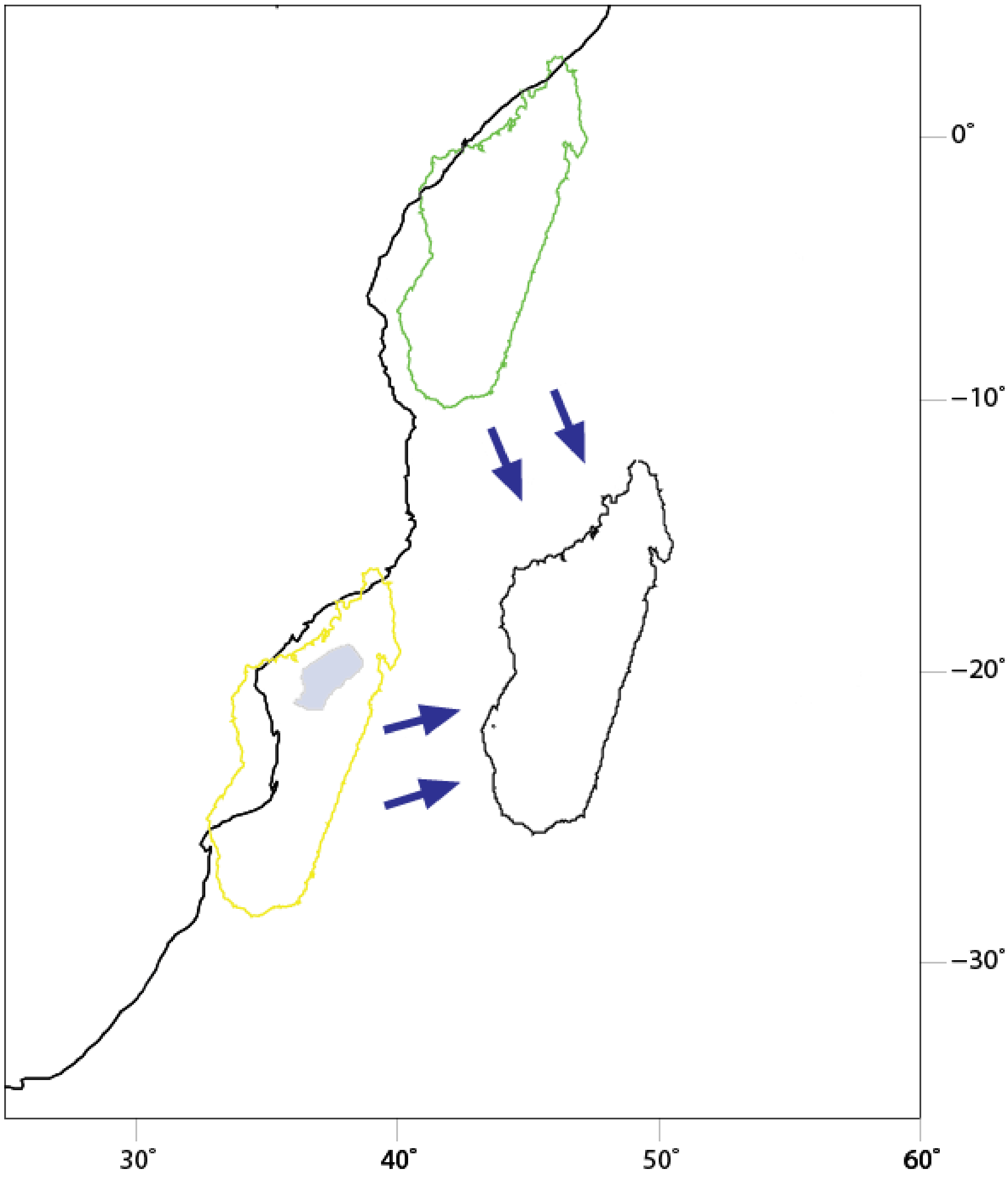

Figure 5: Three possible initial fit positions proposed for Madagascar. (i) Green: a position adjacent to East Africa (Kenya and Tanzania), originally proposed by du Toit (1937) and later favored by Smith and Hallam (1970). (ii) Yellow: a position adjacent to Mozambique proposed originally by Wegener (1929) and supported by Flores (1970, 1972). (iii) Black; Madagascar staying at its present position since the Paleozoic (Francis et al., 1966). In blue: Beira High. Arrows: Madagascar's drift path to present position. (Mercator projection).

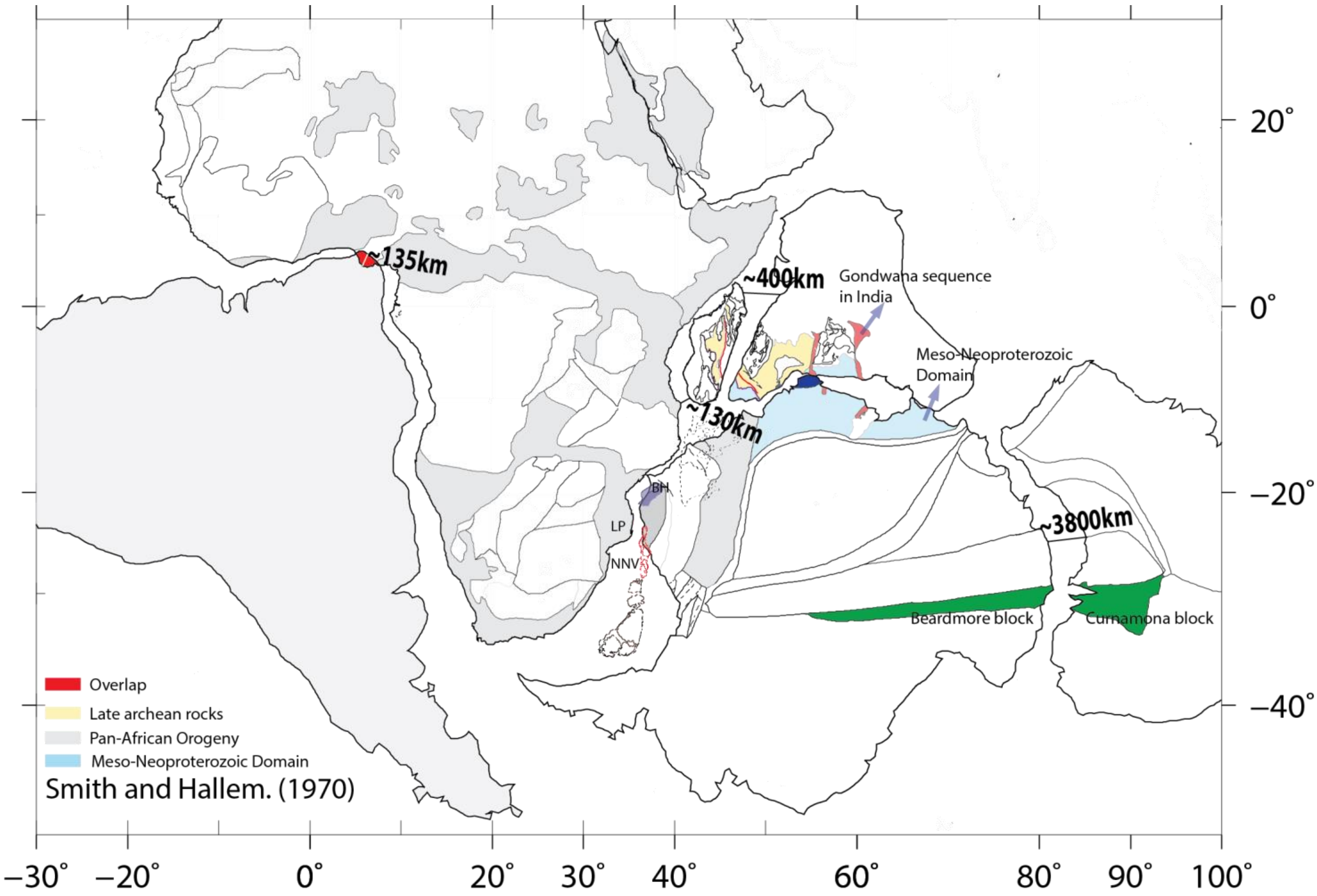

Figure 6: Reconstruction model of Smith and Hallem (1970). Their model presented a good fit of Gondwana, except in Zambezi Basin, where Antarctica overlaps the Beira High. Their model also leads to ~400km between Madagascar and India. Poles for South American plate provided by author. The PanAfrican orogeny in figures 6-23 are represented by author.BH: Beira High, LP: Limpopo Basin, NNV: North Natal Basin. (Mercator projection).

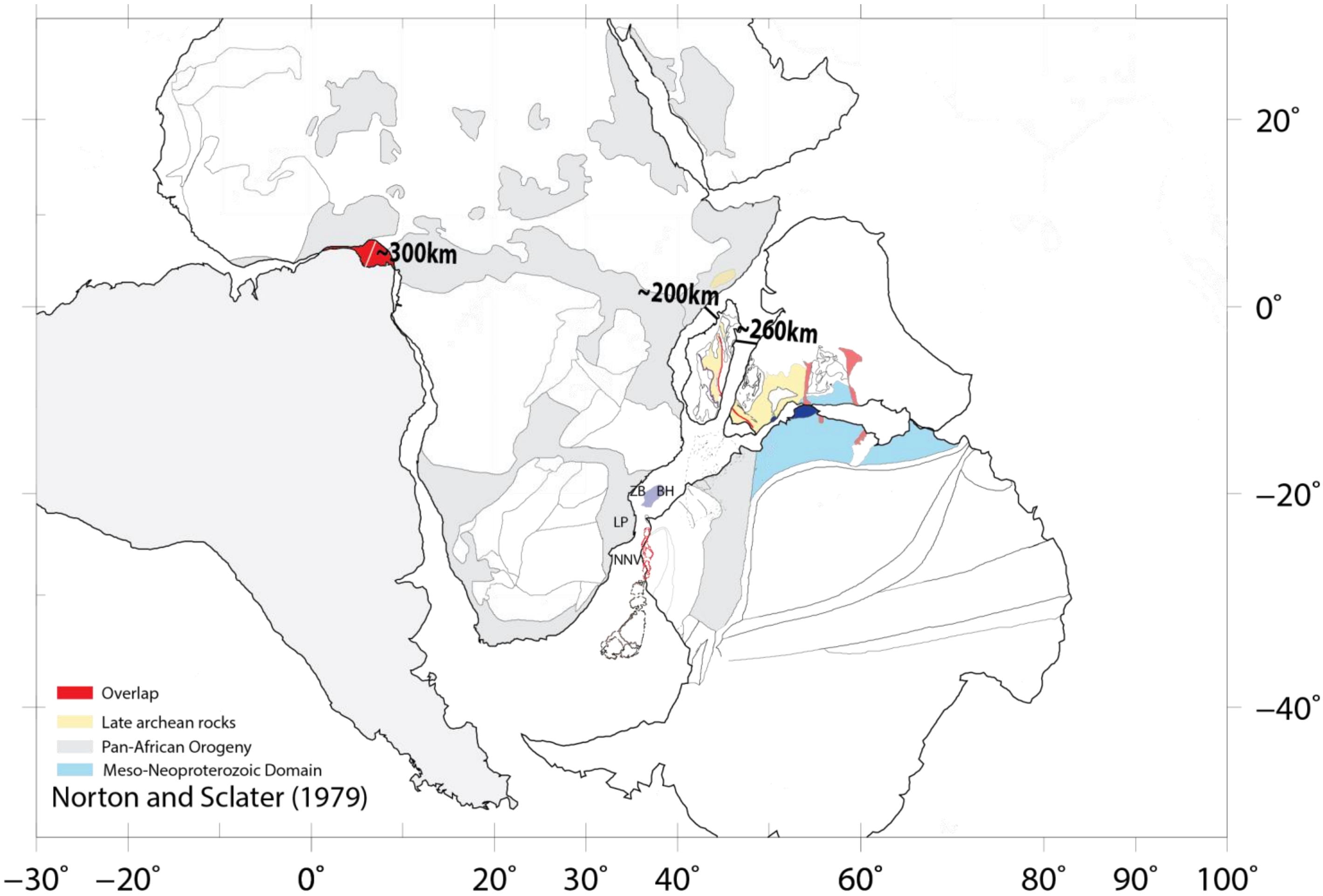

Figure 7: Reconstruction model of Norton and Sclater (1979). They placed the Mozambique Ridge loosely between Africa and Antarctica, treating it as a pre-drift structure. The Gondwana sequence in India and Antarctica are misaligned. The model also results in ~260km of gap between Madagascar and India. Poles for the South American plate provided by Norton and Sclater (1979). BH: Beira High, LP: Limpopo Basin, NNV: North Natal Basin, ZB: Zambezi Basin. (Mercator projection).

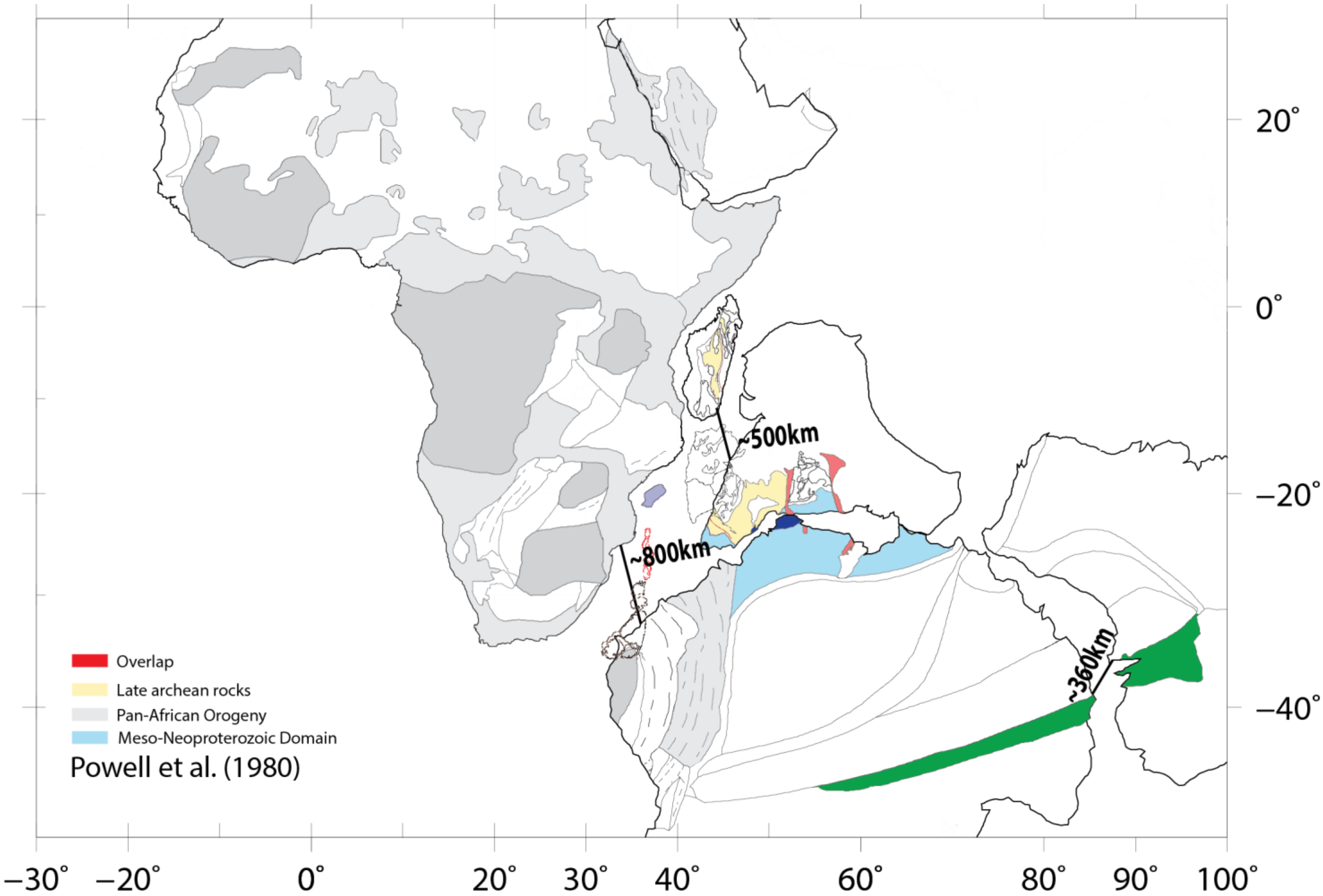

Figure 8: Reconstruction model of Powells et al. (1980). Based on their observation of the pattern of seafloor spreading between Madagascar and India, that India-Antarctica-Australia originally farther south than previously proposed by Smith and Hallem. (1970). Their model results in very large gaps in the initial fit of Gondwana; a 500km gap between India and Madagascar, and 800km gap between Antartica and Africa. (Mercator projection).

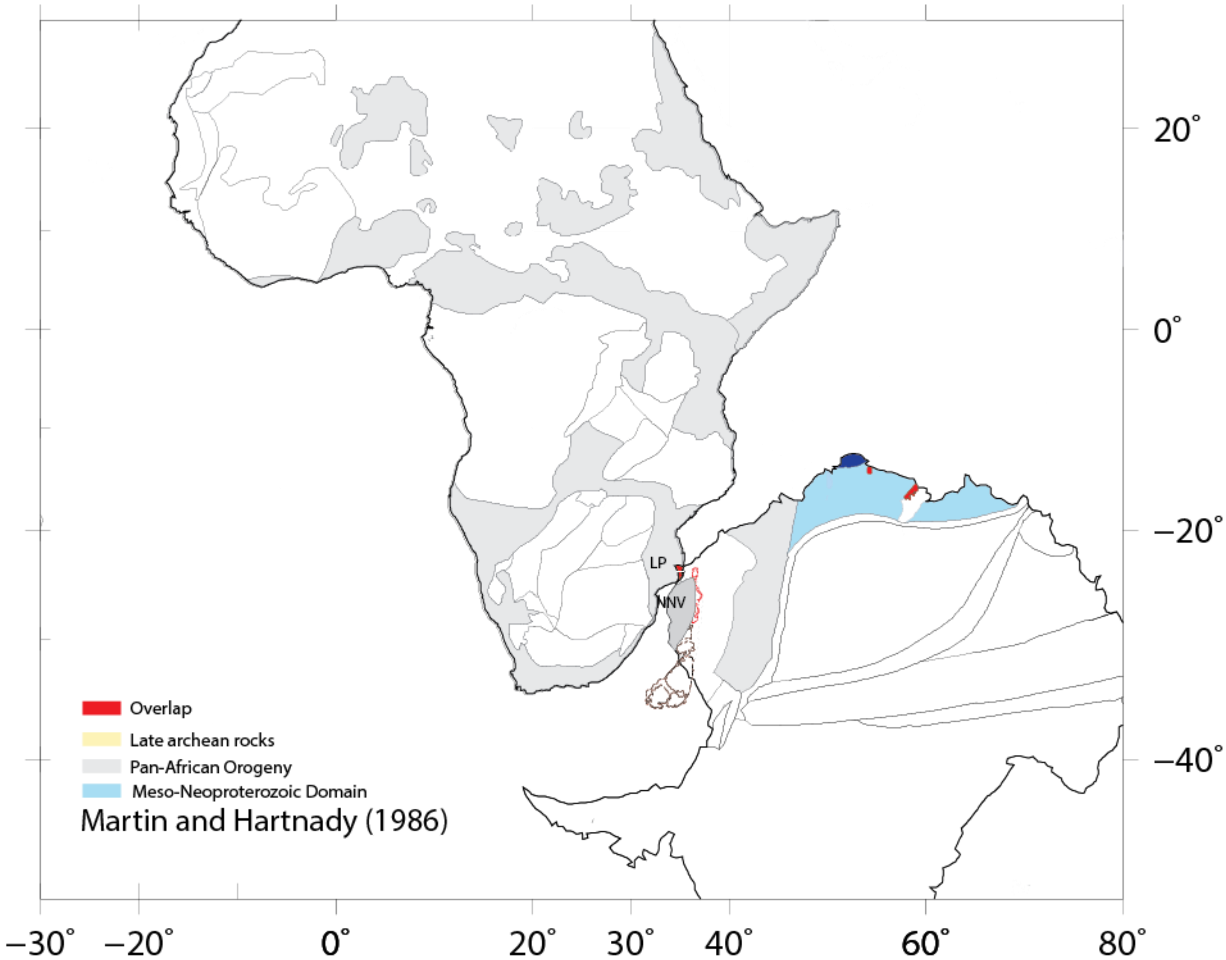

Figure 9: Reconstruction model of Martin and Hartnady (1986). They proposed the Limpopo Basin to be underlained by oceanic crust or very highly extended continental crust, and existence of extinct spreading center northern Natal Valley. (Mercator projection).

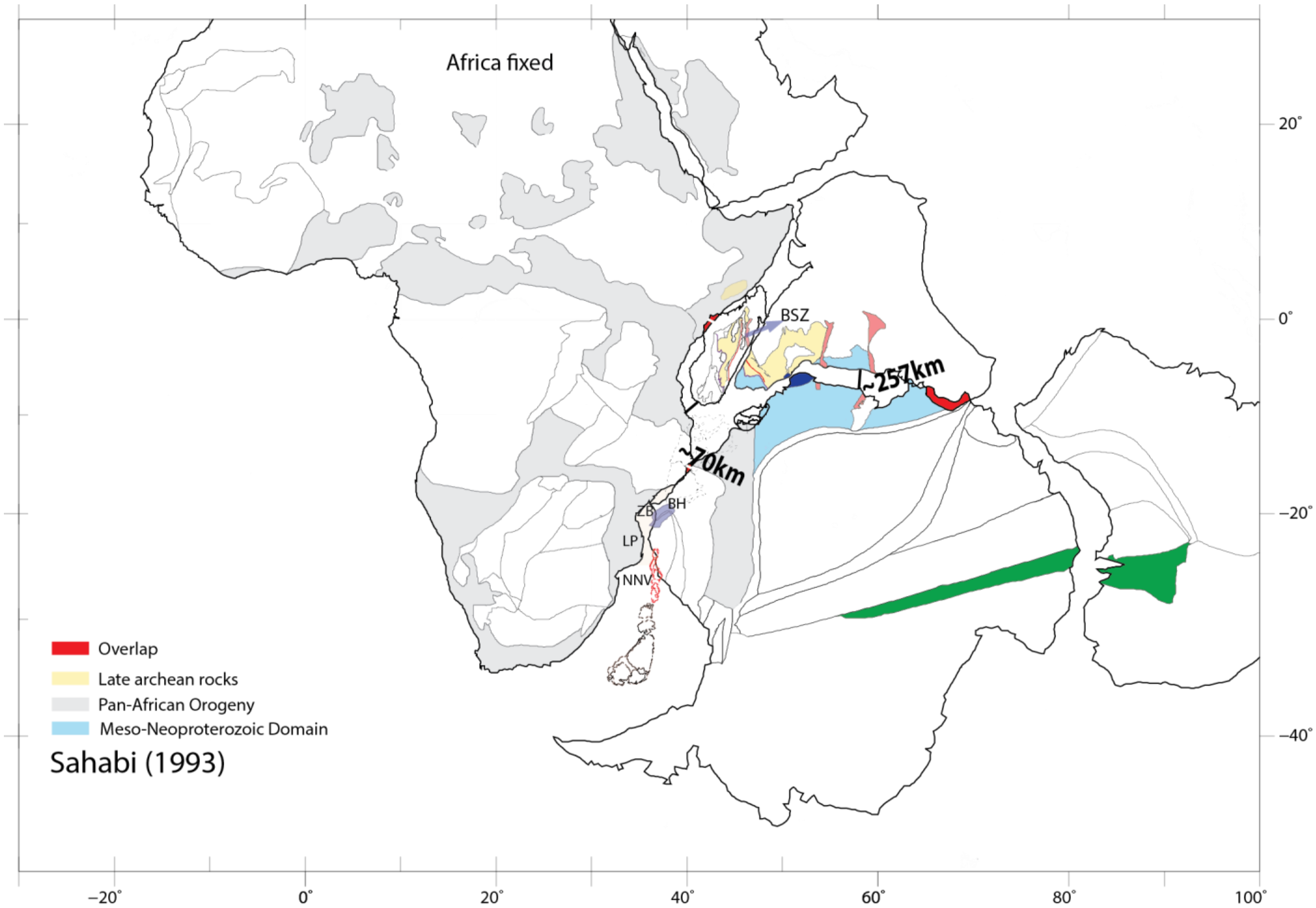

Figure 10: Reconstruction model of Sahabi, (1993). He predicted continental origin for the Limpopo Basin, Natal Valley, and the South Mozambique Ridge, avoiding overlap by Antarctica. However, his model leads to an overlap of Antarctica with the Beira High. The model aligns the Batsimisaraka Shear Zone, to the Moyar Cauvery Shear Zone. BSZ: Batsimisaraka Shear Zone. BH: Beira High, LP: Limpopo Basin, NNV: North Natal Basin, ZB: Zambezi Basin. (Mercator projection).

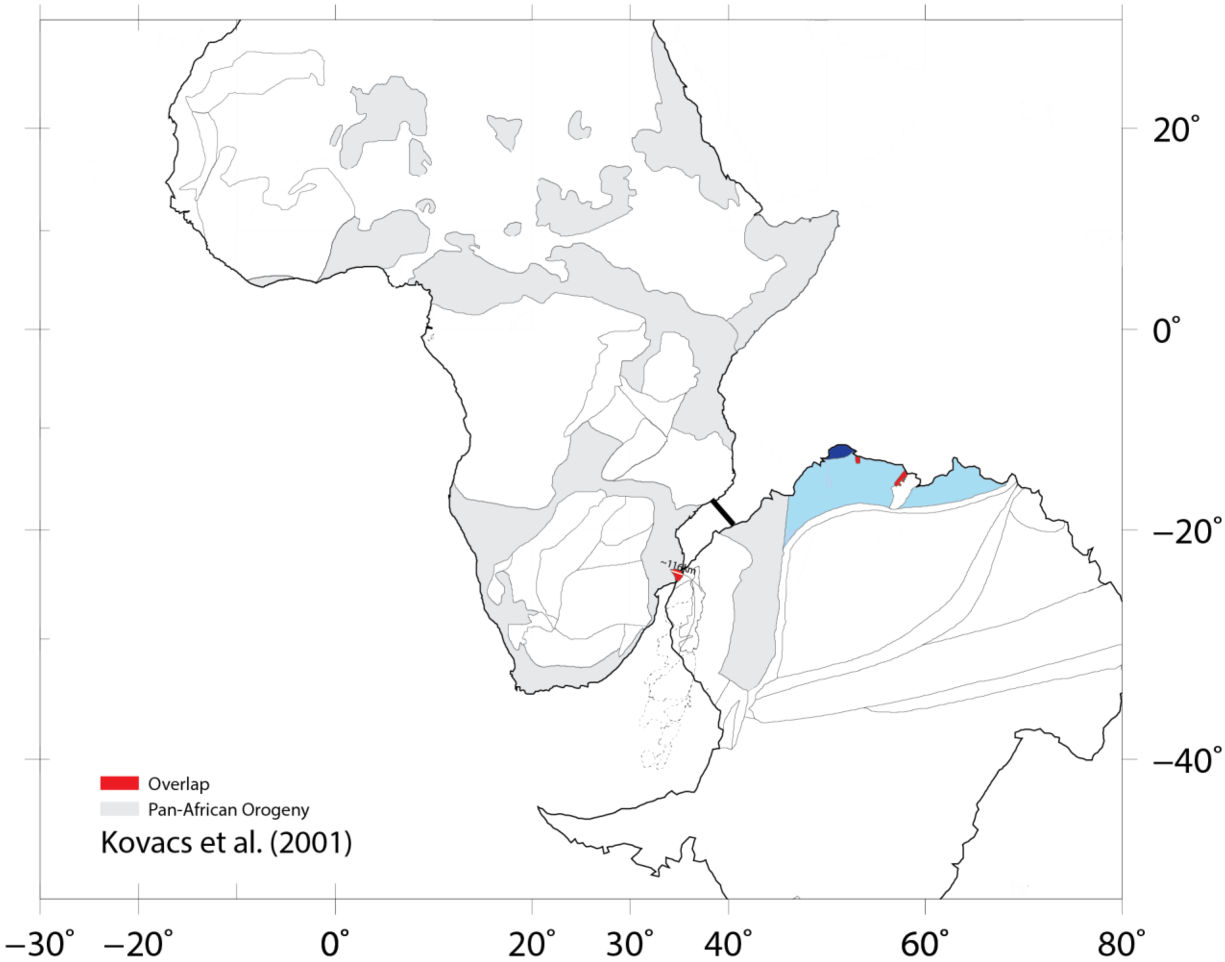

Figure 11: Reconstruction model of Kovacs et al. (2001). They presented a compilation of magnetic data in the Weddell Sea, in agreement with Livermore and Hunter (1996) and Marks and Tikku (2002). Their model results in an overlap of Antarctica on NNV and the Mozambique Ridge. Poles for South American plate provided by author. (Mercator projection).

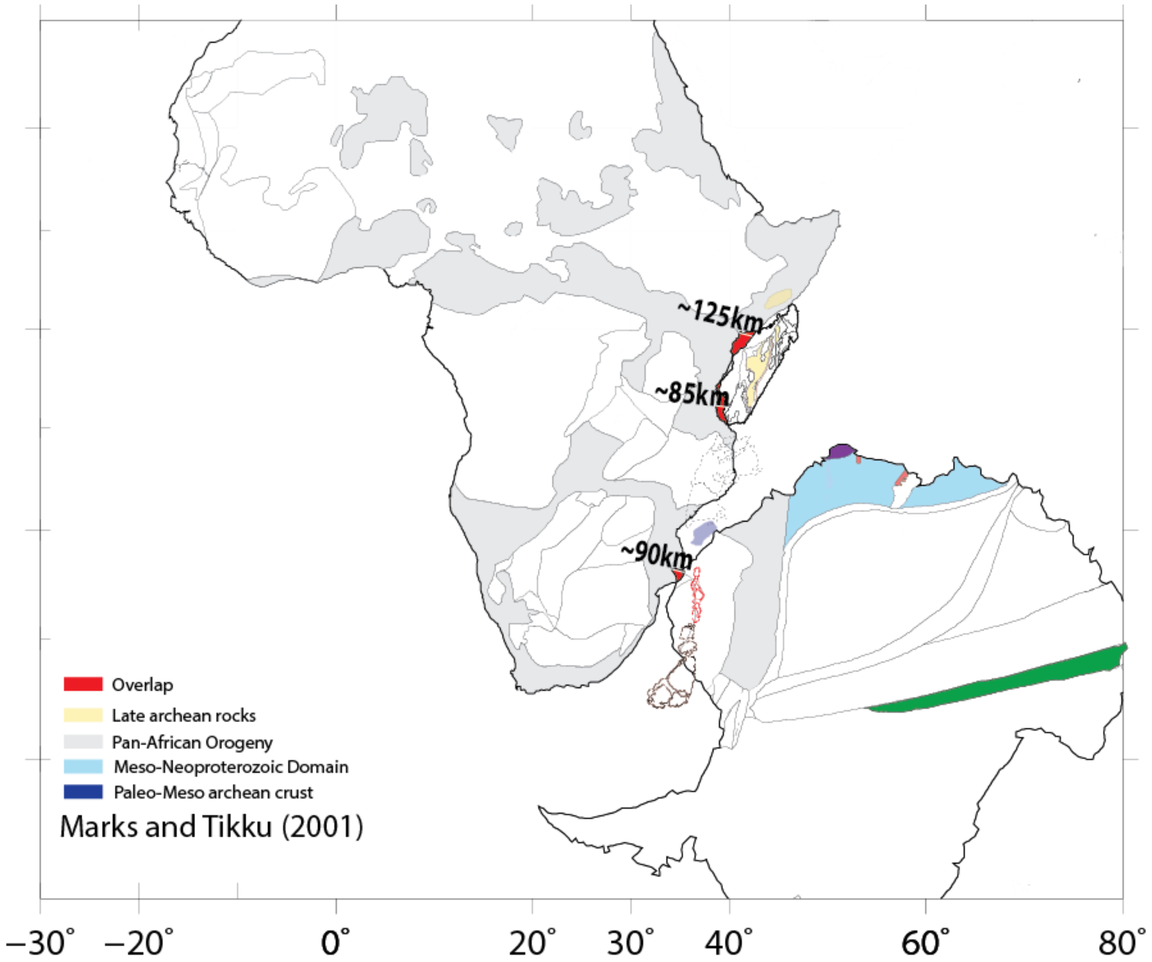

Figure 12: Reconstruction model of Marks and Tikku (2002). They proposed the Mozambique Ridge behaved like a microplate with its own independent motion between anomaly M11 and M2. Their model result overlap of Antarctica across the Mozambique ridge. (Mercator projection).

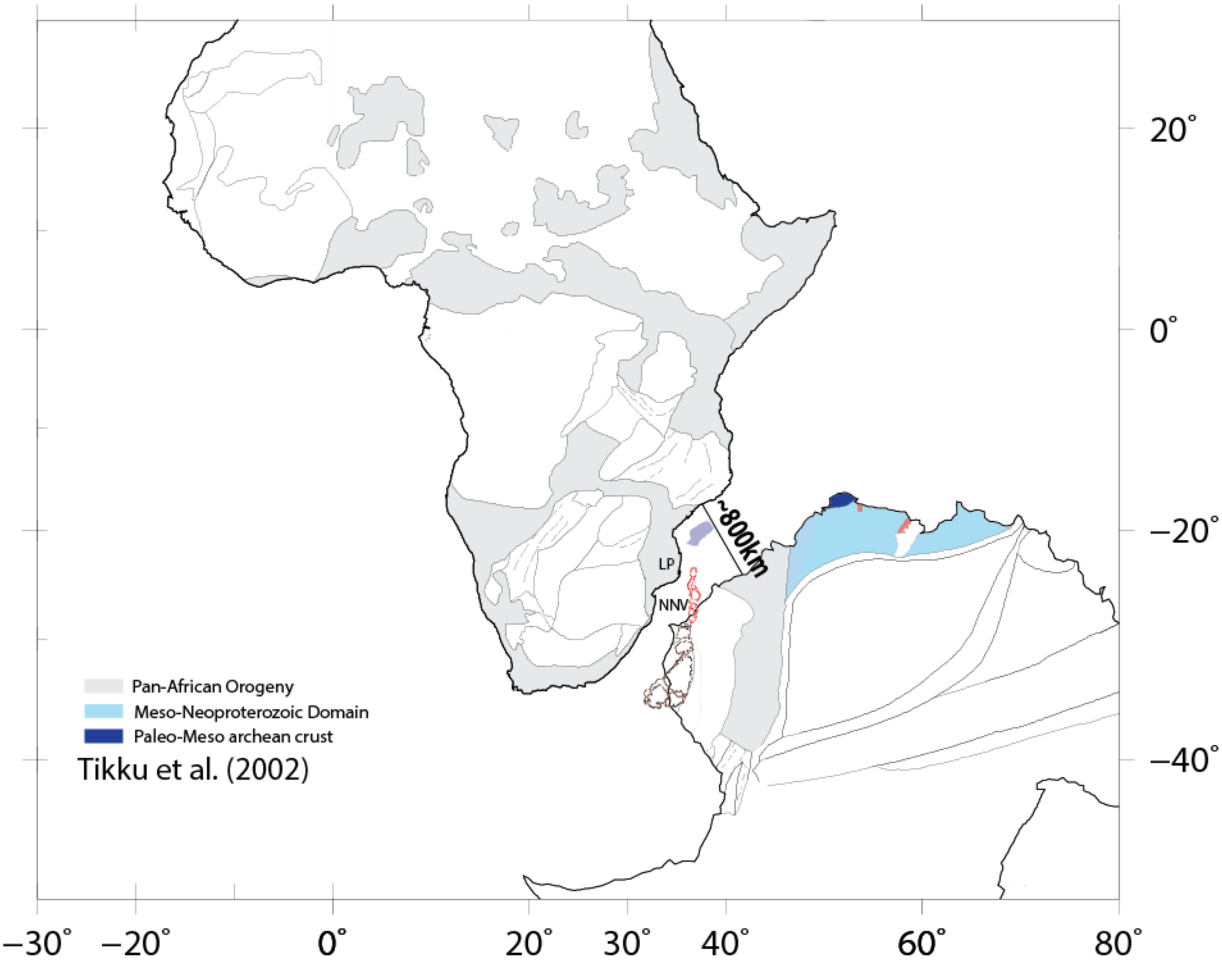

Figure 13: Reconstruction model of Tikku et al. (2002). They suggested a continental origin for the Mozambique Ridge, considering the ridge as a microplate. They suggested the existence of an active spreading center in the North Natal Valley. Their model leads to a gap of ~800km between Antarctica and Mozambique. LP: Limpopo Basin, NNV: North Natal Basin. (Mercator projection).

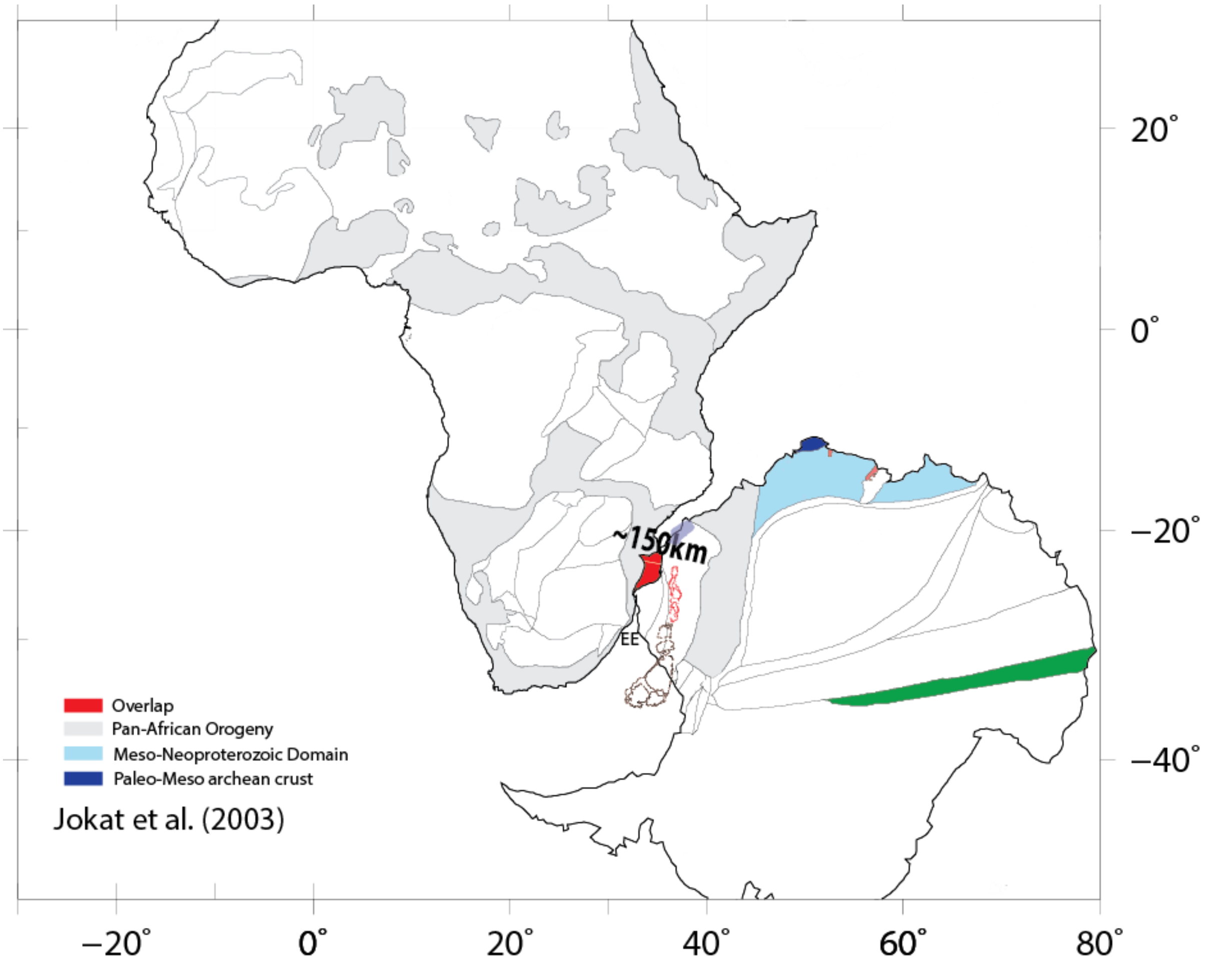

Figure 14: Reconstruction model of Jokat et al. (2003). They argue that the Karoo and Dronning Maud Land magmatism occurred well before any new ocean floor was created in the Indian Ocean, and therefore the oldest oceanic in the ocean cannot be related directly to any plume event. The model results in 150km overlap Antarctica across Africa. ((Mercator projection).

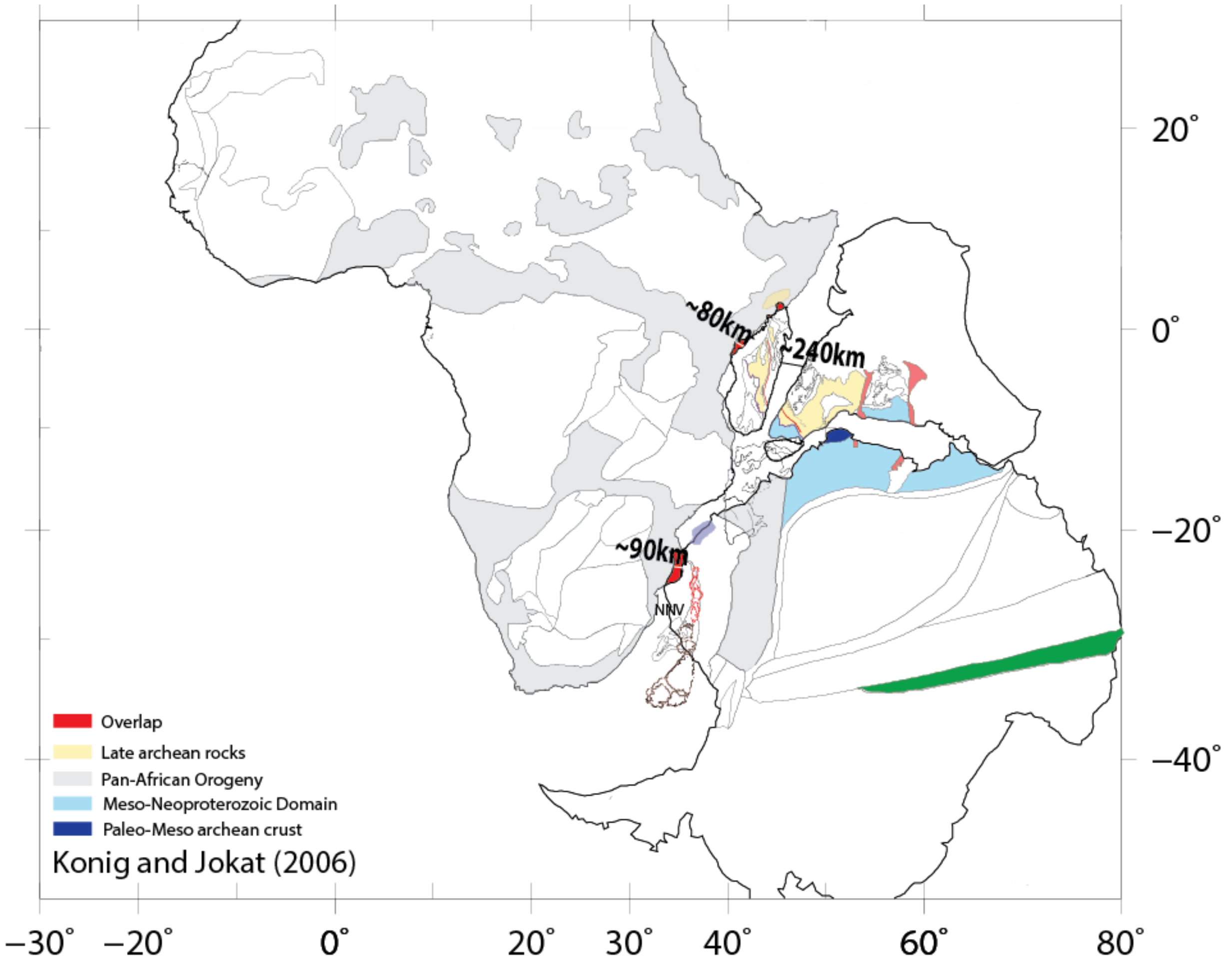

Figure 15: Reconstruction model of Konig and Jokat (2006). They proposed extinct spreading center in the NNV and discussed the existence of an independent Mozambique ridge microplate prior to 120 Ma. Their model results in large overlap of the Mozambique Ridge in the Limpopo Basin in the initial fit of Gondwana. (Mercator projection).

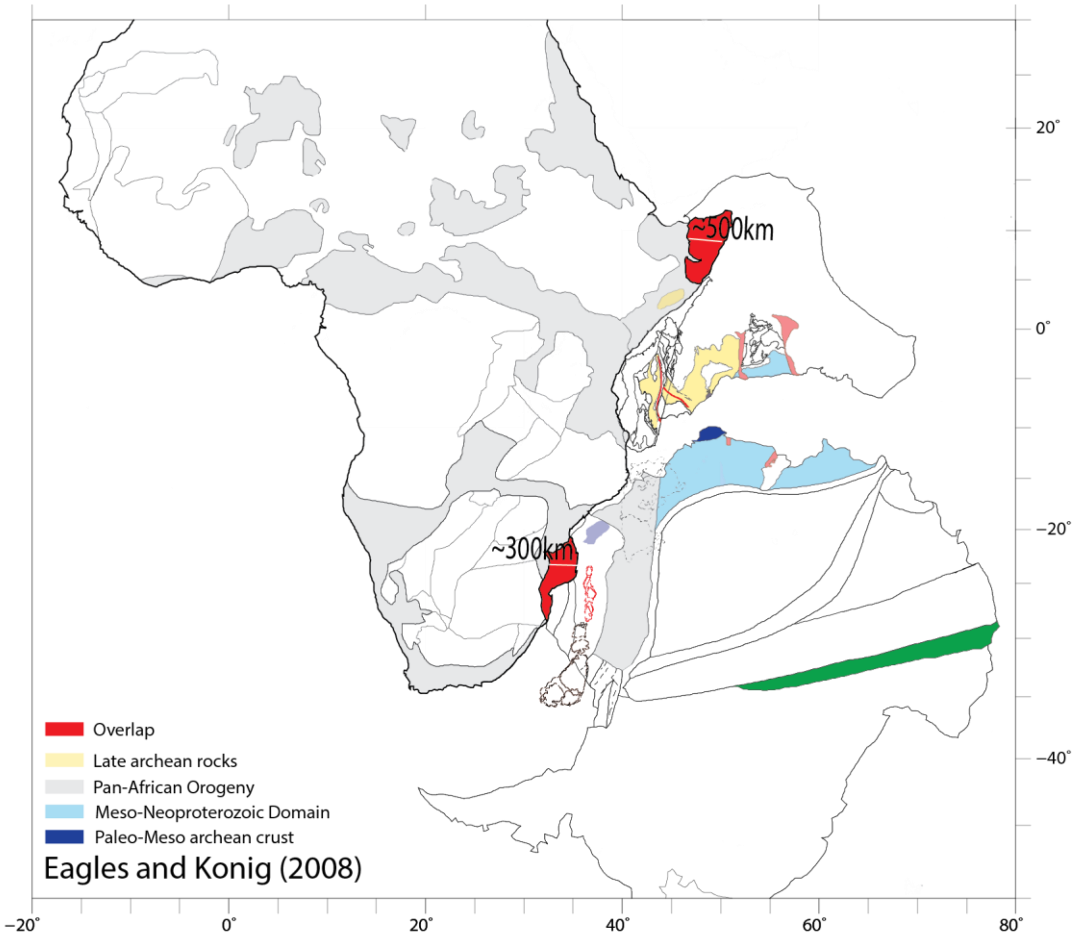

Figure 16: Reconstruction of model of Eagles and Konig (2008). They assumed oceanic origin for the Mozambique ridge and the Southern Mozambique plains. The model results in ~700km overlap between India and Antarctica, and a 300km overlap of the Antarctic plate across Africa. (Mercator projection).

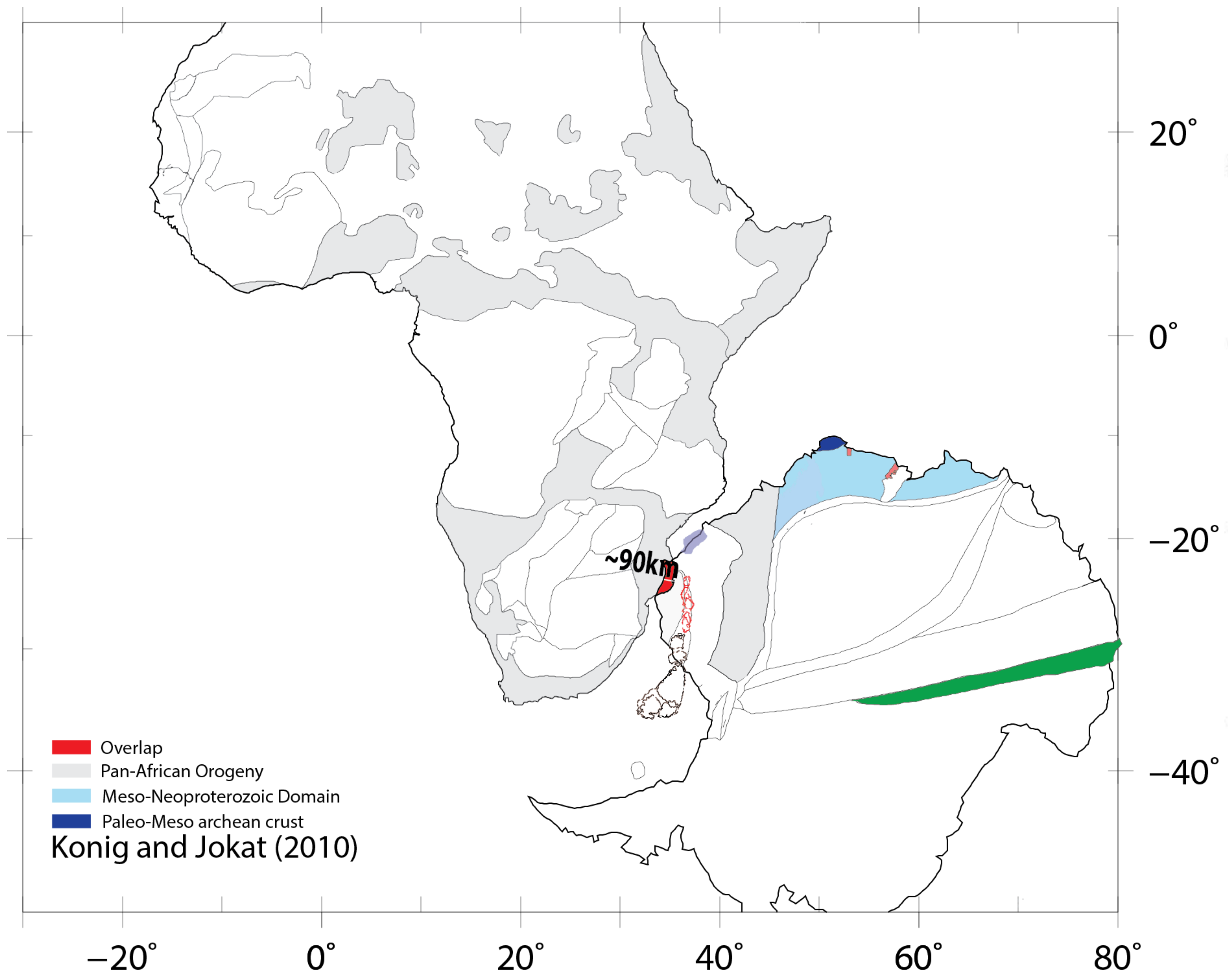

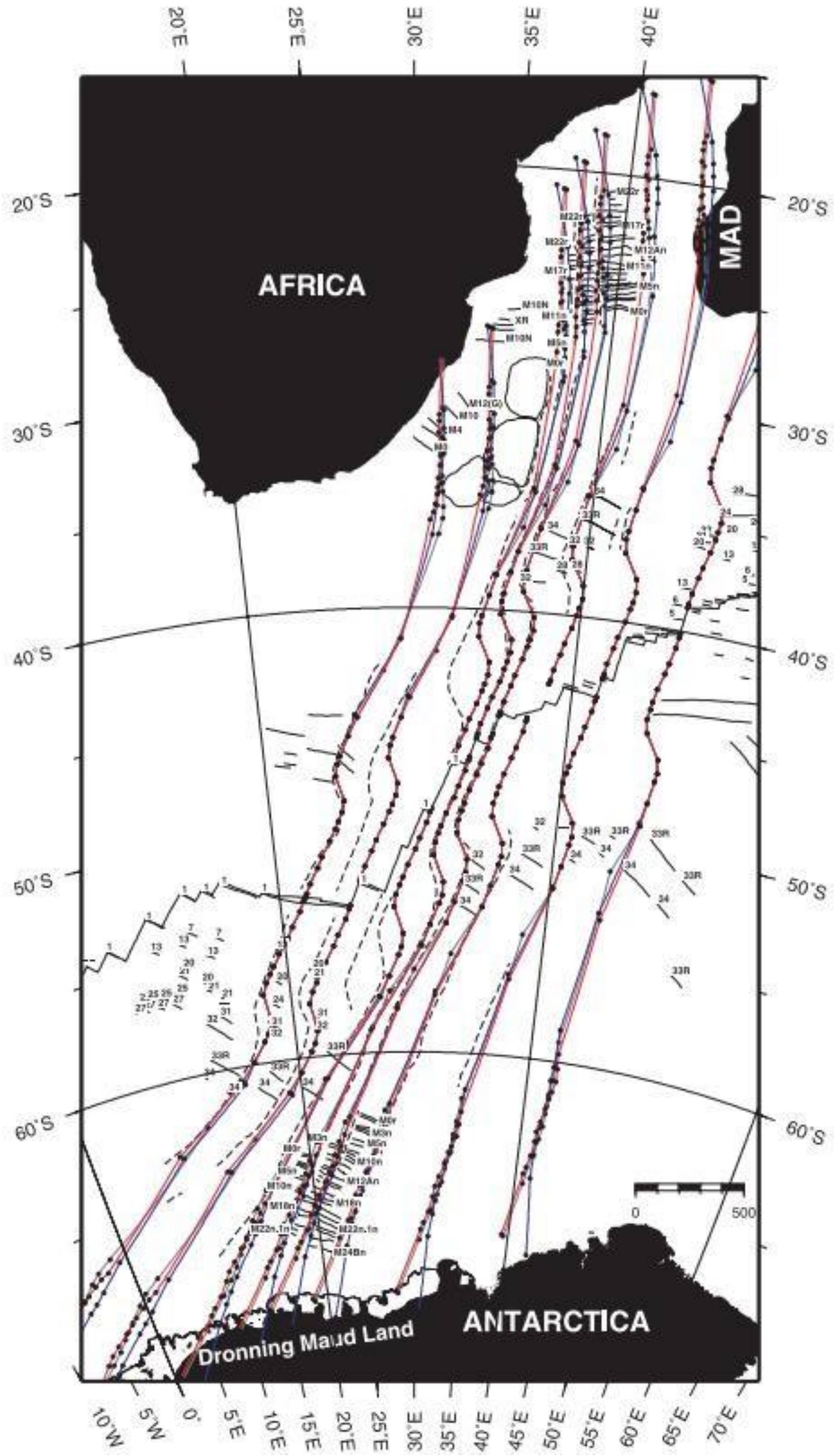

Figure 17: (a) Reconstruction model of Konig and Jokat (2010). They considered oceanic origin for the Mozambique Ridge, with an emplacement between 140-120Ma. The model result in ~90km of overlap between Antarctica and Africa. Mercator projection.

Figure 17 (b) Flowlines for Antarctica proposed in Konig and Jokat (2010). The flowlines crosses the magnetic spreading anomalies in the South Natal Valley (SNV). Implying the SNV was generated between Antarctica and Africa

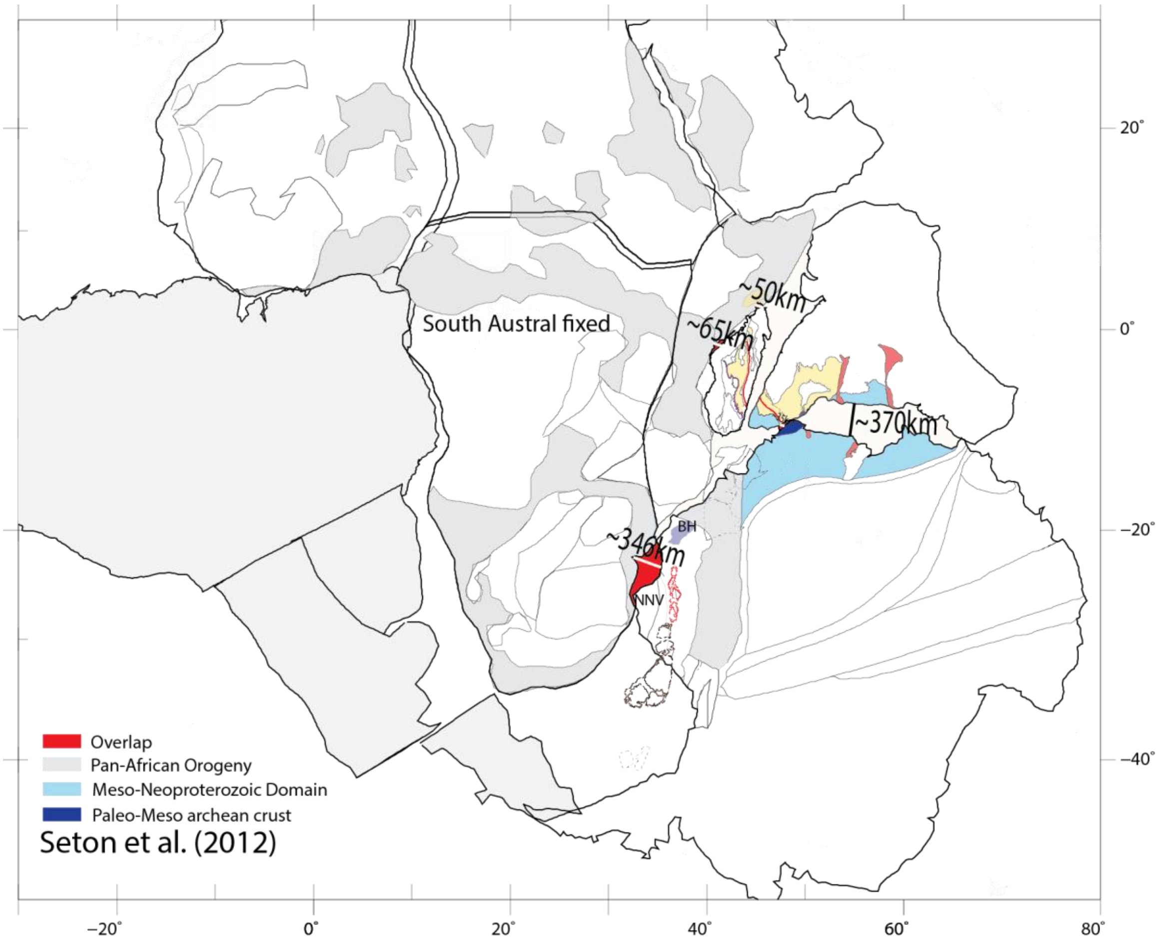

Figure 18: Reconstruction model of Seton et al. (2012). They adopted a model for Gondwana whereby pre-breakup margin extension was initiated at 180 Ma as a response to thermal weakening by the eruption of the Karoo flood basalts, and initiated seafloor spreading at 160Ma along the entire East Africa margin after the cessation of rifting in the Karoo Rift, about 5 million years before the last confidently dated magnetic anomaly (M25). Following Torsvik et al. (2012), they reconstructed Antarctica with an overlap on the Beira High, NNV, N Mozambique Ridge, and Limpopo basin Poles for South American plate provided by Seton et al. (2012). (Mercator projection).

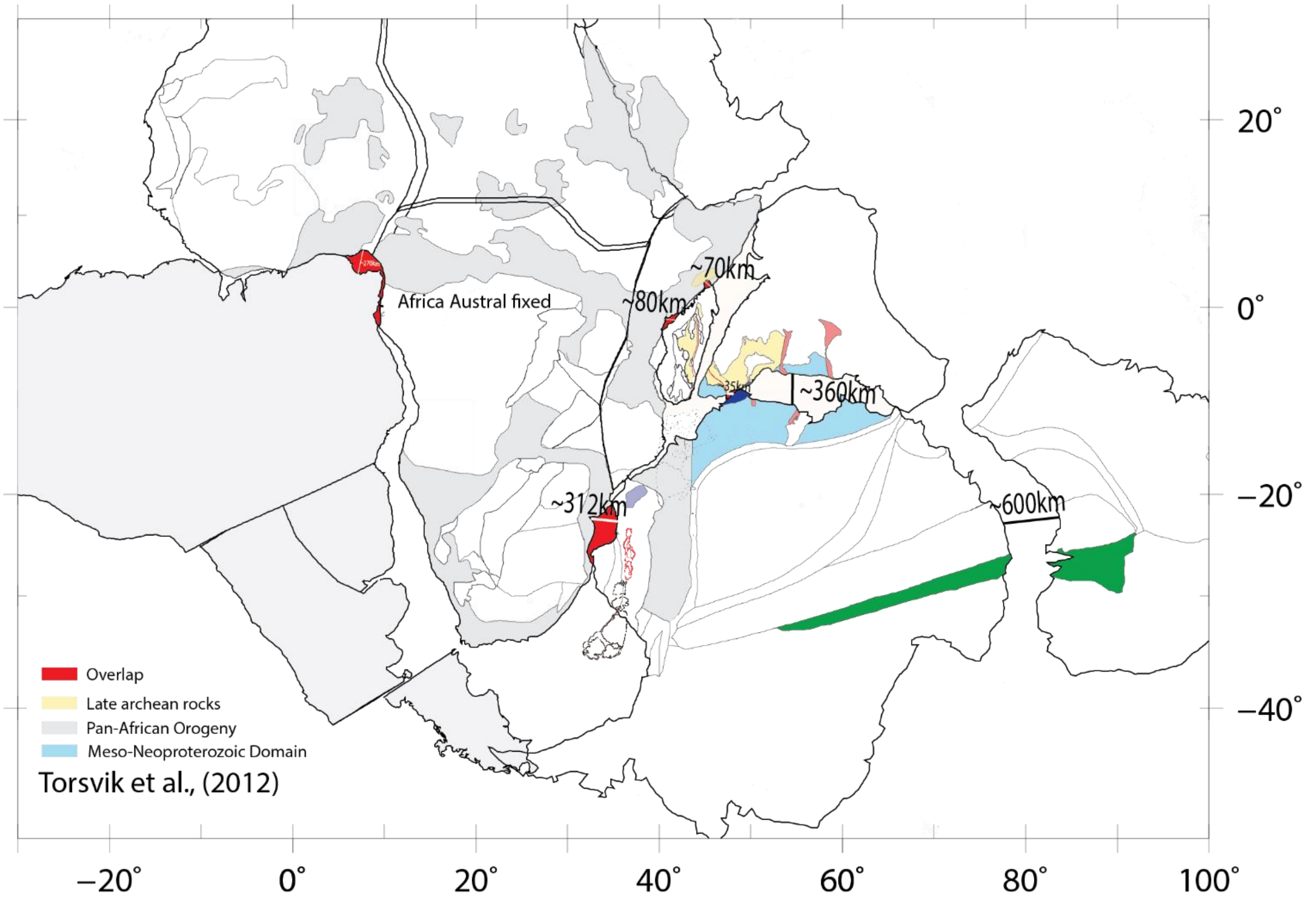

Figure 19: Reconstruction model of Torsvik et al. (2012). Their model assumes oceanic origin for the Limpopo Basin, Natal North Valley, and the Mozambique Ridge. Allowing Antarctica to overlap these structures, and results in ~300km of overlap between Antarctica and Africa. Poles for South American plate provided by Torsvik et al. (2012). (Mercator projection).

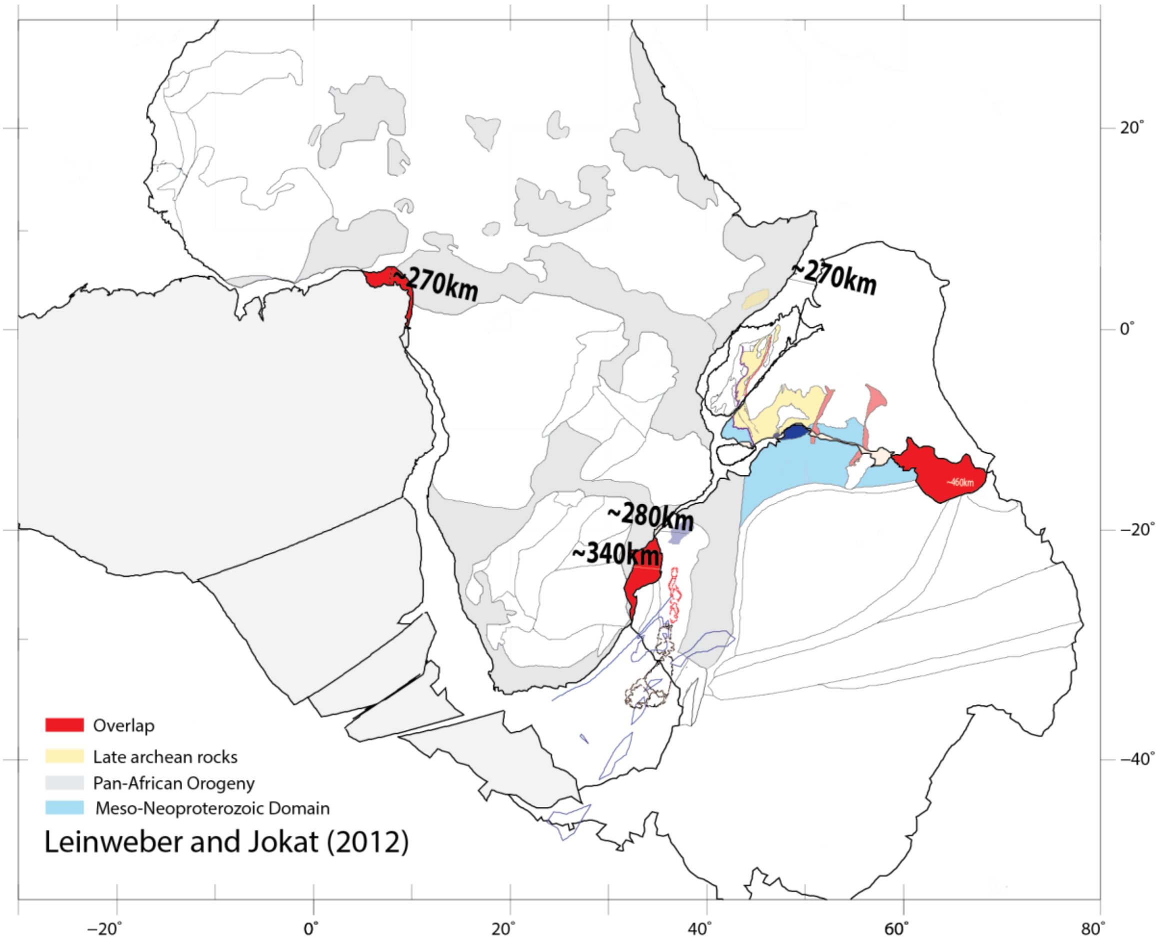

Figure 20: Initial fit of Leinweber and Jokat, (2012). The model is based on interpretation of magnetic anomaly M41 in the Zambezi Basin, and assumption of an Early Jurassic Gondwana breakup, close time wise to the Karoo magmatic activity (179-182Ma). Their initial fit of Antarctica with respect to Africa leads to a tight fit, with a resulting ~300km overlap of Antarctica on Africa inMozambique. They assumed oceanic origin for the Beira High, Limpopo Basin, the North Natal Valley, and the Mozambique ridge, permitting overlap by Antarctica. Poles for South American plate provided by Leinweber and Jokat, (2012. (Mercator projection).

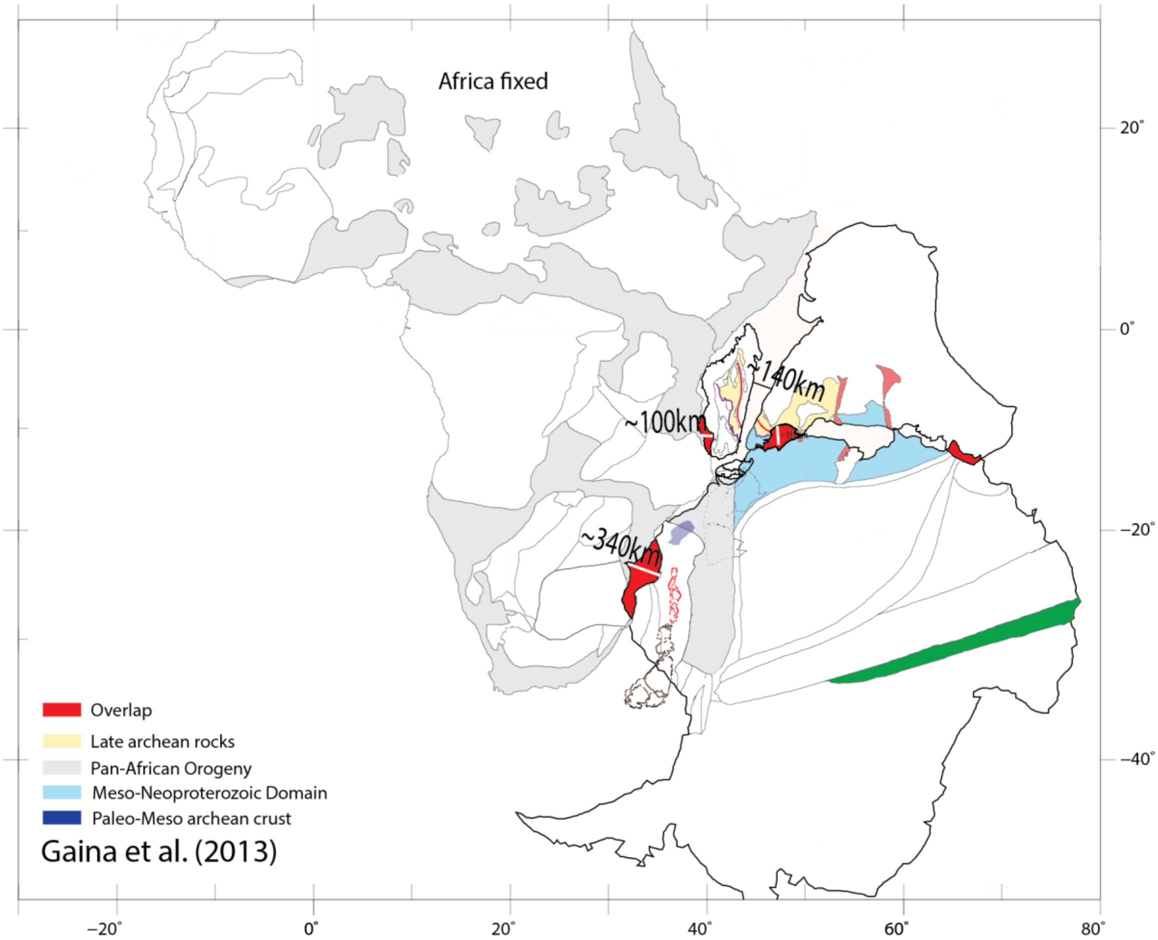

Figure 21: Reconstruction model of Gaina et al. (2013). Following Leinweber and Jokat, (2012), Gaina et al. (2013) assumed magnetic anomaly M41 (167.5 Ma Gradstein et al., 2012) as the oldest Jurassic anomaly in the Mozambique Channel, and additionally proposed anomaly M41 in the Somali to achieve a cohesive initial East-West Gondwana drift from Africa. Their model results in overlap of Antarctica over the Beira High, the Limpopo Basin, the North Mozambique Ridge, and the North Natal Valley. The model further results in ~200km overlap between India and Antarctic, and ~140km gap between India and Madagascar. Poles for South American plate provided by Gaina et al. (2013). (Mercator projection).

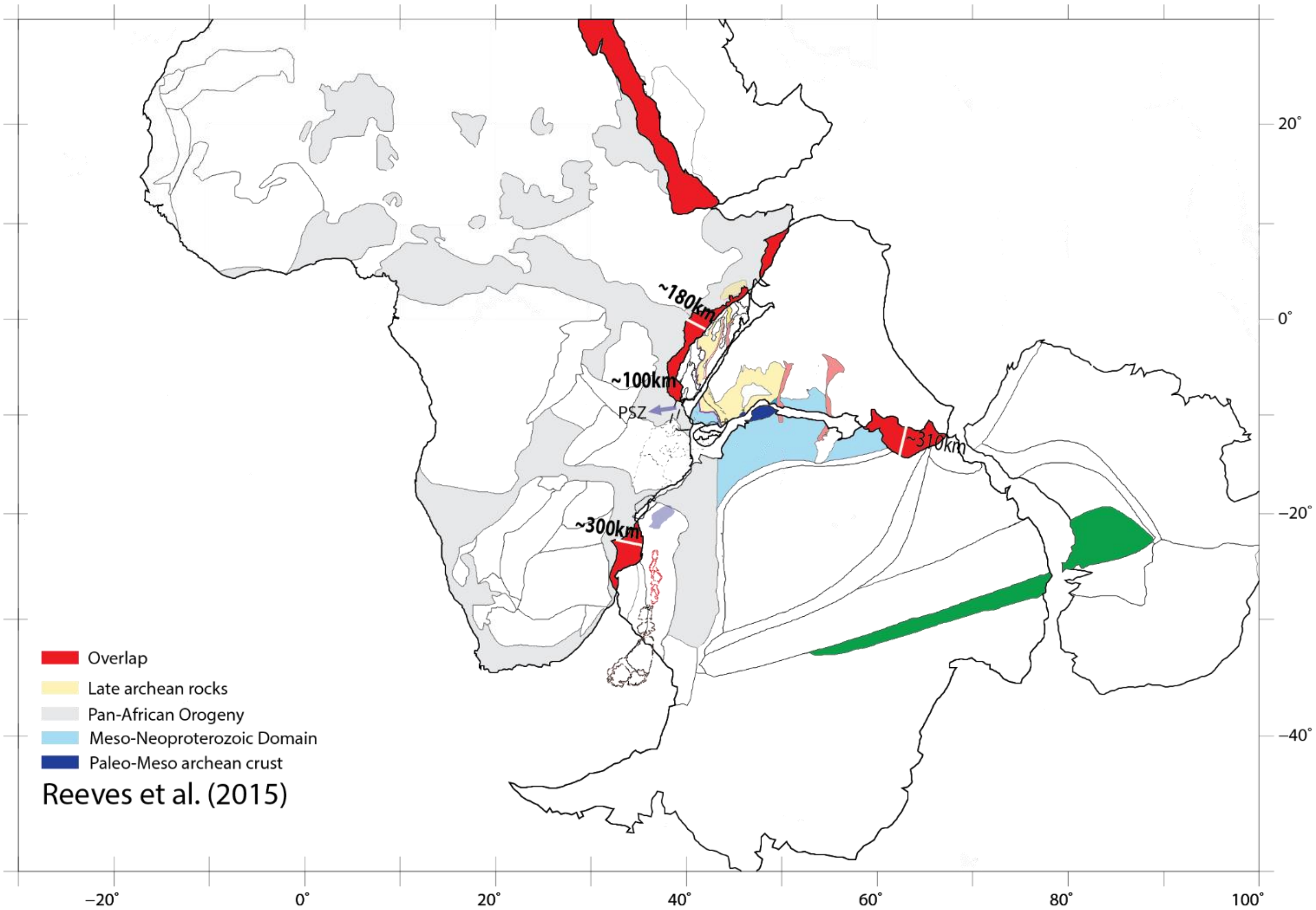

Figure 22: Reconstruction of Reeves et al. (2015). Their original model incorporated reconstruction of distinct rotation poles for several Precambrian cratons and continental fragments. Their fit for India-Madagascar-Sri Lanka-Antarctica was model after Ghosh et al., (2004). They suggested significant extension of the continental crust about 200Km. To examine their model on the same scale as the others, the coastline of the plates was used. The model results in ~300km of overlap of Antarctica on the African plate (in the Limpopo Basin). Notice Antarctica completely overlaps the Beira High, the North Mozambique Ridge and the North Natal Valley. PSZ: PanAfrican Shear Zone after de Wit et al. (2001). (Mercator projection).

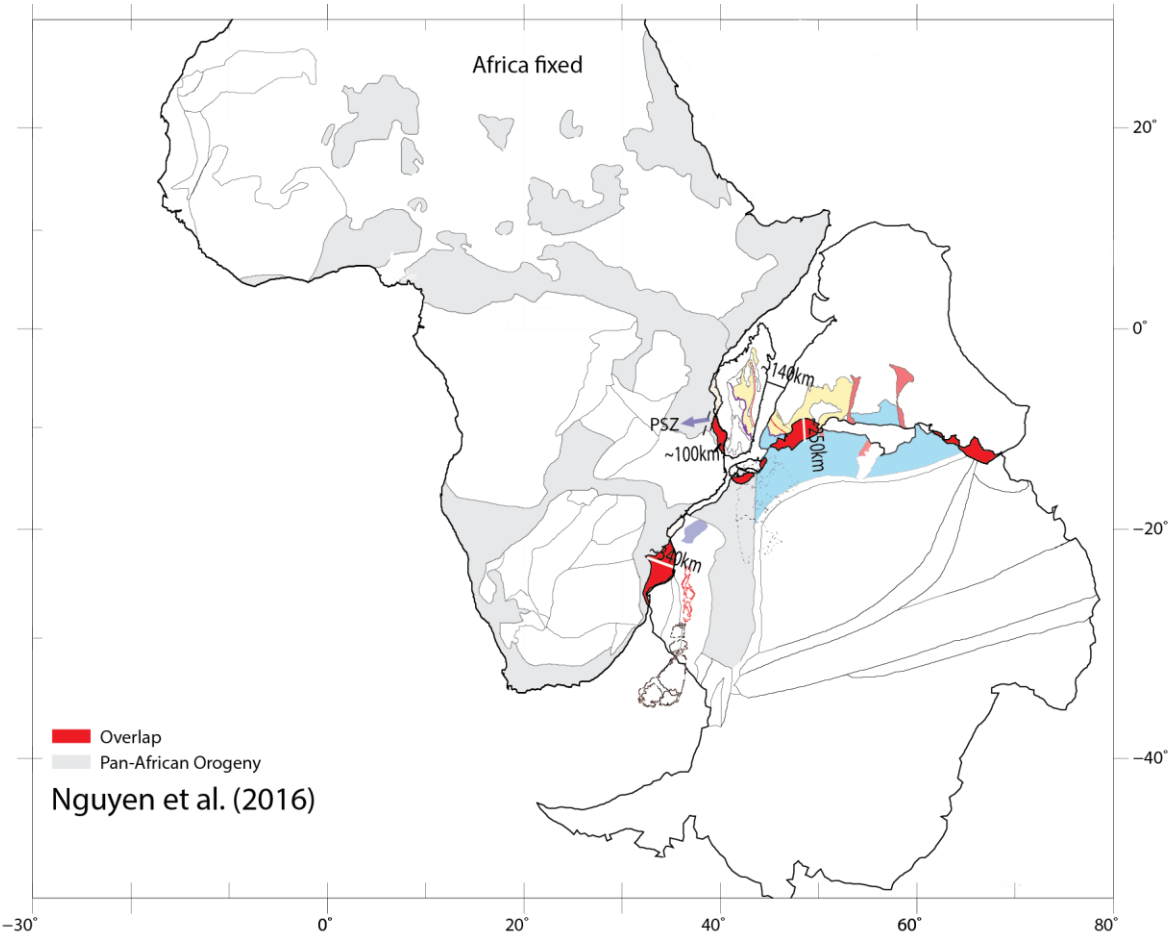

Figure 23: Nguyen et al. (2016) adopted the pole of Gaina et al. (2013) for the initial fit of Madagascar relative to Africa, and Seton et al. (2012) for the rest of the East Gondwana plates. The model results in ~300km overlap of Antarctica over Africa, and ~140km gap between India and Madagascar. PSZ: PanAfrican Shear Zone. (Mercator projection).

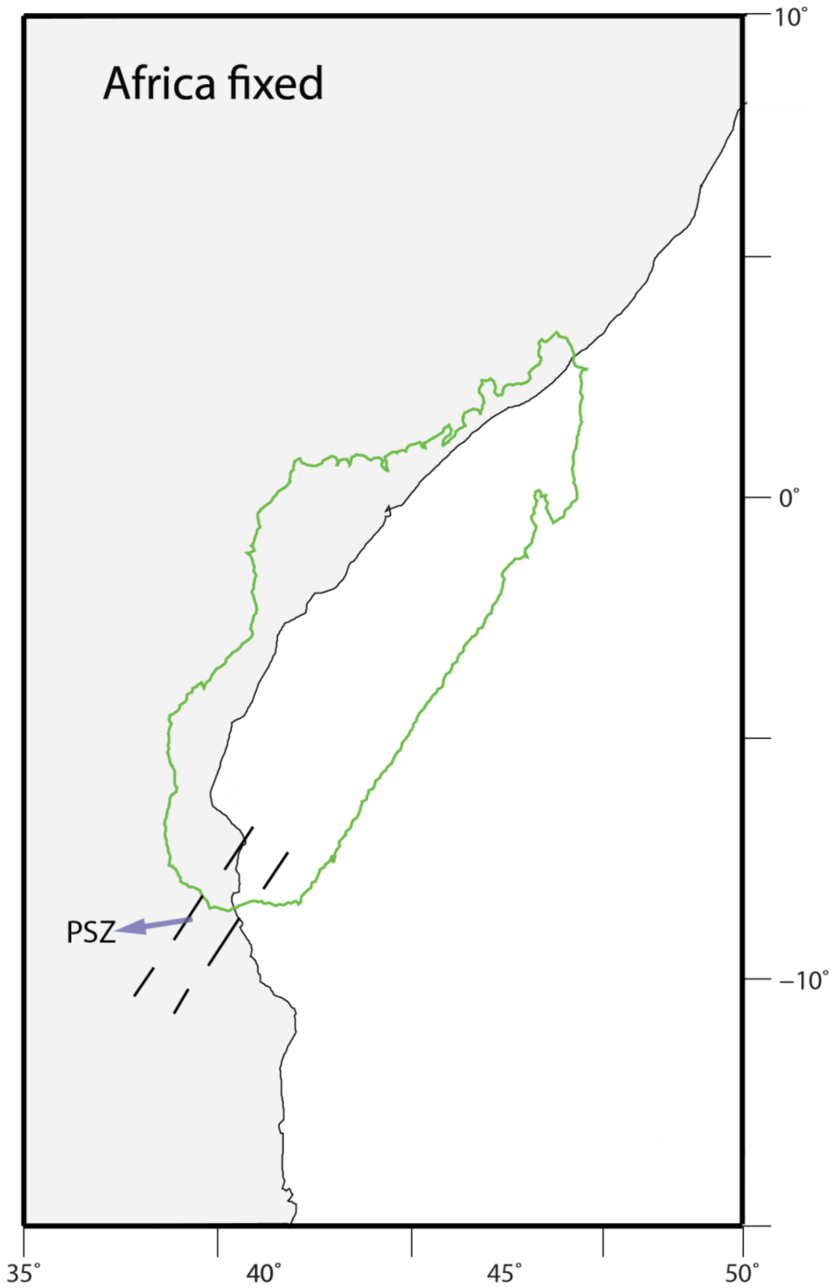

Figure 24: Reconstruction of Madagascar relative to Africa by Phethean et al., (2016). They proposed new spreading lineaments in the Somali Basin, based on directional derivatives of free-air gravity anomalies in support of a tight fit of Madagascar to Africa, with significant crustal extension between the two plates. Their initial fit of Madagascar in their model is after Revees et al. (2015). The model has consequences on the position of Antarctica and the rest of the East Gondwana (India, Sri Lanka, Australia) relative to Africa as it may result in overlap of Antarctica over Africa in Mozambique (see Revees et al. (2015). PSZ: PanAfrican Shear Zone after de Wit et al. (2001). (Mercator projection).

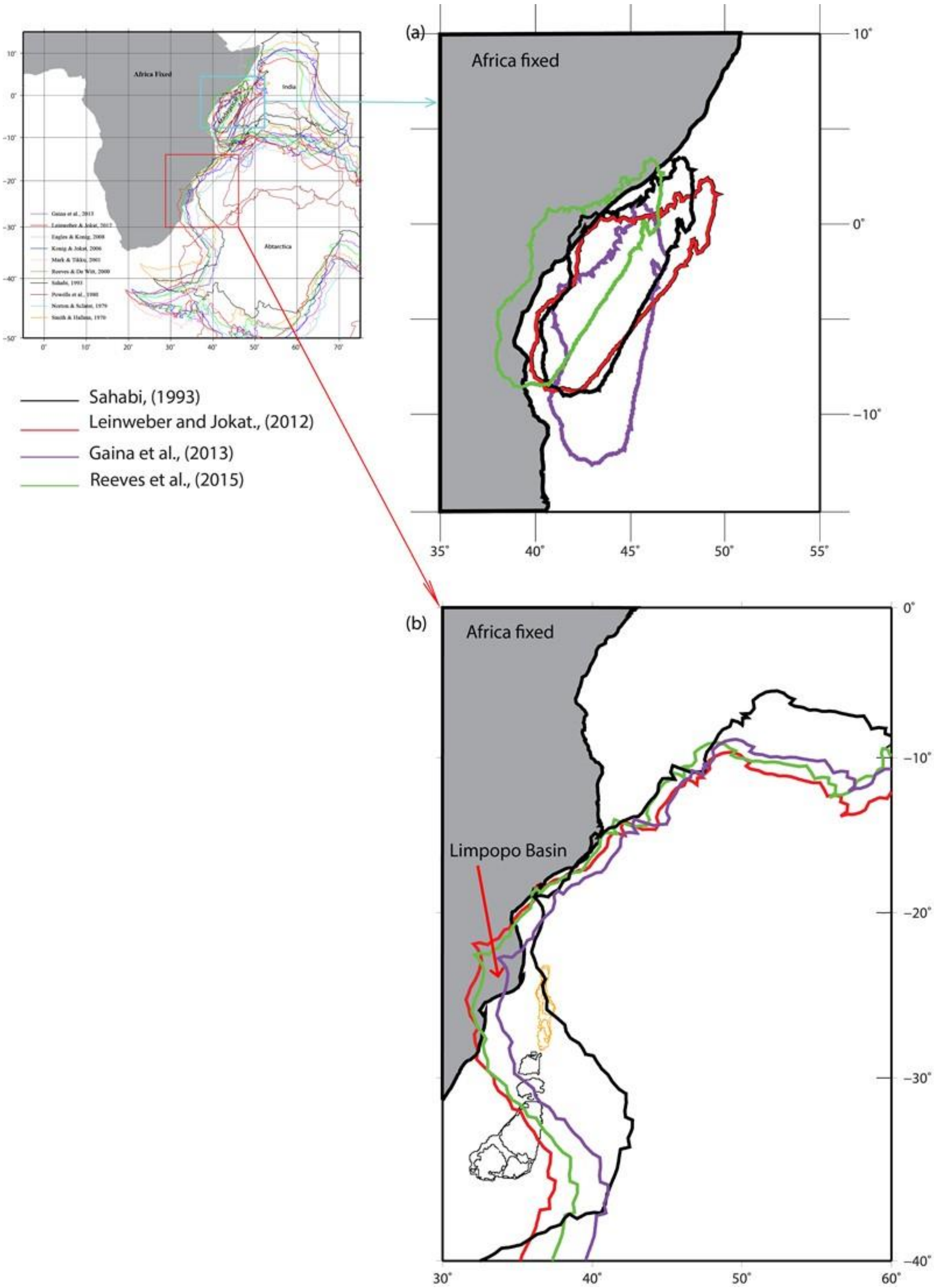

Figure 25: Map showing comparing the reconstruction models of Sahabi, (1993), Leinweber and Jokat, (2012), Gaina et al., (2013), Reeves et al., (2015) at the same scales. Notice the large differences in the placement of the plates in terms of latitude and angle. With regard to the fit between Africa and Antarctica, notice the overlap of Antarctica on the Limpopo basin in (Reeves et al., 2015; Gaina et al., 2013 and Leinweber and Jokat, 2012). The North Mozambique Ridge (In yellow) was found during recent expedition in the Mozambique Basin of MOZ3-5 to consist mainly of sediments on a thinned continental crust (Lepretre et al., 2017; Moulin et al., submitted). The Southern Mozambique Ridge (In black) maybe composed of volcanics (Gohl et al., 2011) possibly emplaced at a triple junction. (Mercator projection).

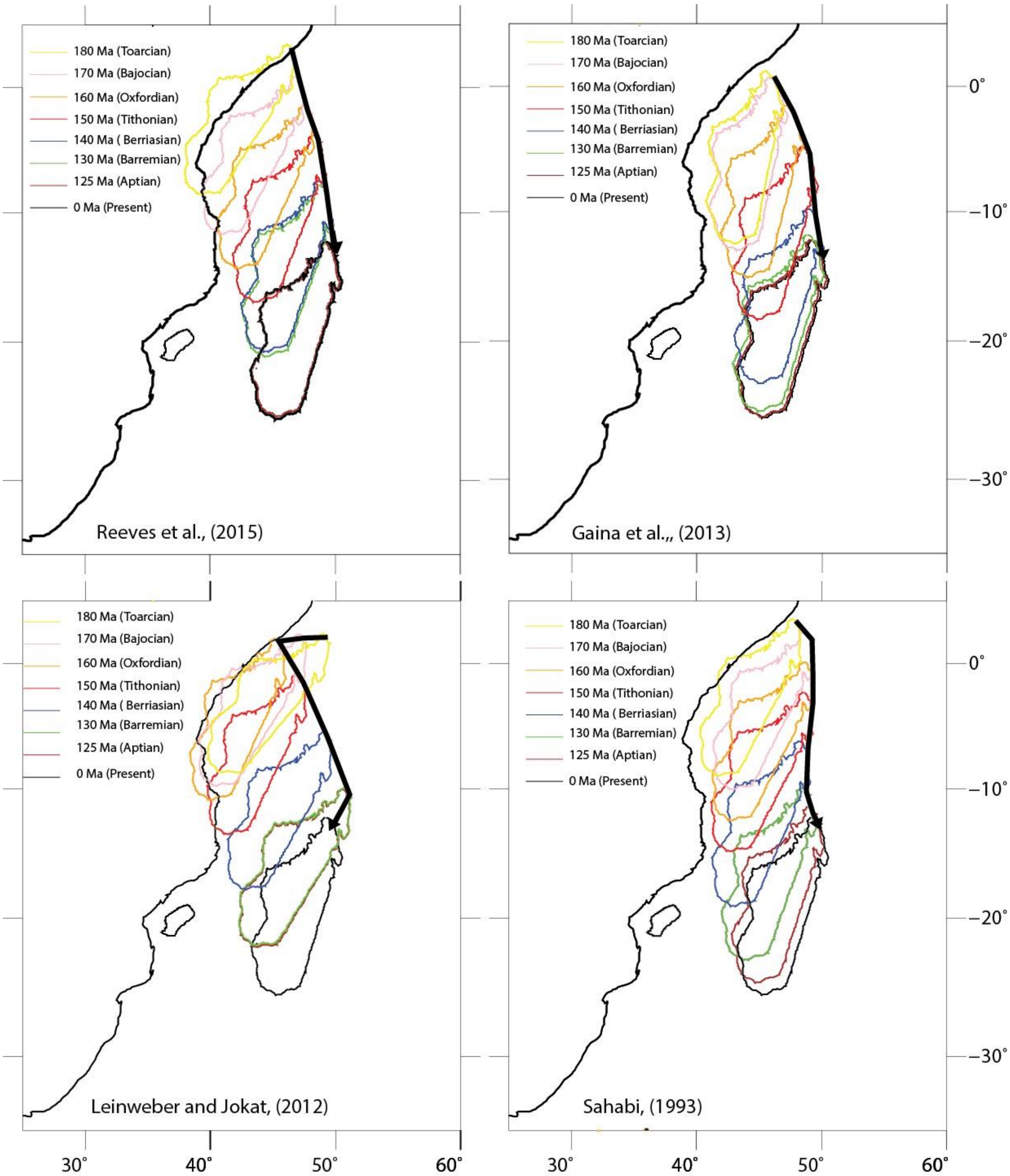

Figure 26: Comparing the evolution partings of Madagascar in (Reeves et al., 2015; Gain et al., 2013; Leinweber and Jokat, 2012; and Sahabi, 1993). The models of Reeves et al., (2015) and Leinweber and Jokat, (2012) starts with an initial overlap of Madagascar on the African plate before a southward drift to the present position. Notice Leinweber and Jokat, (2012) start with an initial phase of compression. (Mercator projection).

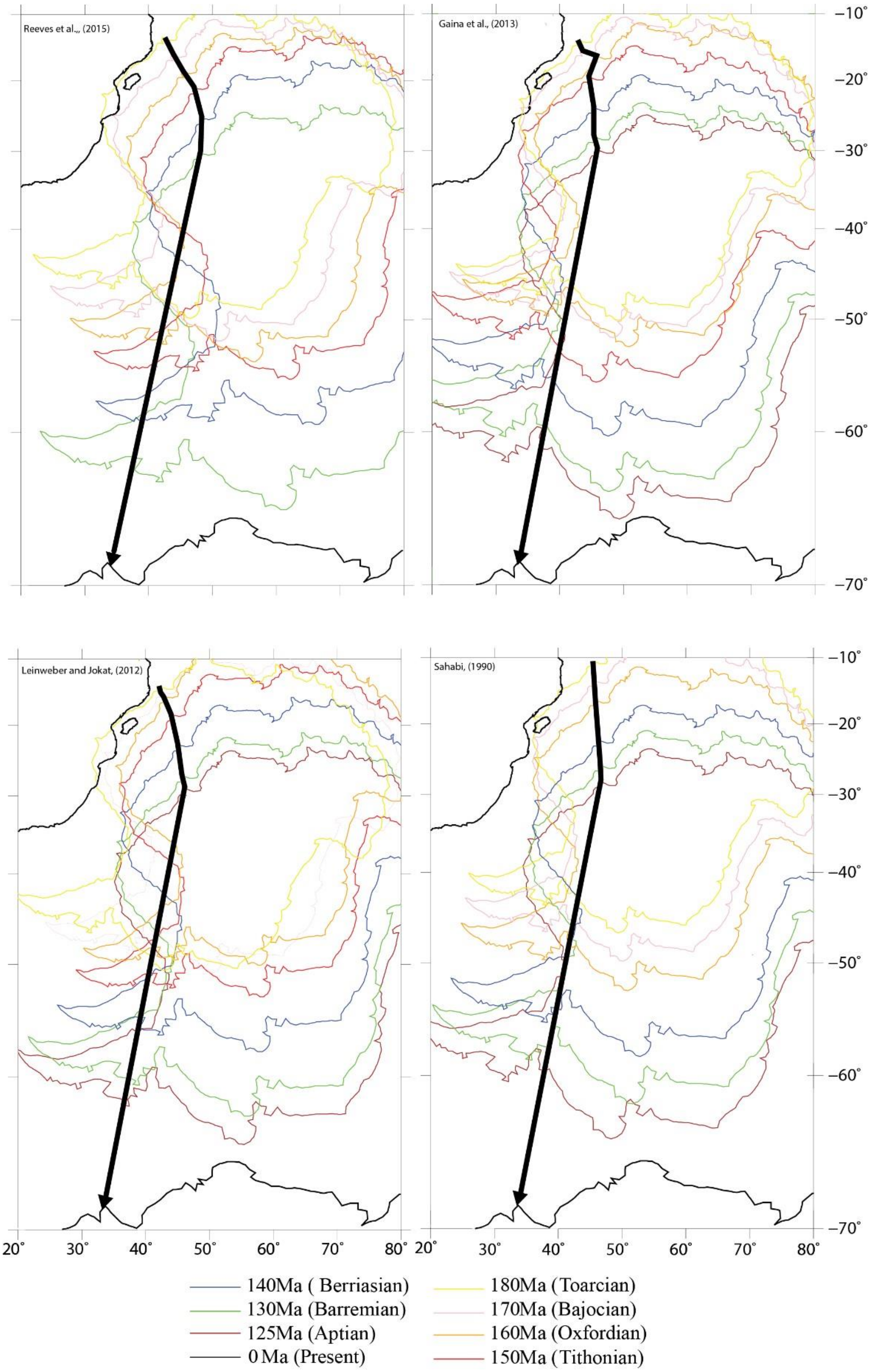

Figure 27: Evolution of Antarctica with respect to Africa in (Reeves et al., 2015; Gain et al., 2013; Leinweber and Jokat, 2012; and Sahabi, 1993). Notice the initial relatively zig zag motion in Gaina et al, (2013), and the overlap of the Antarctic plate and Africa plate in Reeves et al. (2015) Gain et al., (2013), Leinweber and Jokat (2012) calling into question the nature of the crust underlying this area. (Mercator projection).

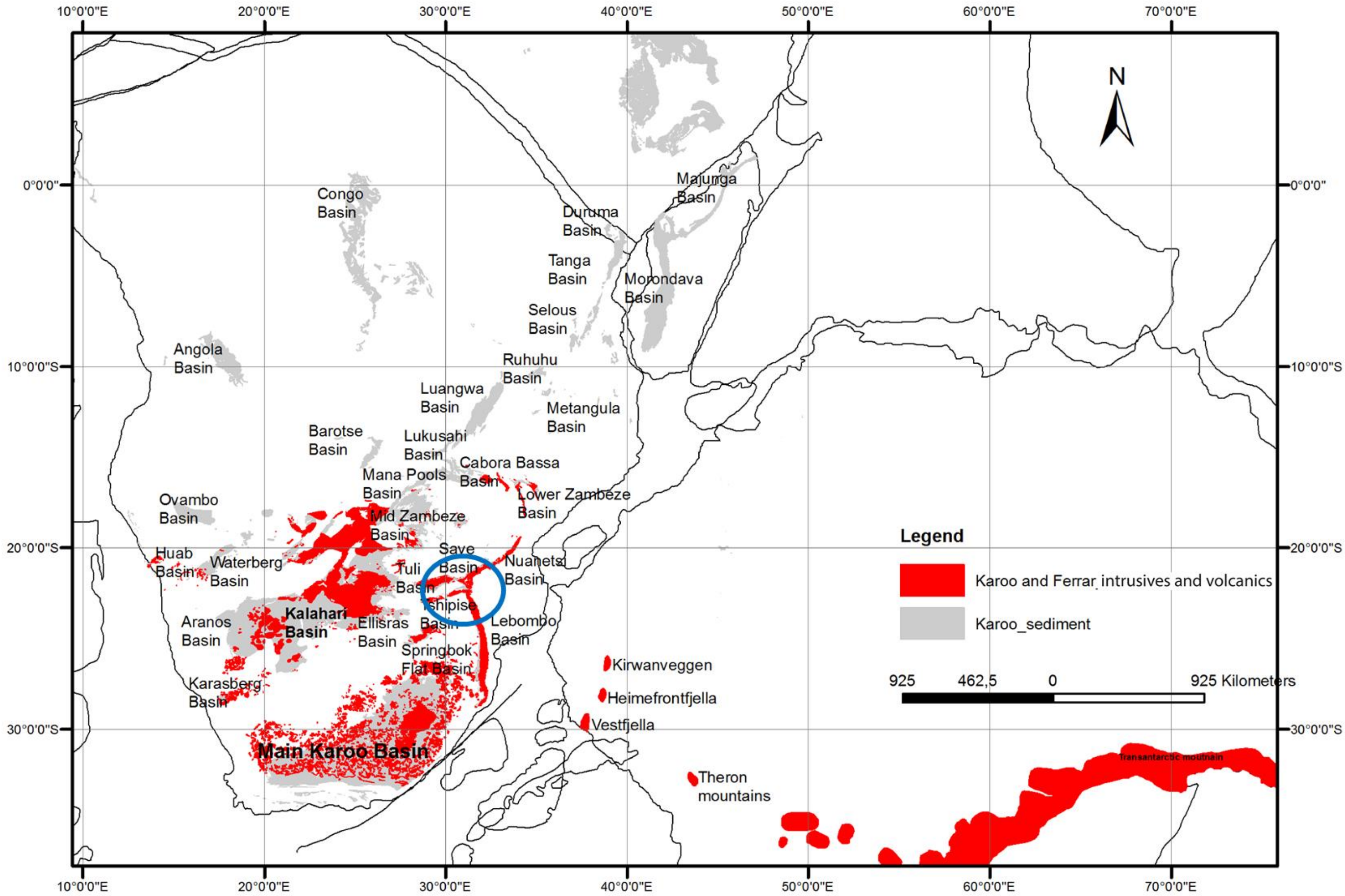

Figure 28: Reconstruction of Thompson et al. (submitted), showing the main distribution of pre-drift Karoo sediments and volcanics in Africa, Madagascar, and Antarctica. The Southern Africa continent is characterized by vast network of sills and dykes (182-183Ma) which are pre-syn-post Karoo magmatism (179-182Ma). This magmatic event was also witnessed in the Dronning Maud Land of Antarctica (Elliot and Fleming 2000), and the Ferrar Province (Antarctica, Elliot and Fleming 2000). World Geodectic System 1984. Blue circle shows the possible location of the tripple junction considered for the plume hypothesis.

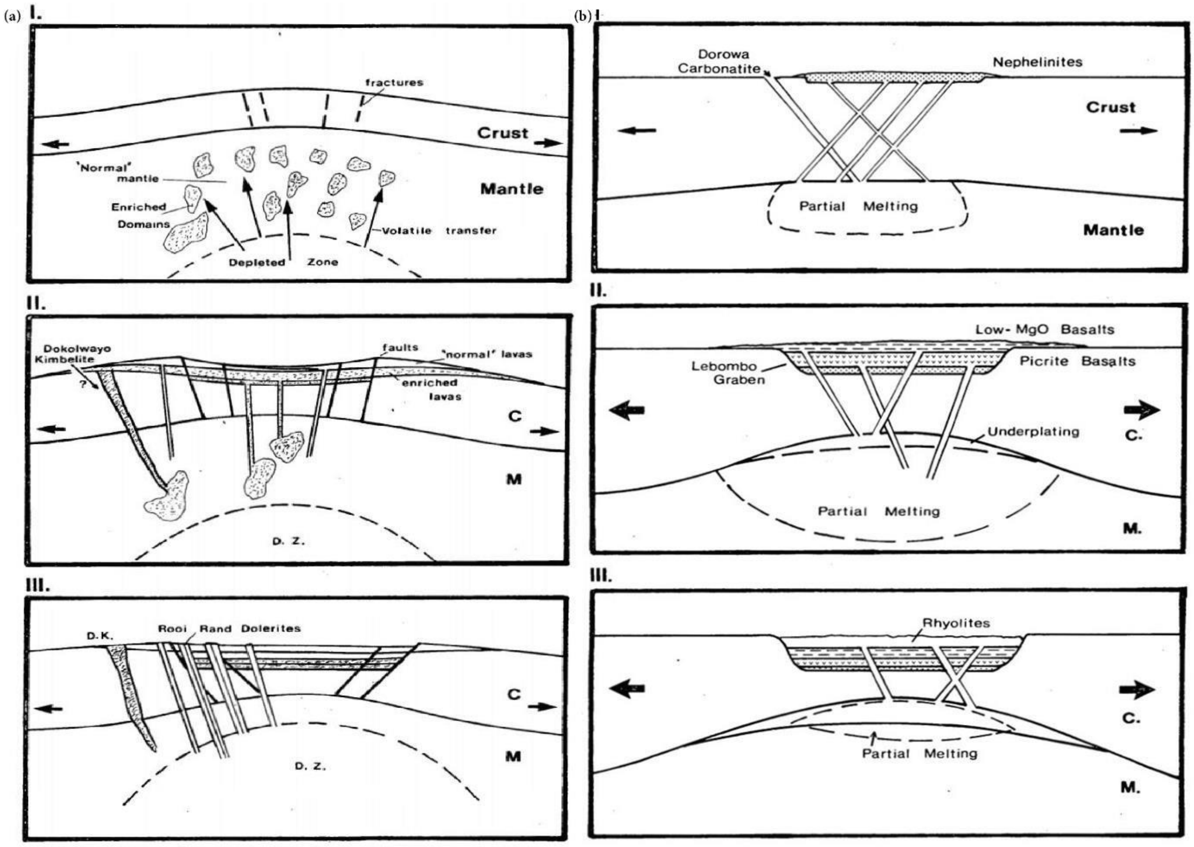

Figure 29: (a) Schematic diagram by Bristow (1980), illustrating the geochemical and isotopic relationships of how the Lebombo volcanics may have been sourced, and how low-MgO volcanics may have developed. (b) A schematic diagram by Bristow (1980), showing how early formed picritic magmas would equilibrate with mantle phases at higher pressures than those magmas formed later in the volcanic event.

Table 1. The ^{40}Ar-^{39}Ar Radiometric Ages for the Karoo Igneous Province in South Africa and Namibia and Correlative Rocks in East Antarctica

Sample	Material	Total Fusion Age, Ma	Plateau Age Ma	^{39}Ar of Total %	Isochron Age, Ma	*N*	$^{40}Ar/^{36}Ar$ Intercept ± 1σ	*J*
				South Africa: Lesotho				
OXB-01	basalt	187.5	186.5 ± 1.9	81	189.6 ± 3.2	5	235.1 ±21.6	0.001686
MLP-172	basalt	180.3	179.5 ± 2.1	79	181.7 ± 2.2	3	280.9 ± 9.6	0.001680
BUS-18	basalt	184.8	182.4 ± 1.7	94	186.4 ± 2.6	5	283.5 ±28.3	0.001690
ROM-01	basalt	180.4	180.0 ± 2.1	88	180.6 ± 4.3	4	253.5 ±39.7	0.001695
		186.8	184.4 ± 1.0	69	181.9 ± 2.3	3	298.2 ± 5.6	0.001593
BMC-04	basalt	184.3	184.3 ± 1.7	95	183.5 ± 1.9	5	292.2 ± 6.4	0.001686
NN-01	basalt	190.4	182.9 ± 2.1	60	184.1 ± 2.5	3	287.2 ±10.9	0.001688
ON-01[a]	basalt	166.7						0.001695
KF-10 Omeg[a]	basalt	173.7	183.9 ± 1.0	77	183.5 ± 1.7	5	302.7 ± 9.1	0.001653
	plagioclase	187.9	183.9 ± 0.7	93	183.8 ± 2.4	6	294.7 ± 2.7	0.001496
MF-09 Moshesh[b]	basalt	185.9						0.001358
KRB-7 Moshesh	andesite	183.2	181.0 ± 1.7	82	182.0 ± 3.2	4	295.8 ±27.9	0.001628
KR-29 Moshesh	basalt	190.5	186.5 ± 1.1	72	184.5 ± 3.2	3	308.9 ±70.6	0.001324
				South Africa: Lebombo				
KVU-5 Jozini	rhyolite	180.3	179.7 ± 0.7	98	180.0 ± 1.8	4	315.3 ±91.7	0.001469
KSA-12 Jozini	rhyolite	177.7	178.1 ± 0.6	91	177.6 ± 1.9	6	308.7 ±38.2	0.001430
RSS-82 Sabie	basalt	179.0	181.2 ± 1.0	79	182.6 ± 2.1	4	296.0 ±13.9	0.001398
KOL-2 Sabie	basalt	186.2	183.2 ± 1.3	83	181.4 ± 3.7	4	306.0 ± 9.5	0.001680
RSV-4 Sabie[c]	basalt	180.8						0.001503
RSV-35 Sabie	basalt	188.4	184.2 ± 1.0	81	182.8 ± 4.9	3	305.6 ±51.7	0.001525
	plagioclase	190.4	184.2 ± 0.6	76	182.9 ± 2.5	6	295.1 ± 3.4	0.001574
RSS-8 Sabie[b]	basalt	186.7						0.001621
KP-121 Letaba	picrite	184.5	182.7 ± 0.8	90	182.2 ± 2.5	4	356.6 ±31.6	0.001675
KP-111 Letaba	picrite	129.5	141.9 ± 1.5	62	139.8 ± 2.5	3	267.0 ±14.1	0.001385
KP-83 Mashikiri[d]	nephelinite	219.4						0.001382
KP-92 Mashikiri	nephelinite	194.2	182.1 ± 1.6	54	181.7 ± 3.9	2	313.1 ±29.0	0.001436
KOL-17 Mashikiri[b]	nephelinite	206.3						0.001599
				South Africa: Transvaal Dikes and Sills				
TRA-71[c]	plagioclase	177.2						0.001378
TRA-76	plagioclase	180.6	181.4 ± 1.1	95	183.5 ± 1.6	7	257.2 ±35.5	0.001391
TRA-84	plagioclase	189.4	182.8 ± 1.6	68	182.4 ± 2.8	4	309.0 ±25.0	0.001470
TRA-95	plagioclase	207.6	180.3 ± 1.8	65	184.1 ± 2.2	4	294.8 ±16.0	0.001353
				Namibia: Hardap				
HAR-02[b]	basalt	188.4						0.001265
	plagioclase	183.4	183.0 ± 0.6	100	184.4 ± 1.8	6	294.6 ± 2.6	0.001448
HAR-07[b]	basalt	182.7						0.001746
HAR-08	basalt	177.4	184.2 ± 1.0	50	185.4 ± 1.9	4	290.2 ± 3.7	0.001275
HAR-13	basalt	185.4	186.0 ± 0.8	92	187.4 ± 2.0	5	291.0 ± 2.1	0.001605
				Namibia: Keetmanshoop				
KEE-02[c]	basalt	179.8				0.001305		
KEE-03	plagioclase	183.4	84.7 ± 0.5	95	183.8 ± 1.7	8	268.1 ±37.6	0.001548
KEE-05	plagioclase	176.0	181.5 ± 0.8	50	182.9 ± 2.8	3	295.2 ± 8.5	0.001641
KEE-07[b]	basalt	185.0						0.001774
KEE-10	basalt	184.1	184.7 ± 0.7	100	185.8 ± 2.0	6	292.5 ± 3.8	0.001710
	plagioclase	189.0	180.5 ± 0.7	90	181.8 ± 2.3	4	294.7 ± 4.1	0.001591
KEE-11[a]	basalt	181.7						0.001255
				Antarctica: Kirwan Mountains				
LAD-7	plagioclase	183.9	180.6 ± 0.6	89	182.0 ± 3.2	5	294.9 ± 3.1	0.001650
LAG-22	plagioclase	182.1	182.7 ± 0.6	97	180.9 ± 2.0	6	294.9 ± 0.9	0.001630
LAG-31	plagioclase	183.4	182.8 ± 0.6	98	181.5 ± 1.5	7	293.2 ± 4.3	0.001640

Figure 30: Radiometric ages of Karoo volcanism presented Duccan et al. (1997) in Africa compared to Antarctica. The ages suggest contemporanous emplacement.

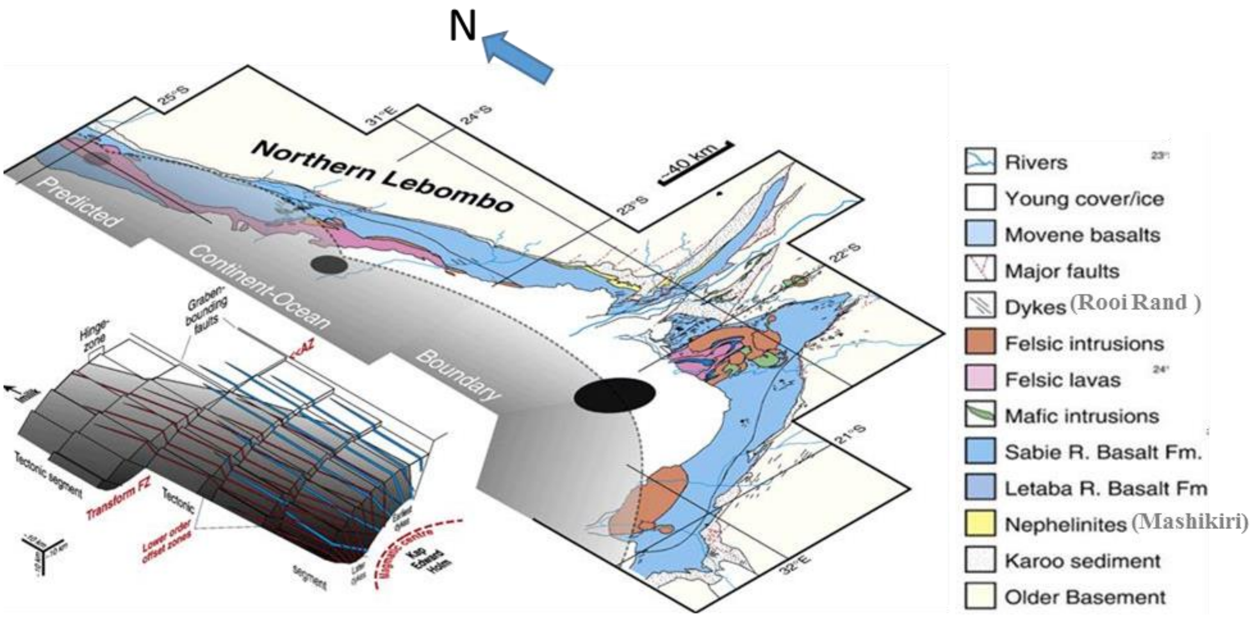

Figure 31: Geological map of the Lebombo Monocline by Klausen (2009). Distribution of Karoo sediments (Late Carboniferous to Middle Jurassic) and overlying volcanic rocks in Klausen (2009), showing the distribution of earliest nephelinite, overlain by picritic Letaba River basalt formation, and lateral high- to low-(Ti, Zr) transition in Sabie River basalt Formation. Note northward disappearance of younger lava formations beneath unconformable cover of Cretaceous–Tertiary sediments. The insert describes the distribution of dykes on the Lebombo. The N–S and NW–SE trending dykes are Jurassic dykes. The predominant SW–NE dykes are cut by the N–S and NW–SE; therefore older than the Karoo Supergroup.

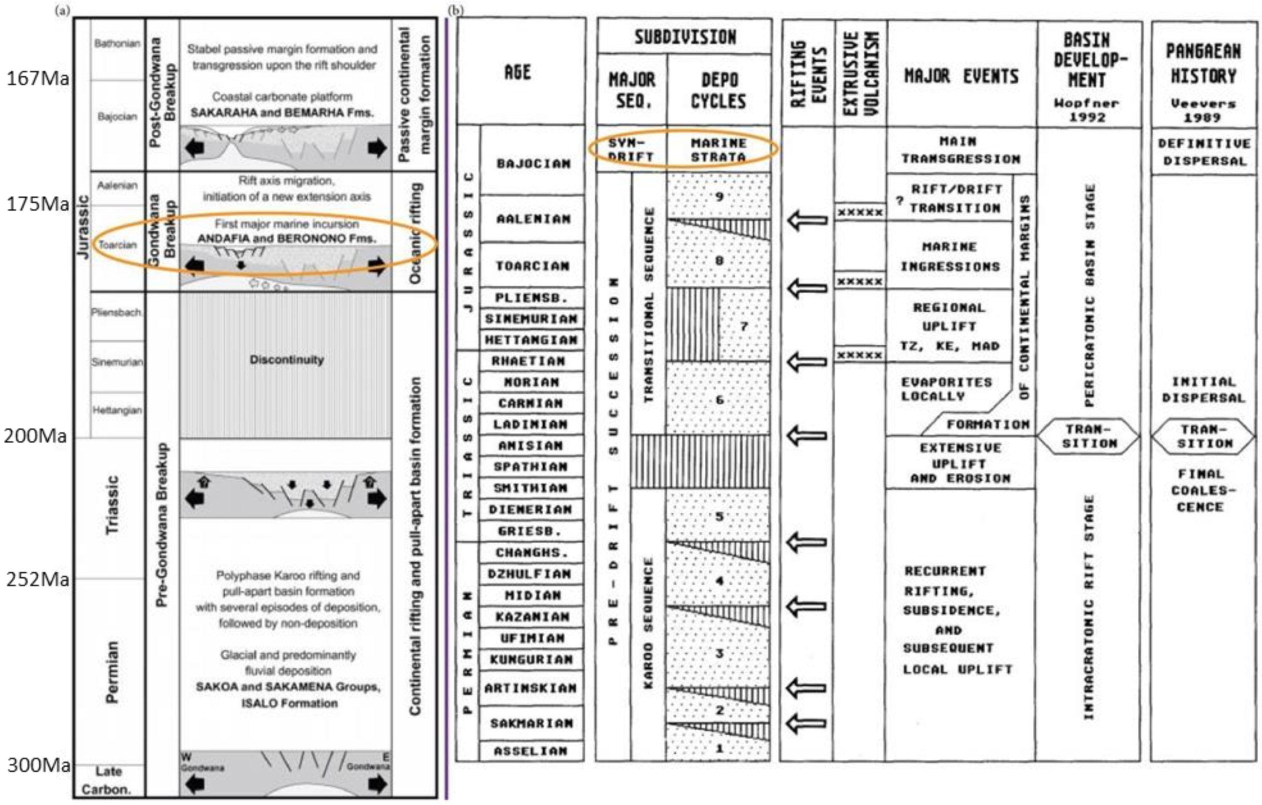

Figure 32: (a) Lithotectonic model by Geiger e al. (2004). In their model, Gondwana breakup was preceded by several Karoo rifting events, but only the Early Jurassic (Toarcian) Andafia rift finally resulted in crustal separation. (b) Generalized stratigraphic scheme by Hankel (1994) for pre-drift sediments of East Africa and Madagascar showing major subdivisions and events. Notice the age difference predicted for the start of drifting in the two schemes Toarcian in Geiger and Bajocian in Hankel (1994).

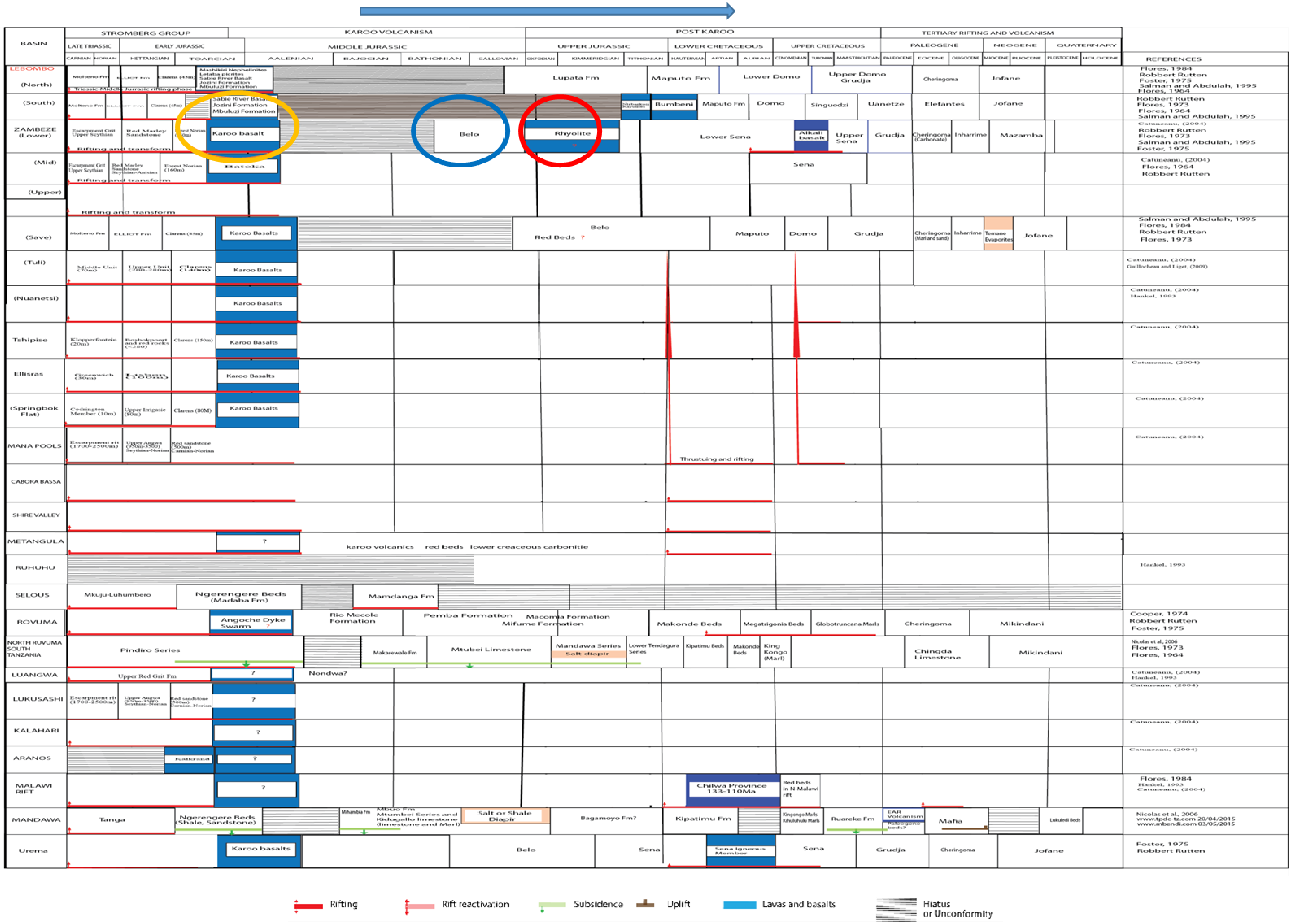

Figure 33: Lihotectonic chart of Karoo Basins in Africa. The yellow circle correspond to breakup contemporanous with the Karoo magmatic event. The blue circle age of magnetic anomaly M41, and the red circle corresponds to the confidently dated magnetic anomlay in the Somali Basin. Legend same as figure 34.

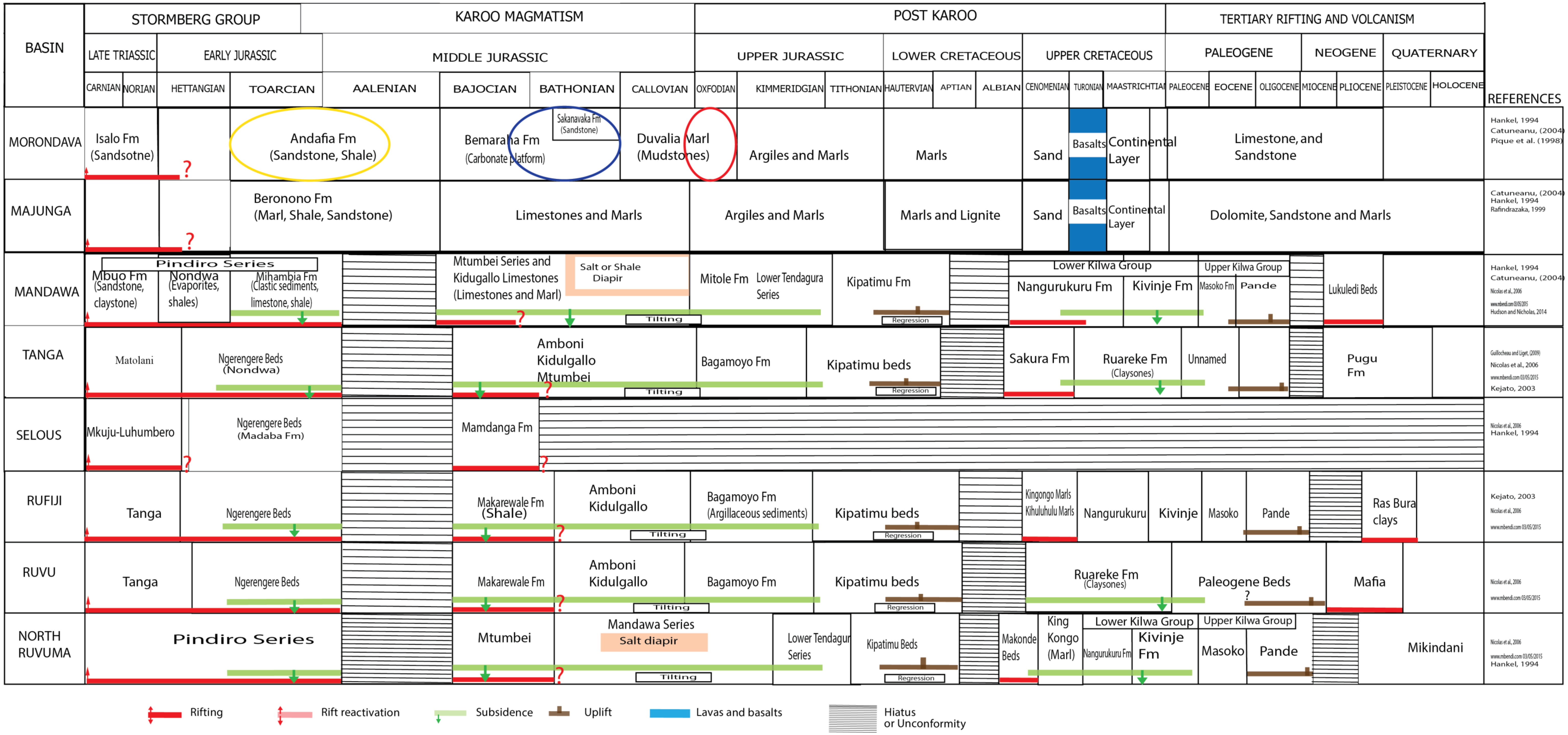

Figure 34: Litotectonic chart of Karoo basins in East Africa and Madagascar Basin. Notice the different ages predicted for the start of drift in Gondwana; the yellow and blue circles correspond to the predictions of Geiger et al. (2004) and Hankel, (1994), respectively. The red circle correspond to the age of the first oceanic crust in Somali Basin. Legend same as figure 33.

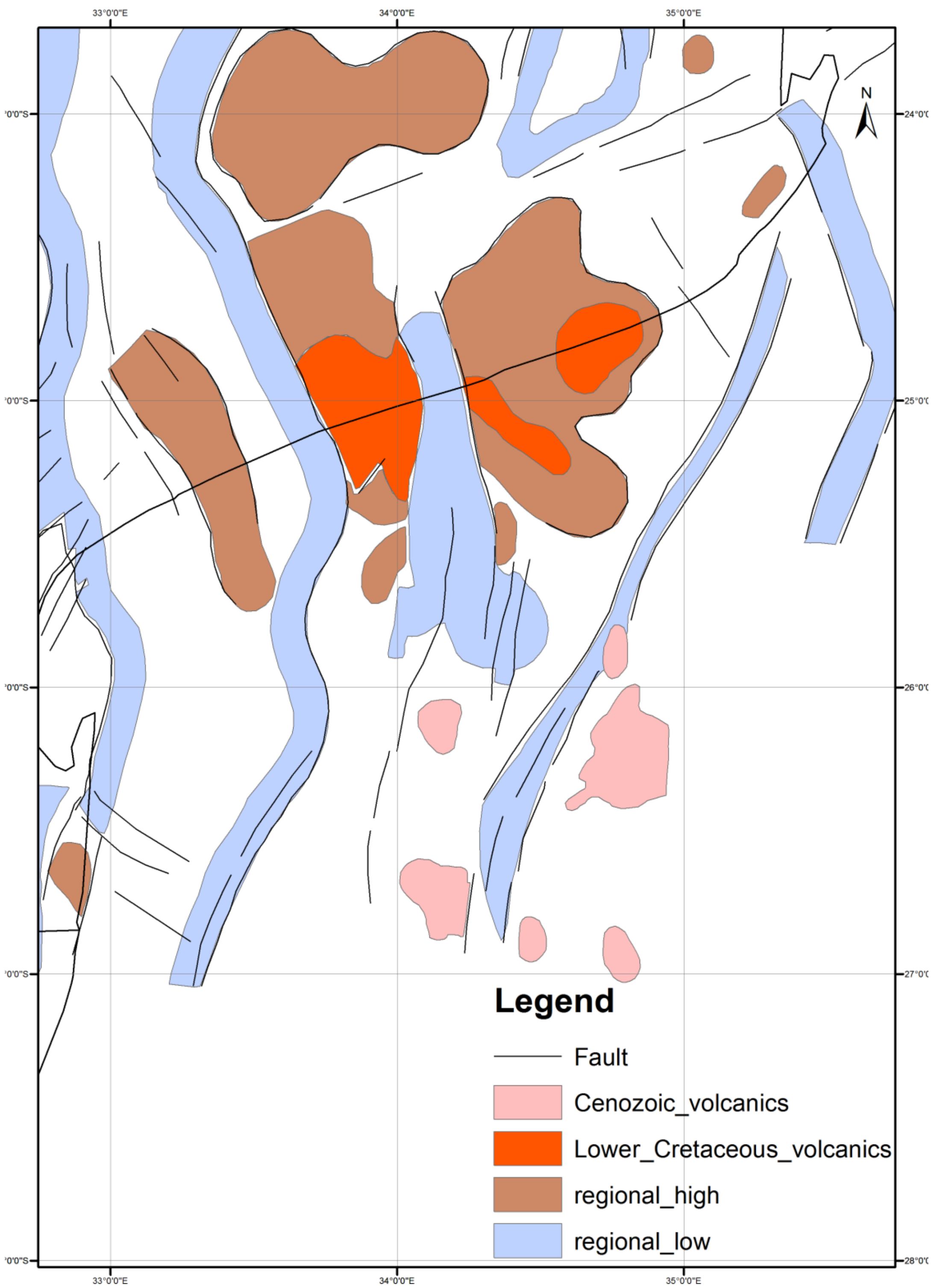

Figure 35: Structural map of the Limpopo basin after Salman 1985. The nature of the crust underlying the Limpopo basin remains unknown. Cox (1992) proposed the basin's development to be related to a plume event that resulted in suppressed breakup, extensive volcanism, and subaerial spreading. Salman and Abdulla (1995) and Flores (1975), however, interpreted the basin to be characterized by the existence of a series of parallel, trending fractures issuing ever younger magma from west to east. The regional low and high are derived from gravity.. Map drawn after Salman, (1985).

Table 1. Mozambican wells that encountered volcanics*

No.	Name	Elevation (sea level)	Thickness (m)	Radiometric age, MM yrs.	Rock type
1	2	3	4	5	6
1	Balano 1	-2,861.1	256.1	-	Basalt
2	Domo 1	-2,980.9	57.0	K/Ar - 137.0	Olivine, basalt
3	Zandamela 1	-1,770.2	926.0	-	Basalt, rhyolites
4	S.Massinga 1	-4,169.0	27.4	-	Basalt
5	Mambone 1	-3,247.9	353.6	-	Basalt, alkali basalt
6	Nhamura 1	-5,140.1	301.2	(Karroo?)	Dolerite
		-5,441.3	27.4	(PreCambrian)	Dolerite
7	Nhachangue 1	-4,479.6	46.9	-	Olivine basalt
8	NE Palmeira 1	-4,441.2	13.7	K/Ar - 285.6±14.3	Basalt
9	NW Macia 1	-2,122.0	152.2	-	Basalt
10	Funhalouro 1	-4,054.1	49.7	-	Weathered basalt,tuffs
11	Nemo 1x	-3,709.4	396.3	-	Tuffs,alkali basalt
12	Sunray I IA	-3,507.0	38.4	K/Ar - 129.6±4.0	Basalt
13	Sunray 2 IA	-1,105.2	118.8	K/Ar - a)116.8±1.8 b)8.47±1.0(?)	Weathered basalt
14	Sunray 3	-3,552.7	28.0	-	Weathered basalt
15	Sunray 4 IB	-1,325.9	19.5	K/Ar - 74.2±3.0	Basalt
16	Sunray 7	-2,595.7	463.3	-	Basalt
17	Sunray 12 I	-2,159.8	282.8	K/Ar - 18.1±0.3	Tuffs, basalt

Figure 36: Chart of Mozambique well that encountered volcanics by Flores (1984)**, showing the **episodic event of the Karoo volcanism.

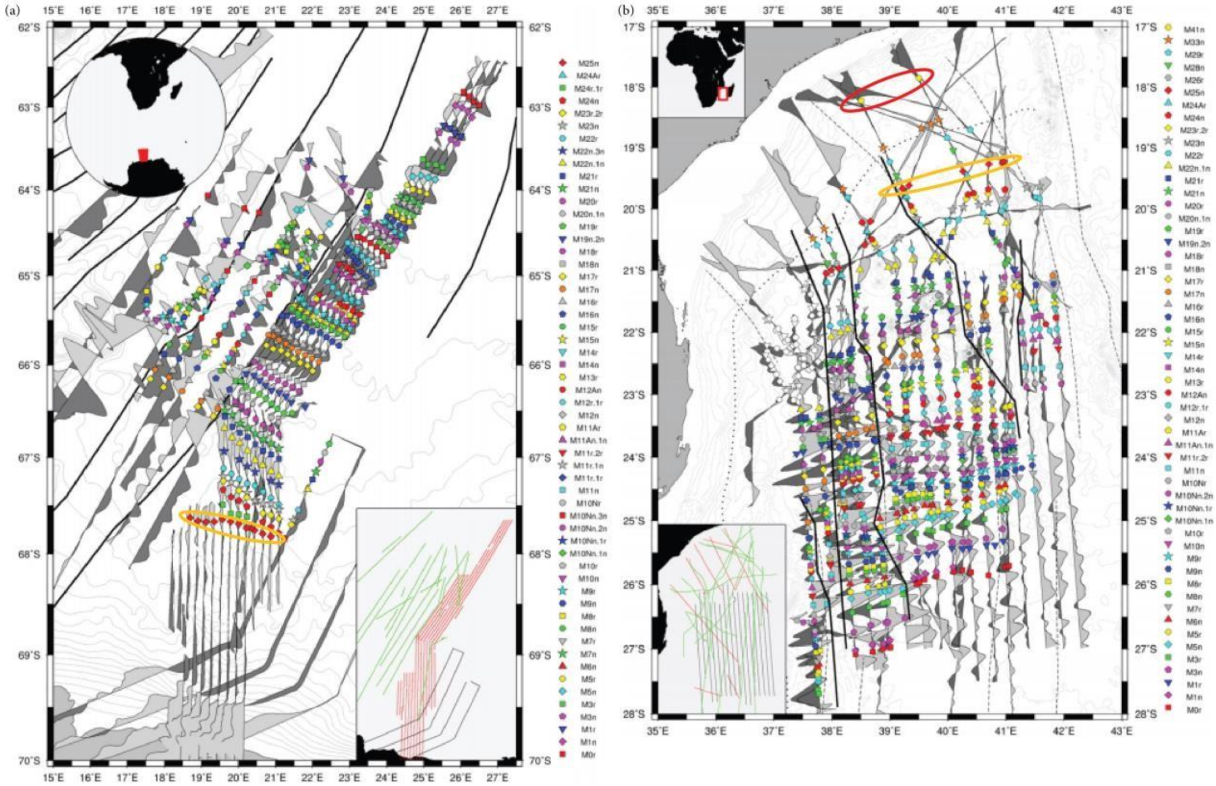

Figure 37: Magnetic anomaly identification in the Riiser-Larsen Sea and Mozambique Basin. (A) Magnetic anomaly identification in the Riiser-Larsen Sea by Leinweber and Jokat (2012). The lower right inlet shows the tracks of their lines. The yellow elipse marks anomaly M25 (157Ma), the oldest magnetic anomaly identified in the Riiser Larson Sea. (B) Magnetic anomaly in the Mozambique Basin. The small inset map in the left bottom shows their lines used. The yellow and red circle marks magnetic anomaly M25 and M41 (166Ma) respectively, identified by Leinweber and Jokat (2012), who identified anomaly M41 as the oldest magnetic anomaly in the Riiser Larson Sea. Dash lines indicate the Continent Ocean Transition Boundary (COTB) by Raillard (1990).

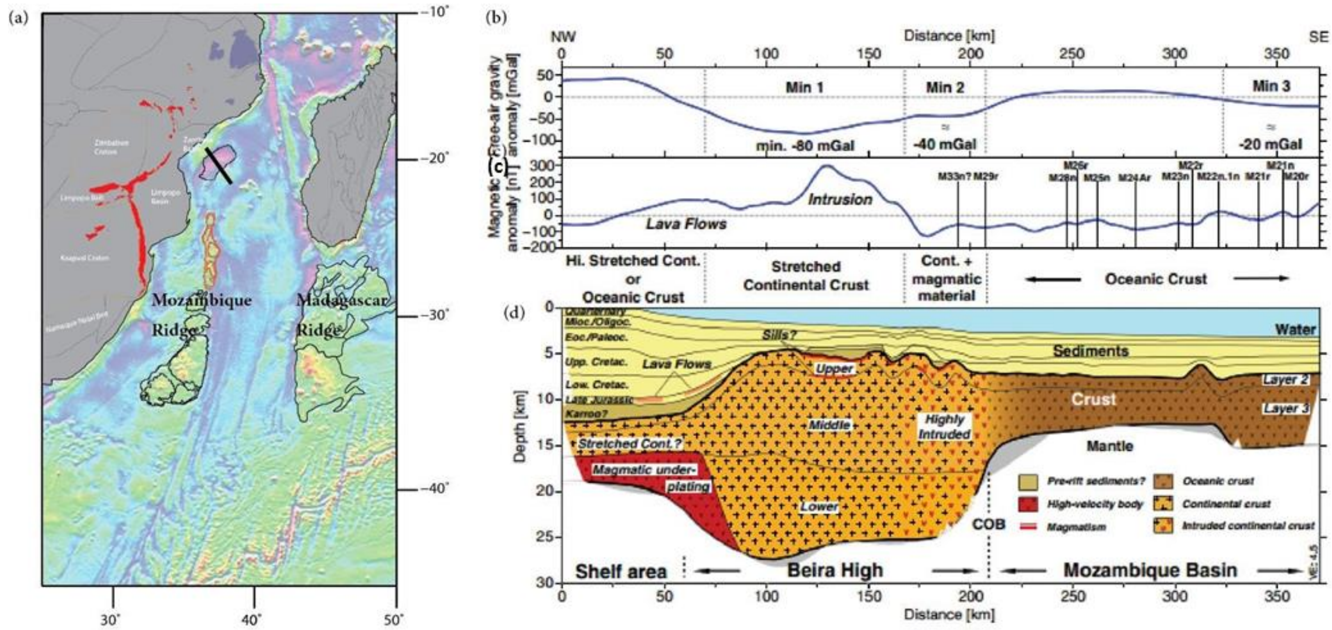

Figure 38: (a) Free-air satellite-derived gravity anomaly of the Mozambique Channel by Sandwell et al., (2014). The black line across the Beira High shows the location of the seismic refraction profile 2014001014 of Muller et al. (2016). The north Mozambique Ridge (in red) discovered in recent expedition in the Mozambique Basin of MOZ3-5 to be compose mainly of sediment on a thinned continental crust (Lepretre et al., 2017; Moulin et al., submitted). The southern Mozambique Ridge (in black) maybe composed of volcanics (Gohl et al., 2011) possibly emplaced at a triple junction. (b) The free-air gravity anomaly along the profile (c) Magnetic anomaly along the profile. The magnetic anomalies were from Leinweber and Jokat (2012). (d) Wide-angle seismic profile 2014001014 seismic across the Beira High and the Zambezi depression by Muller et al., (2016). They interpreted the Beira High to be of continental origin, and that the Zambezi depression consists of stretched continental crust. (Mercator projection figure 11-23).

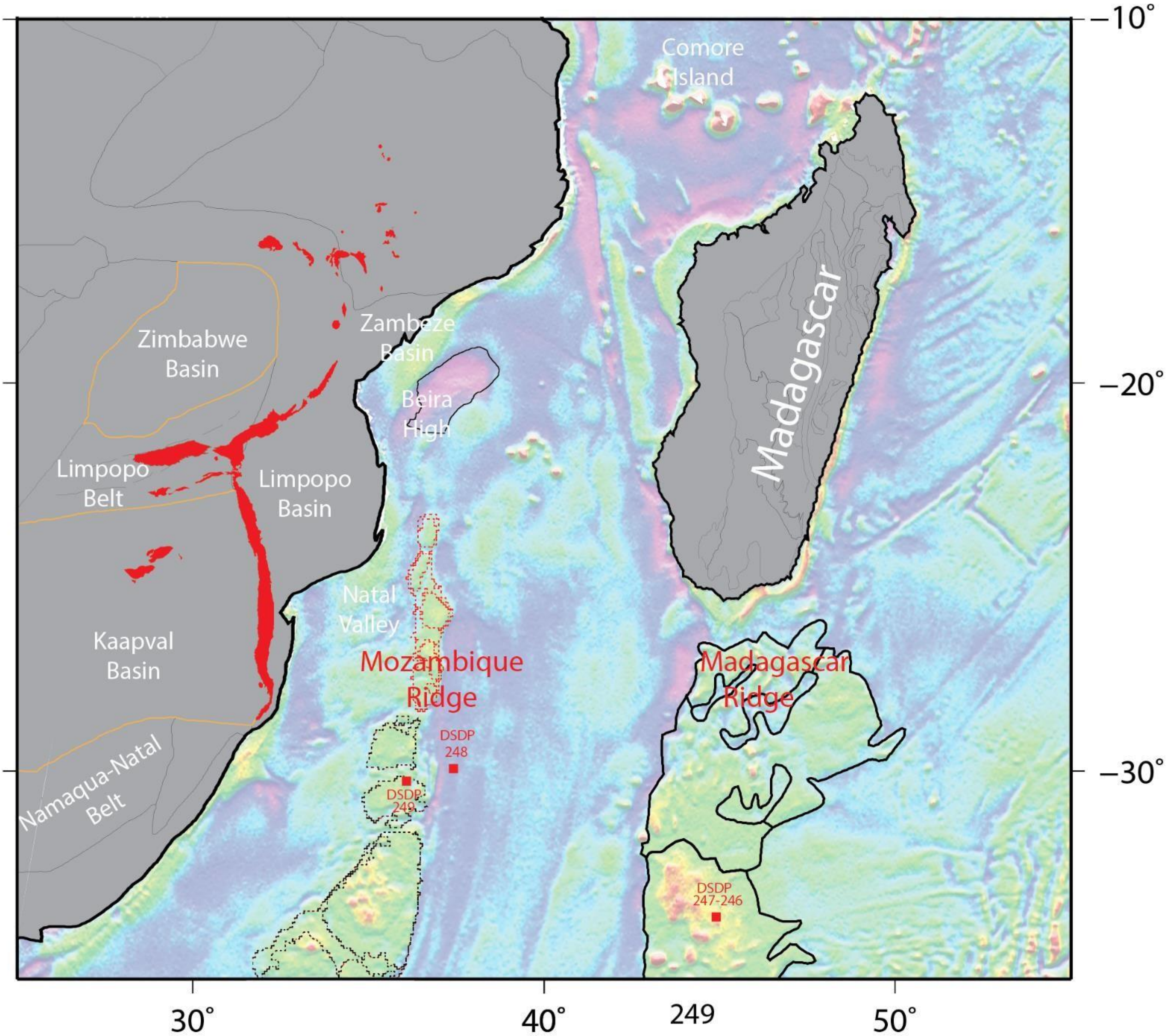

Figure 39: Free-air satellite-derived gravity anomaly (Sandwell et al. 2014) of Mozambique and Madagascar. The Mozambique ridge is formed of several bathymetric plateaus rising up to 3500m from the ocean floor. It has broad, elevated topography especially on its southern half, falling away steeply into the Mozambique basin to its east (Gohl et al., 2011). The Madagascar Ridge extends a distance of 1300km from the southern tip of Madagascar, and ~400 km across. The ridge protrudes at water depth between 2 and 3 km across most of the plateau. (Mercator projection).

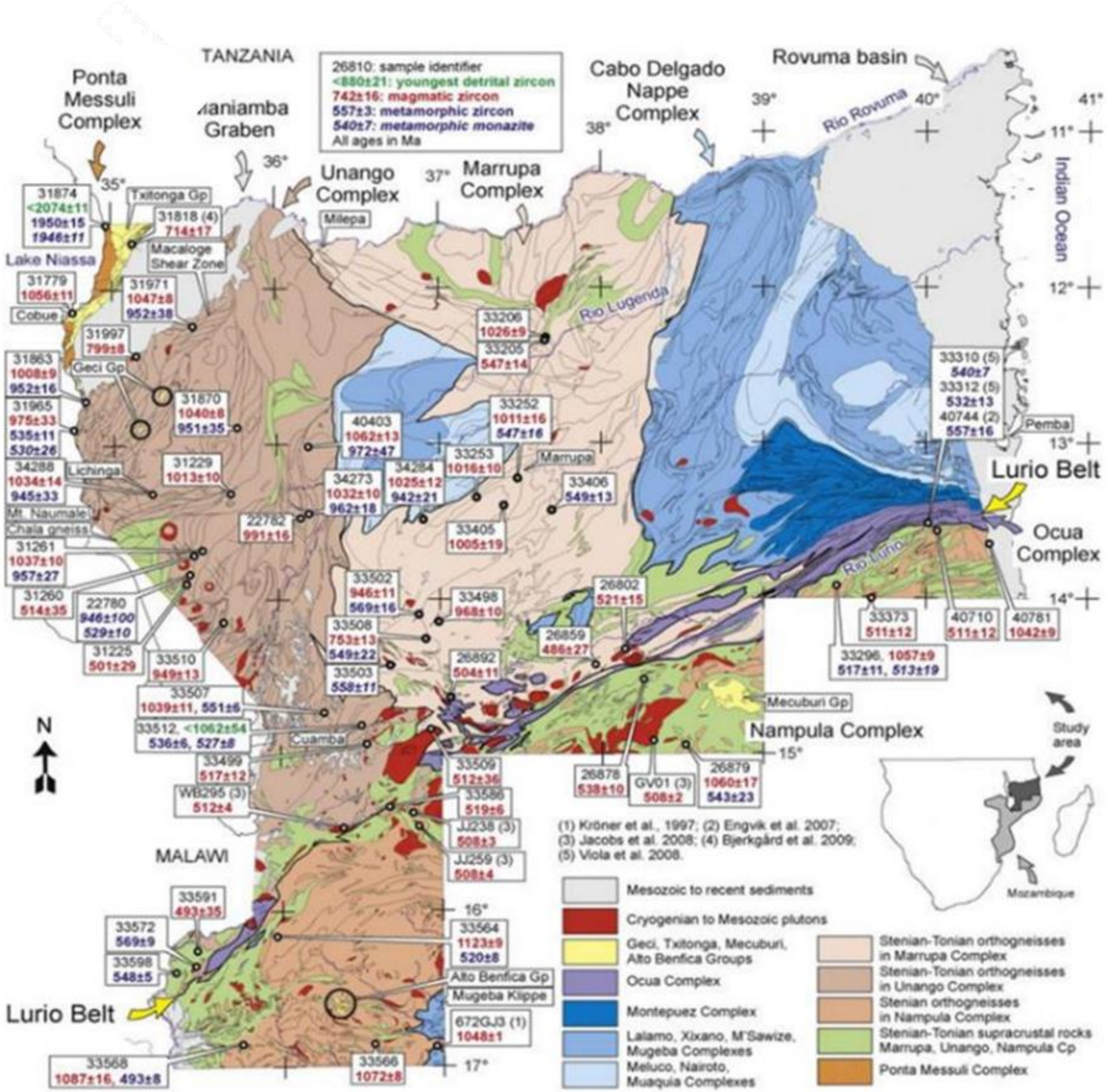

Figure 40: Geology of North Mozambique by Bingen et al. (2009), showing Mozambique Belt, a complex rift-orogenic belt. At least three orogenic episodes are recognized along the belt.

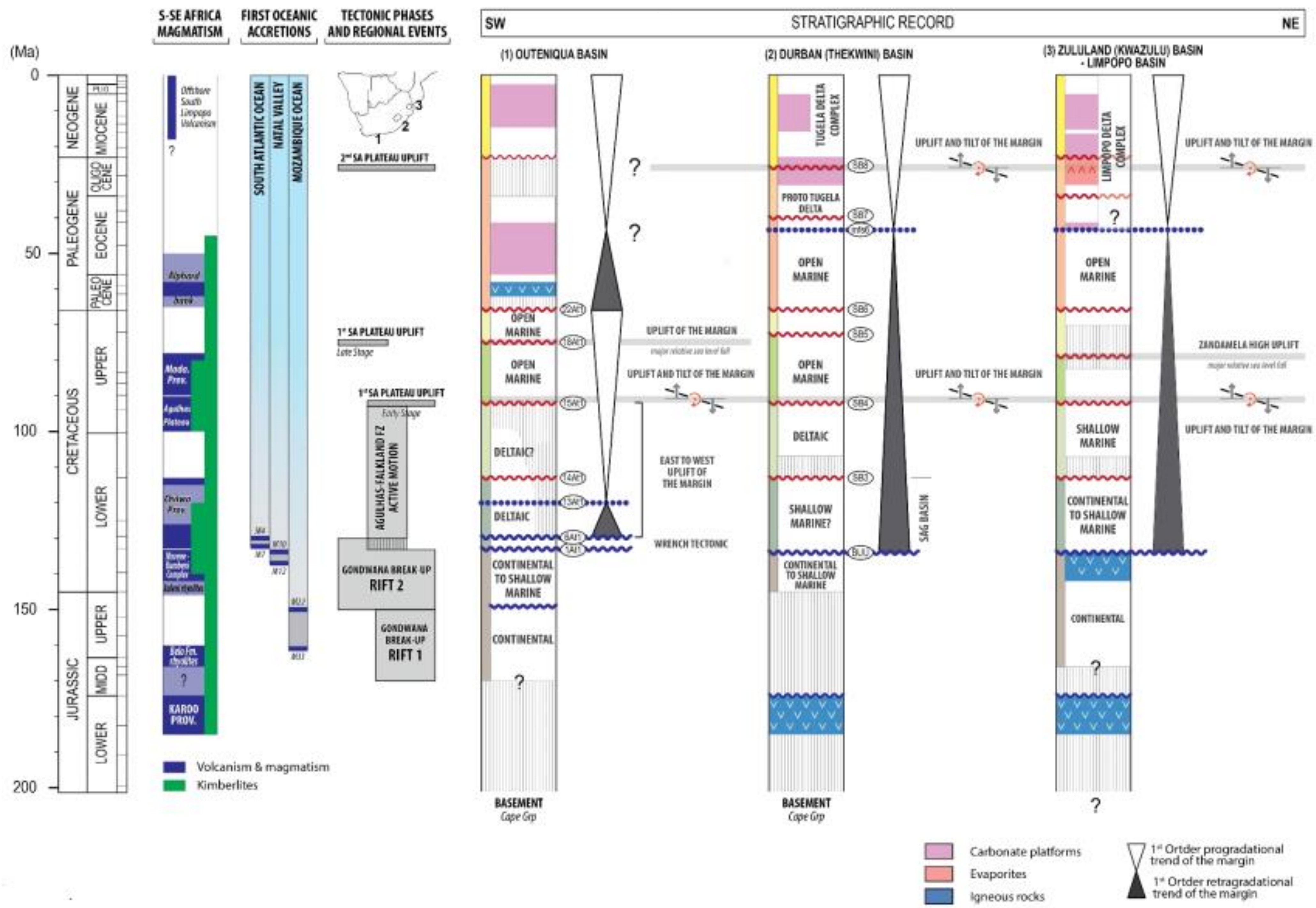

Figure 41: Synthetic chart of the passive margin of southern Africa: magmatism, oceanic accretions, regional scale deformations and stratigraphic record by Baby (2017).

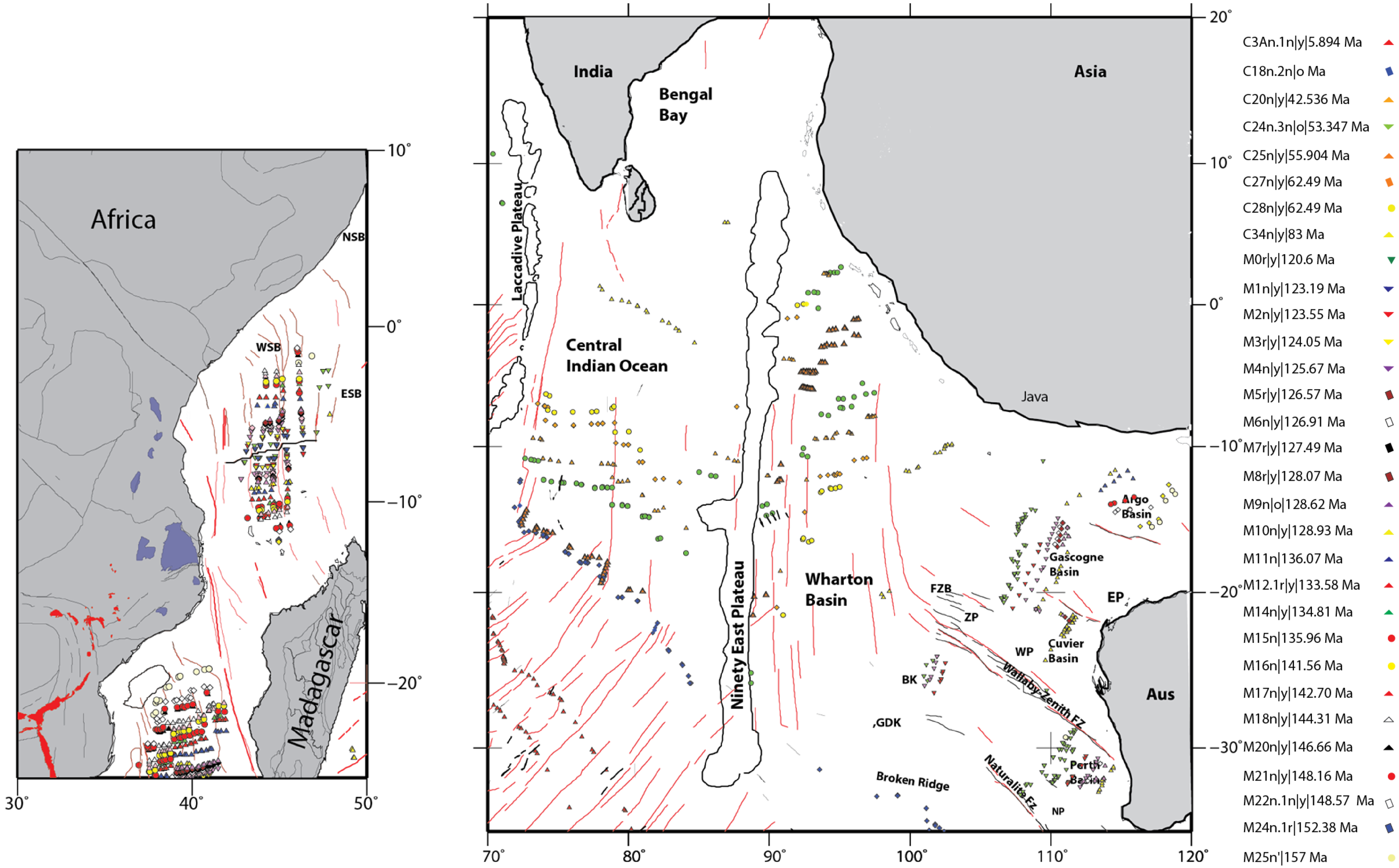

Figure 42: Map of seafloor fabric and magnetic anomalies data used in the study in the Somali Basin and East Indian Ocean. The magnetic anomaly plots were derived from EMAG3 and Williams et al. (2013). ZP: Zenith Plateau, NP: Naturaliste Plateau, WZFZ: Wallaby Zenith Fracture Zone. BK: Batavia Knoll, GDK: Gulden Draak Knol,; DHR: Dirck Hartog Ridge, BR: Broken Ridge, FZB: Fracture Zone Bends. (Mercator projection).

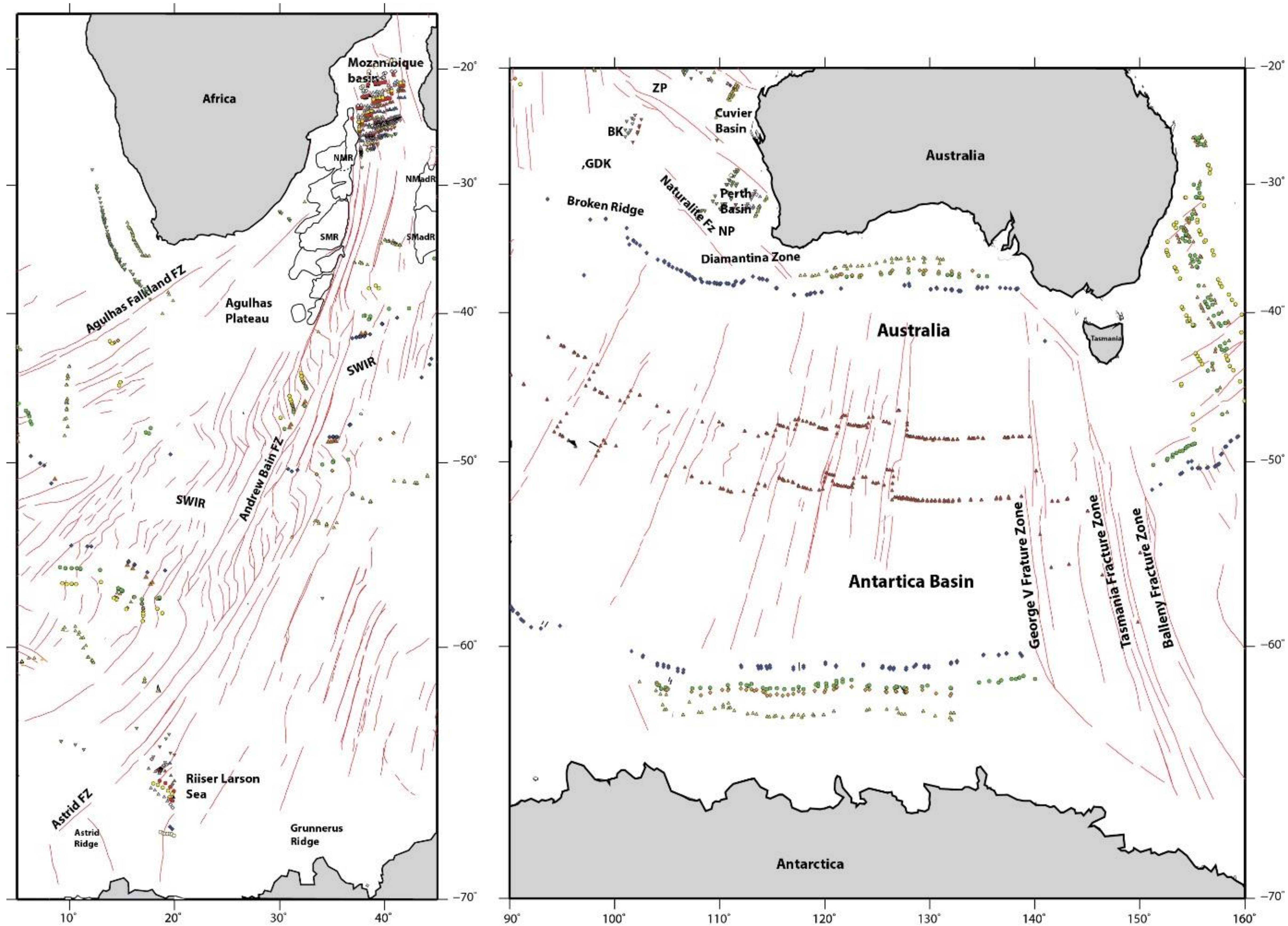

Figure 43: Map of seafloor fabric and magnetic anomalies data used along the study in the Africa-Antarctic corridor and the Australia-Antartic Basin. (Mercator projection).

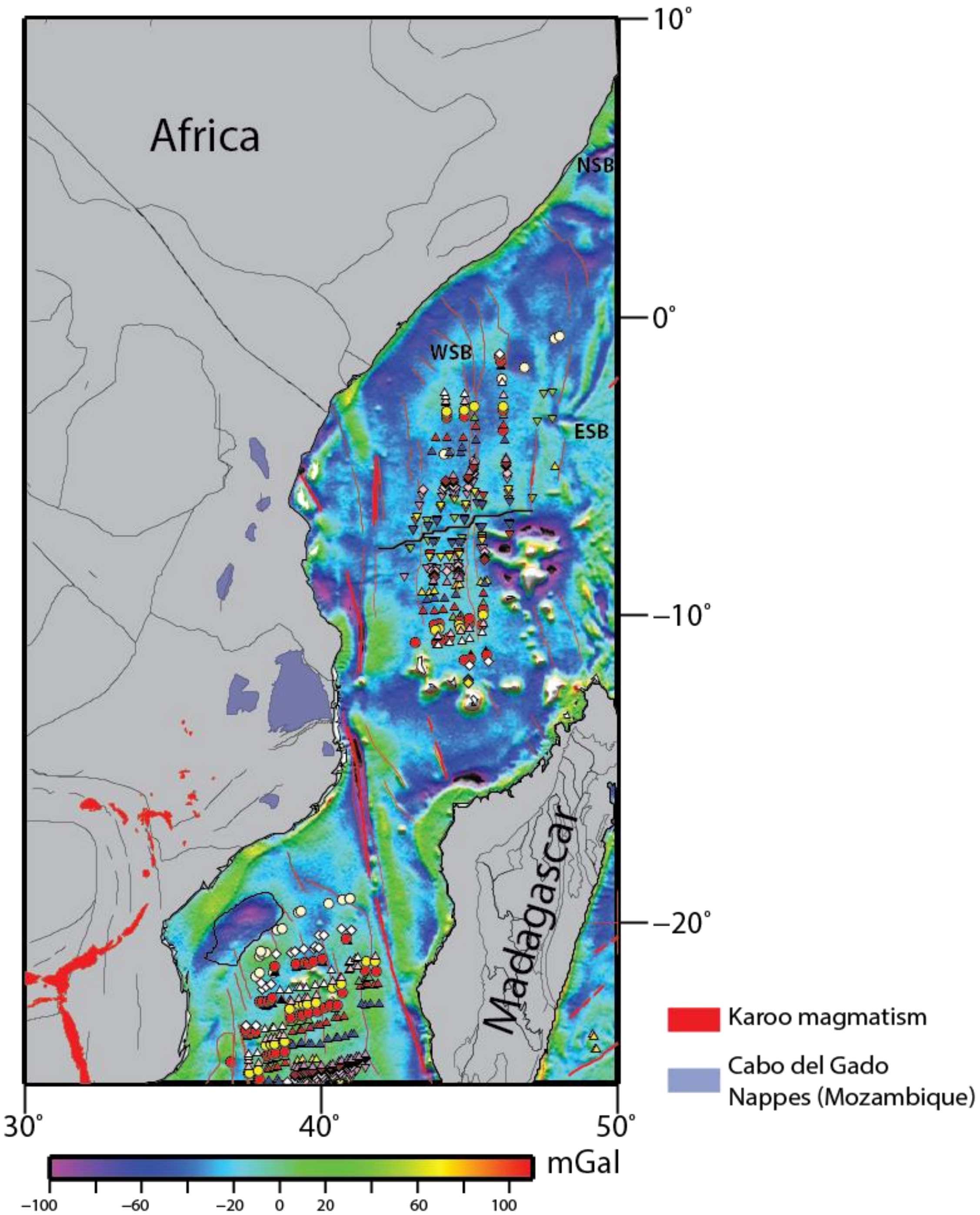

Figure 44:) Free-air satellite-derived gravity anomalies of the Somali Basin by Sandwell et al. (2014. Magnetic anomalies are from Dais et al. (2016) in Somali Basin, and Leinweber and Jokat et al., 2012 for the Zambezi basin. Gravity grid legend is same for figures 46-49.. (*Mercator projection).*

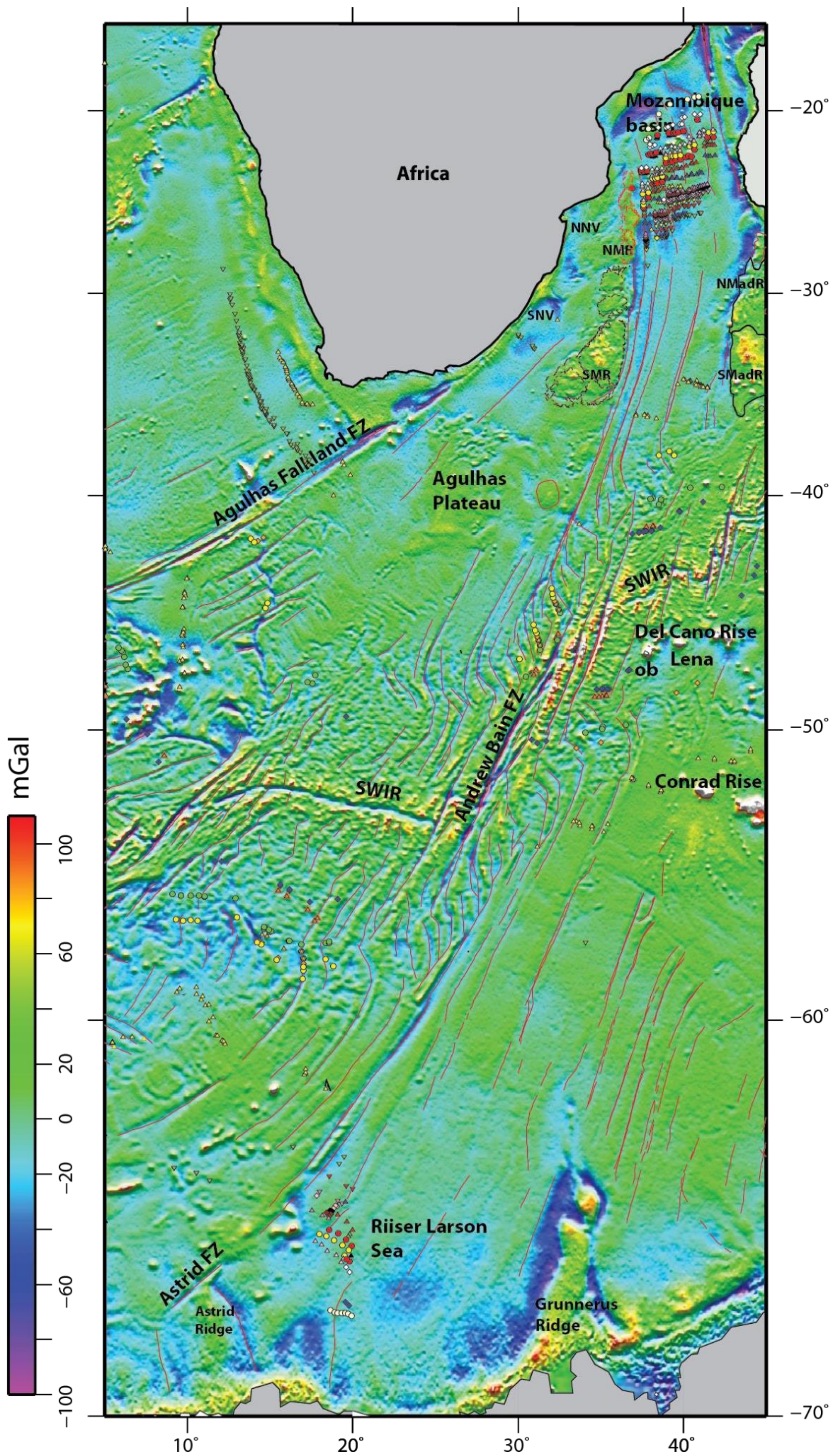

Figure 45: Map of satellite-derived free-air gravity data of the Antarctica Africa corridro by Sandwell et al. (2014); MozR: Mozambique Ridge; SMR: Madagascar Ridge, NMR: North Mozambique Ridge,; NNV: Northern Natal Valley, SWIR: Southwest Indian Ocean. (Mercator projection).

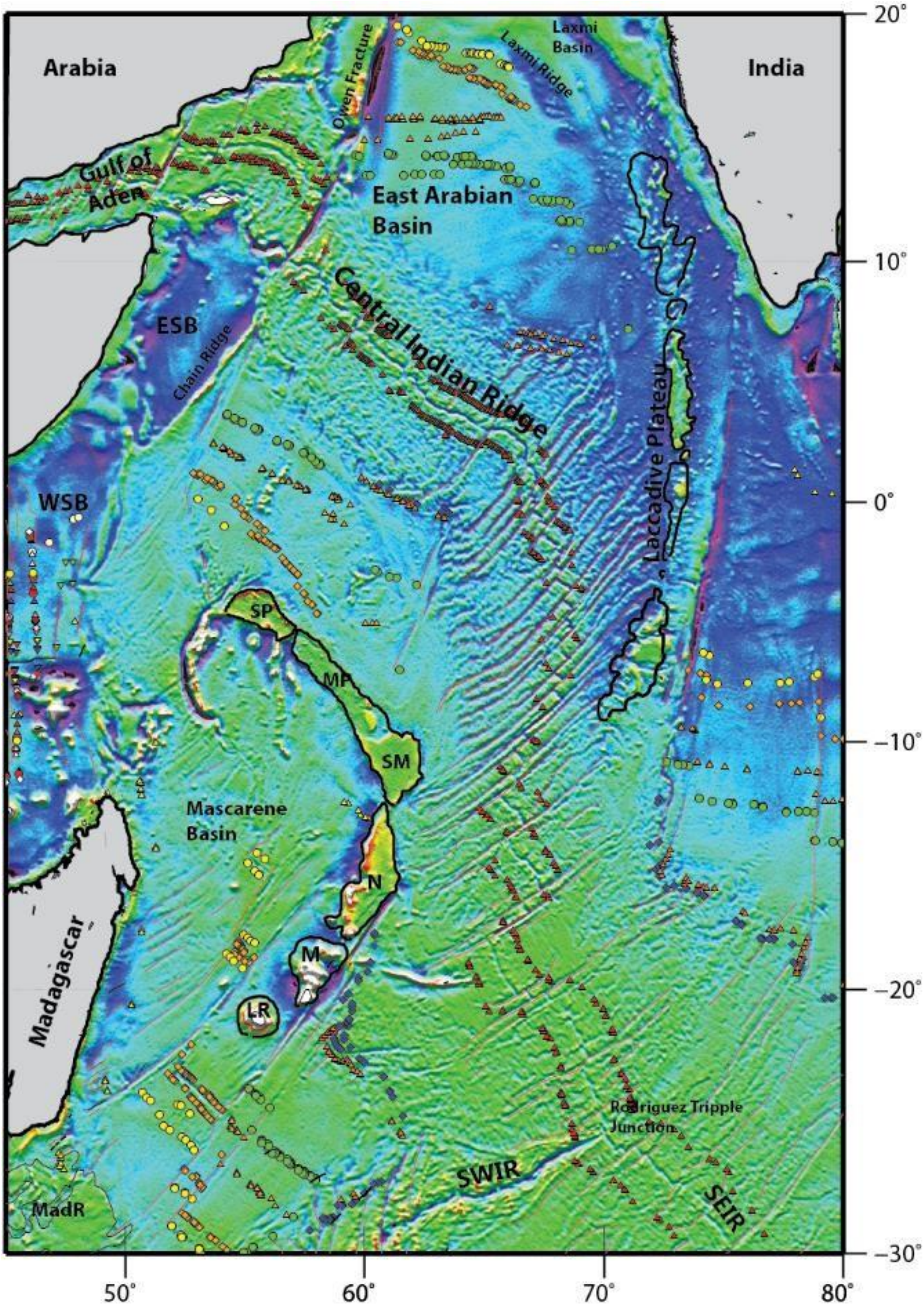

Figure 46: Map of Sandwell et al. (2014) satellite-derived free-air gravity data of the Central Indian Ocean Ages of magnetic anomalies are same for figure 45-49. LR: La Réunio, M: Mauritius, MP: Mascarene Plateau, N: Nazareth Plateau, SM: Saya de Malha Bank, SP: Seychelles Plateau; SEIR: Southeast Indian Ocean; SWIR: Southwest Indian Ocean. (Mercator projection).

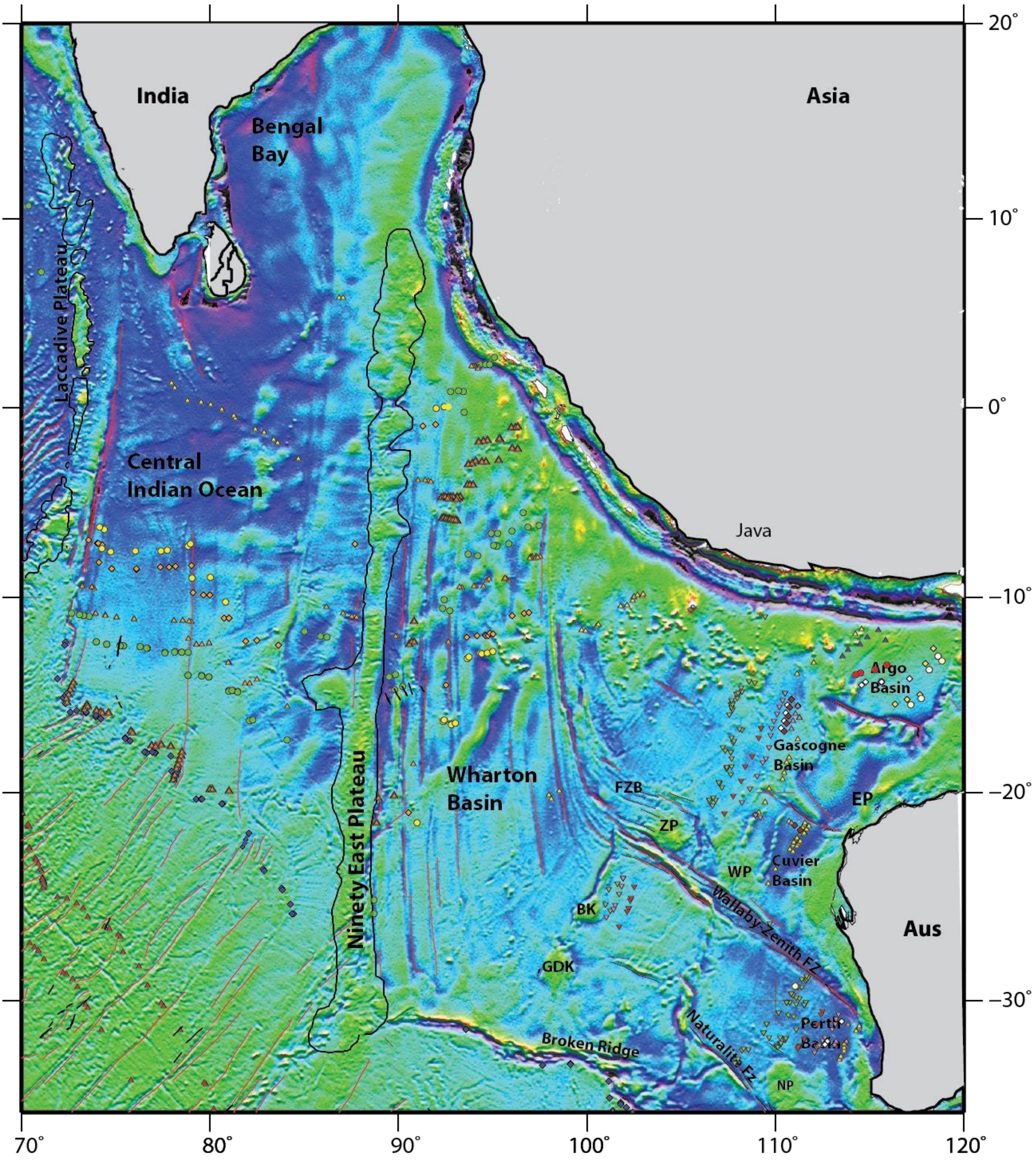

Figure 47: Free-air satellite-derived gravity anomalies of Eastern Indian Ocean by Sandwell et al. (2014). EP: Exmouth, Plateau. ZP: Zenith Plateau, WP: Wallaby Plateau, NP: Naturaliste Plateau, WZFZ: Wallaby-Zenith Fracture Zone. BK: Batavia Knoll; GDK: Gulden Draak Knoll; DHR: Dirck Hartog Ridge; BR: Broken Ridge: FZB, Fracture Zone Bends : NP: Naturaliste Plateau: ZP: Zenith Plateau, WP; Wallaby Plateau. (Mercator projection).

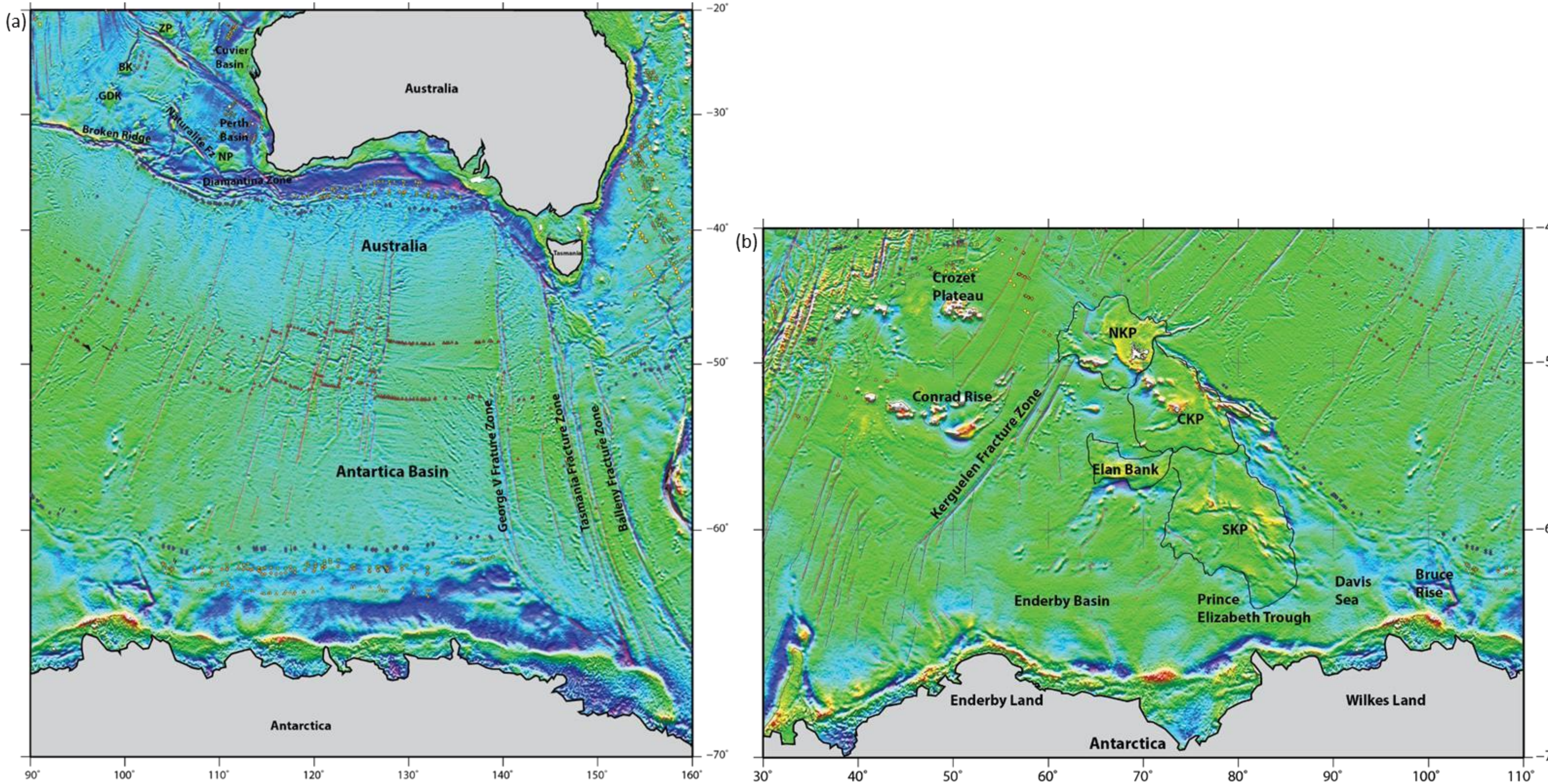

Figure 48: Free-air satellite-derived gravity anomalies by Sandwell et al. (2014) (a) Antarctic-Australia Basin (b) Enderby and surrounding basins. Ages of magnetic anomalies are same as in figure 45 BK: Batavia Knoll; CKP: Central Kerguelen Plateau; DHR: Dirck Hartog Ridge; GDK: Gulden Draak Knol, NKP: North Kerguelen Plateau, WP: Wallaby Plateau, NP: Naturaliste Plateau, SKP: South Kerguelen Plateu, NP: Naturaliste Plateau, ZP: Zenith Platea. (Mercator projection).

Figure 49: Chart of event compilation in the Indian Ocean. Notice the lack of conscensus on the age of the rst oceanic crust in some of the basins (Mozambique basin, Enderby basin, Bay of Bengal etc.

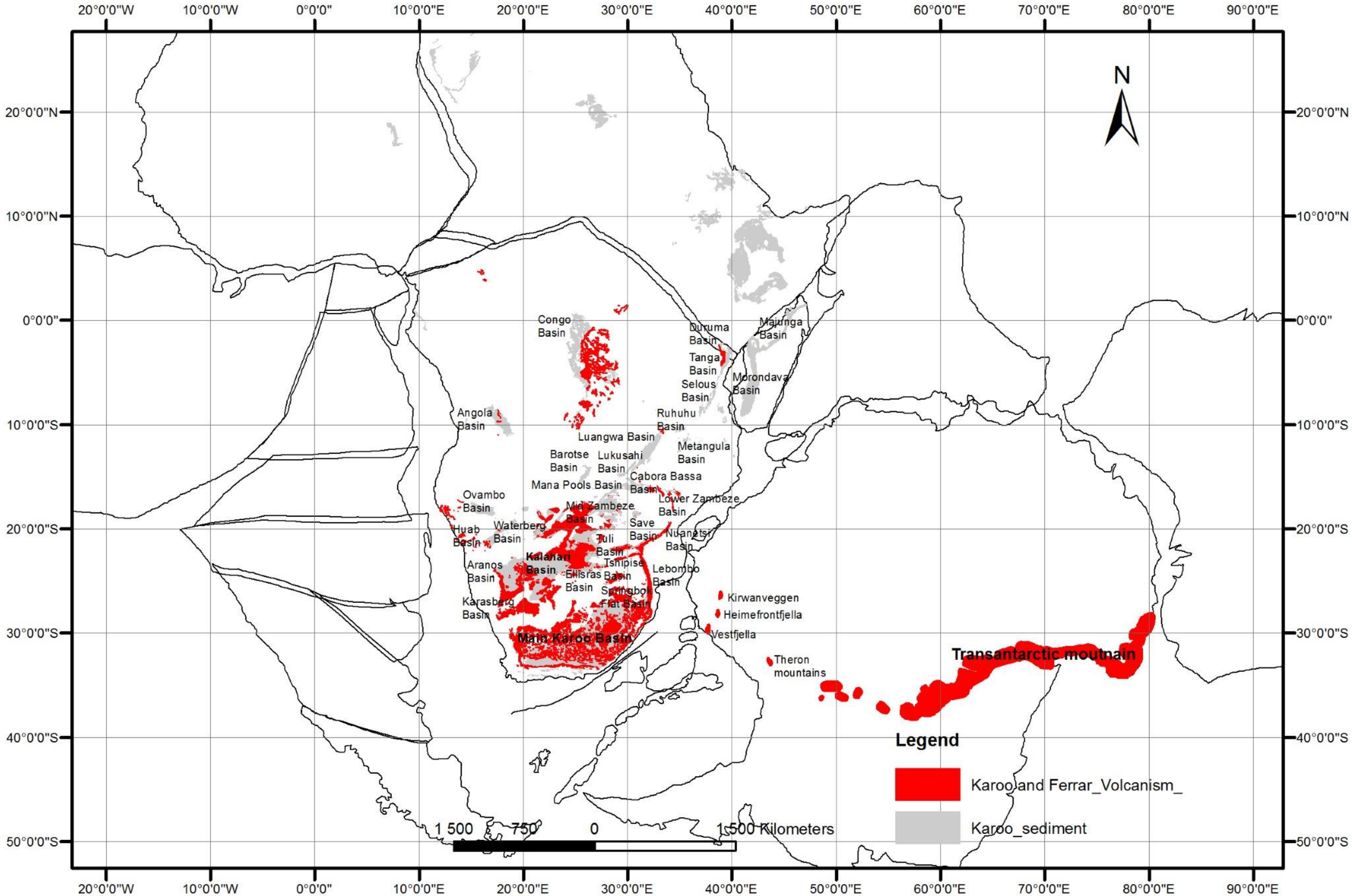

Figure 50: Map Karoo sediments and igneous rockss distribution in Gondwana. World Geodectic System 1984.

KAROO BASINS AFRICA

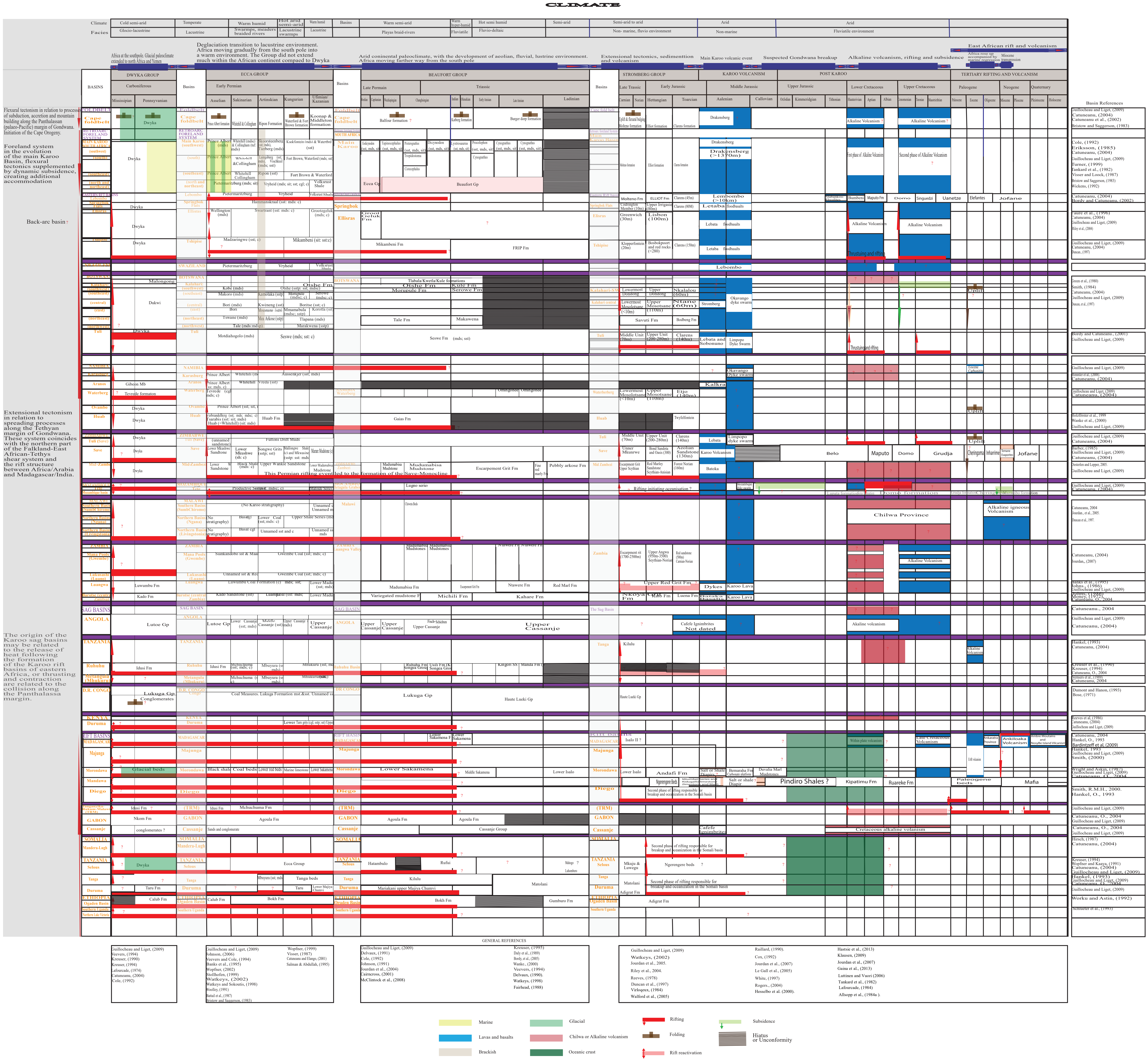

Figure 51: Litho-stratigraphic and event chart of Karoo basins in Africa. The Karoo basins preserve the sedimentary record from Late Carboniferous–Early Jurassic of the Karoo Supergroup deposited into intracratonic rift basins in Gondwana, and the formation of these basins was influenced by the pre-existing crustal architecture of the African continent. The deposition of sediments was controlled mainly by tectonic and climatic changes.

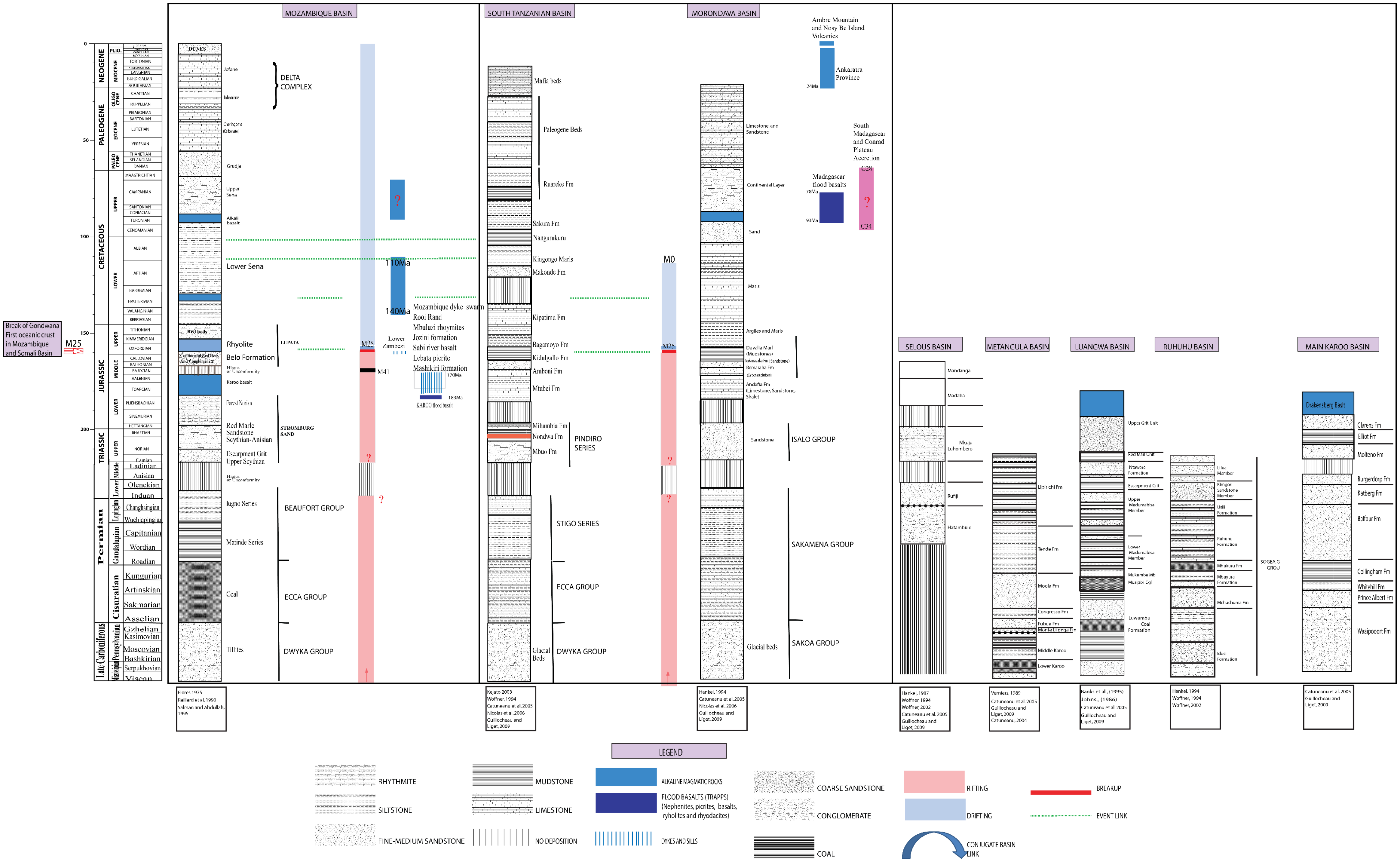

Figure 52: Litostratigraphic chart of Karoo basins in Africa.

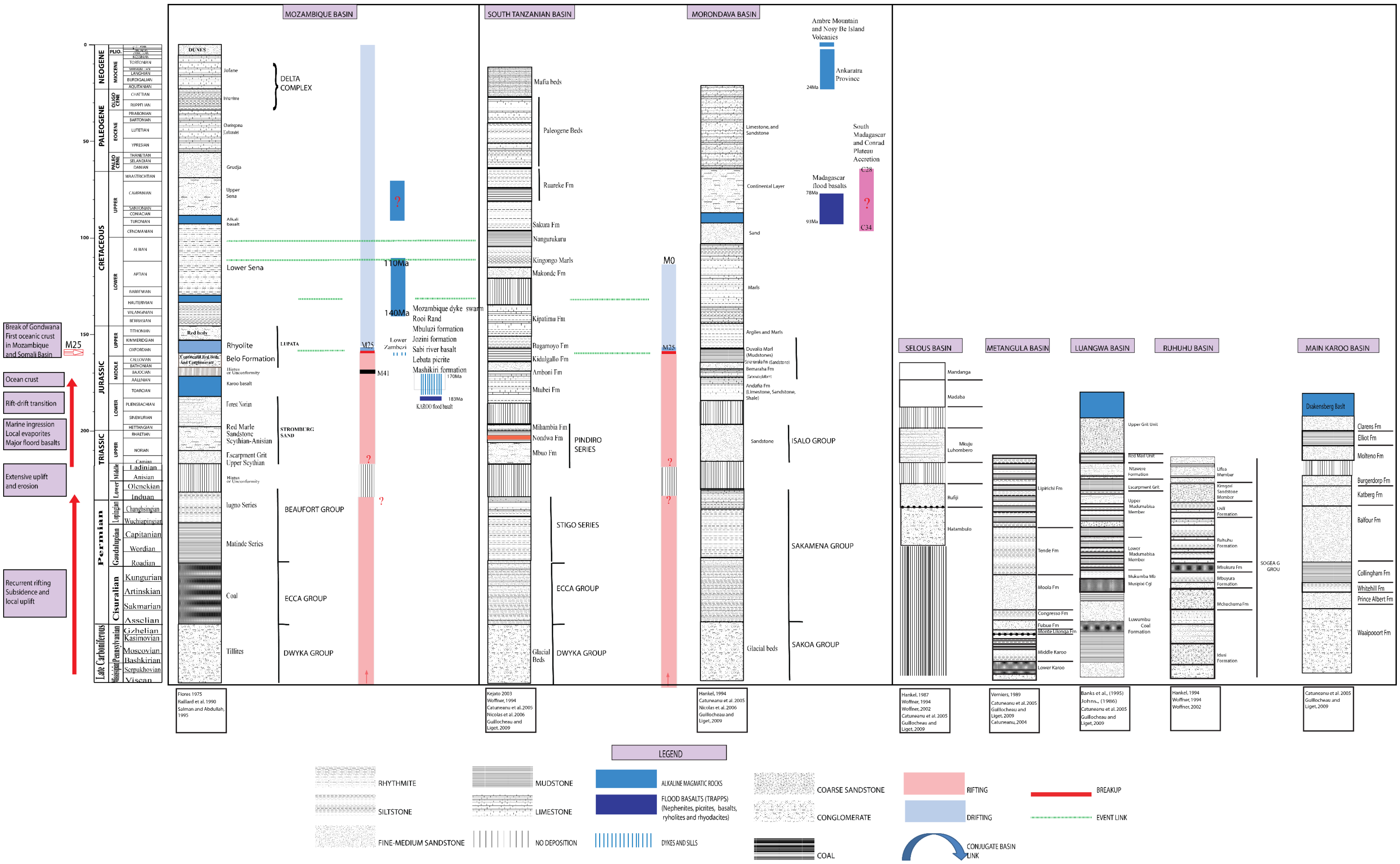

Figure 53: Litostratigraphic and event chart of Karoo basins in Africa.

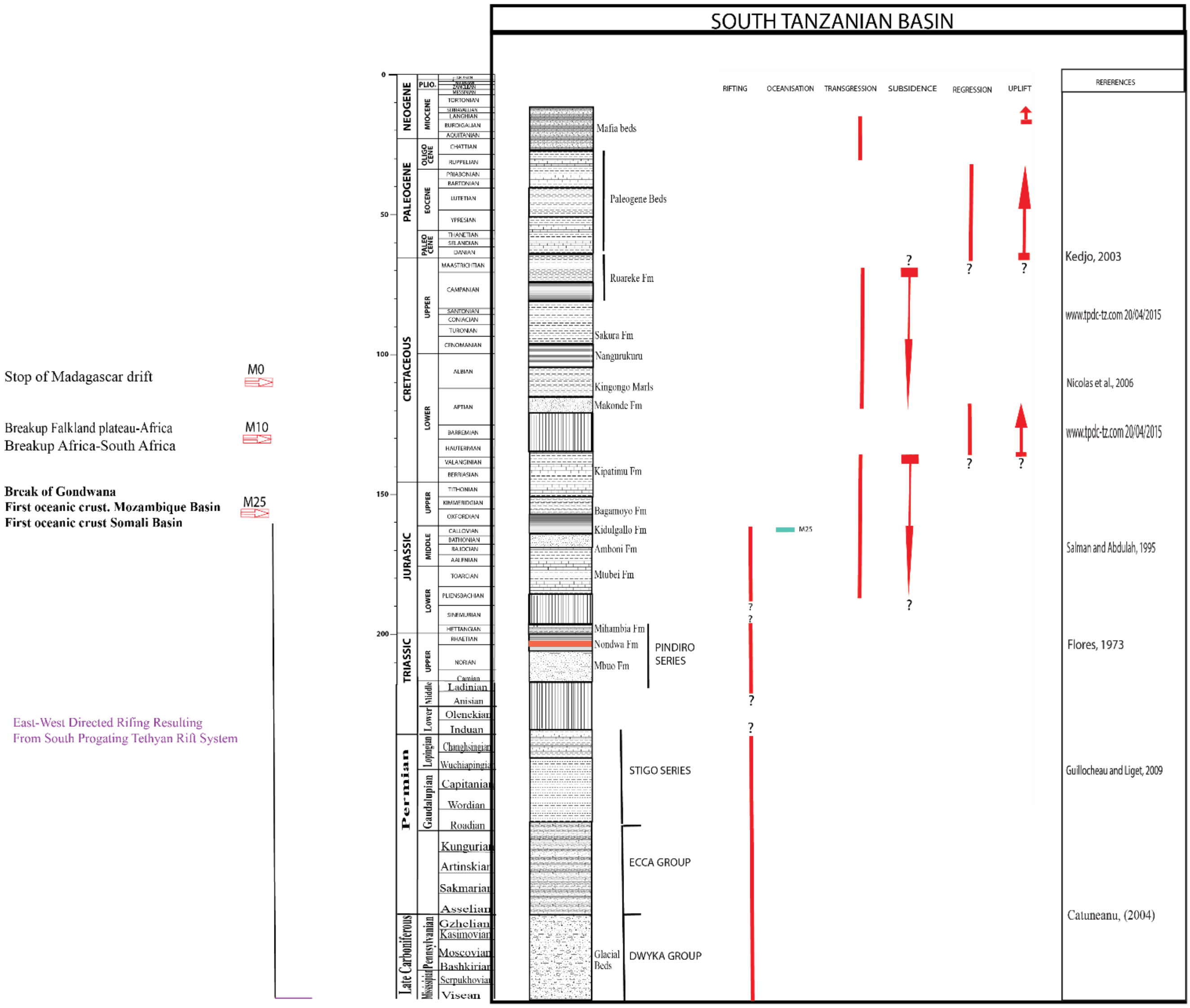

Figure 54: Lithostratigraphic and event chart in the south Tanzania Basins, the figure shows the general incoherencies in the predicted periods of oceanization and breakup in the Somali. Breakup ages start from as early as Late Triassic to Oxfordian, but oceanization is predicted to start with the Toarcian with the deposition of the Andafia beds.

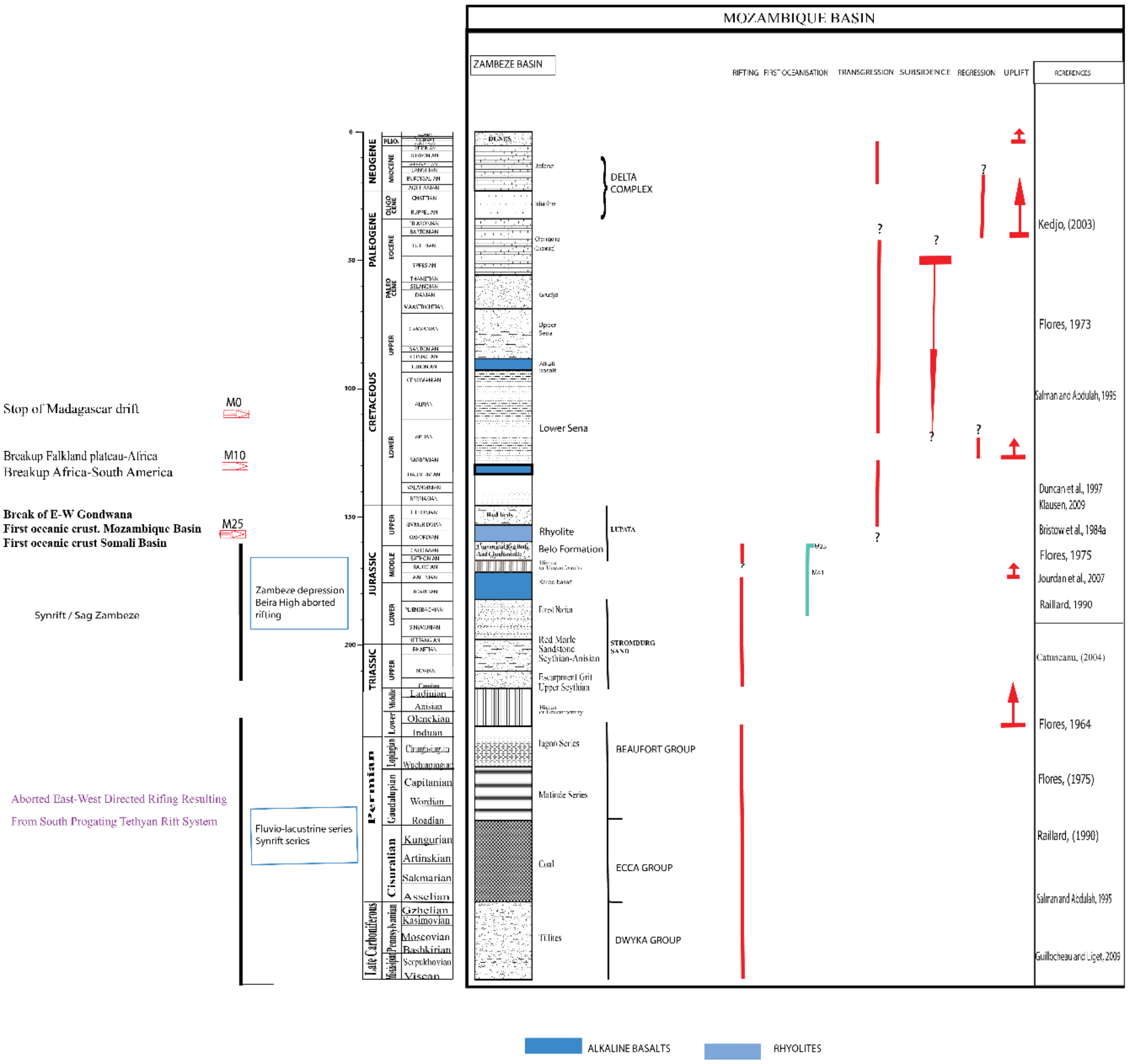

Figure 55: Lithostratigraphic and event chart in the Mozambique Basin, the highlights the general incoherencies in the predicted periods of oceanization and breakup in the basin. The rifting is predicted to have started in the Late Triassic and ended in the Lower Jurassic with the Karoo volcanic event, but Salazar et al. (2013) and others, argue rifting to have continued into the Late-Middle Jurassic affecting the Belo Formation

Figure 56: Summary of major lithotectonic events recorded in the Indian Ocean and the Tethys Ocean. The Tethys Ocean existed before the breakup of Gondwana, and its proximity to the Indian Ocean permitted recording of major tectono-magmatic events that affected the two ocean.

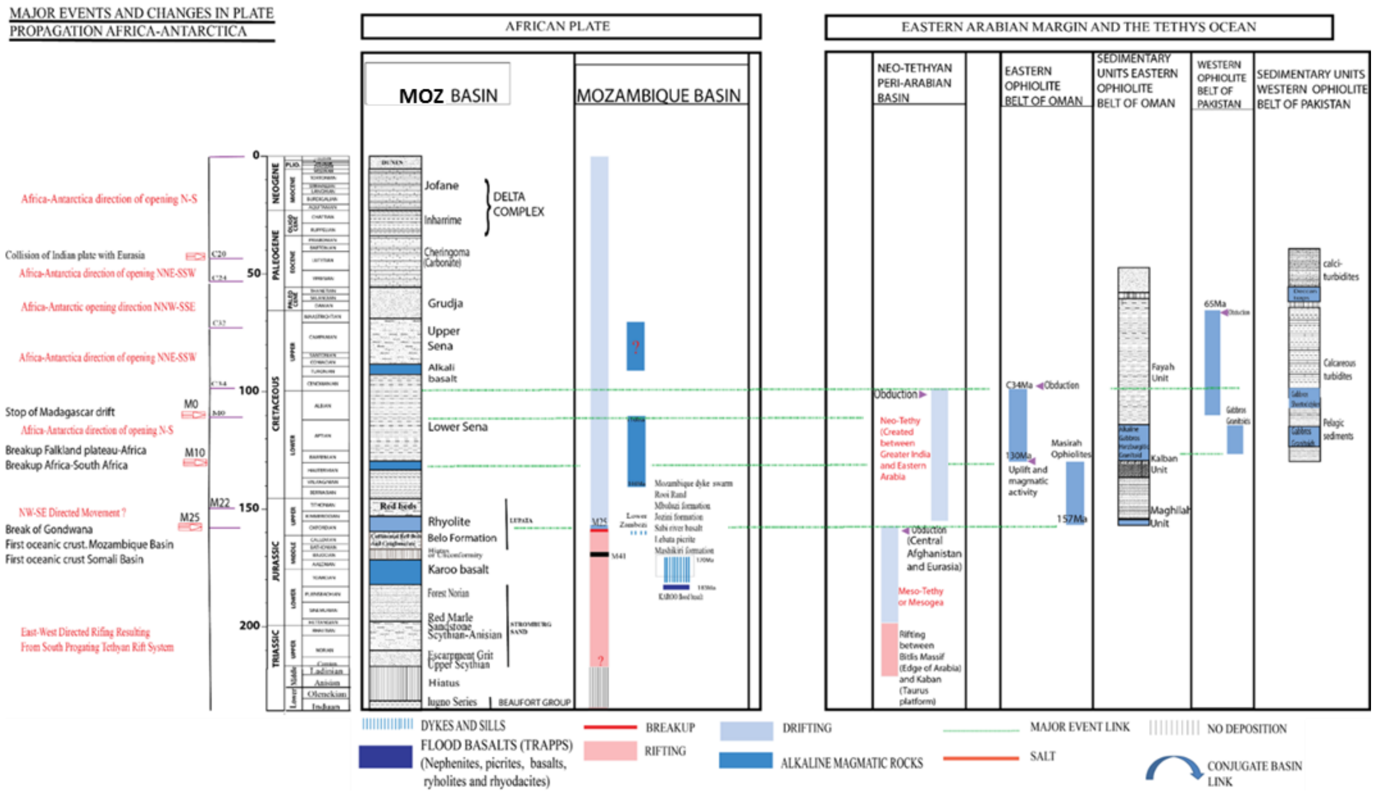

Figure 57: Summary of major events recorded Mozambique basin and the Tethys Ocean (in the ophilitic belt of Eastern Oman and Western Pakistan from figure 56. Notice the good correlation of the tectonic events with the Indian Ocean, and the absence of record of the M41 event in both the Mozambique basin and the Tethys Ocean.

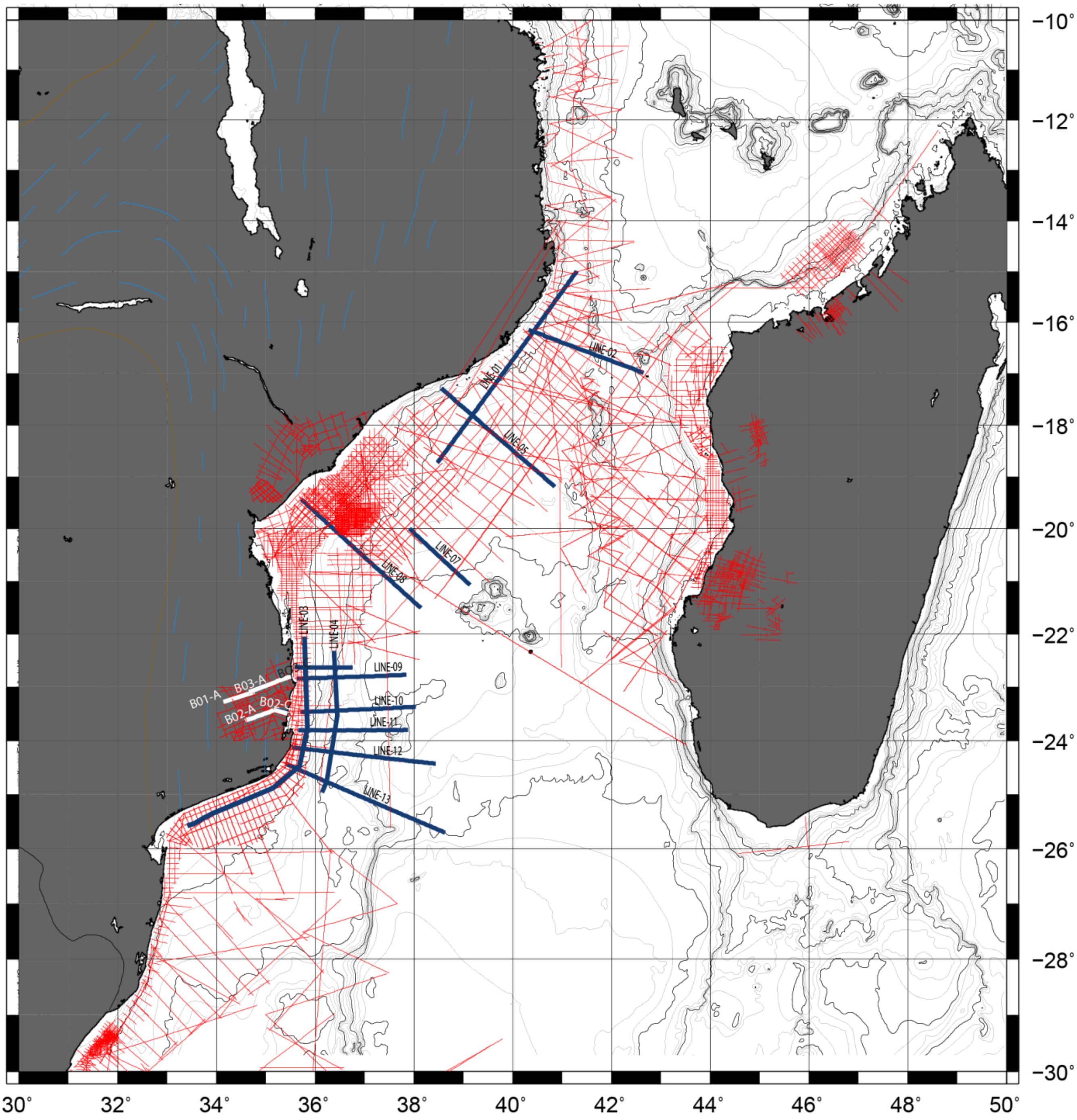

Figure 58: Map showing the seismic lines used in the study in the Mozambique Channel. (offshore lines in white) (Mercator projection)

Legend figures 59-63

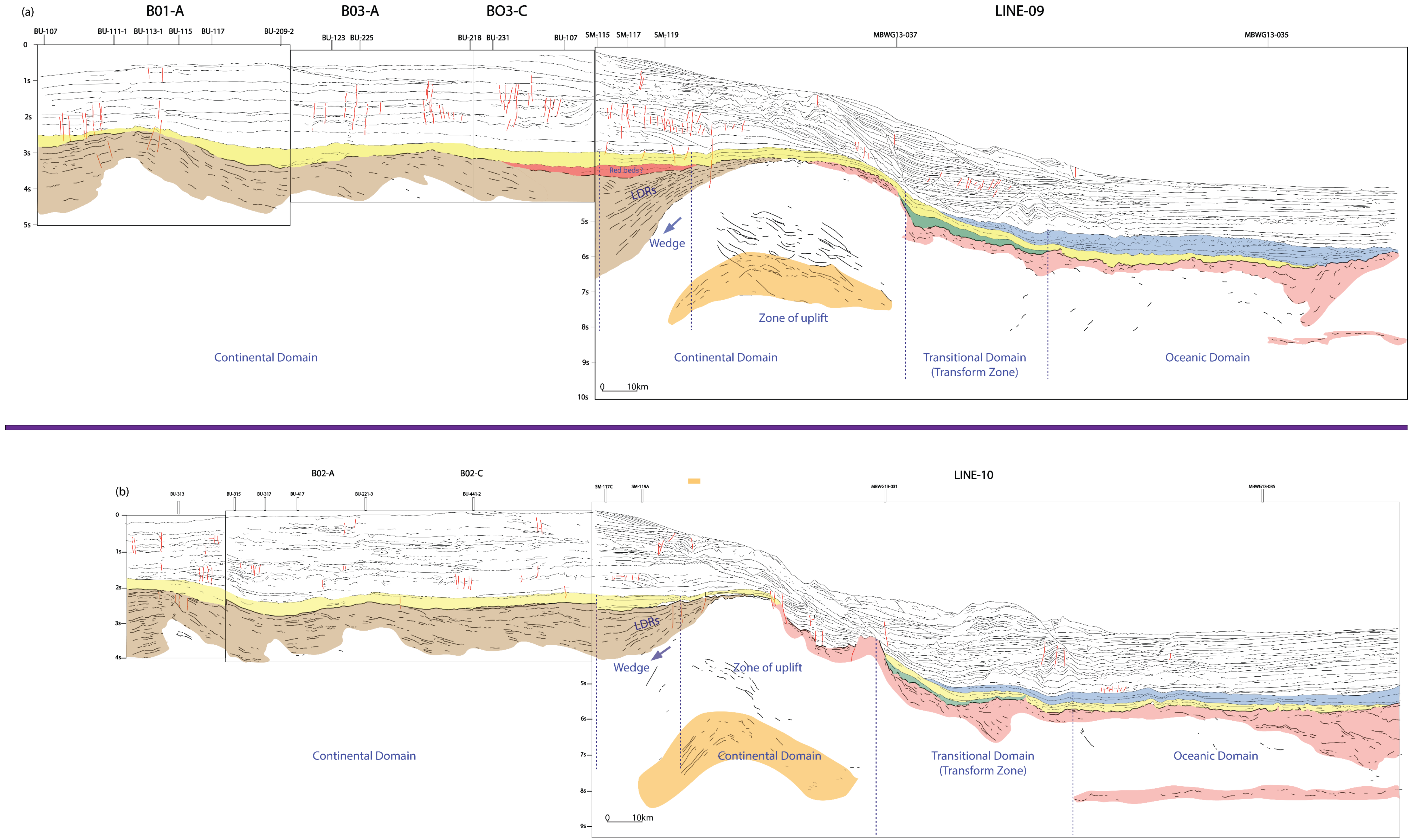

Figure 59: Seismic interpretations of lines LINE- 09 and LINE- 10 delineating different identified domains across the Limpopo basin. LINE- 09 was combined with lines B03-A B03-B, and B01-A, and LINE- 10 was similarly combined with lines B02-A and B03-B to extend our interpretations onshore and to investigate the trend of the landwarding reflectors, previously interpreted Karoo volcanics and SDR's (Cox, 1992, Klausen, 2009) . The brown horizon (Pre-drift Karoo sediemnts) continues landwards into intracratonic basins from the uplifted zone where it sharply dips into the basin and into the intracratonic basins. The uplifted zone is characterized by flexural uplift and uplift of the basement leading to margin morphology change and erosion of the Maputo sediments.

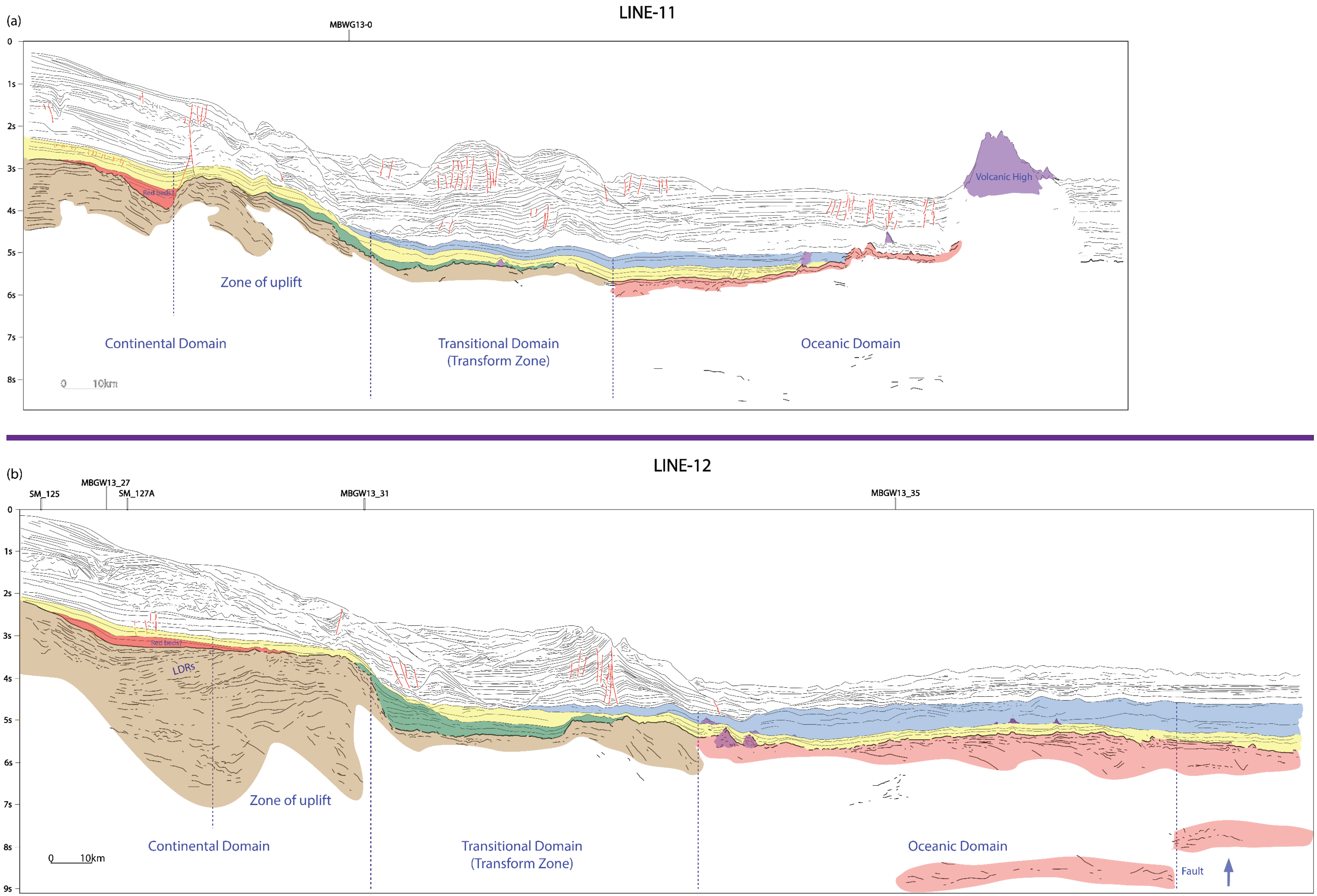

Figure 60: Interpretations on seismic lines LINE-11 and LINE-12. The green horizon lies directly above basement offshore, mostly in the transition zone. It represent the first rift infilling to flexural uplift and early drift sediments in the Limpopo basin. Notice the thickening of the progradational blue horizon (The Lower Domo Shales) seaward, and the major fault deformation within the oceanic domain. Line LINE-11 show evidence of recent volcanic activity.

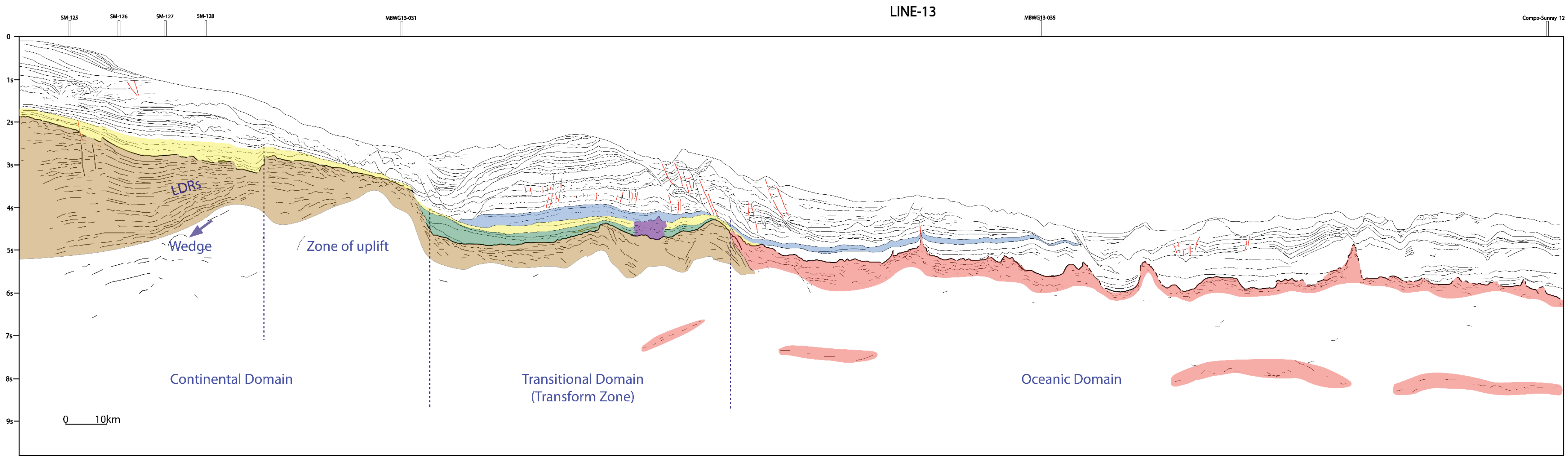

Figure 61: Seismic line LINE-13 in the Limpopo basin. Notice in the wedging zone, the trend landward dipping reflectors previously interpreted as Karoo volcanics, and the more recent volcanic activity within the transitional domain; intruding the green, yellow and blue horizons.

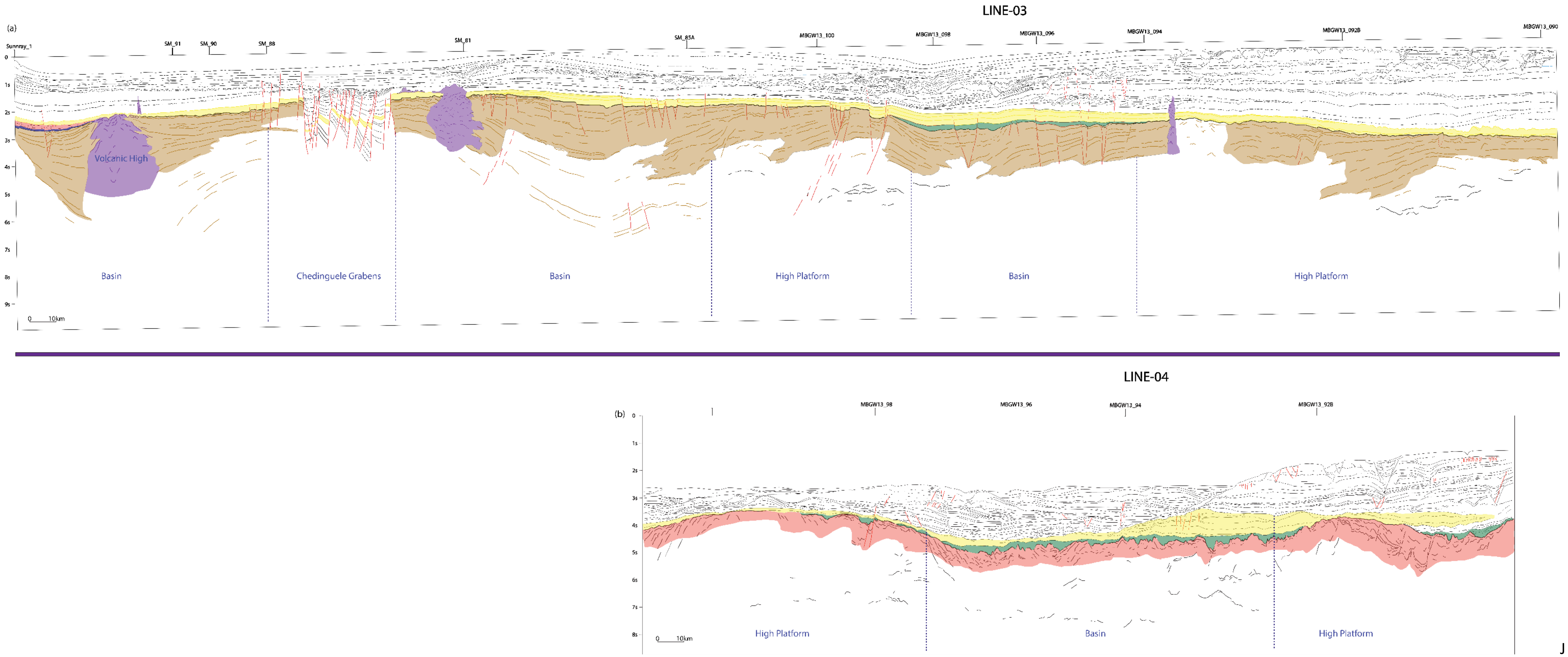

Figure 62: Seismic lines LINE-03 and LINE-04. Notice the different volcanic episodes on seismic MBGW13-027, and the capping of the brown horizon by ''Karoo volcanics''.

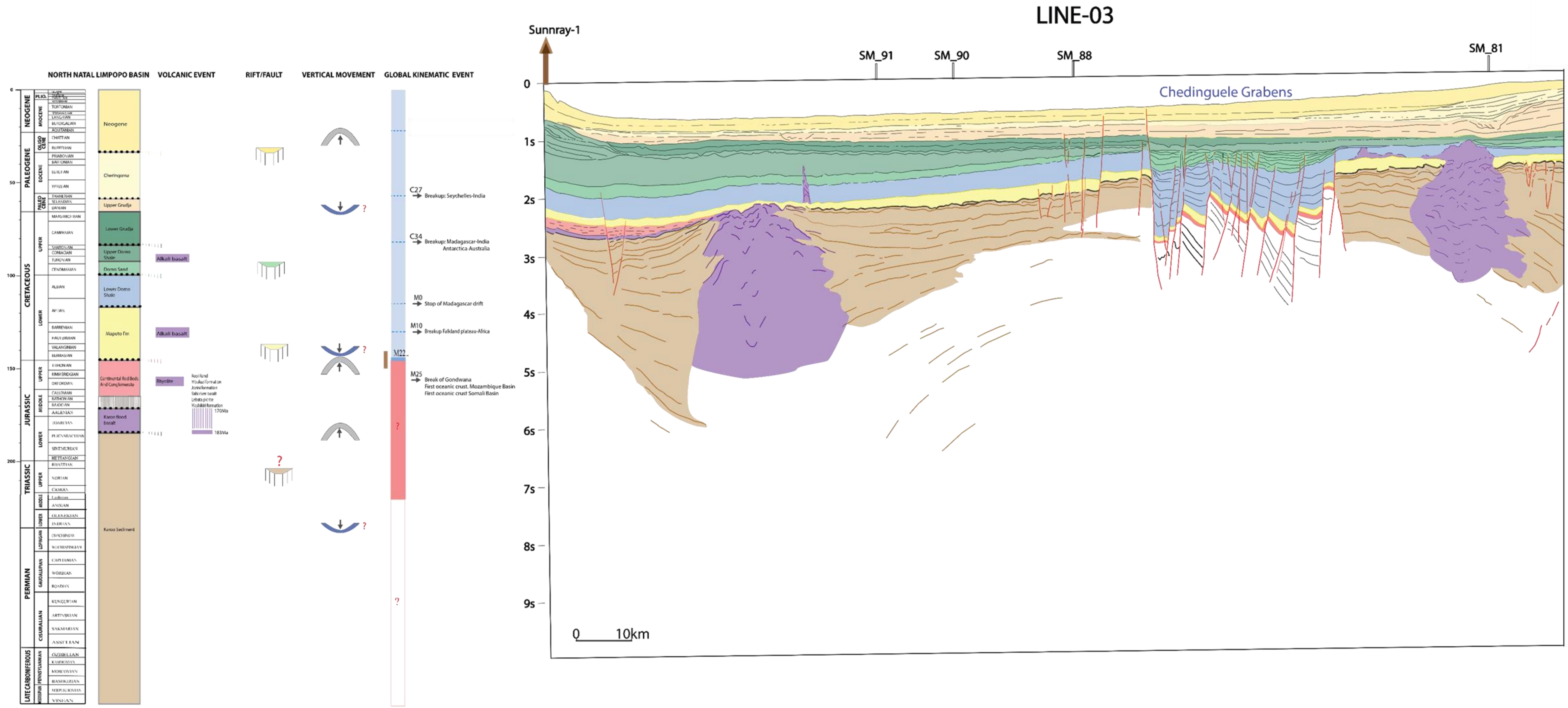

Figure 63: Event and chronostratigraphic chart of Natal and Limpopo Basins compared to major global tectonic events.

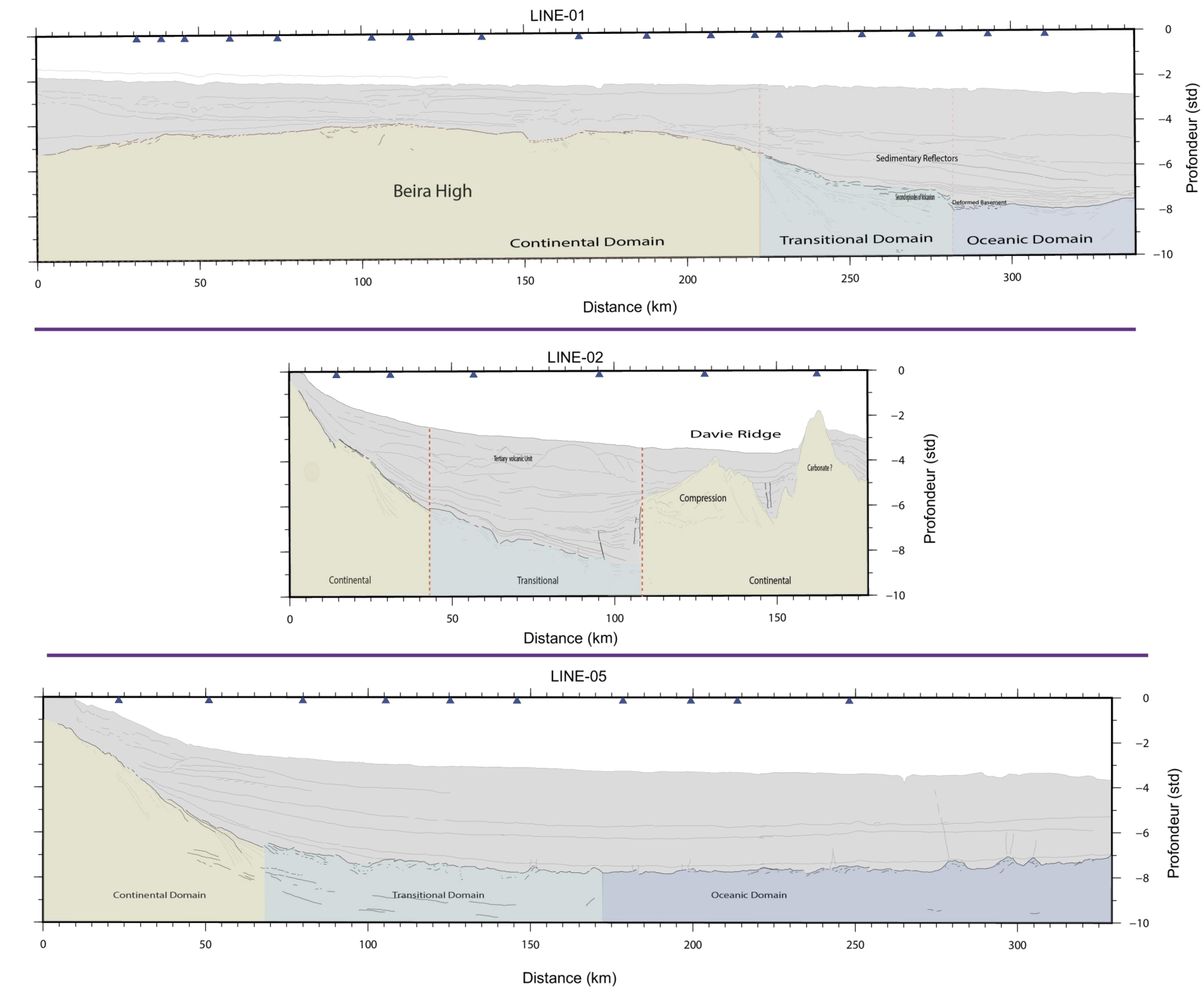

Figure 64: Seismic lines LINE- 01, LINE- 02, and LINE- 05 of the Zambezi basin delineating the extent of the continental, transitional domains and oceanic domains in the basin.

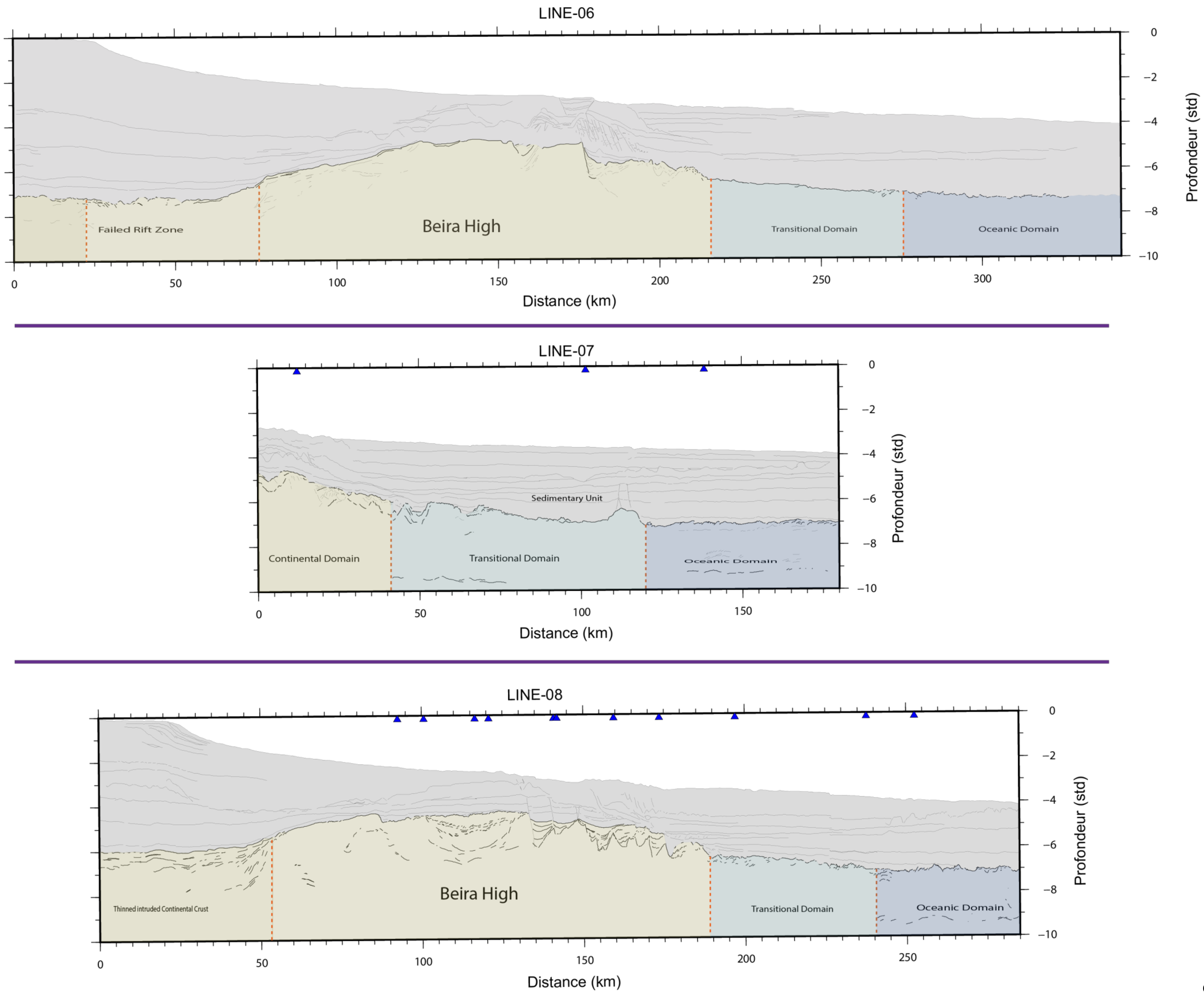

d

Figure 65: Seismic lines LINE- 06, LINE- 07, and LINE- 08 of Zambezi basin, showing margin structuration and delimitation

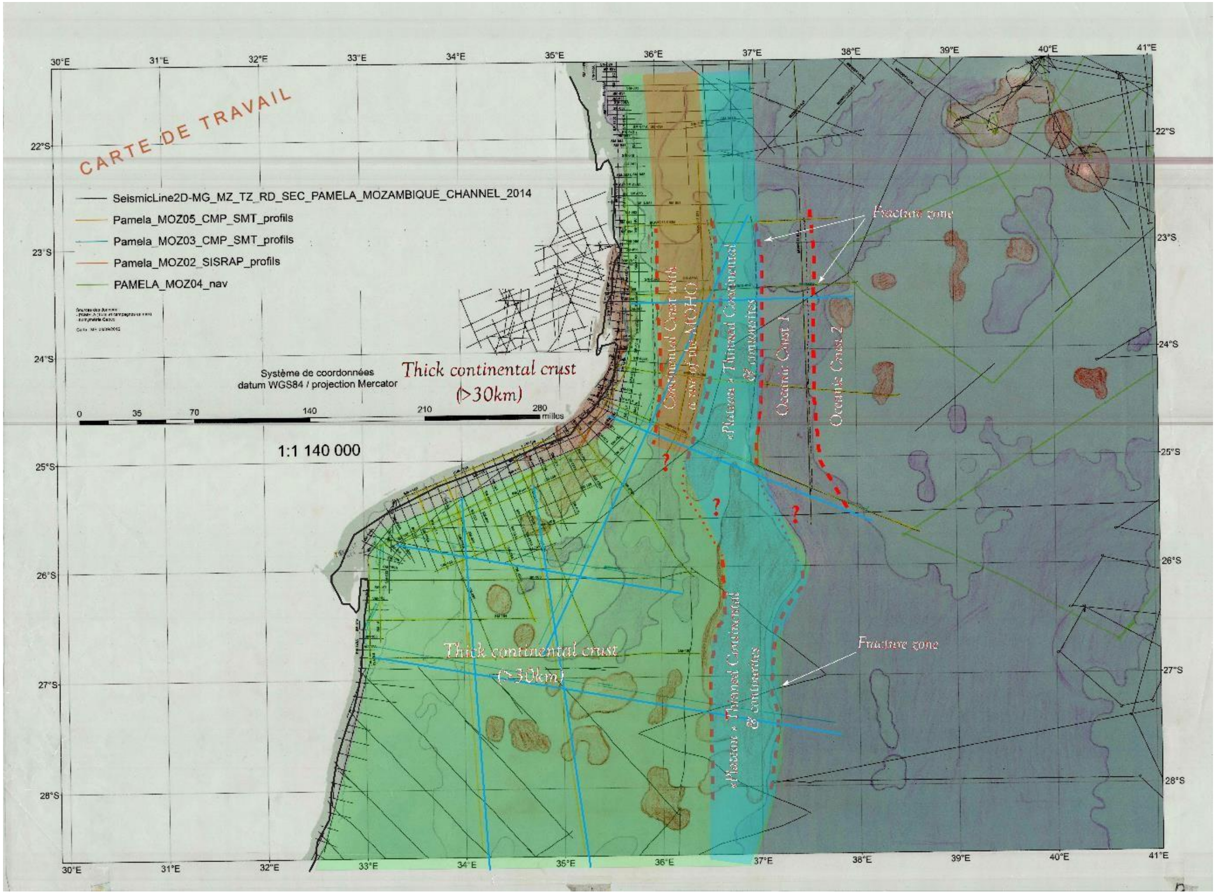

Figure 66: Map of Limpopo-Natal Basin showing the structure of the margin and the delineation of the different domains (Oceanic, continental, and thinned continental crust).

.

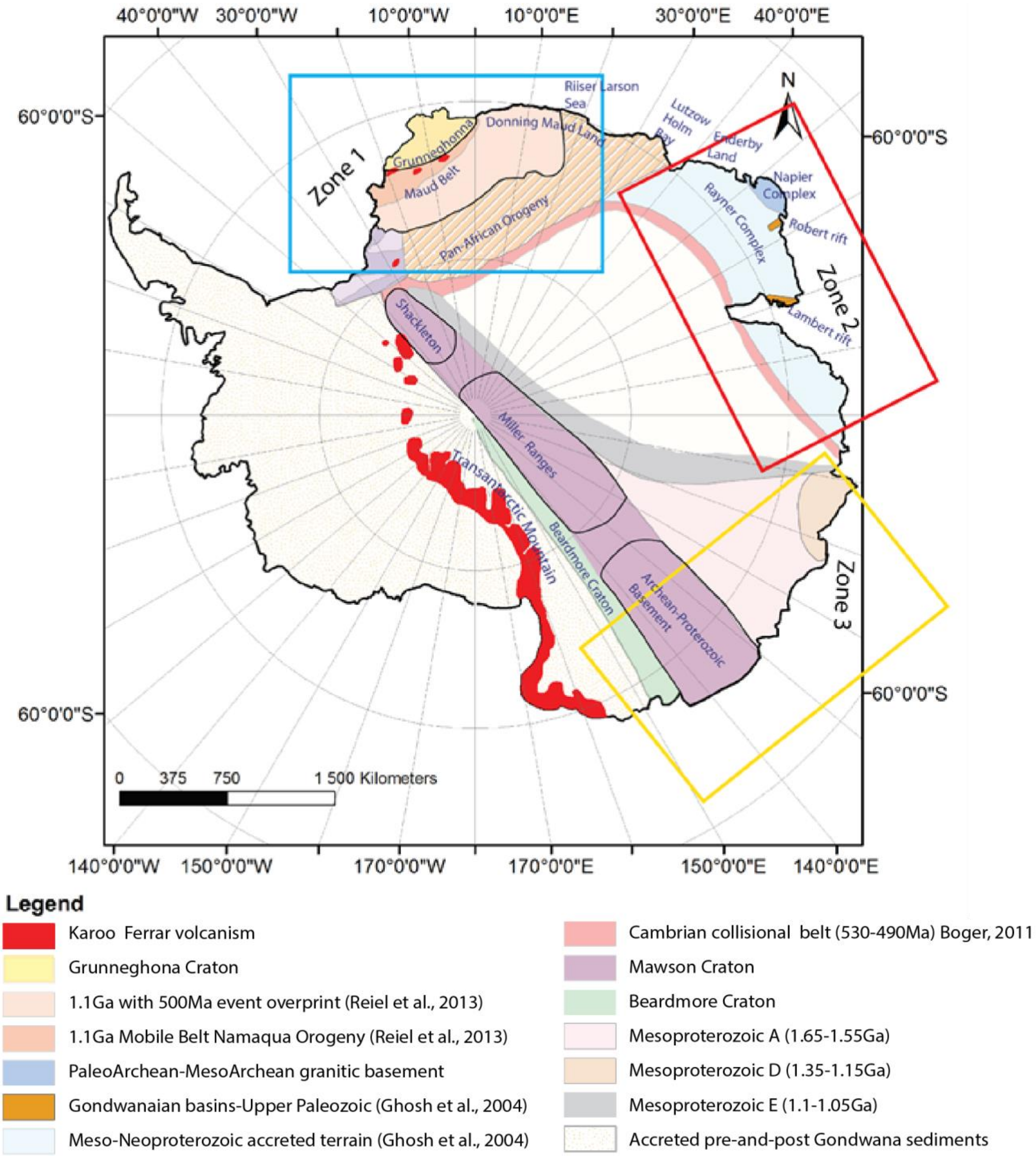

Figure 67: Basement geology of Antarctica compiled from (Rediel et al., 2013: Boger, 2011: Gosh et al., 2004: Kelly et al., 2002 – see Plate 1 supplementary material). Base on geochronological properties and similar orogenic history, the area marked Zone 1 (Blue rectangle) is related to the Kaapval craton of Southern Africa, Zone 2 (Red rectangle) is related to the Eastern Ghats craton of Eastern India, and Zone 3 (Yellow rectangle) is related to the Australian plate. The trace of the Beardmore, Mawson, Mesoproterozoic A, D, E, and the accreted pre and post Gondwana sediments in Antarctica and Australia is After Boger (2011). World Geodectic System 1984 figures 68-74.

(a)

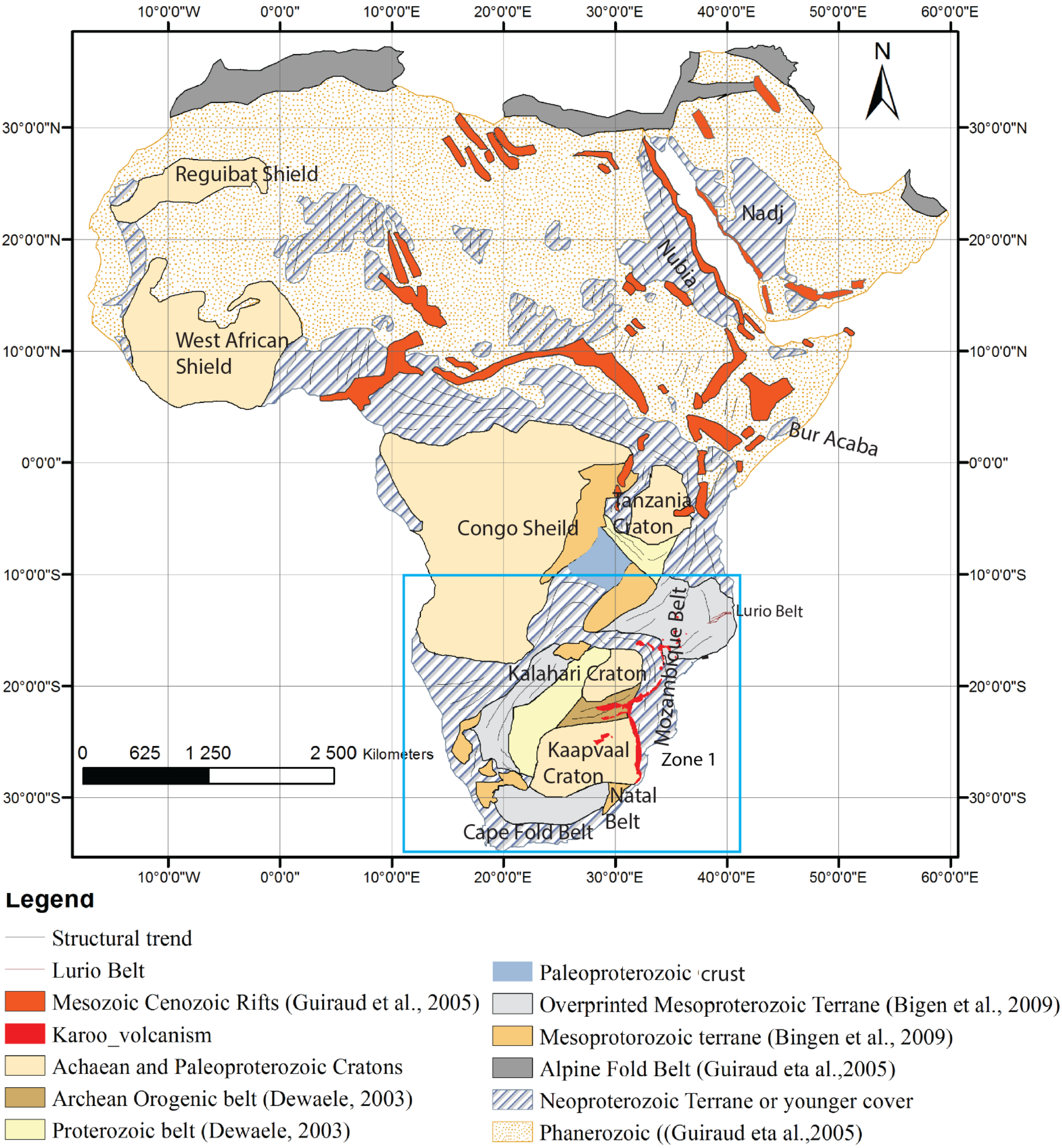
10°0'0"W
0°0'0"
10°0'0"E
20°0'0"E
30°0'0"E
40°0'0"E
50°0'0"E
60°0'0"E
30°0'0"N
20°0'0"N
10°0'0"N
0°0'0"
10°0'0"S
20°0'0"S
30°0'0"S
N
Reguibat Shield
West African Shield
Nadj
Nubia
Bur Acaba
Congo Sheild
Tanzania Craton
Lurio Belt
Mozambique Belt
Kalahari Craton
Kaapvaal Craton
Zone 1
Natal Belt
Cape Fold Belt
0 625 1 250 2 500 Kilometers
Legend
Structural trend
Lurio Belt
Mesozoic Cenozoic Rifts (Guiraud et al., 2005)
Karoo_volcanism
Achaean and Paleoproterozoic Cratons
Archean Orogenic belt (Dewaele, 2003)
Proterozoic belt (Dewaele, 2003)
Paleoproterozoic crust
Overprinted Mesoproterozoic Terrane (Bigen et al., 2009)
Mesoprotorozoic terrane (Bingen et al., 2009)
Alpine Fold Belt (Guiraud eta al.,2005)
Neoproterozoic Terrane or younger cover
Phanerozoic ((Guiraud eta al.,2005)

(b)

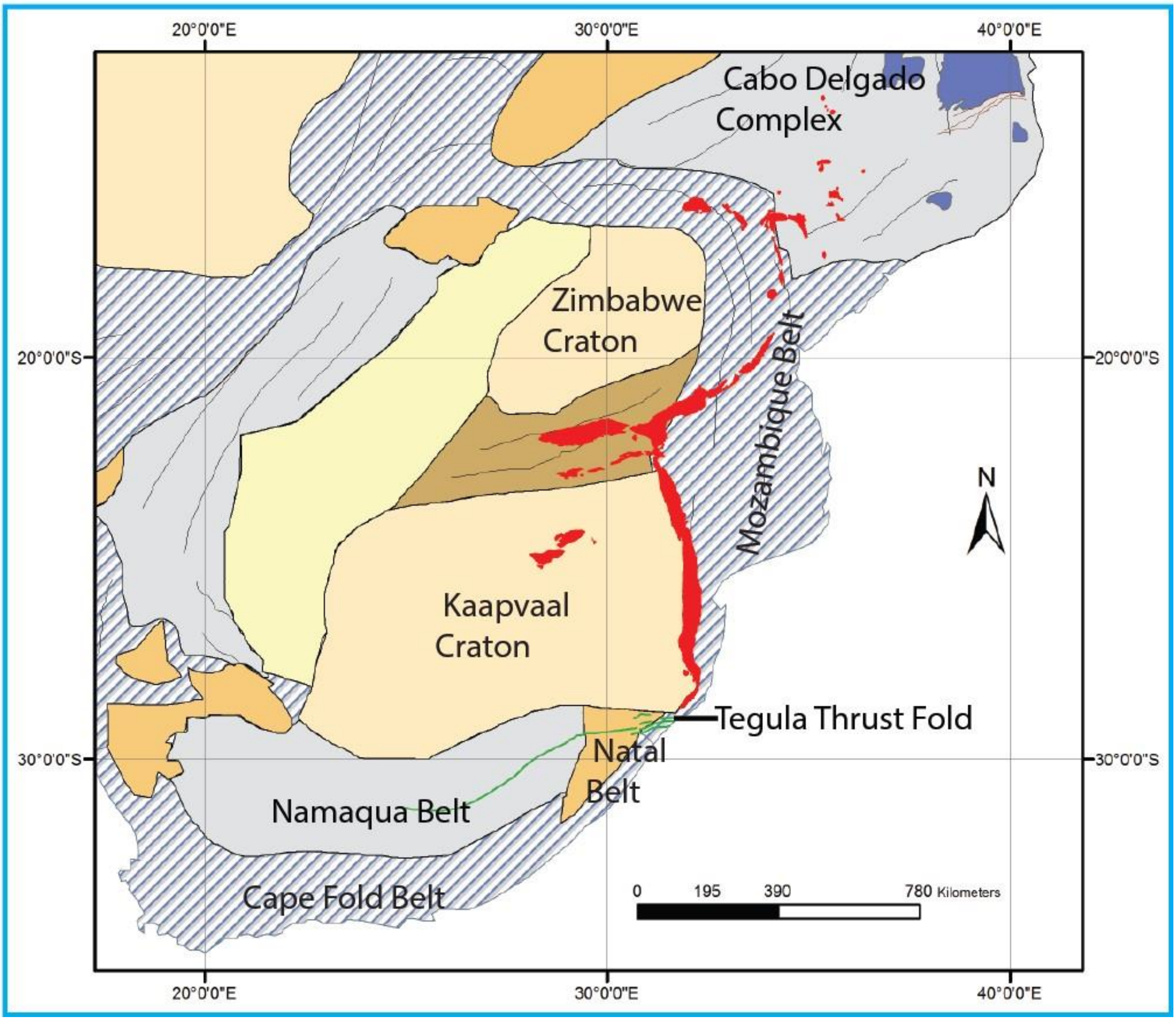

Figure 68: (a) Geological map of Africa compiled from (Foster et al., 2015: Rekha et al., 2014: Jacobs et al., 2008: Guiraud et al., 2005: Dewaele, 2003: Daly et al., 1989. The zone 1 (blue rectangle figure 67), marks a domain of similar geochronological properties with Antarctica. (b) Zoom on figure 5a showing the domain of shared geological history with the Antarctica plate. The archean Kaapvaal Craton bear similar geochemical signatures similar to archean Grunnehogna Craton, most likely forming a single craton. The Namaqua-Natal belt formed during the Namaquan Orogeny (1.1-10Ga), and is regarded as an extension of the Mesoproterozoic Maud Belt (1.1Ga) in Antarctica.

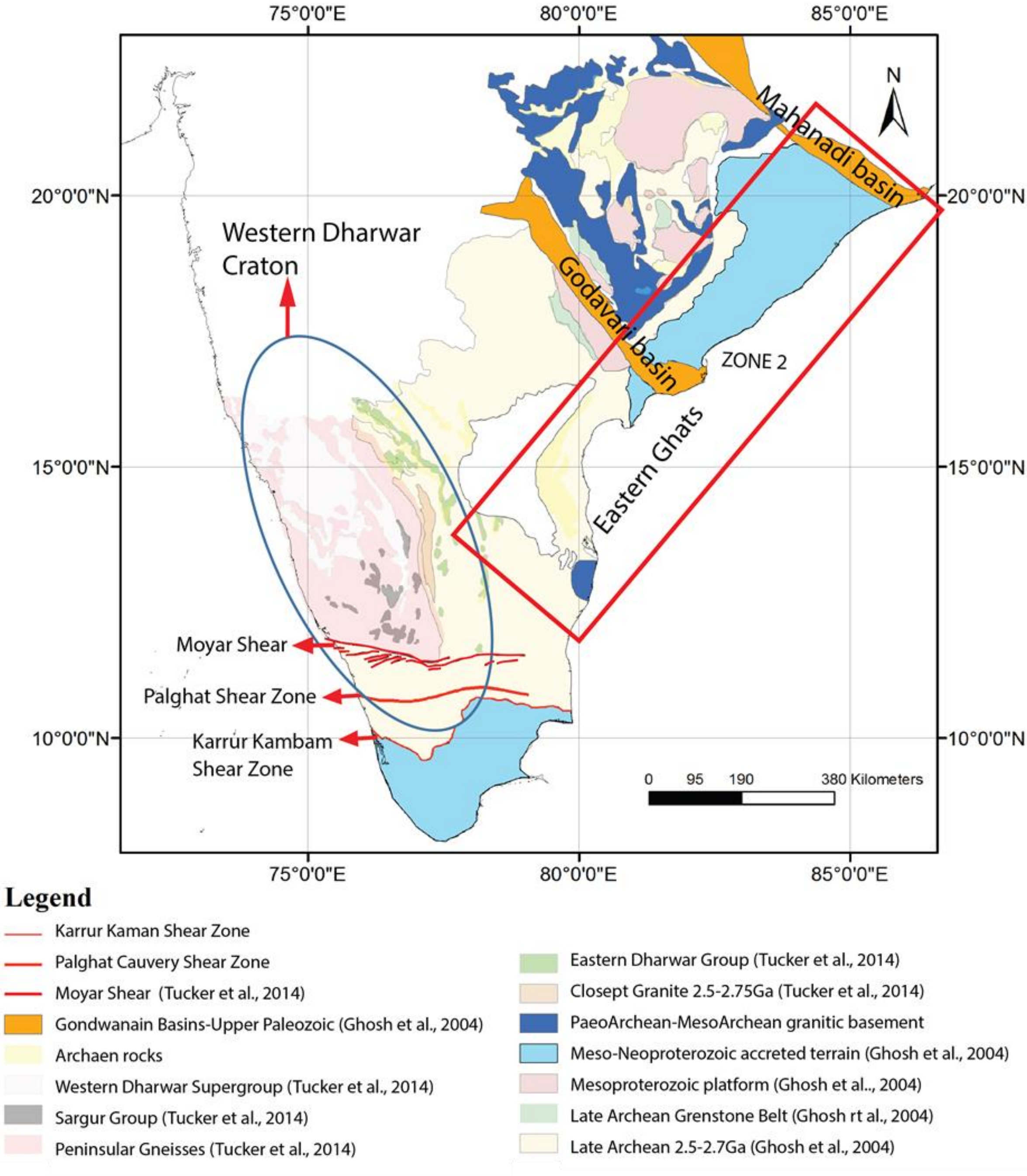

Figure 69: Geology of India basement compiled from (Tucker et al., 2014; Rajaprian et al., 2014; Dasgupta et al., 2013; Ghosh et al., 2004; and [www.portal.gsi.gov.in/portal 11/07/2016](www.portal.gsi.gov.in/portal) . The marked area zone 2 (figure 67), indicates area of similar geological similarities with Antarctica. Rocks of the Ghats share similar geochronological properties with rocks of Enderby Land in East Antarctica. The Dharwar Craton of India shares similar geochemical and geochronological properties with the archean rocks of earstern Madagascar.

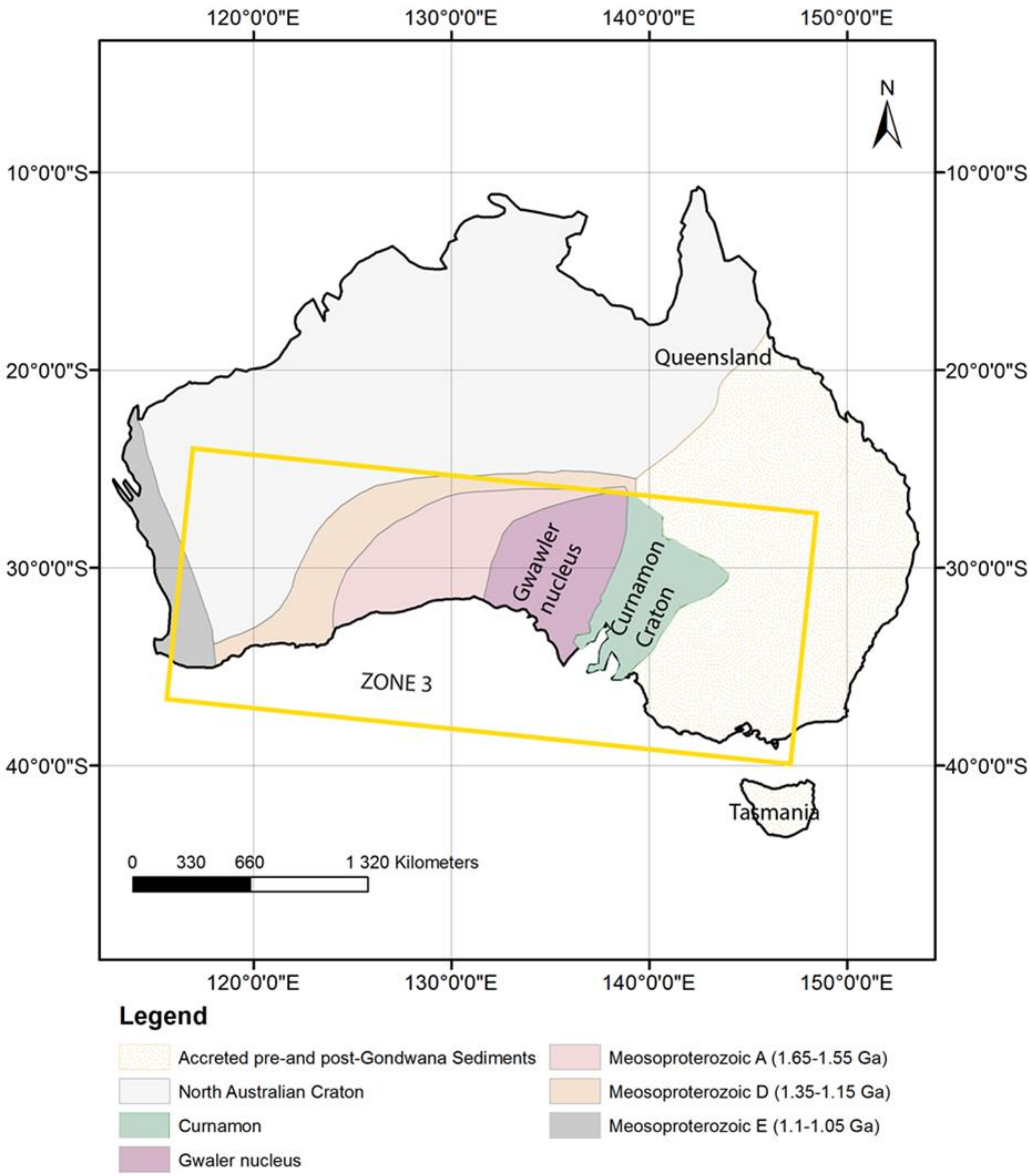

Figure 70: Basement geology of the Australian modified (after Borg and DePaolo, 1991 and Boger, 2011). Zone 3 indicates area of sheared geological similarities with Antarctica. The Mawson and Beadmore cratons of Antarctica continue into the Gawler and Curnamon blocks in Antarctica respectively, bearing similar geochemical and geochronologically characteristics.

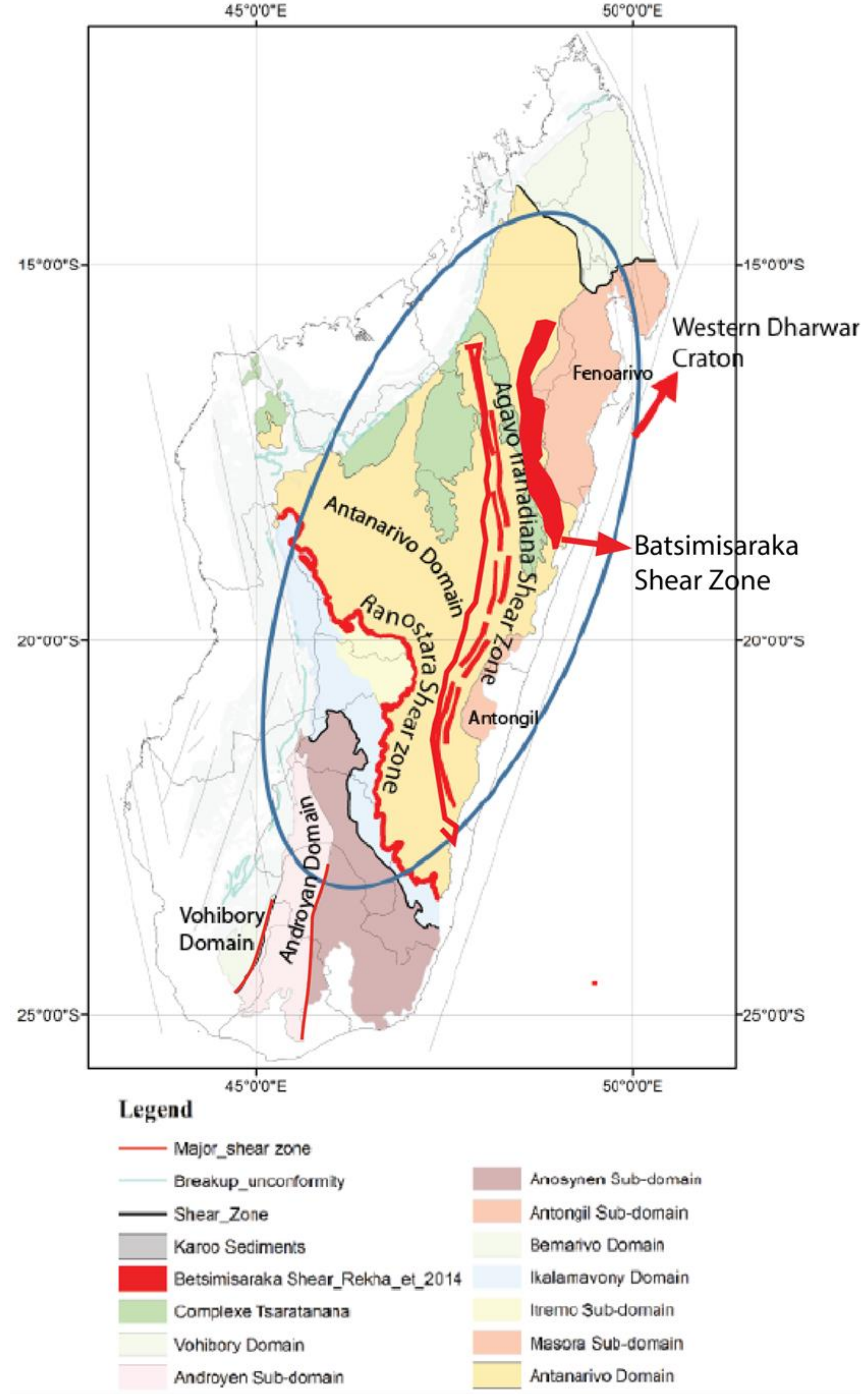
45°0'0"E
50°0'0"E
15°0'0"S
20°0'0"S
25°0'0"S
Western Dharwar Craton
Fenoarivo
Agavo Ifanadiana Shear Zone
Antanarivo Domain
Batsimisaraka Shear Zone
Ranostara Shear zone
Antongil
Androyan Domain
Vohibory Domain
Legend
Major_shear zone
Breakup_unconformity
Shear_Zone
Karoo Sediments
Betsimisaraka Shear_Rekha_et_2014
Complexe Tsaratanana
Vohibory Domain
Androyen Sub-domain
Anosynen Sub-domain
Antongil Sub-domain
Bemarivo Domain
Ikalamavony Domain
Itremo Sub-domain
Masora Sub-domain
Antanarivo Domain

Figure 71: Geology of Madagascar compiled from (Tucker et al., 2014: Rekha et al., 2014: Rasoamalala et al., 2013; de Wit et al. 2003; Nesen et al., 198;: Courrier and Lafont, 1987; Besairie and Collignon, 1972). The Western Dharwar craton Of Madagascar shares similar geochemical and geochronological properties with the Dharwar craton in India. The Batsimisaraka shear zone in Rekha et al., 2014, is argued by Tucker et al., 2014 not to be evident.

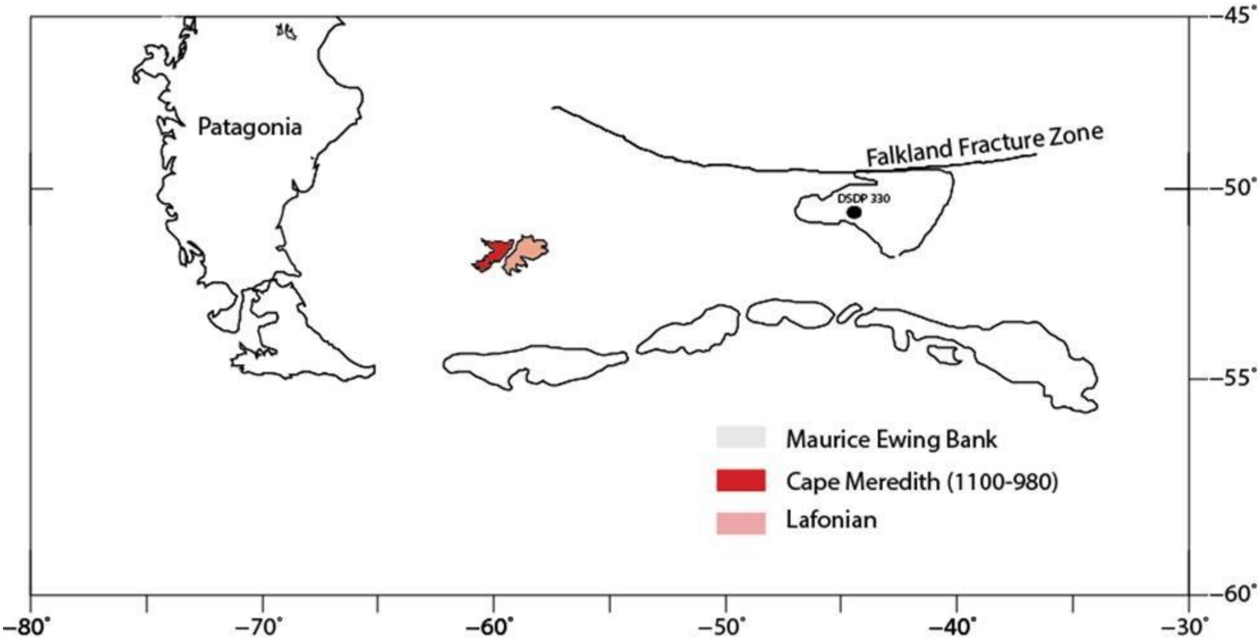

Figure. 72: Geological map of the Falkland Plateau compiled from (Lock, 1978; Martin et al., 1981; Marshall, 1994; Curtis and Hyam, 1998). DSDP Hole 330 was bottomed in Precambrian rocks (554± 66Ma Lorenzo and Mutter, 1988) correlative with the Pan-African ~650-500Ma Cape basement of Southern Africa.

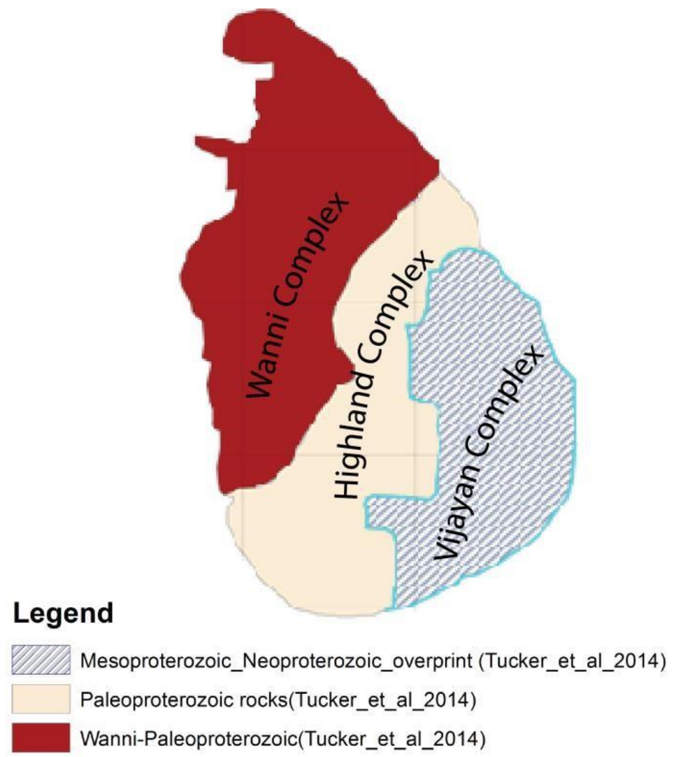

Figure 73: Basement geology map of Sri Lanka (modified after Koner et al., 2003; Bingen et al., 2009; Kelly et al., 2002; and Tucker et al., 2014– see Plate 6 supplementary material).

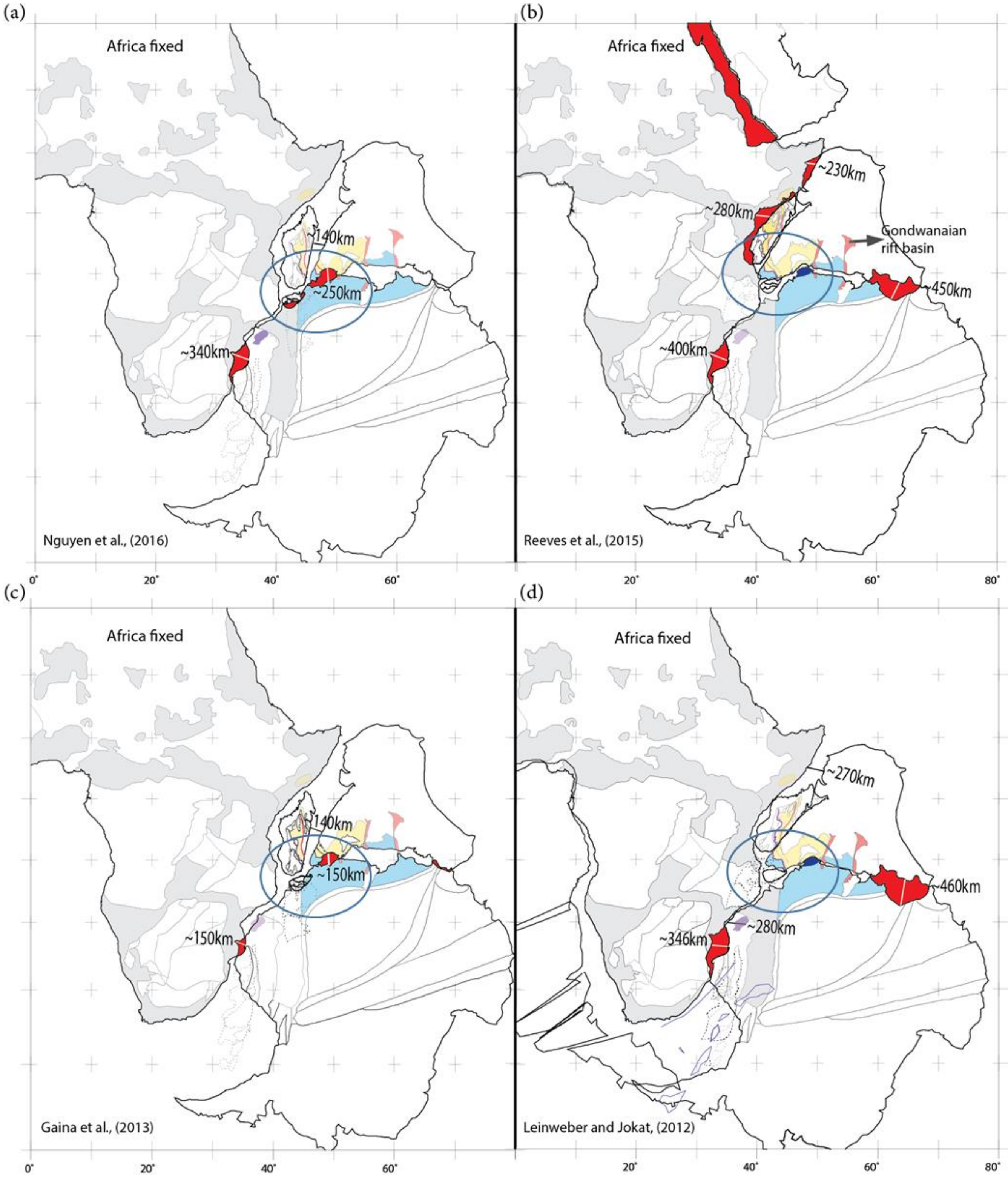
(a)
Africa fixed
~140km
~250km
~340km
Nguyen et al., (2016)
(b)
Africa fixed
~230km
~280km
Gondwanaian
rift basin
~450km
~400km
Reeves et al., (2015)
20°
10°
0°
−20°
−40°
0°
20°
40°
60°
80°
(c)
Africa fixed
~140km
~150km
~150km
Gaina et al., (2013)
(d)
Africa fixed
~270km
~460km
~346km
~280km
Leinweber and Jokat, (2012)
20°
0°
−20°
−40°
0°
20°
40°
60°
20°
40°
60°
80°

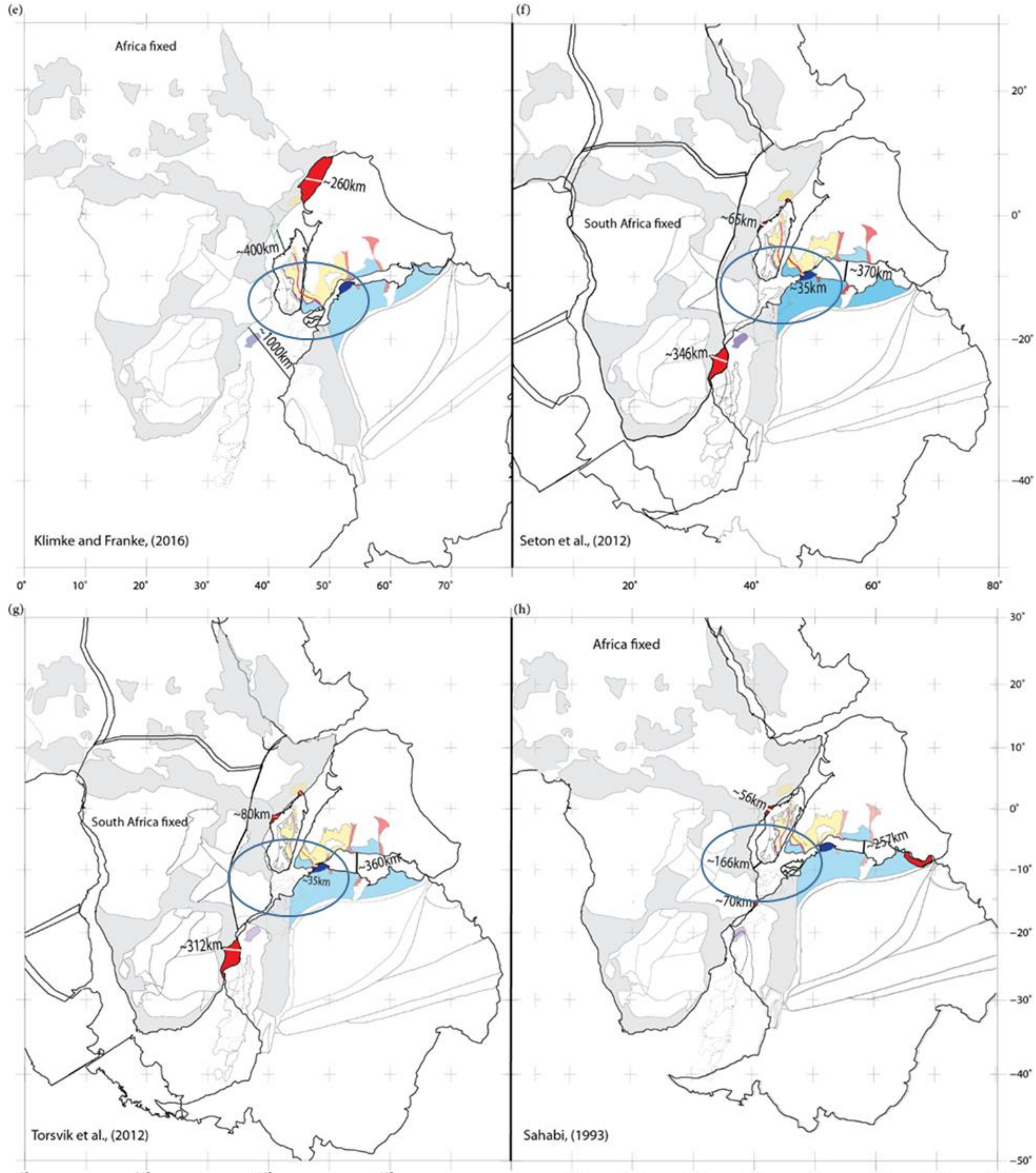
(e)
Africa fixed
~260km
~400km
~1000km
Klimke and Franke, (2016)
(f)
South Africa fixed
~65km
~35km
~370km
~346km
Seton et al., (2012)
(g)
South Africa fixed
~80km
~35km
~360km
~312km
Torsvik et al., (2012)
(h)
Africa fixed
~56km
~166km
~257km
~70km
Sahabi, (1993)

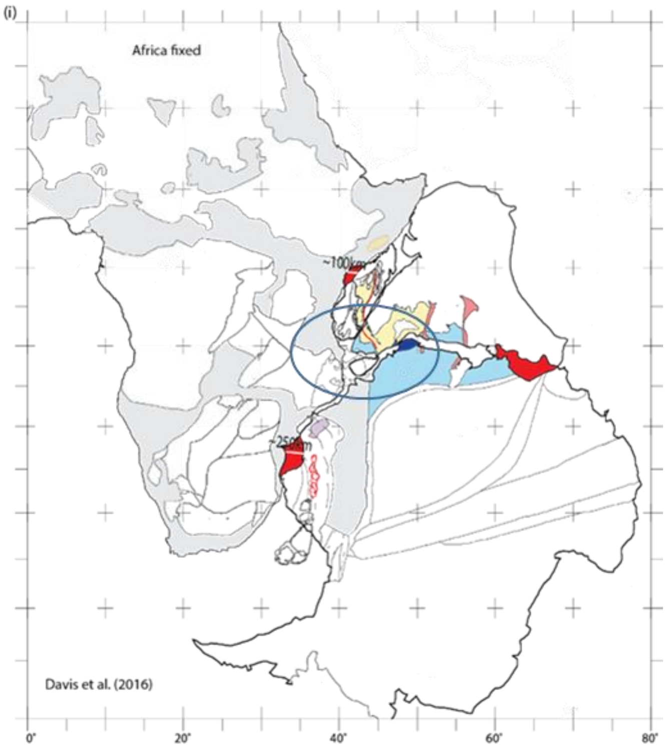

Figure.74 Comparing the kinematic models of Nguyen et al. (2016), Klimbe and Franke (2016), Davis et al. (2016), Reeves et al. (2015), Gaina et al. (2013), Leinweber and Jokat, (2012), Seton et al. (2012), Torsvik et al. (2012) and Sahabi (1993). The red, ash, blue, yellow and deep blue polygons represents overlap, Neoproterozoic terrain, Mesoproterozoic accreted terrain, Late Archean rocks, Paleo-Meso Archean rocks respectively.. The blue circle compares the geology of the India-Madagascar-Sri Lanka-Africa domain. Leinweber and Jokat (2012), Reeves et al. (2015), Davis et al. (2016) are model after the geochronological studies of Ghosh et al., 2004. In these models, the Agavo Ifanadiana shear zone (Madagascar) is aligned with the Moyar shear zone (West India). This results in overlap between India and Antarctica. Gaina et al. (2013) and Sahabi (1993) on the other hand, fit the Batsimisaraka shear zone to the Moyar shear zone avoiding the overlap, but inaccurately fit Mesoproterozoic rocks to Archean rocks. The models of Seton et al. (2012) and Torsvik et al. (2012) result in misalignment of Archean rocks of the Napier complex (Antarctica) and the Eastern Ghat craton (East India), and the conjugate Gondwanaian rifts basins. Sahabi (1993) and Davis et al. (2016), on the other hand presents alignment of Archean rocks of the Napier complex and the Ghat craton and a good alignment of the Gondwanian rifts basins. Klimbe and Franke (2016) prefer a more southward position of Madagascar leading to huge gap of about 1000km between Antarctic and Africa taken into consideration current information and observations we have gathered on the surrounding plates. (Mercator projection).

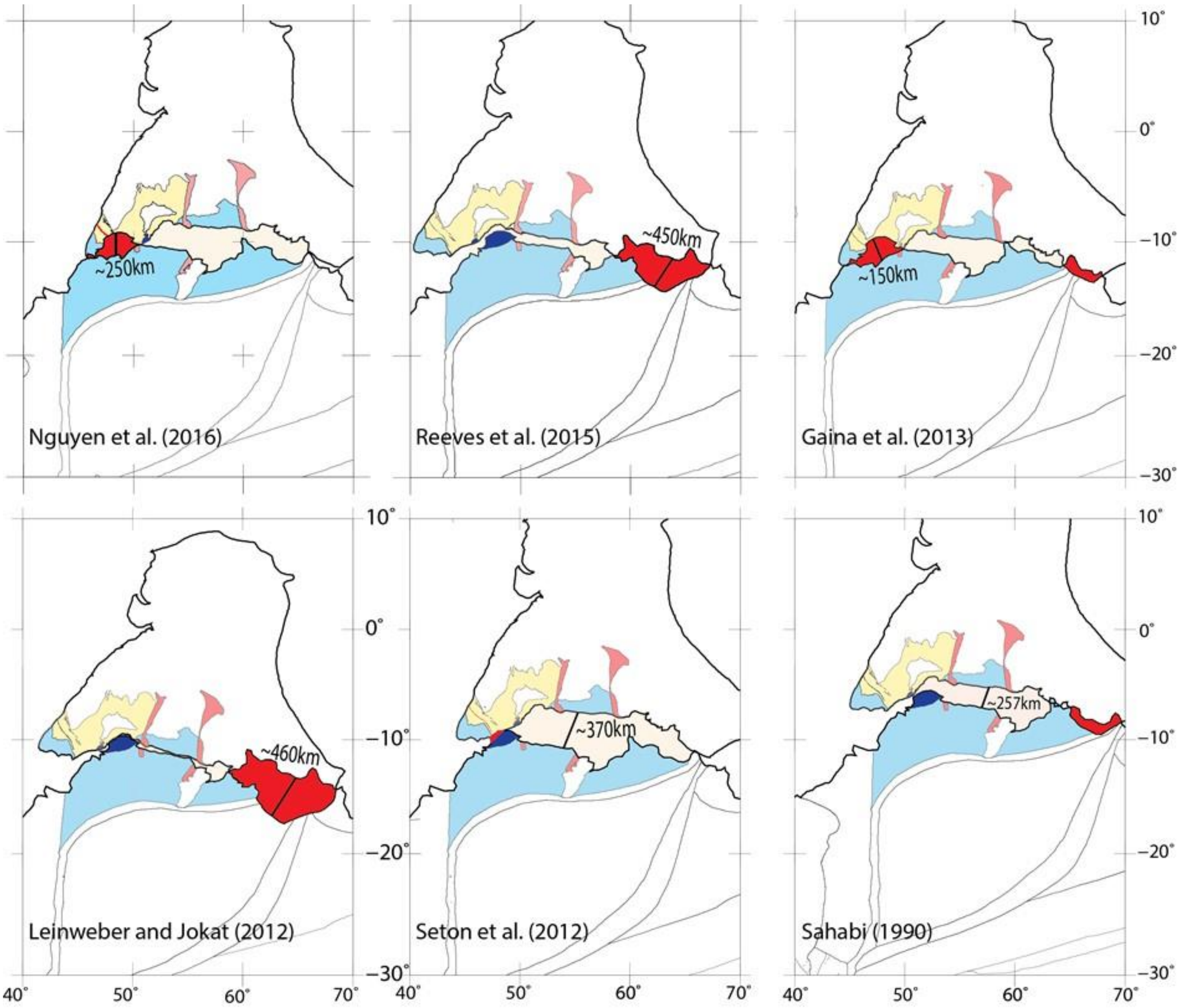

Figure 75: Comparism (zoom) of India and Antarctica with referencee to Africa for the models of Nguyen et al. (2016), Reeves et al. (2015), Gaina et al. (2013), Leinweber and Jokat (2012), Seton et al. (2012), and Sahabi (1993). The models of Nguyen et al. (2016), Gaina et al. (2013) and Seton et al. (2012) result in misalignment of Archean rocks of the Napier complex and the Ghat craton, and the Gondwanaian rifts basins. Reeves et al. (2015), Leinweber and Jokat (2012) and Sahabi (1990), on the other hand results in a perfect alignment of Archean rocks of the Napier complex and the Ghat craton, and Gondwana rifts basins. Notice the large overlaps in Nguyen et al. (2016), Reeves et al. (2015), Gaina et al. (2013) and Leinweber and Jokat, (2012). The pink color represent gap between the plates. (Mercator projection).

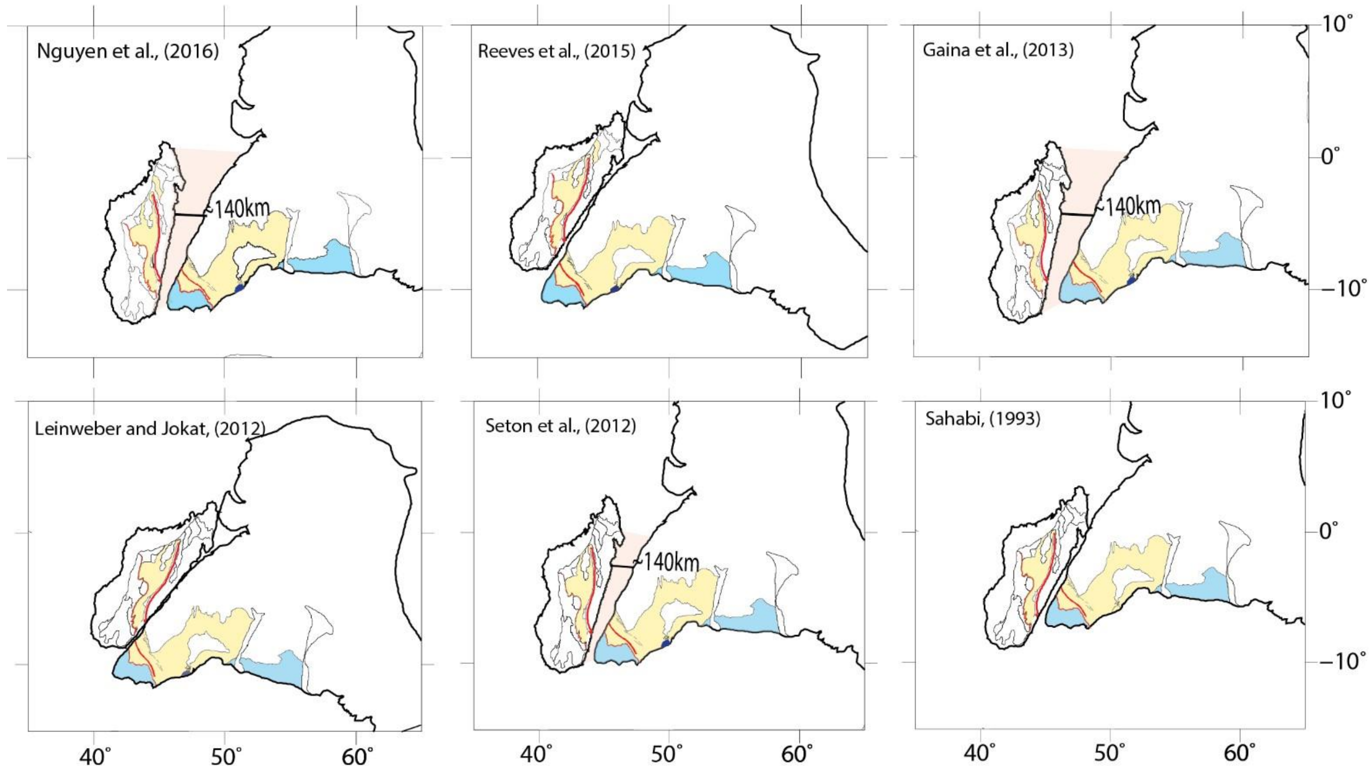

Figure 76: Comparing reconstruction of Madagascar and India with referencee to Africa in Nguyen et al. (2016), Reeves et al. (2015), Gaina et al. (2013) and Leinweber and Jokat (2012) Seton et al, (2012), and Sahabi (1993). In Reeves et al. (2015) and Leinweber and Jokat (2012), the Agavo Ifanadiana shear zone is aligned with the Moyar shear zone, resulting in Mesoproterozoic rocks of Ikalamavony in Madagascar fitted with Archean rocks Dharwar craton in India. Nguyen et al. (2016), Gaina et al, (2013) and Seton et al. (2012), on the other hand results in about ~140km gap between India and Madagasca, and fits Mesoproterozoic rocks to Archean rocks between the two plates. The pink color represent gap betweeen the plates. (Mercator projection).

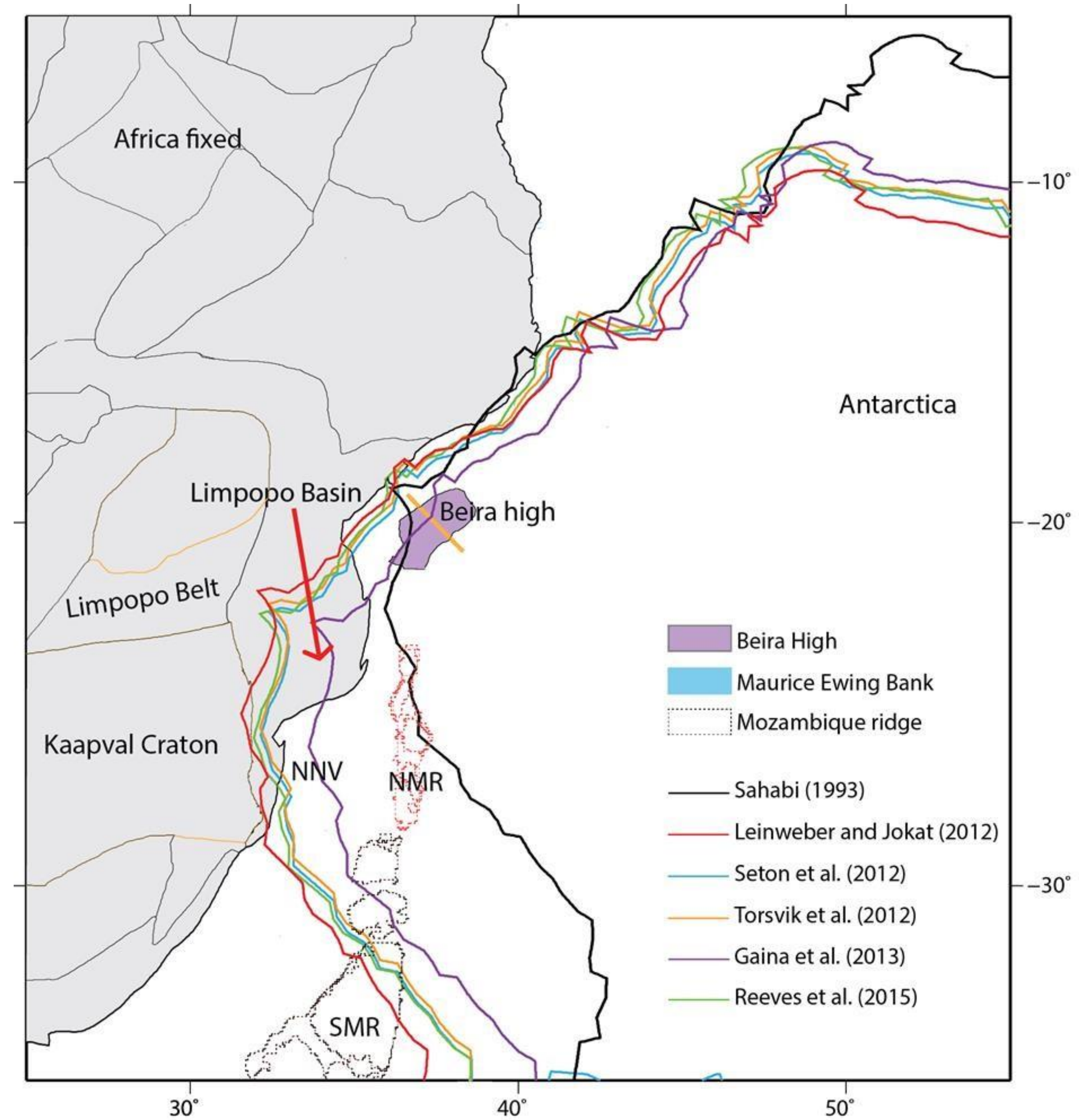

Figure 77: Comparing the fits between Antarctica with respect to Africa, and the consequence on the Beira High continental crust and the Limpopo basin. The yellow line crossing the Beira High continental block shows the location of the seismic refraction profile 2014001014 of the MOCOM-Cruise (See figure 11). Notice all the models except Sahabi, (1993) overlap on the Beira high, the North Natal Valley, a part or the total Limpopo Basin and the North Mozambique ridge. The North Mozambique Ridge (NMR, in red) consist mainly of sediments muscle on a thinned continental crust (Lepretre et al., 2017; Moulin et al., submitted). The Southern Mozambique Ridge (SMR, in black) maybe composed of volcanics (Gohl et al., 2011). (Mercator projection).

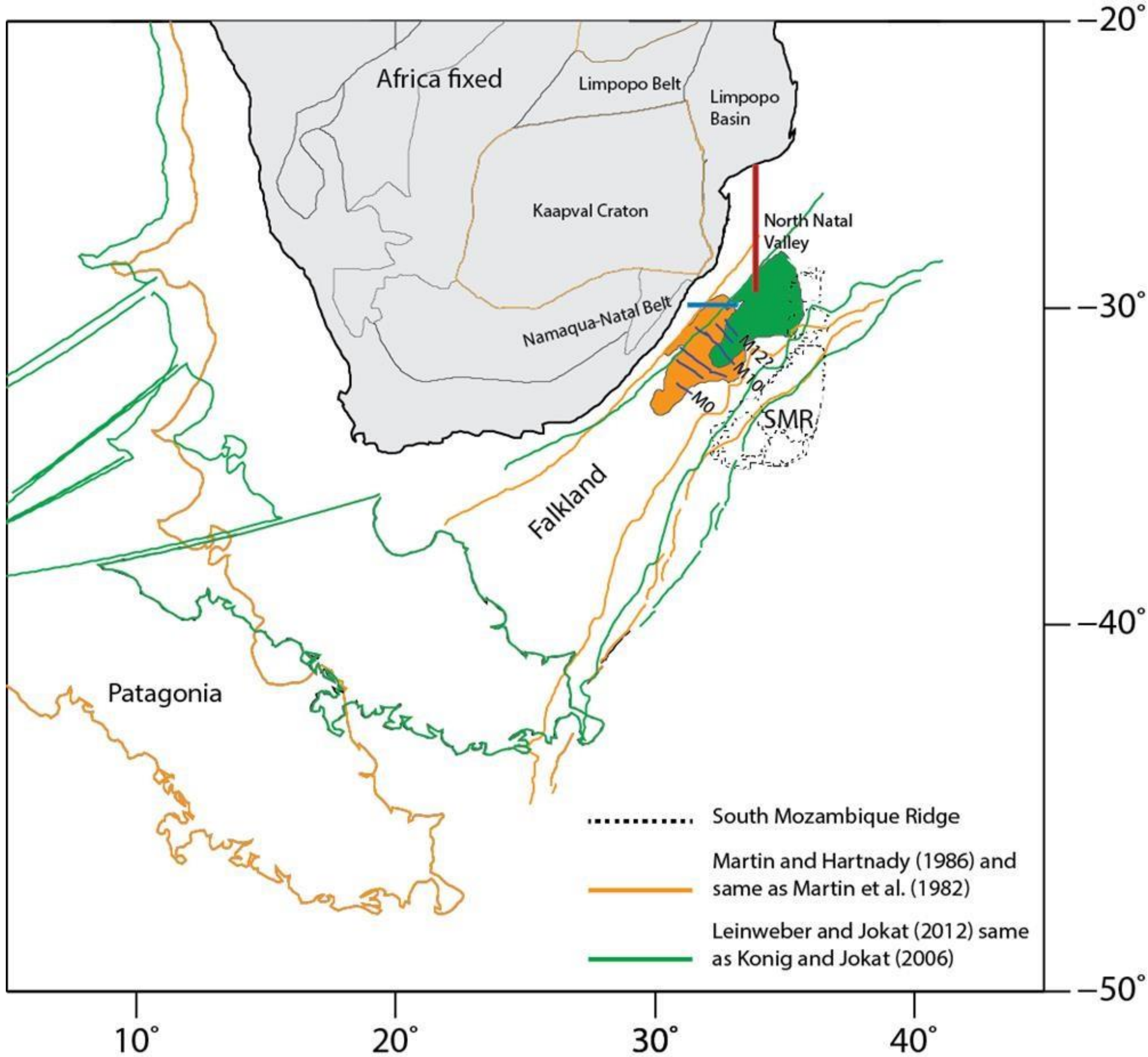

Figure 78: Comparing the proposed fit for the Falkland-Patagonia in the reconstruction of Martin and Hartnady (1986) and Martin et al. 1982 (green) and the models Leinweber and Jokat (2012) and Konig and Jokat (2006) (orange) relative to African plate. Notice Leinweber and Jokat (2012) and Konig and Jokat (2006) (orange) significantly overlap the North Natal Valley, which is underlain by continental crust (Moulin et al., submitted). Red line: refraction profile M7 Pamela Moz3-5 of Lepretre et al. (2017); Blue line the limit of the South Tegula Ridge. SMR= South Mozambique Ridge. (Mercator projection).

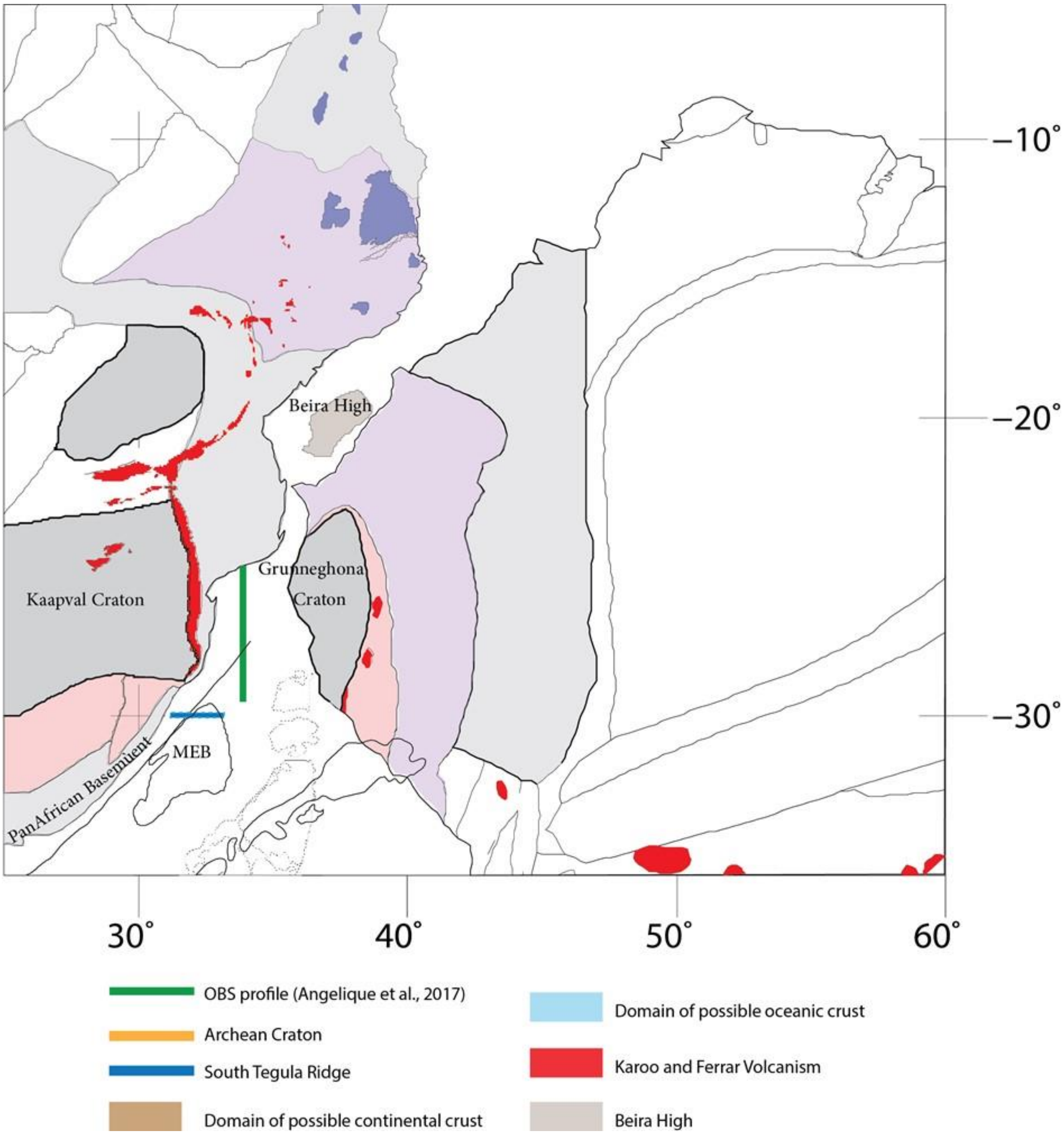

Figure 79: Map showing our reconstruction of Antarctica with respect to Africa. . Notice the Antarctica plate do not overlap the Beira High continental crust, and the extent of the Archean Kaapval and Grunneghona Craton. The two cratons bears strong geochemical signatures with each other. The reconstruction of the Falkland Plateau to Africa shows the similarities between the geology of the Pan-African basement and the rocks of the Maurice Ewing Bank. Green line: refraction profile M7 Pamela Moz3-5 of Lepretre et al. (2017); Blue line the limit of the South Tegula Ridge. (Mercator projection)

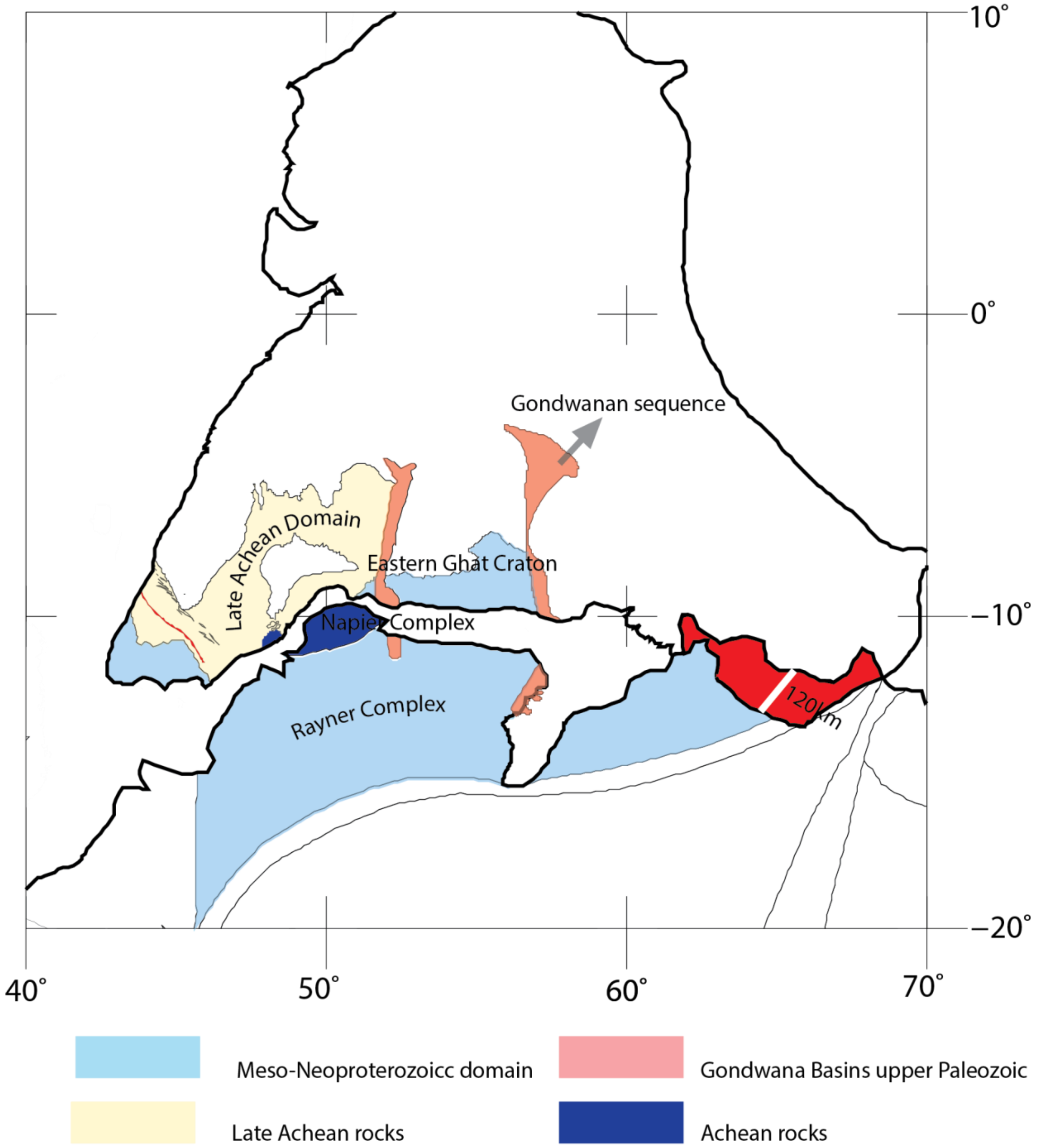

Figure 80: Map showing our reconstruction of India and Antarctica (with respect to Africa). The Archean rocks of the Napier complex in Antarctica and the Eastern Ghats craton share similarly geochemical characteristics. The Rayner Complex extends from Enderby Land (Antarctica) into the Mesoproterozoic rocks of the Eastern Ghats Granulite in India. Notice the alignment of the conjugate Carboniferous-PermoCretaceous rift basins of Godavari and Mahanadi in India, and the Lambert and Robert rift valleys in Antarctic. The ~120km overlap between India and Antarctica (red area) within Southern Bangladesh is explained by the not clearly defined limits of the India plate within the region, and the characterization of the region by Large compressional deformation. (Mercator projection)

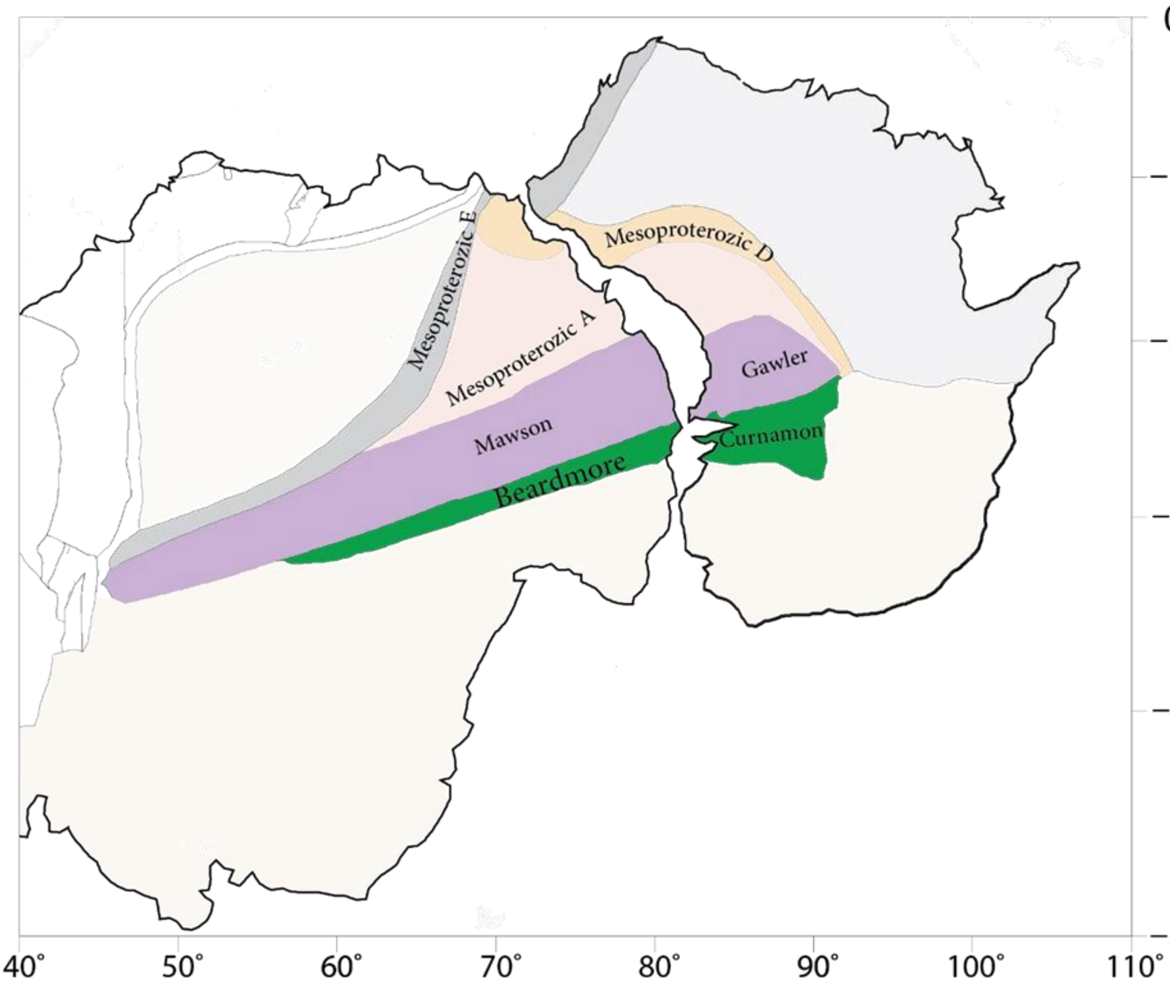

Figure 81: Map showing our reconstruction of Australia and Antarctica (with respect to Africa). Notice the alignment of the Beardmore and Curnamona cratons, and the continuation of the Mesoproretozoic rocks (Boger, 2011) between Antarctica and Australia. (Mercator projection).

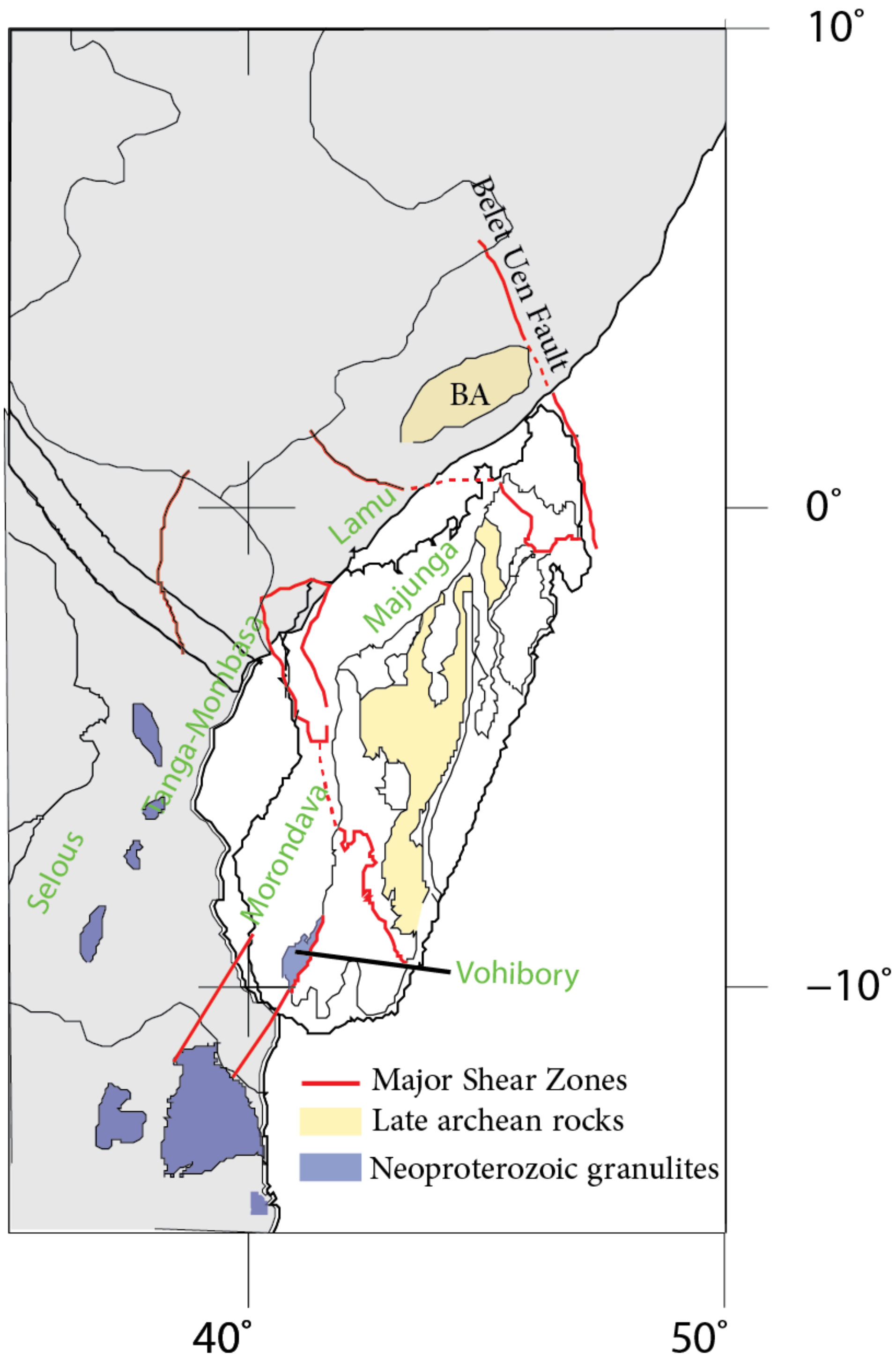

Figure 82: Map showing our reconstruction of Madagascar with respect to Africa The continuation of the Vohibory Pan-African shear zone to the Pan-African shear zone in Tanzania (de Wit et al., 2001; Reeves and de Wit., 2000), the Brava fault in Kenya to continue with the Andreaparaty shear zone in Madagascar, and the Belet Uen fault to be continues with the fault lying to the northern fringe of Madagascar. (Mercator projection).

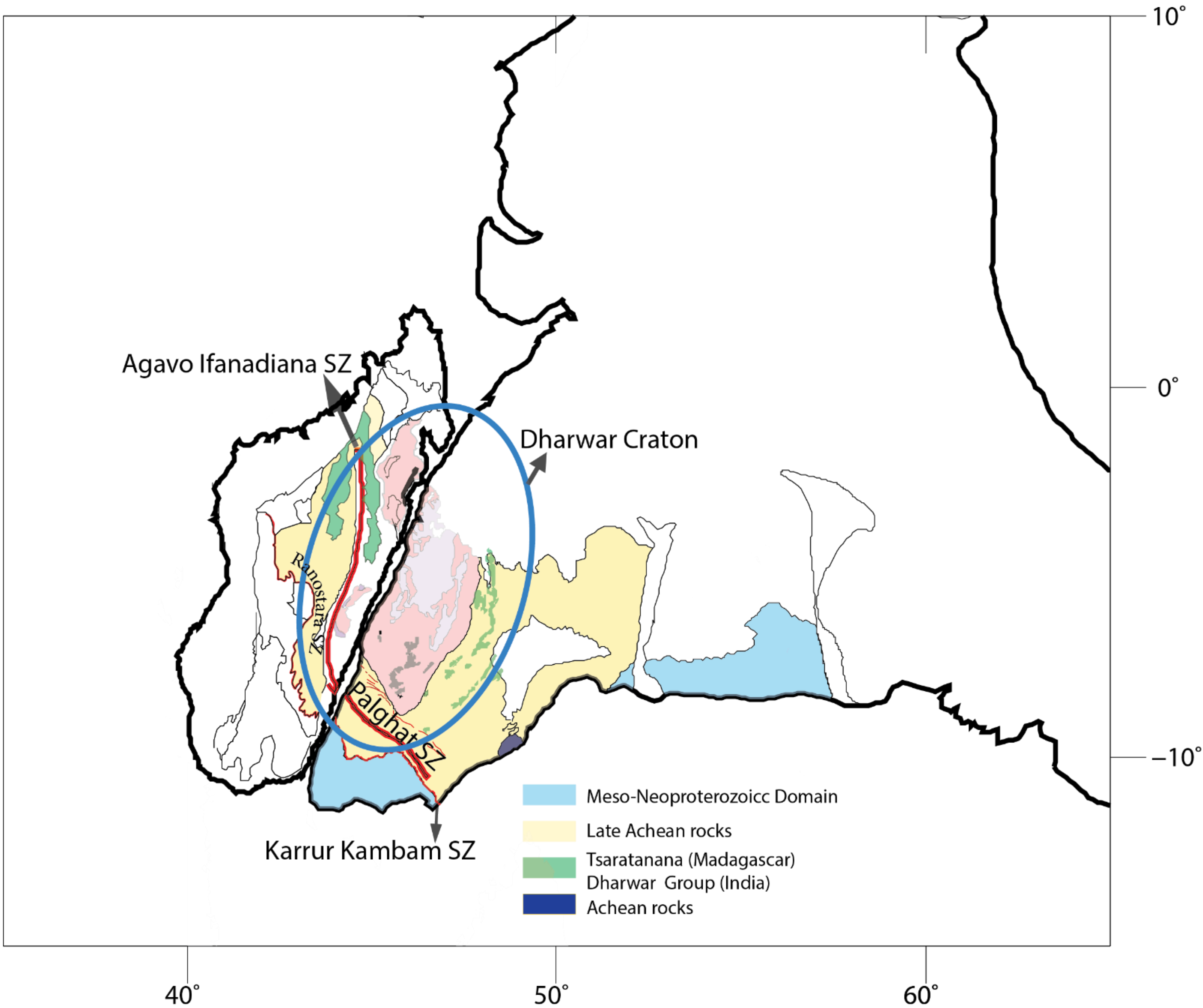

Figure 83: Map showing our reconstruction of India and Madagascar. Note the correspondence of Eastern Dharwar craton of India and the Western Dharwar craton of Madagascar. We fit the Precambrian shear zones of Agavo Ifadiana shear zone of Madagascar to the Palghat shear zones of India. This results in alignment of Archean and Mesoproterozoic rocks in both in Madagascar and India. (Mercator projection).

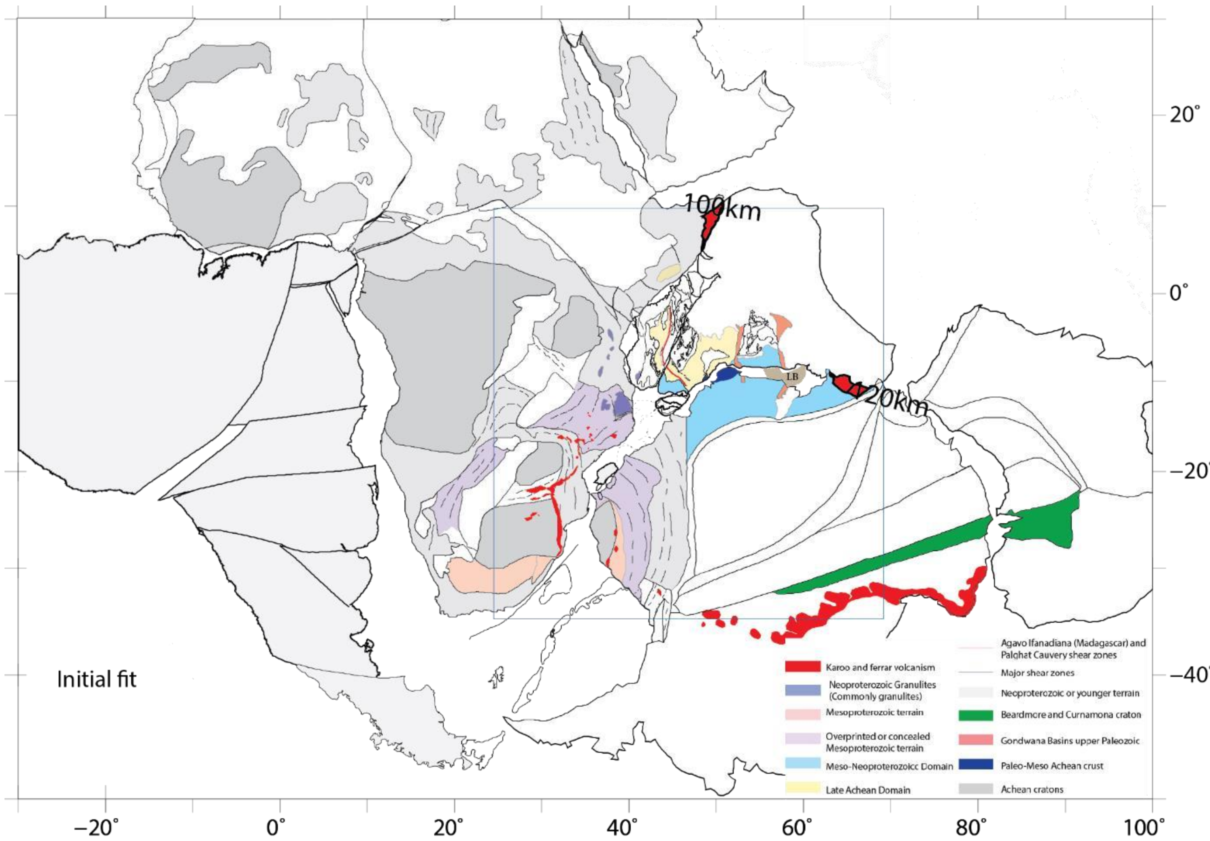

Figure 84: Our proposed initial fit of Gondwana. This new model shows the full extent of the Dharwar craton traced from the India plate into Madagascar and possibly into the Bur Acaba of Africa and beyond. It permits a very good alignment of the Beardmore and Mawson cratons in Antarctica and Australia, and allows a good trace of Mesoproterozoic rocks of Antarctica and Australia to be traced into each other. It also grants a perfect alignment of Archean rocks of the Napier complex and the Ghat craton, and a good alignment of Gondwana rifts basins. LB: Elan Bank. (Mercator projection).

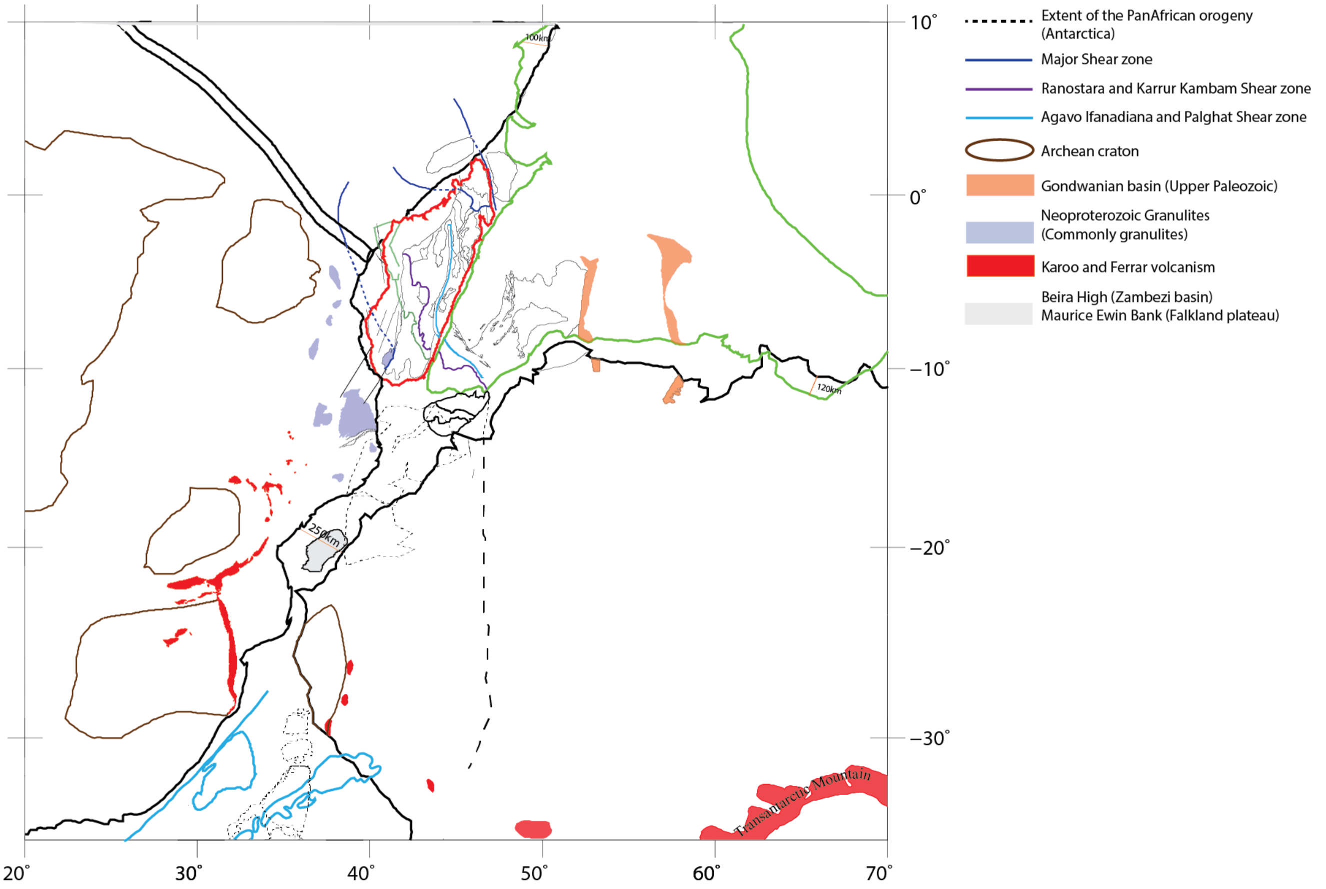

Figure. 85: Zoom on figure 22, showing perfect alignment of Precambrian shear zones of the Agavo Ifadiana shear zones of Madagascar, to the Palghat shear zones of India respectively. It also shows the full extent of the Pan-African orogenic event and the Karoo volcanism in Gondwana. (Mercator projection).

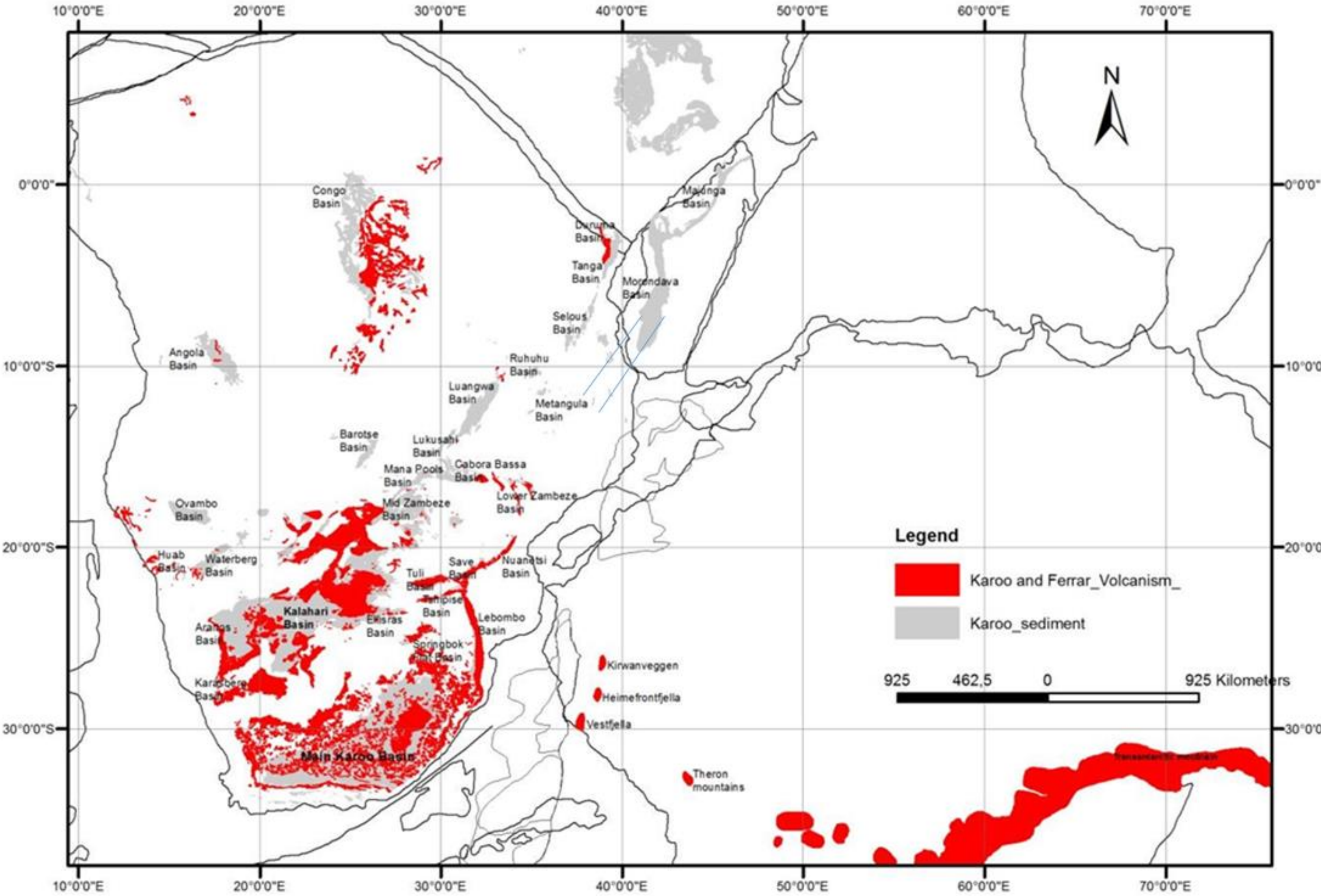

Figure. 86: New reconstruction model showing the main distribution of Karoo sediments and volcanics in Africa, Madagascar, and Antarctica. The Southern Africa continent is characterized by vast network of sills and dykes which are pre-syn-post Karoo volcanism.

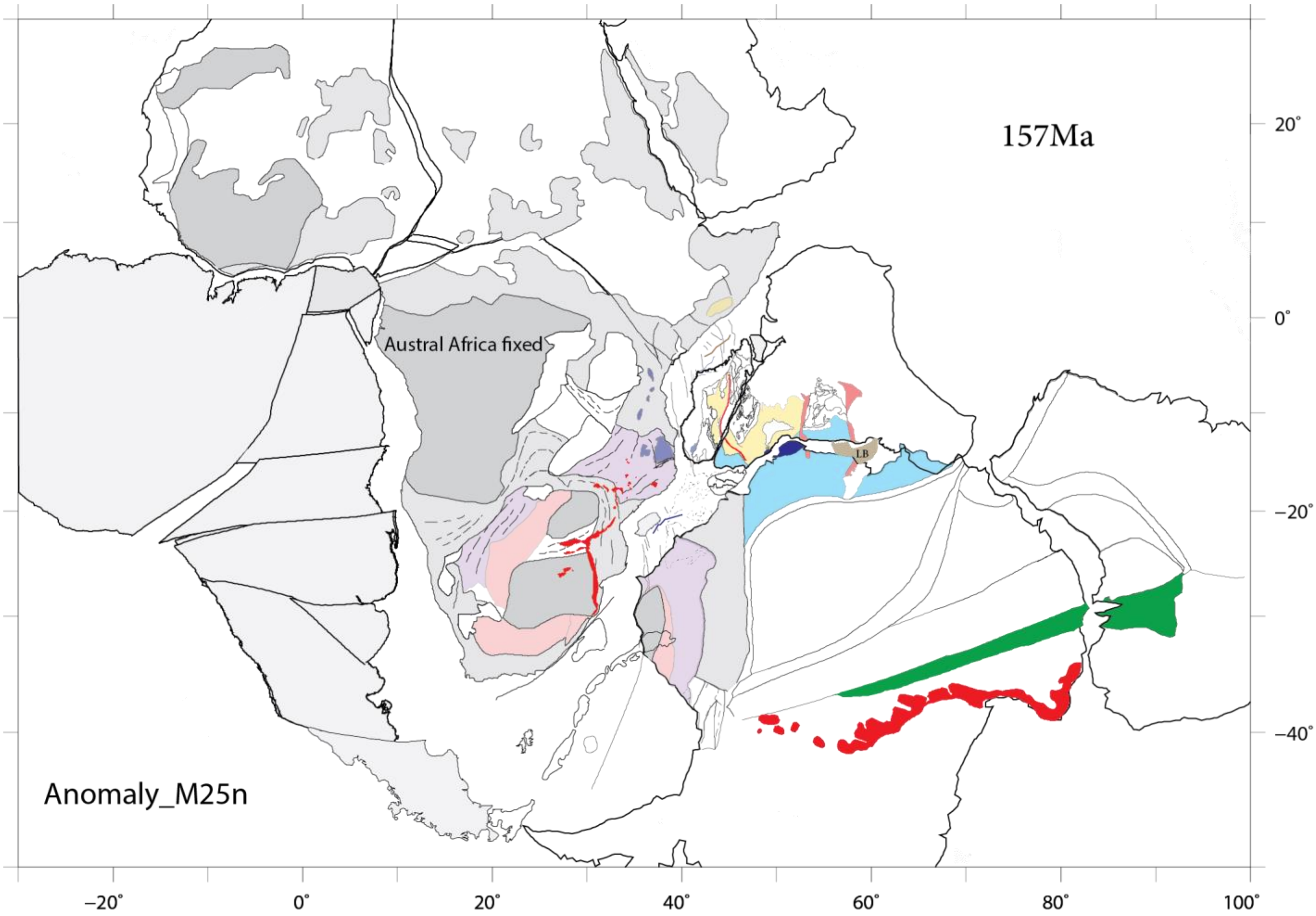

Figure 87: Reconstruction of the Indian Ocean at anomaly during the mid-late Jurassic, East -West Gondwana separated. The break-up of Gondwana was accompanied by active seafloor spreading in the Western Somalia and Mozambique Basins with the formation of first oceanic crust at M25 (157Ma). LB: Elan Bank. (Mercator projection).

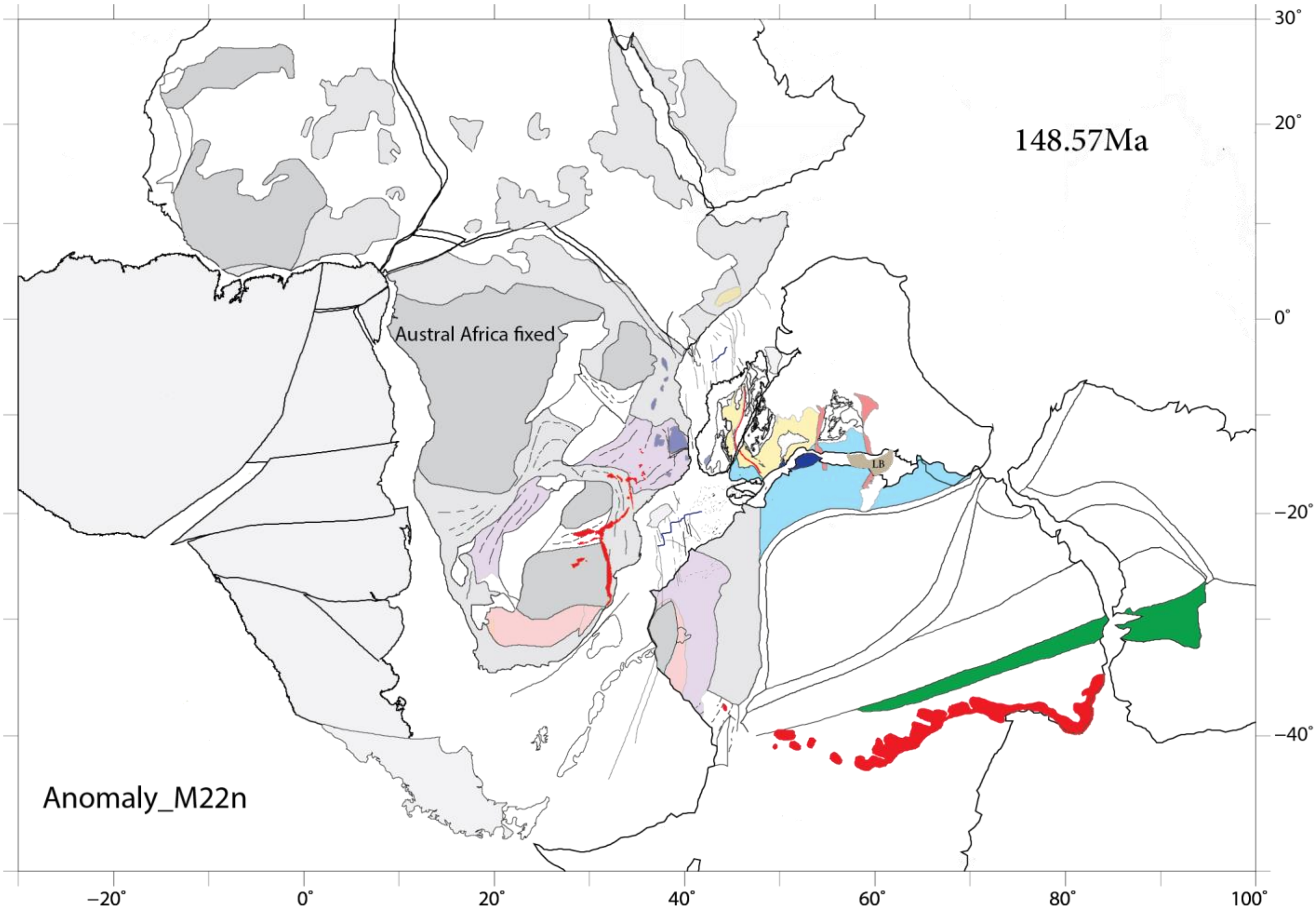

Figure: 88: Reconstruction of the Indian Ocean at anomaly at M22 (48.57Ma). (Mercator projection).

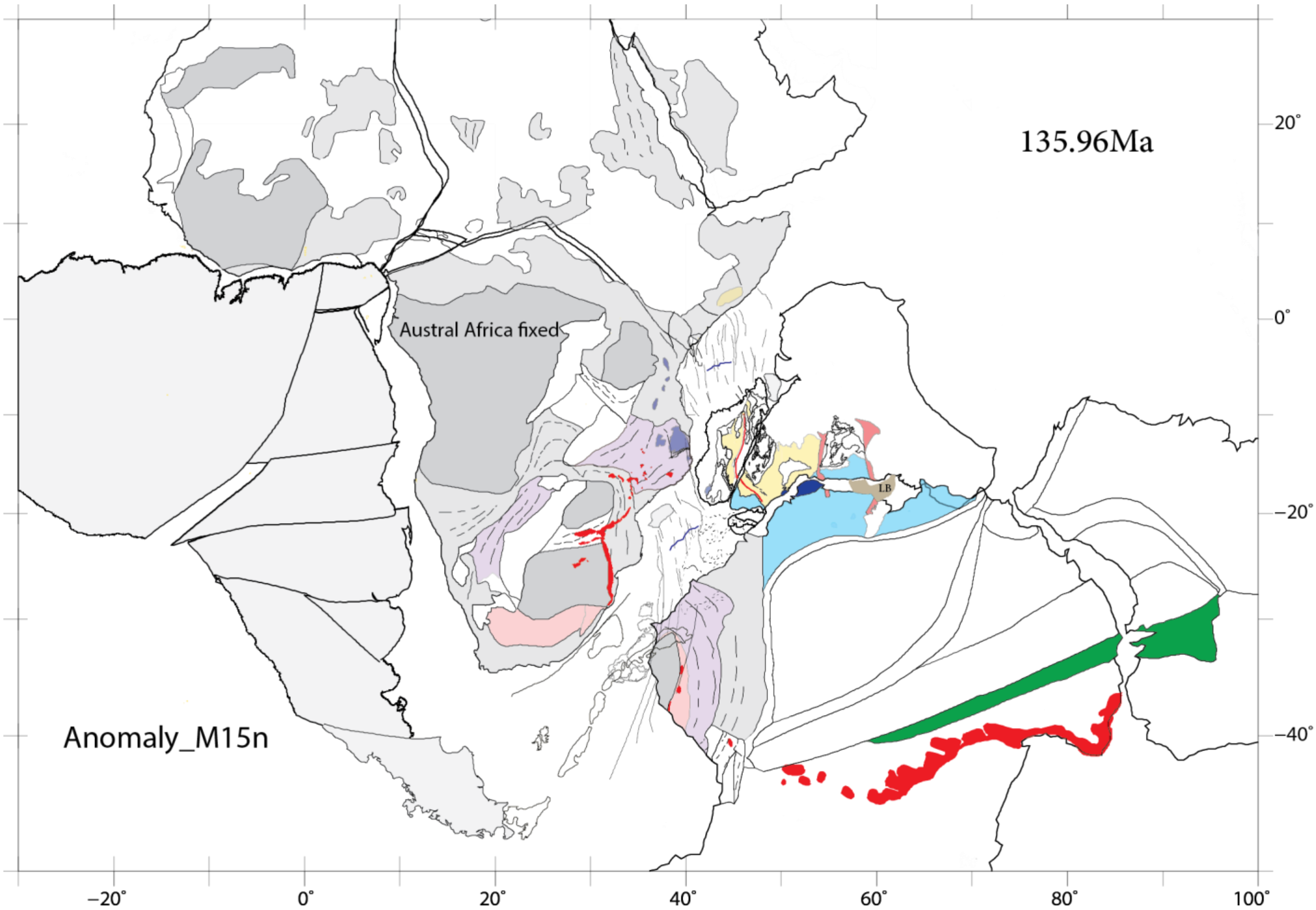

Figure 89: Reconstruction of the Indian Ocean at anomaly at M15 (135.96Ma). (Mercator projection).

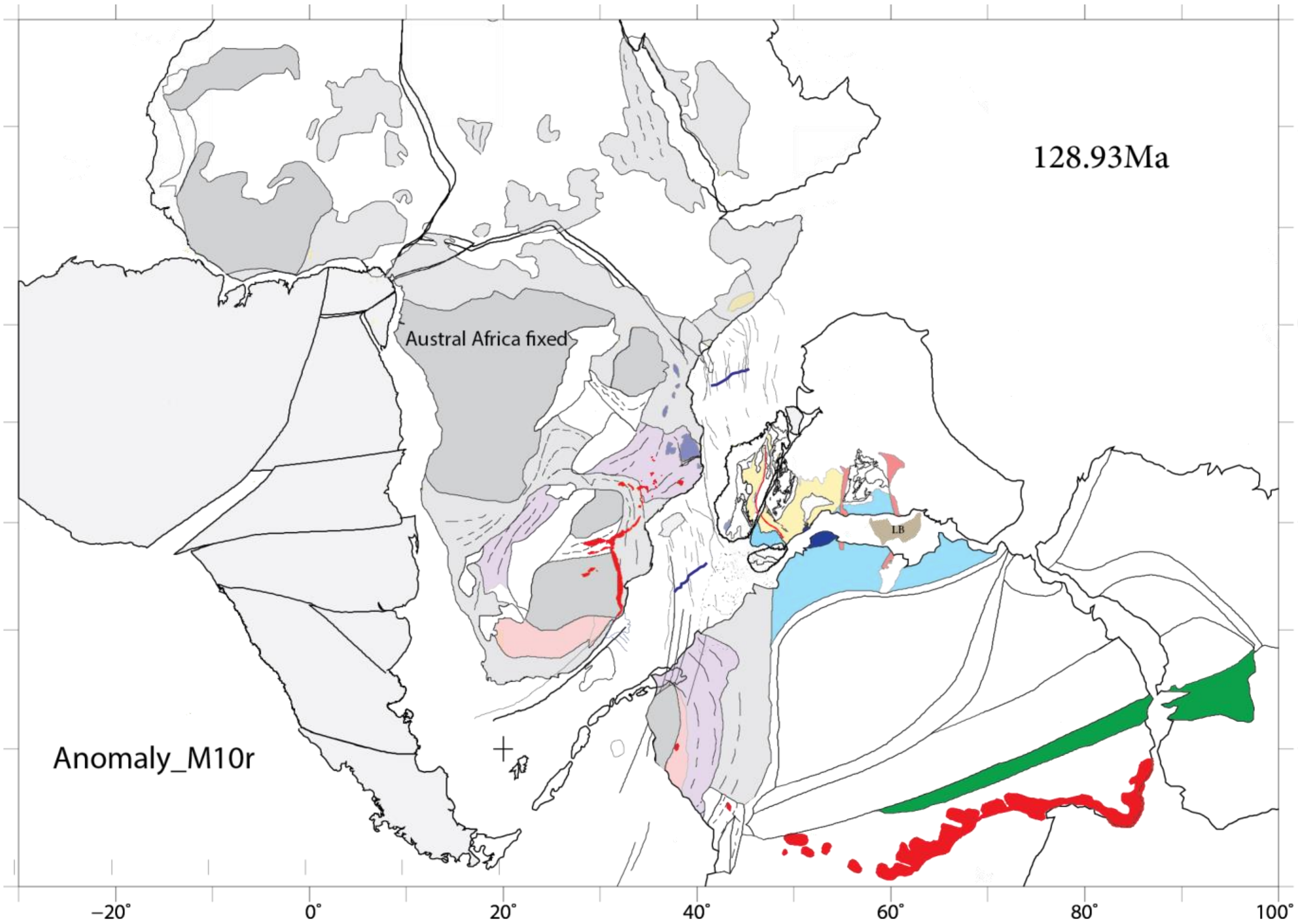

Figure 90: Reconstruction of the Indian Ocean at anomaly at M10r (128.93Ma). This period saw large scale plate reorganisation in the Indian Ocean, leading to the formation of Curvier, Perth and Gascogne basins on the northwestern Australian margin (Veevers et al., 1988), and breakup of the South Atlantic Ocean the formation of the first oceanic crust in the North Natal Valley. EB: Elan Bank (Mercator projection).

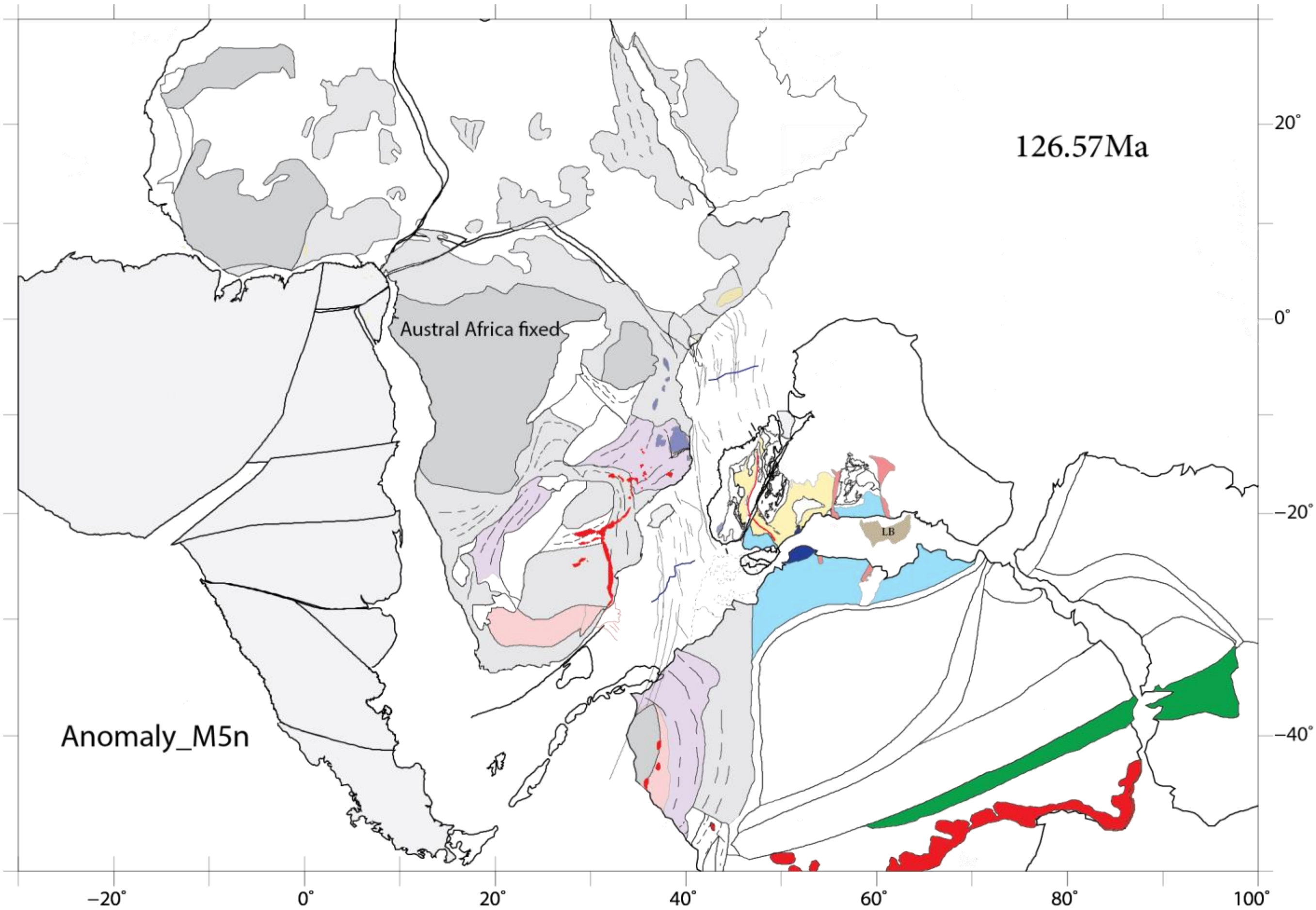

Figure 91: Reconstruction of the Indian Ocean at anomaly at M5 (126.57Ma). (Mercator projection).

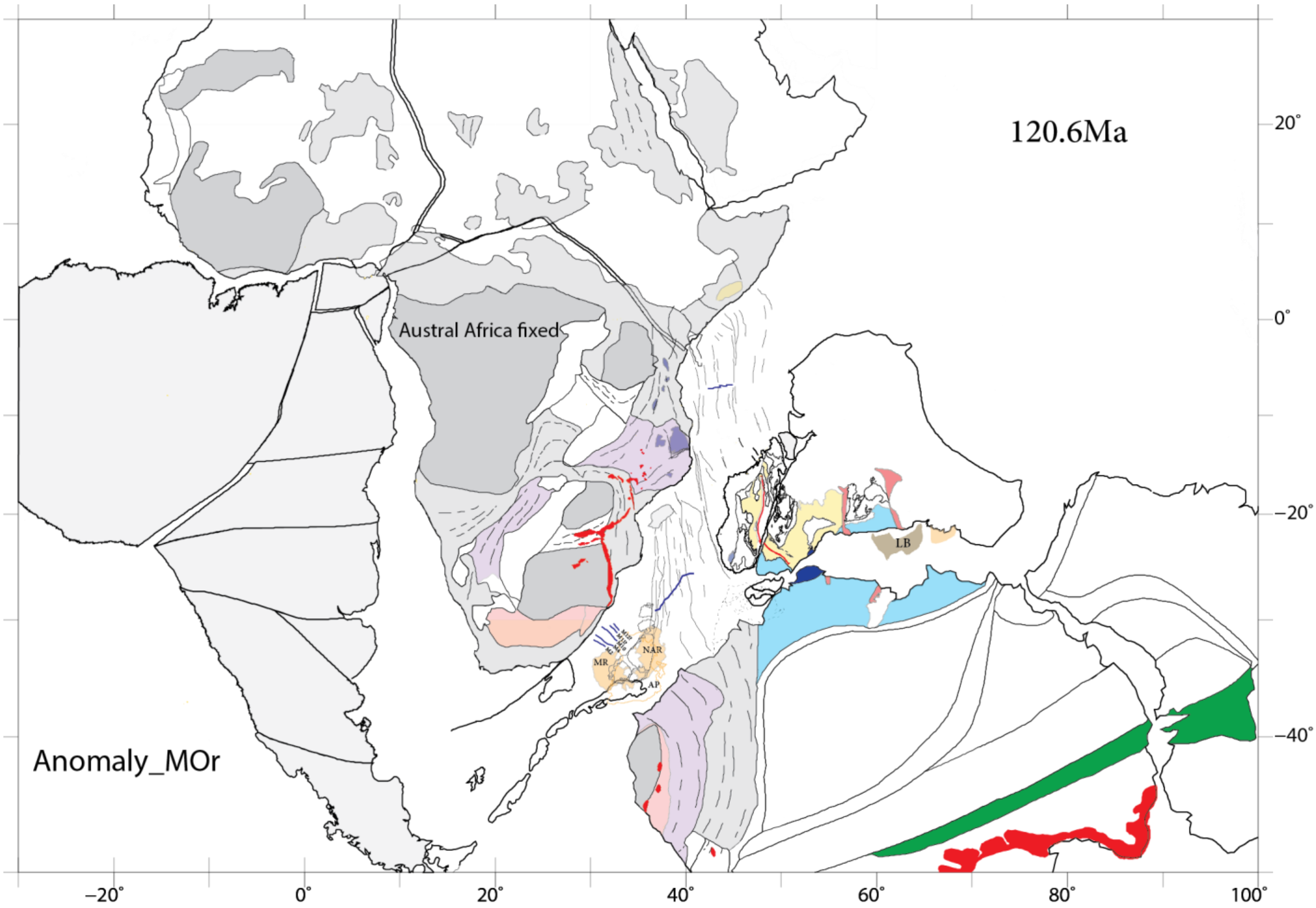

Figure 92: Reconstruction of the Indian Ocean at anomaly at M0r (120.6Ma). The Madagascar-Greater India-Sri Lanka block stopped its southward drift from Africa at M0. The accretion in the Curvier, Perth and Gascogne basins also stopped at M0. The South Mozambique Ridge, Maud Rise, Aqulhas Plateau, and northern part of the Astrid Ridge these four ridges overlap at the Southern Mozambique Ridge at M0, which means they may hve emplaced during tht time, possibly due to anormalous volcanism. The North Kerguelen Plateau may have been initiated around this time. (Mercator projection).

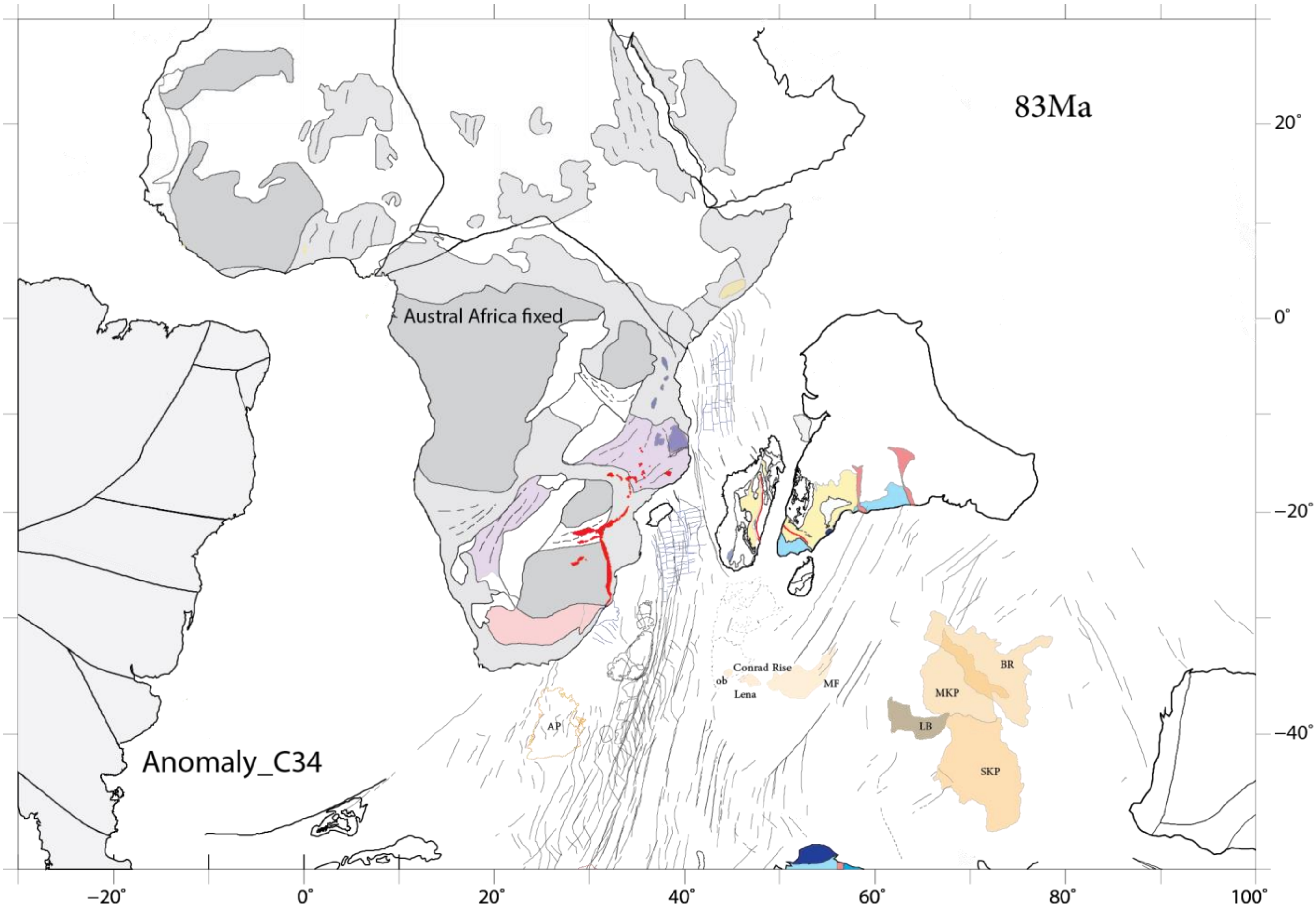

Figure 93: Reconstruction of the Indian Ocean at anomaly C34 (83Ma). Breakup and first oceanic recorded between Madgascar and India, and Australia and Antarctica. Anomalous oceanic plateaus (Conrad Rise, Crozet Ridge, Del Cano Rise and the South Madagascar Ridge) became emplaced during this period. The Del Cano Rise is a companion feature of the southern Madagascar according to Goslin et al., 1981. The Middle Kerguelen Plateau and the Broken Ridge were emplaced around this time. AP: Agulhas Plateau; BR: Broken Ridge; CB: Crozet Bank; CKP: Central Kerguelen Plateau; DCR: Del Cano Rise; LR: Chagos- Laccadive; LA: La Réunion; M: Mauritius; MP: Mascarene Plateua; N: Nazareth Plateau; SB: Saya de Malha Bank; NKP: North Kerguelen Plateau; South Kerguelen Plateau; SP: Seychelles Plateau. (Mercator projection).

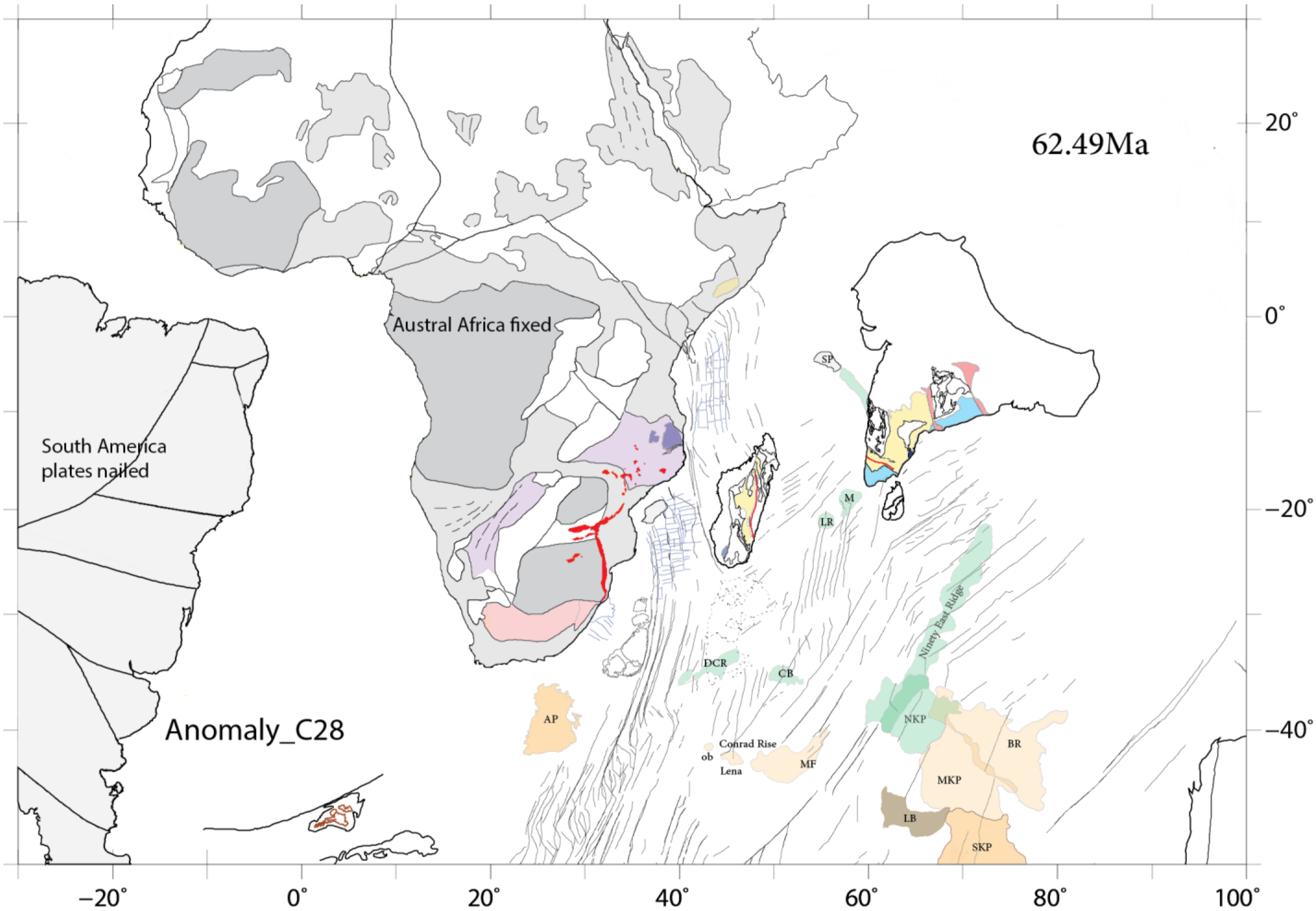

Figure 94: Reconstruction of the Indian Ocean at anomaly C28 (62.49Ma). The Mascarene Basin stopped its accretion at C27, and a ridge jump initiated seafloor spreading between Seychelles and India at C27. The Chagos- Laccadive (LR), the Ninetyeast Ridges, North Kerguelen Plateau may have been emplaced during this period. AP: Agulhas Plateau; BR: Broken Ridge; CB: Crozet Bank; CKP: Central Kerguelen Plateau; DCR: Del Cano Rise; LR: La Réunion; M: Mauritius; MP: Mascarene Plateua; N: Nazareth Plateau; SB: Saya de Malha Bank; NKP: North Kerguelen Plateau; South Kerguelen Plateau; SP: Seychelles Plateau. (Mercator projection).

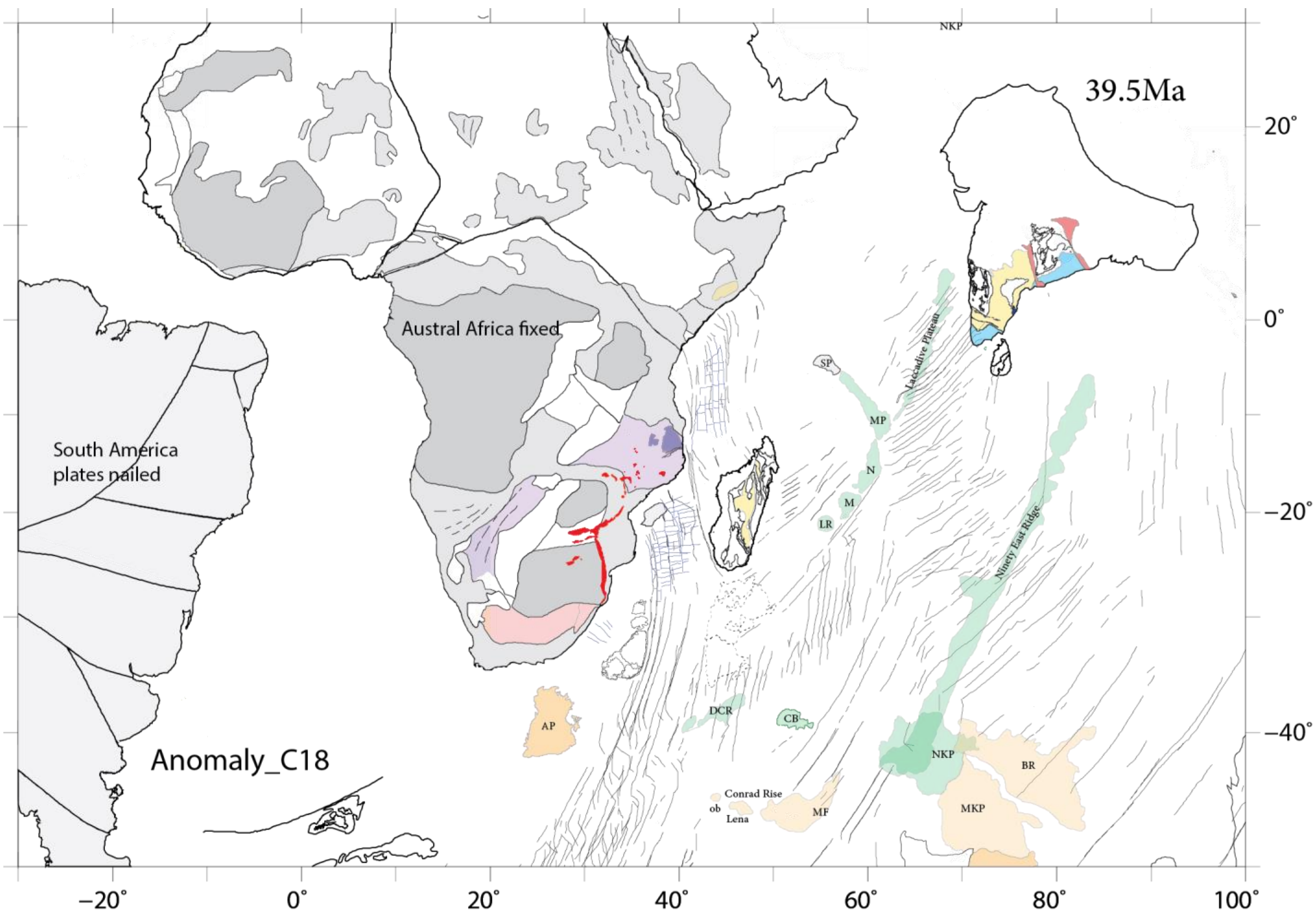

Figure 95: ***Reconstruction of the Indian Ocean at anomaly C18 (39.5Ma). formation of first oceanic crust between Arabia and Africa. AP: Agulhas Plateau; BR: Broken Ridge; CB: Crozet Bank; CKP: Central Kerguelen Plateau; DCR: Del Cano Rise; LR: Chagos- Laccadive; LA: La Réunion; M: Mauritius; MP: Mascarene Plateua; N: Nazareth Plateau; SB: Saya de Malha Bank; NKP: North Kerguelen Plateau; South Kerguelen Plateau; SP: Seychelles Plateau. (Mercator projection)***

-

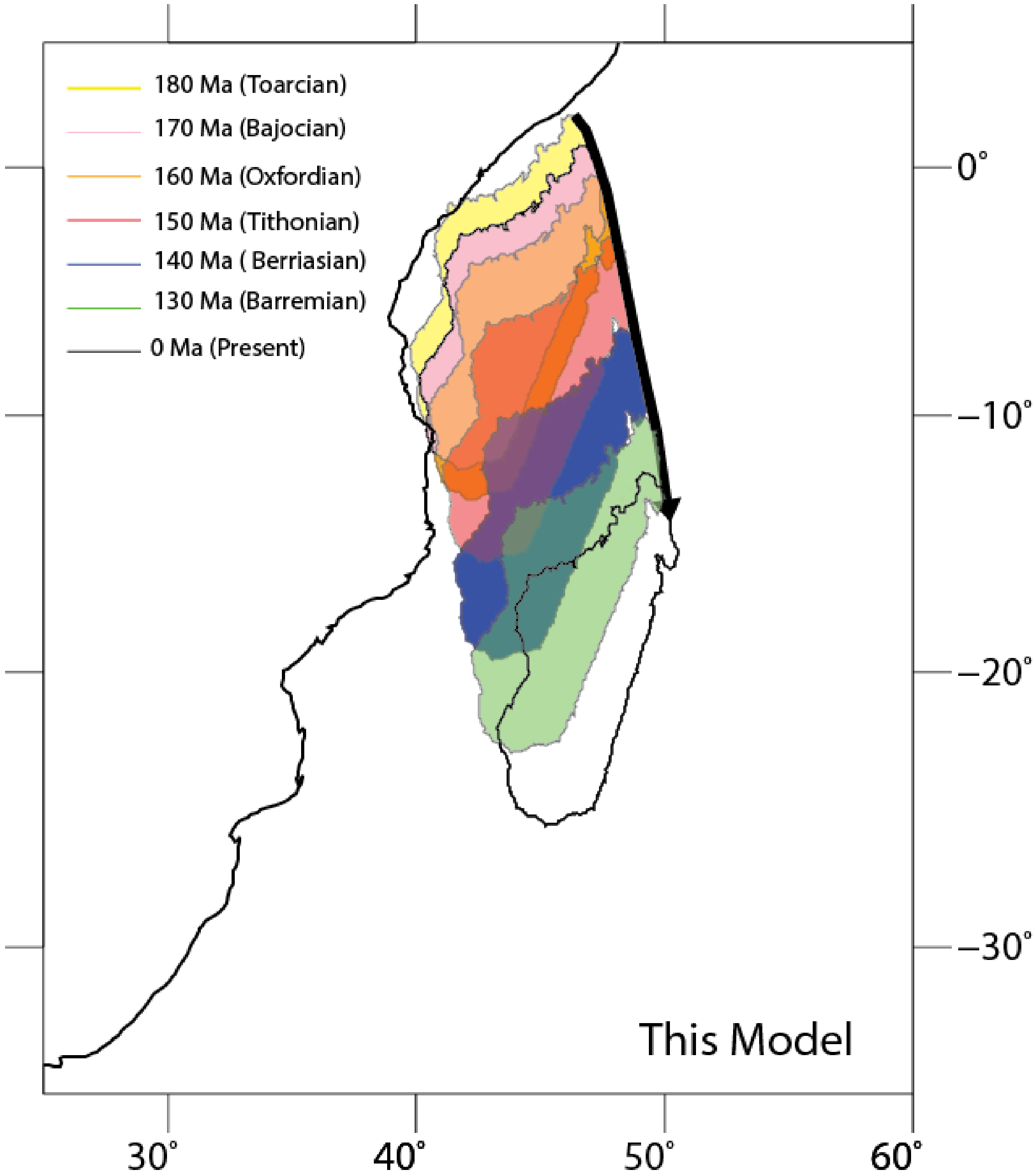

Figure 96: Map showing the evolution of the Madagascar in our model from fit to present position. (Mercator projection).

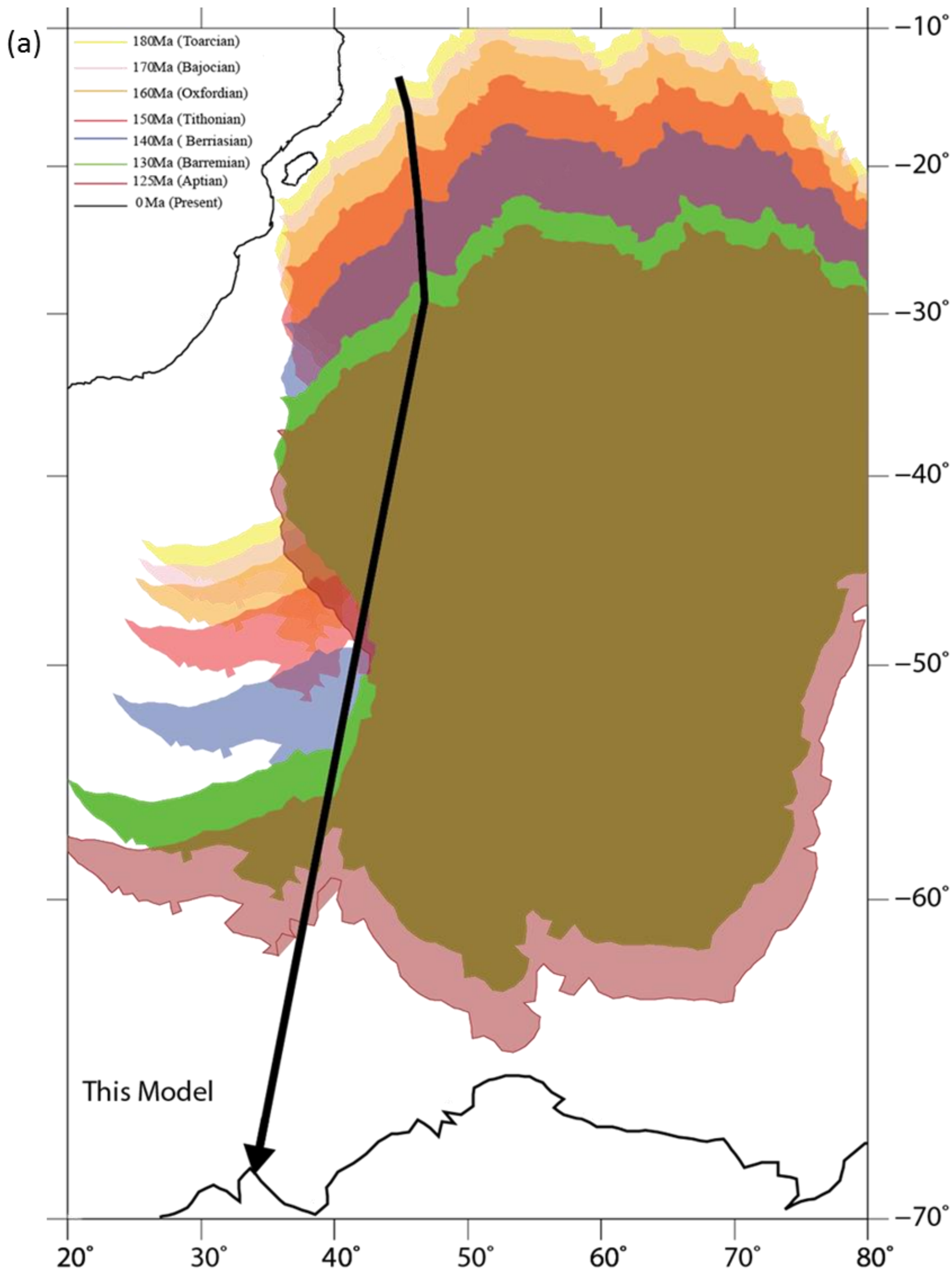
(a)
180Ma (Toarcian)
170Ma (Bajocian)
160Ma (Oxfordian)
150Ma (Tithonian)
140Ma (Berriasian)
130Ma (Barremian)
125Ma (Aptian)
0 Ma (Present)
This Model
−10°
−20°
−30°
−40°
−50°
−60°
−70°
20°
30°
40°
50°
60°
70°
80°

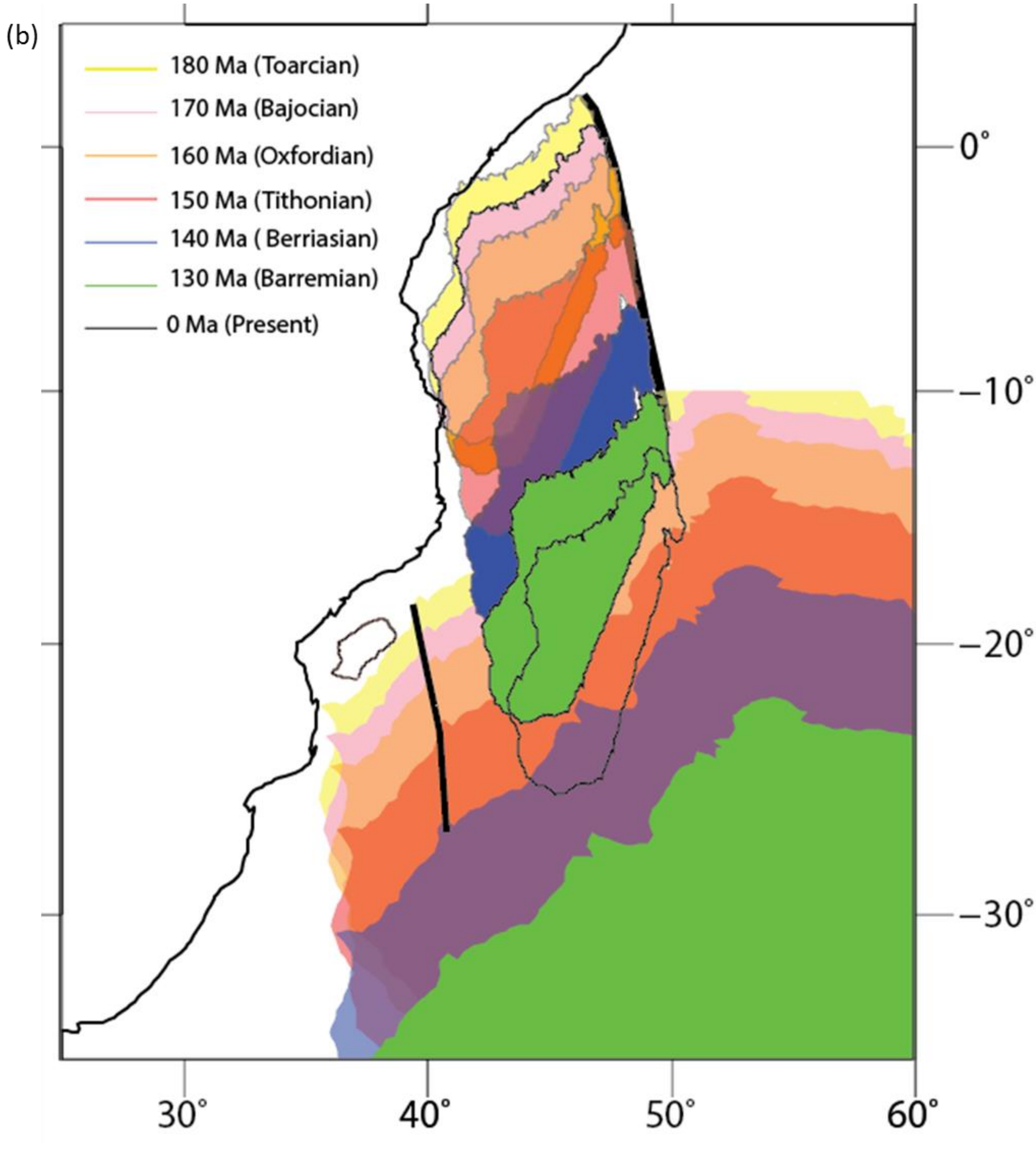

Figure 97: (a) Map showing the evolution of the Antarctica in our model from fit to present position. (b) Comparism of the evolution of the Antarctica and Madagascar in our model (Mercator projection).

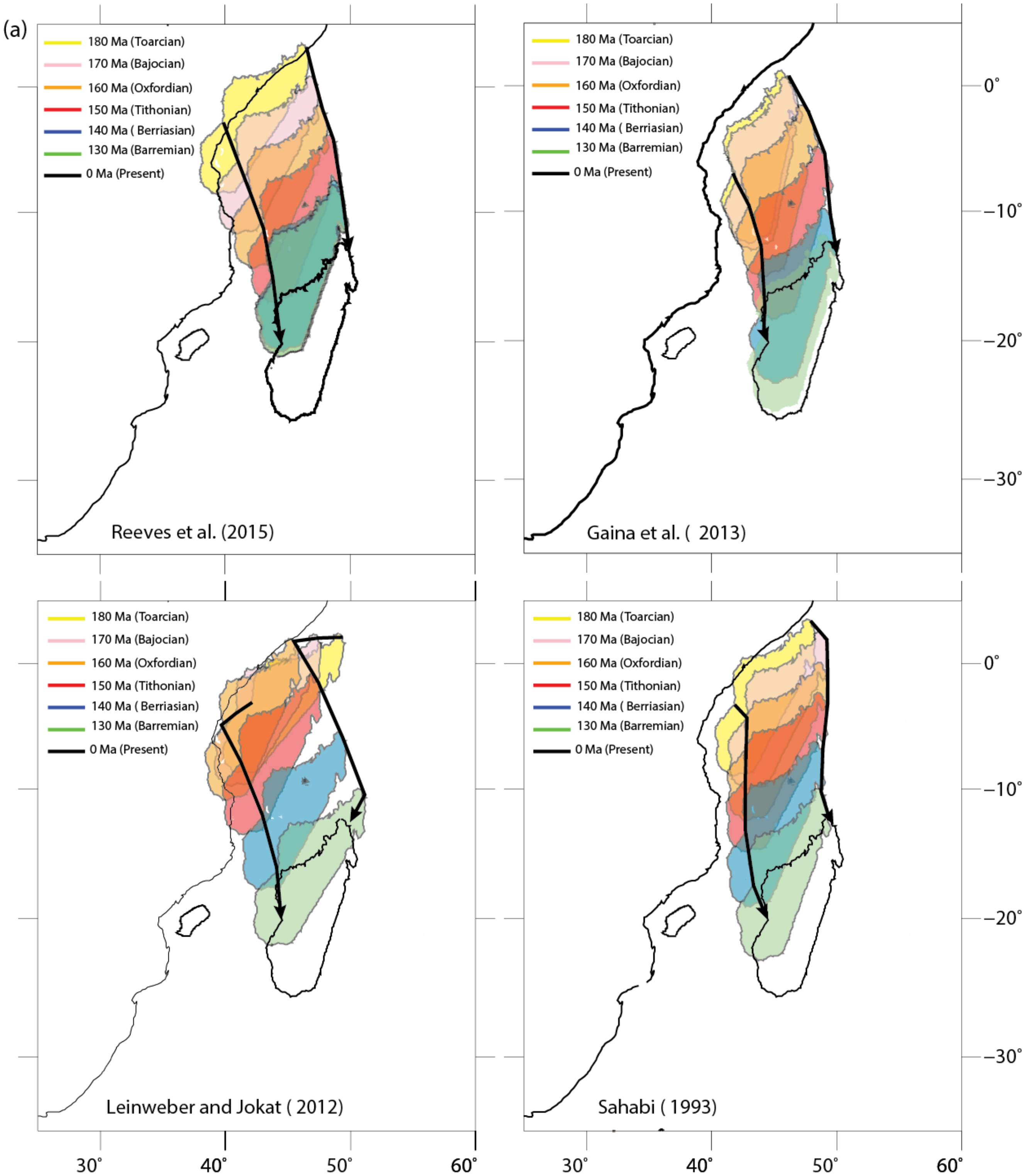
(a)
180 Ma (Toarcian)
170 Ma (Bajocian)
160 Ma (Oxfordian)
150 Ma (Tithonian)
140 Ma (Berriasian)
130 Ma (Barremian)
0 Ma (Present)
Reeves et al. (2015)
Gaina et al. (2013)
Leinweber and Jokat (2012)
Sahabi (1993)
0°
−10°
−20°
−30°
30°
40°
50°
60°

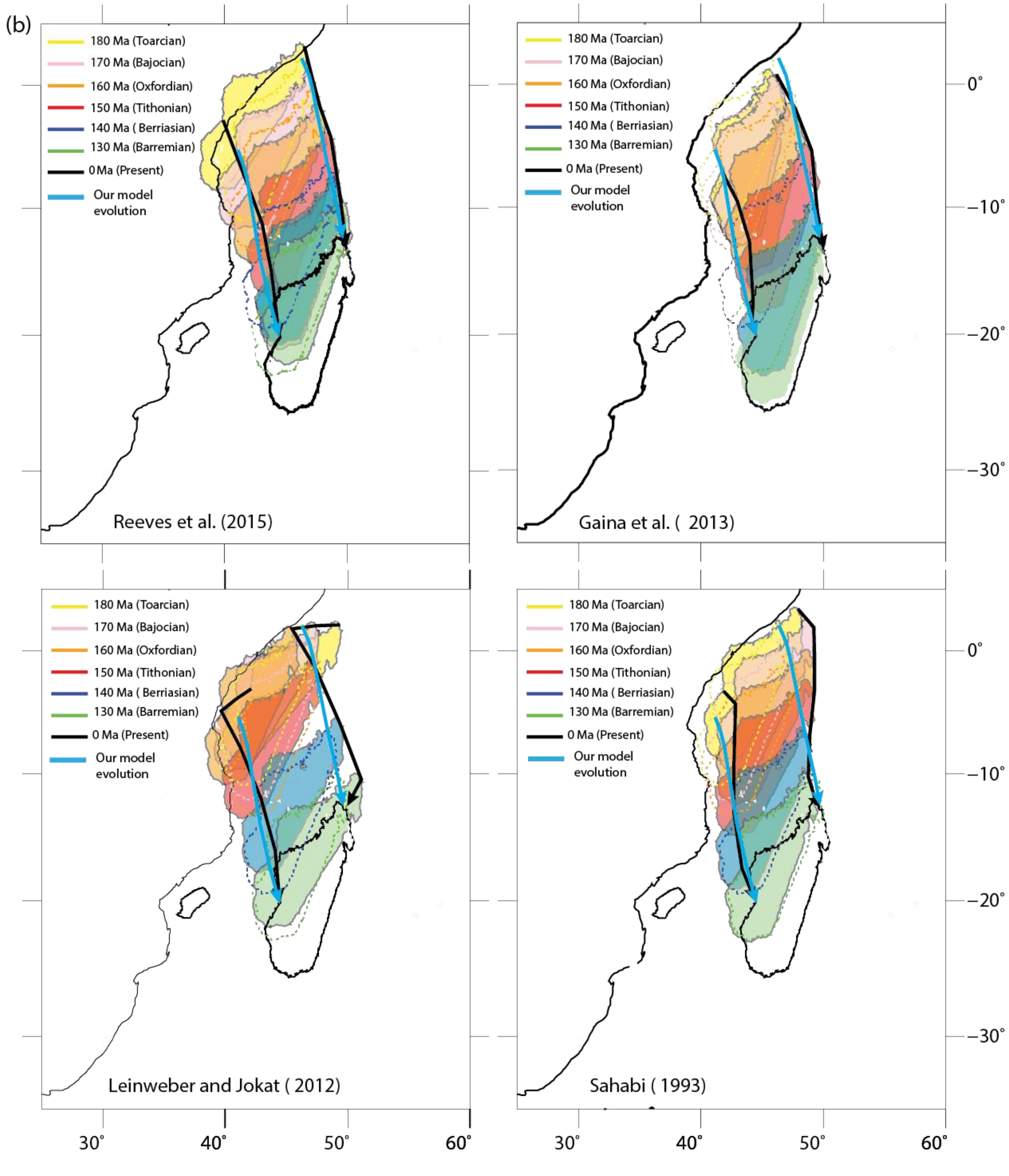

Figure 98: (a) Map showing the evolution of Madagascar in (Reeves et al., 2015; Gain et al., 2013; Leinweber and Jokat, 2012; and Sahabi, 1993), compared in (b) with the evolution of Madagascar in our model. The black arrows indicate the direction of movement of the plates through time. Reeves et al., 2015 closest tour model. (Mercator projection).

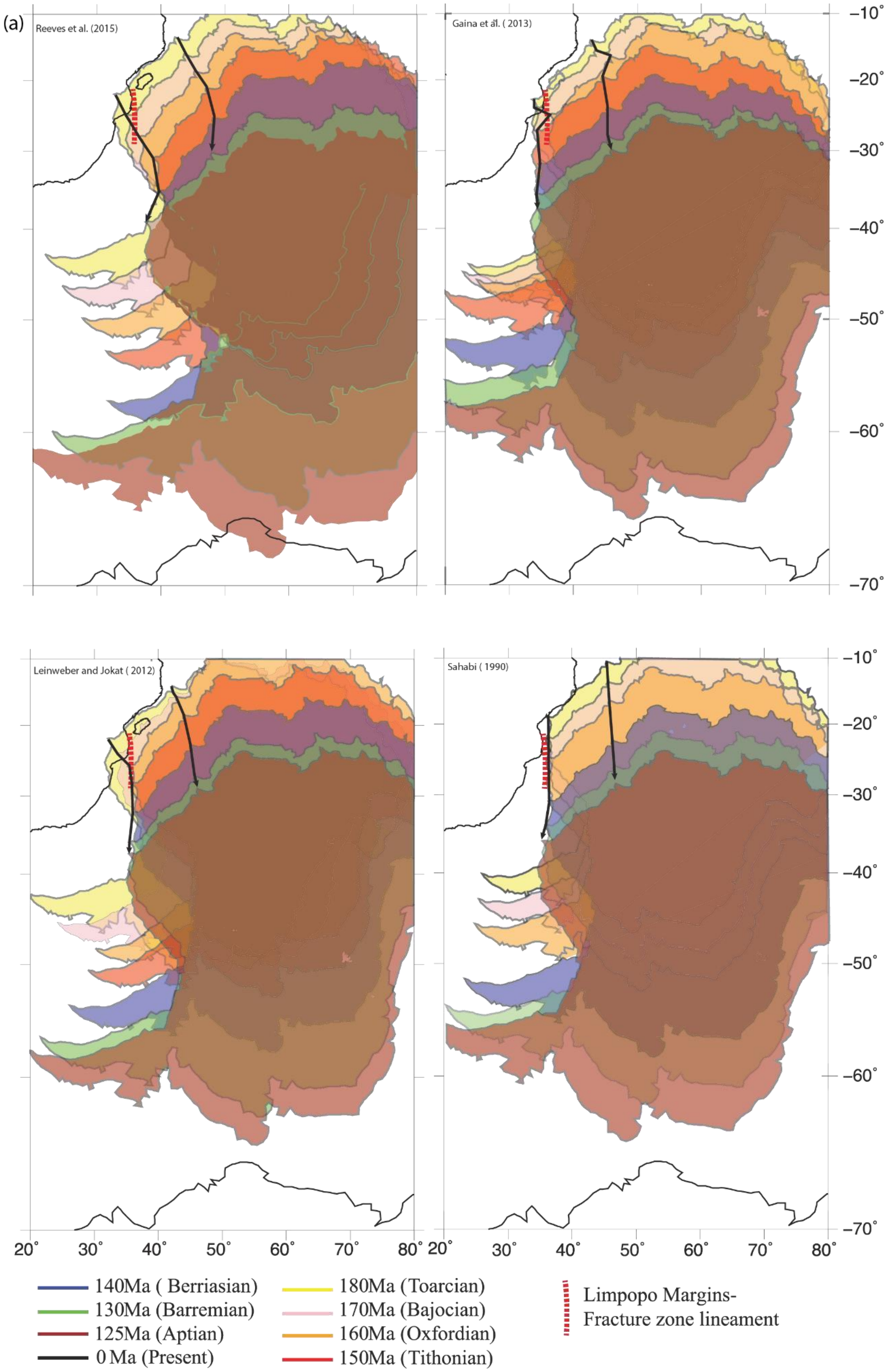

(a)
Reeves et al. (2015)
Gaina et al. (2013)
Leinweber and Jokat (2012)
Sahabi (1990)
−10°
−20°
−30°
−40°
−50°
−60°
−70°
20°
30°
40°
50°
60°
70°
80°
140Ma (Berriasian)
130Ma (Barremian)
125Ma (Aptian)
0 Ma (Present)
180Ma (Toarcian)
170Ma (Bajocian)
160Ma (Oxfordian)
150Ma (Tithonian)
Limpopo Margins-
Fracture zone lineament

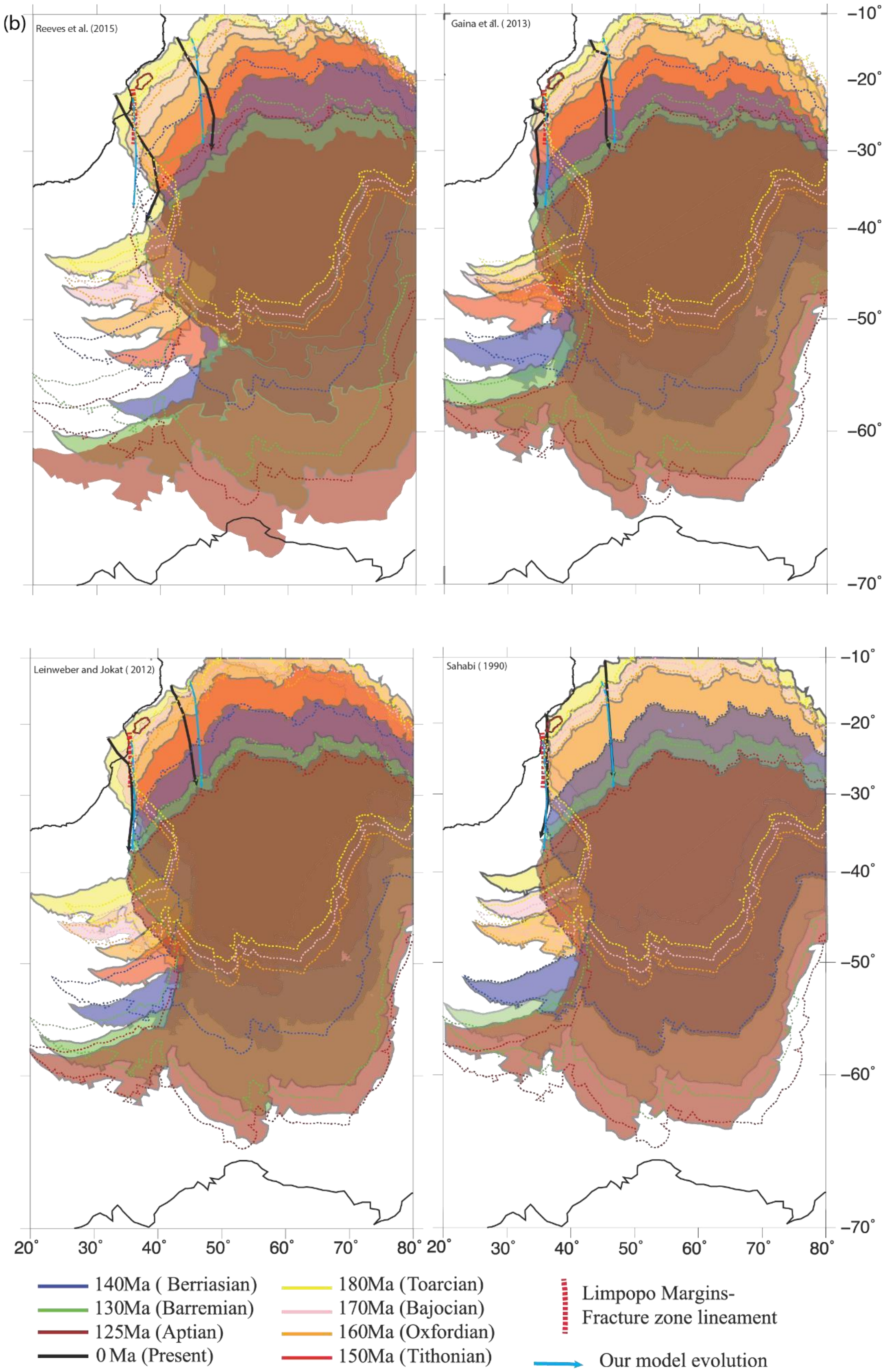

Figure 99: (a) Map showing the evolution of Antarctica in (Reeves et al., 2015; Gain et al., 2013; Leinweber and Jokat, 2012; and Sahabi, 1993), compared in (b) with the evolution of Antrctica in our model. The black arrows indicate the direction of movement of the plates through time in published models. Sahabi, 1993, closest to our model. (Mercator projection).

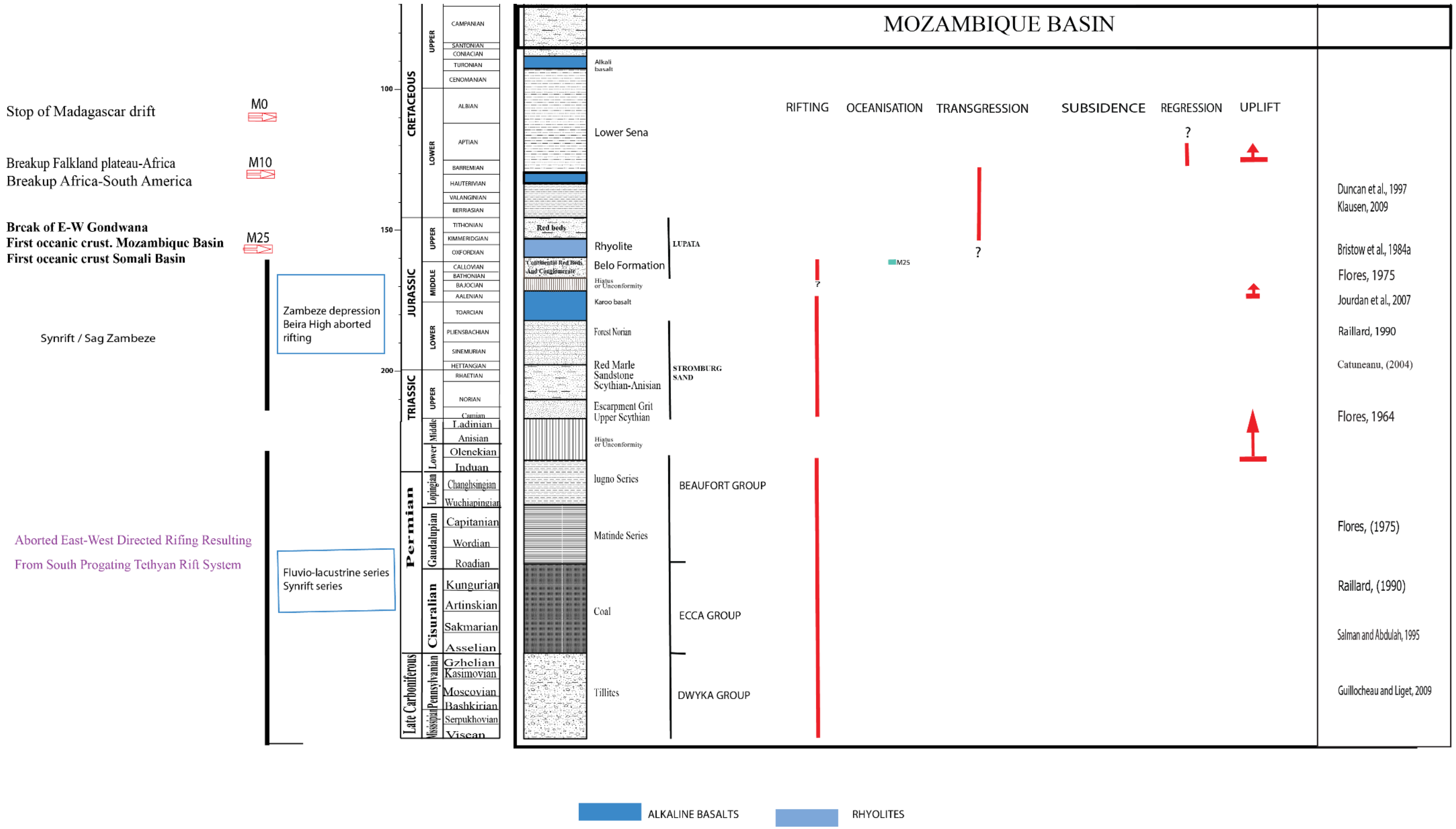

Figure 100: Reinterpretation of the lithostratigraphic and event chart in the Mozambique Basin (figure 55). We propose rifting may have continued until late-Middle Jurassic. This implies the Belo formation maybe is a synrift formation, as has previously proposed by [(Salazar et al., 2013 See figure 101)], and oceanization did not occur with the Karoo magmatic event (182-186), but was initiated around anomaly M25 in the early-Upper Jurassic (157Ma).

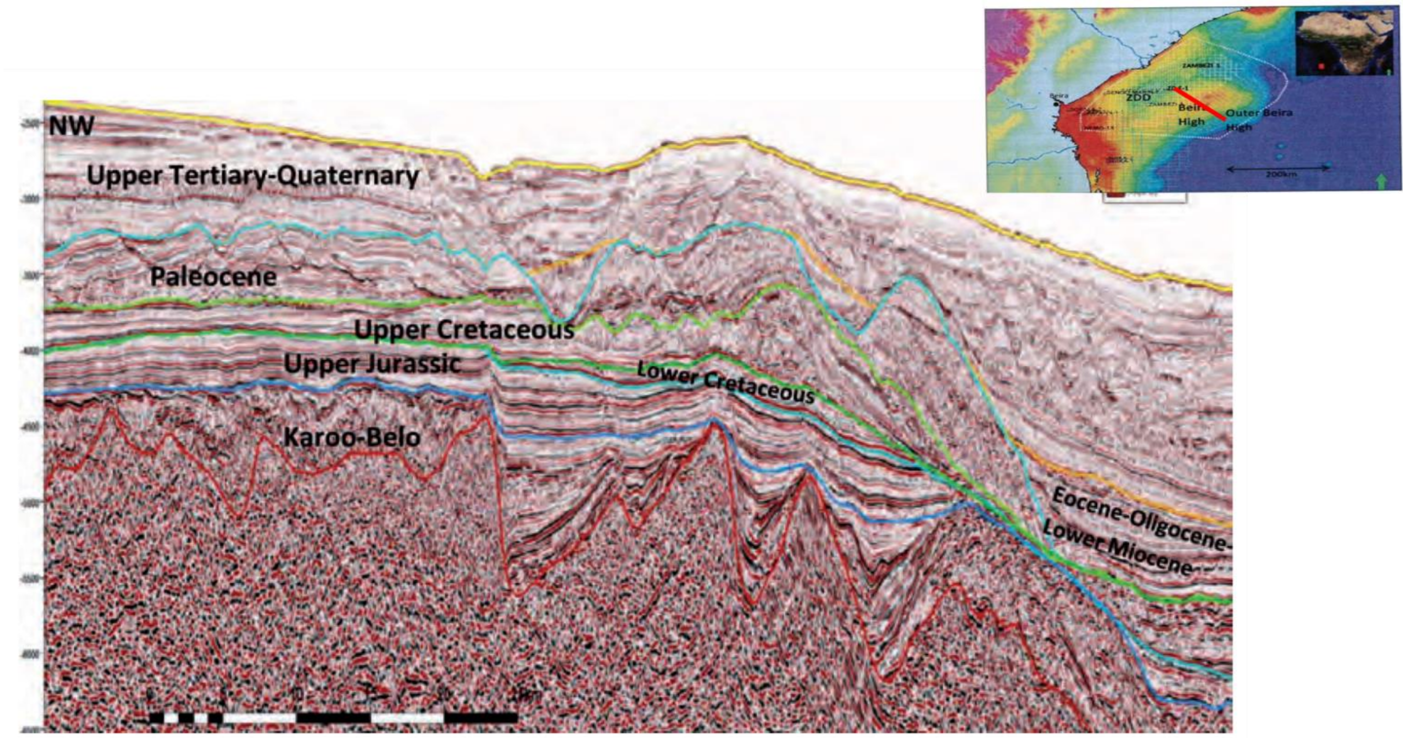

Figure 101:2D seismic reflection interpretation offshore Zambezi Basin by (Salazar et al., 2013). Notice the Karoo and the Belo Formation are interpreted as syn-rift formation. The insert above: location of the seismic lines use in their study.

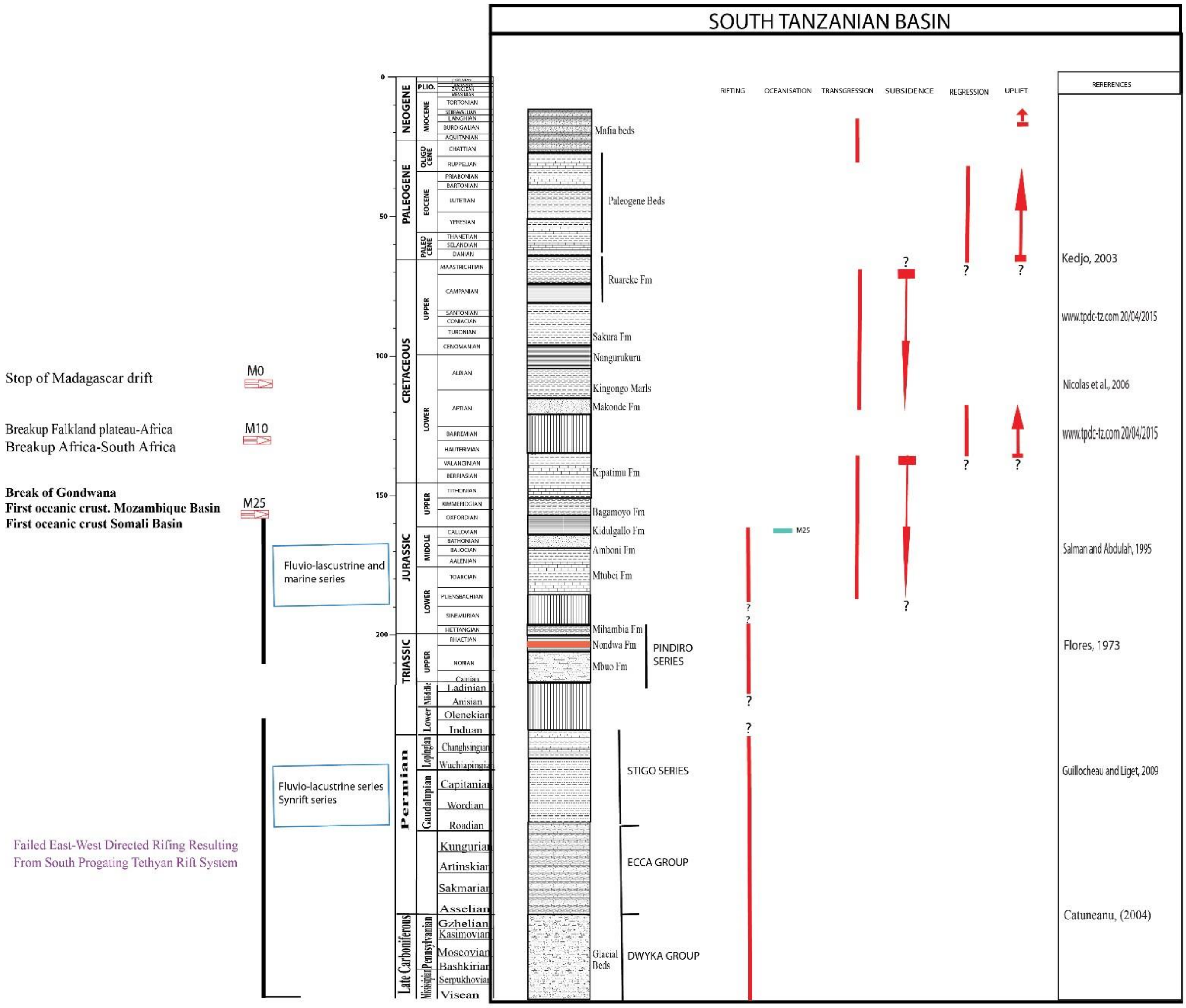

Figure 102: Reinterpretation of the lithostratigraphic and event chart in the South Tanzania Basin (figure 56). The rifting may have started in Triassic and ended in the Callovian, initiating breakup and oceanization onwards.

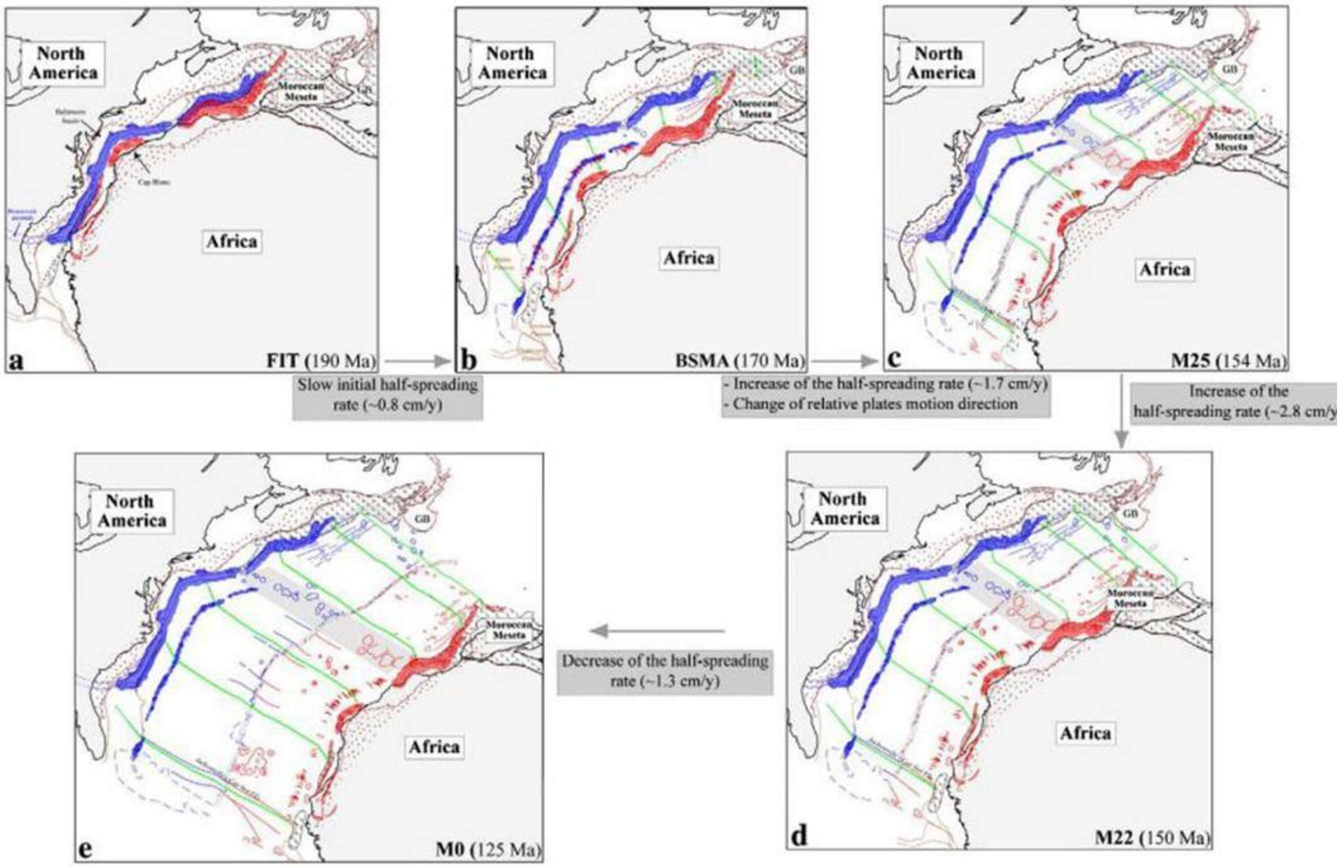

Figure 103: Labails et al. (2010), observed in the Central Atlantic a major change in direction of plate propagation from NW-SE to WNW-ESE. Notice the huge change in direction of propagation between BSMA and anomaly M25 (b and c).

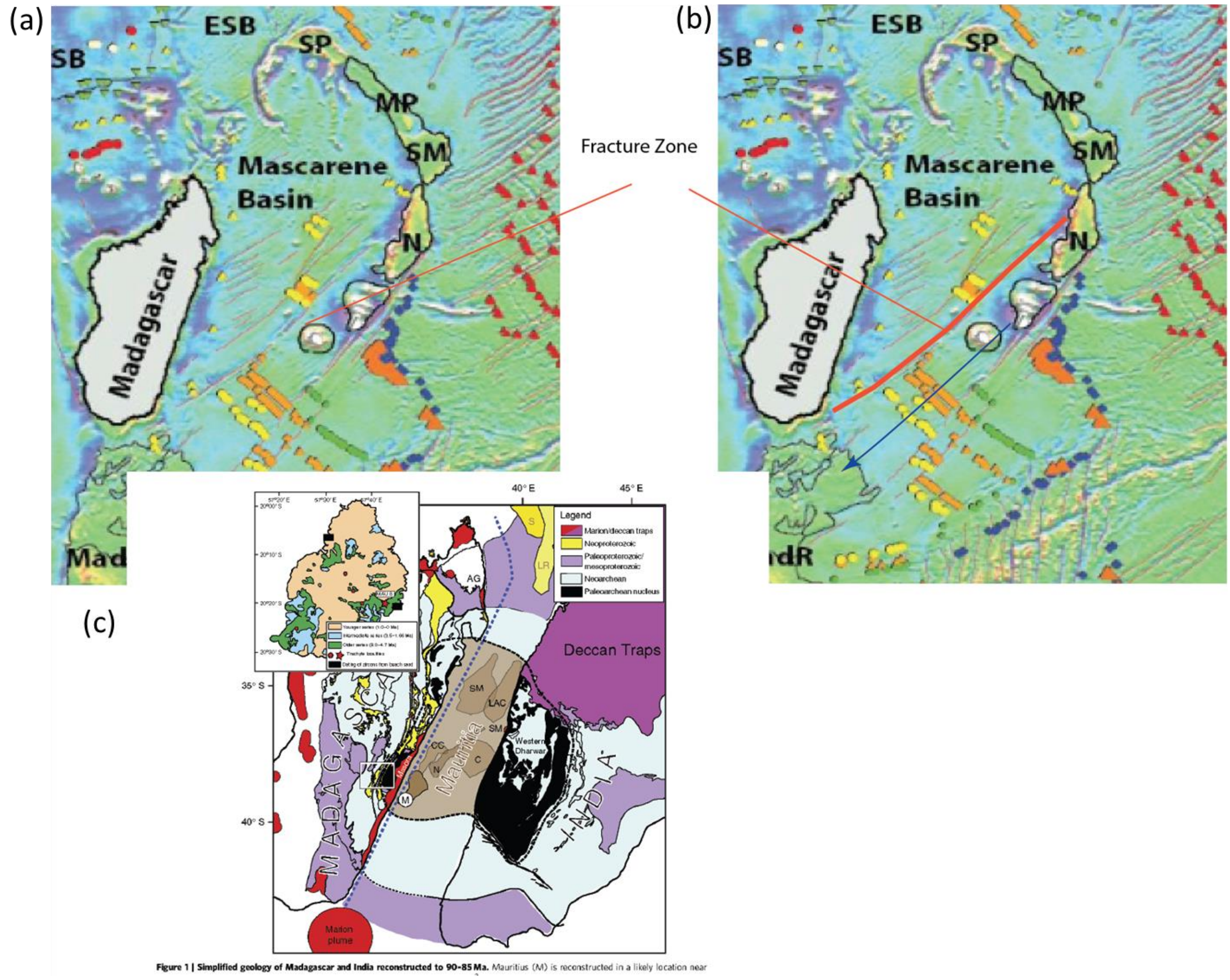

Figure 104:.(a) (c) Sandwell et al. (2014) free-air satellite-derived gravity anomaly of the Mascarene showing clear fracture zones between Madagascar and India. (b) Satellite-derived gravity anomaly of the Mascarene Basin The red lineindicate major fracture along which the India plate moved. (c) Reconstruction of Madagascar and India by Aswhal et al. (2016). They found Archaean zircons in Miocene oceanic hotspot rocks and establish ancient continental crust beneath Mauritius. They proposed the Mauritius continental plate bewteen Madagascar and India.

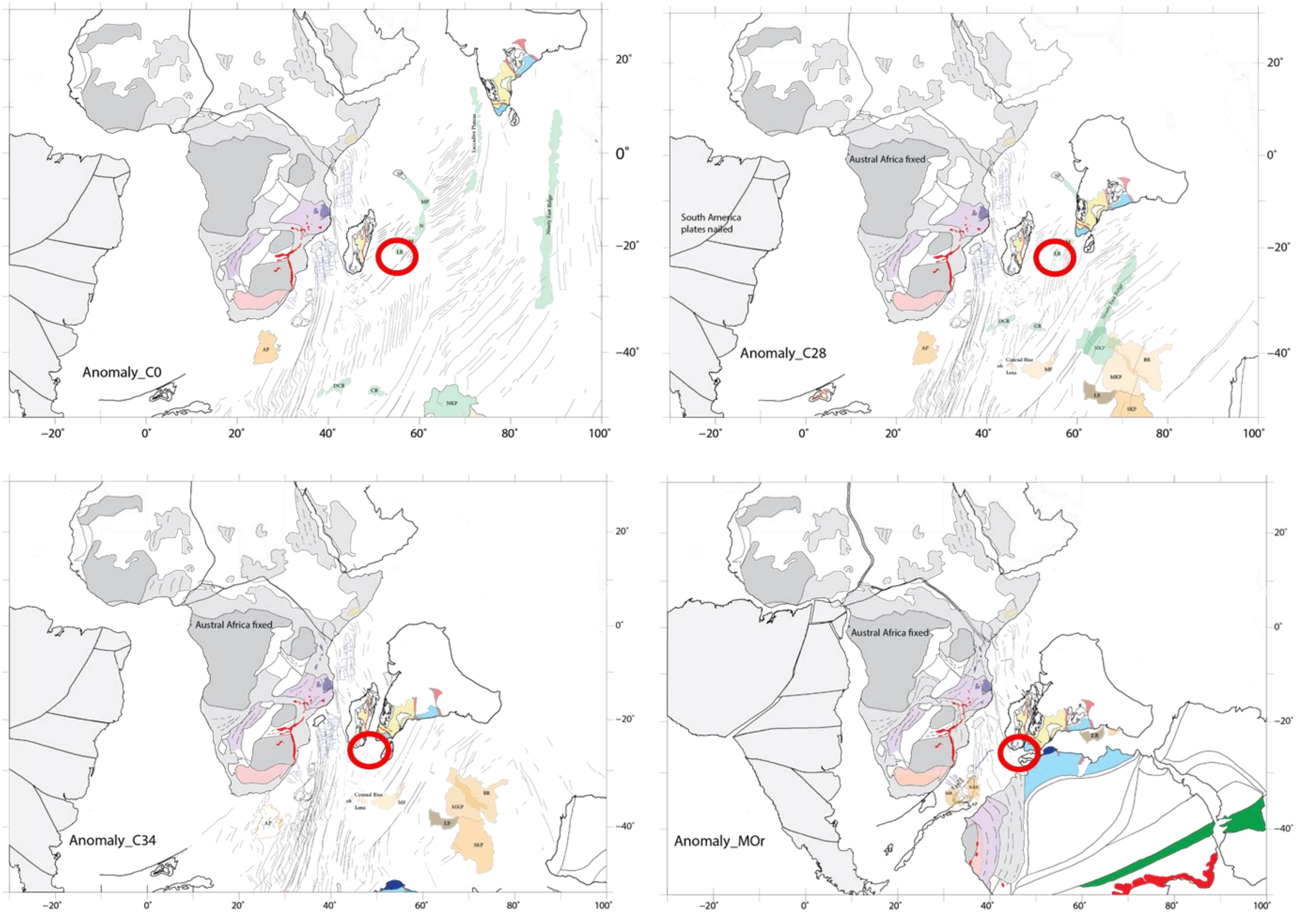

Figure 105:Map showing the reconstruction of India to Madagascar and the possible position of the Archaean zircons . The clear fracture zones between India and Madagascar indicates that the two plates separated from each other. Hence, the retrieve Archean rocks could well be fragments of India as it continued it drifting from Madagascar. (Mercator projection).

Table 1: Poles Antactica-Africa

Age	Latitude	Longitude	Rotation	Source
Ano18	13.6	-41.4	7.47	Bernard et al. (2005)
Ano23	8.5	-40.8	10.01	Bernard et al. (2005)
Ano28	11.3	-49.6	11.11	Bernard et al. (2005)
Ano32	-1.2	-42.4	12.38	Bernard et al. (2005)
Ano34	-1.3	-34.7	17.78	Bernard et al. (2005)
M0	11.72991	154.0759	-42.51146	This study
M5n	12.68688	154.0827	-44.66053	This study
M10r	9.705075	152.8902	-46.33414	This study
M15n	9.864203	153.7544	-50.71872	This study
M22n	8.271569	152.2943	-53.09270	This study
M25n	8.428259	152.0446	-55.43329	This study
Fit	8.969426	151.6038	-58.75505	This study

Table 2: Poles Madagascar-Africa

Age	Latitude	Longitude	Rotation	Source
Initial fit	9.384853	117.2845	-15.40567	This study
M25n	5.161909	110.0051	-12.69742	This study
M22n	2.188300	102.7732	-10.97189	This study
M15n	4.675859	97.03268	-8.123477	This study
M10r	3.488152	-98.77951	6.404223	This study
M5n	8.683980	-107.8003	5.789815	This study

M0r	0.000	0.000	0.000	

Table 3: Poles India-Africa

Age	**Latitude**	**Longitude**	**Rotation**	**Source**
Ano5	22.1900	33.4100	-4.7100	Eagles and Hoang (2013).
Aoo18	16.2000	48.4700	-25.2400	Eagles and Hoang (2013).
Ano21	17.8400	44.4200	-25.7700	Eagles and Hoang (2013).
Ano22	18.1100	42.3000	-27.2100	Eagles and Hoang (2013).
Ano24	18.4800	37.8600	-29.9500	Eagles and Hoang (2013).
Ano25	18.5300	33.6600	-34.4300	Eagles and Hoang (2013).
Ano26	19.1200	31.6200	-35.9000	Eagles and Hoang (2013).
Ano27	20.1500	28.4900	-38.0500	Eagles and Hoang (2013).
Ano28	21.6700	25.8200	-39.8000	Eagles and Hoang (2013).
Ano31	22.6100	24.0400	-45.1600	Eagles and Hoang (2013).
Ano32	22.4900	24.2200	-47.5200	Eagles and Hoang (2013).
Ano34	22.4300	24.9600	-53.6300	Eagles and Hoang (2013).
M0r	22.22783	24.40480	-56.71661	This study
M5n	22.16459	29.60182	-60.14409	This study
M10r	23.17356	30.41119	-60.07137	This study
M15n	25.46677	32.16216	-59.68924	This study
M22n	26.59191	35.30000	-59.83694	This study
M25n	28.44201	36.86446	-59.31655	This study
Fit	31.31943	38.96307	-58.86290	This study

Table 4: Poles Australia-Africa

Age	Latitude	Longitude	Rotation	Source
AnoO	O.000	O.000	O.000	This study
Ano18	16.30318	50.92139	-22.41163	This study
Ano28	10.92827	61.22190	-26.94301	This study
Ano34	16.90723	75.47579	-27.48594	This study
M0	24.73430	107.5313	-41.06655	This study
M5n	26.15952	109.5644	-42.60602	This study
M10r	23.21838	111.0177	-44.40272	This study
M15n	24.13406	115.6568	-47.28139	This study
M22n	22.52906	116.5607	-49.91948	This study
M25n	22.88478	118.0439	-51.93749	This study
Fit	23.67146	119.8226	-54.90728	This study

Table 5: Poles Sri Lanka-Africa.

Age	Latitude	Longitude	Rotation	Source
M0r	10.11700	42.55943	-81.32627	This study
M5n	10.18472	45.66046	-85.58115	This study
M10r	10.99839	46.09781	-85.72527	This study
M15n	12.82913	47.08052	-85.77724	This study
M22n	2.044542	52.97449	-52.31302	This study
M25n	15.41446	49.81841	-86.50547	This study
Fit	17.65087	50.91434	-86.33724	This study

From anomaly C34 Sri Lanka together with India.

Table 6: Poles Seychelles-Africa.

Age	Latitude	Longitude	Rotation	Source
M0r	2.905783	-136.6054	45.91607	This study
M5n	2.311616	-133.3757	51.06846	This study
M10r	1.266099	-132.3603	51.14625	This study
M15n	1.030455	49.95525	-51.10443	This study
M22n	2.044542	52.97449	-52.31302	This study
M25n	3.771343	55.01324	-52.15144	This study
Fit	6.548114	57.69930	-52.07016	This study

Seychelles move India after the separation of India and Madagascar until the final drift at anomaly C28.

Table 7: Poles Falkland-Africa

Age	Latitude	Longitude	Rotation	Source
Fit	46.92559	-33.09283	57.66492	This study

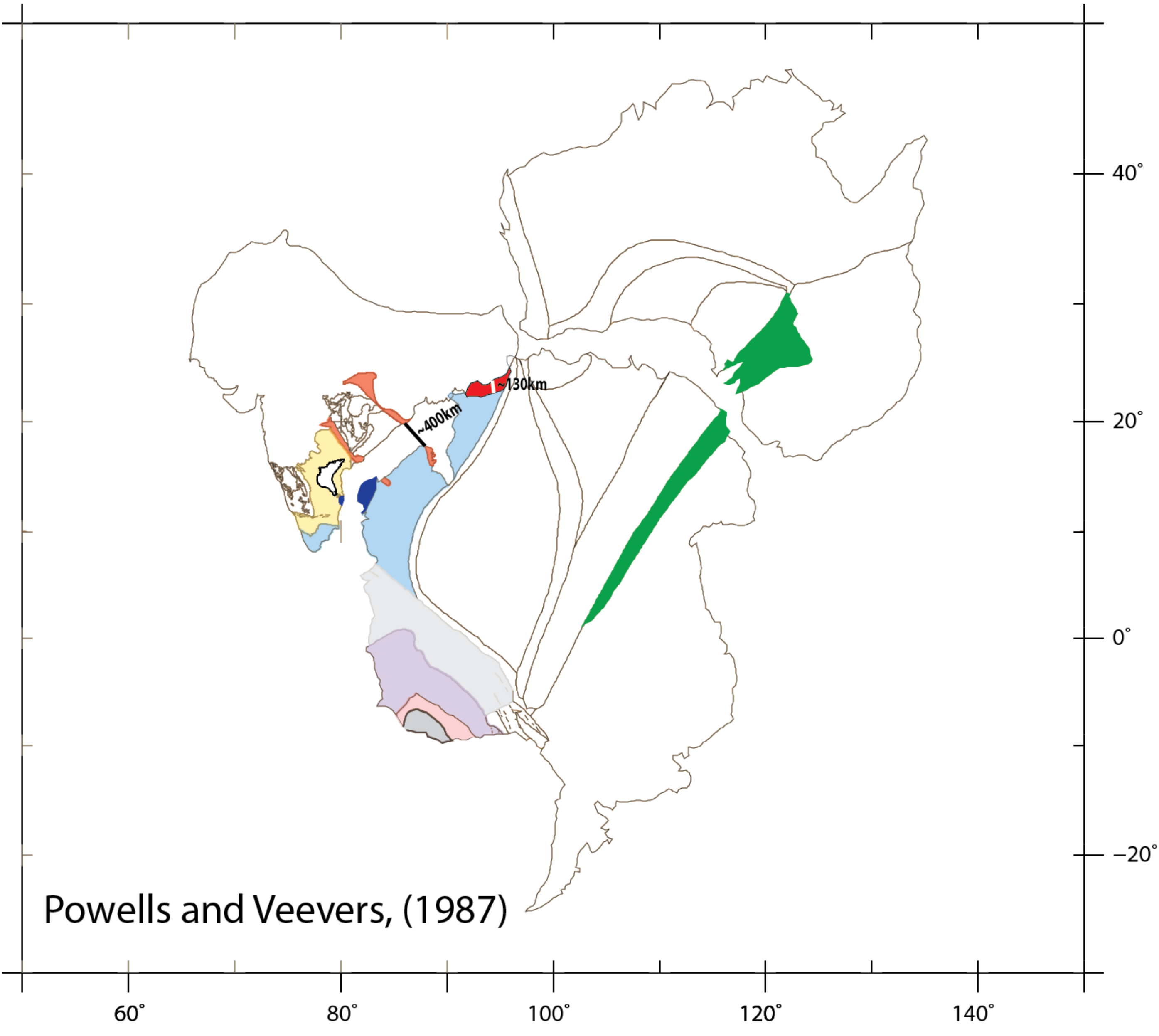

Figure 1: ***Reconstruction model of Powells and Veevers (1987). Mercator projection.***

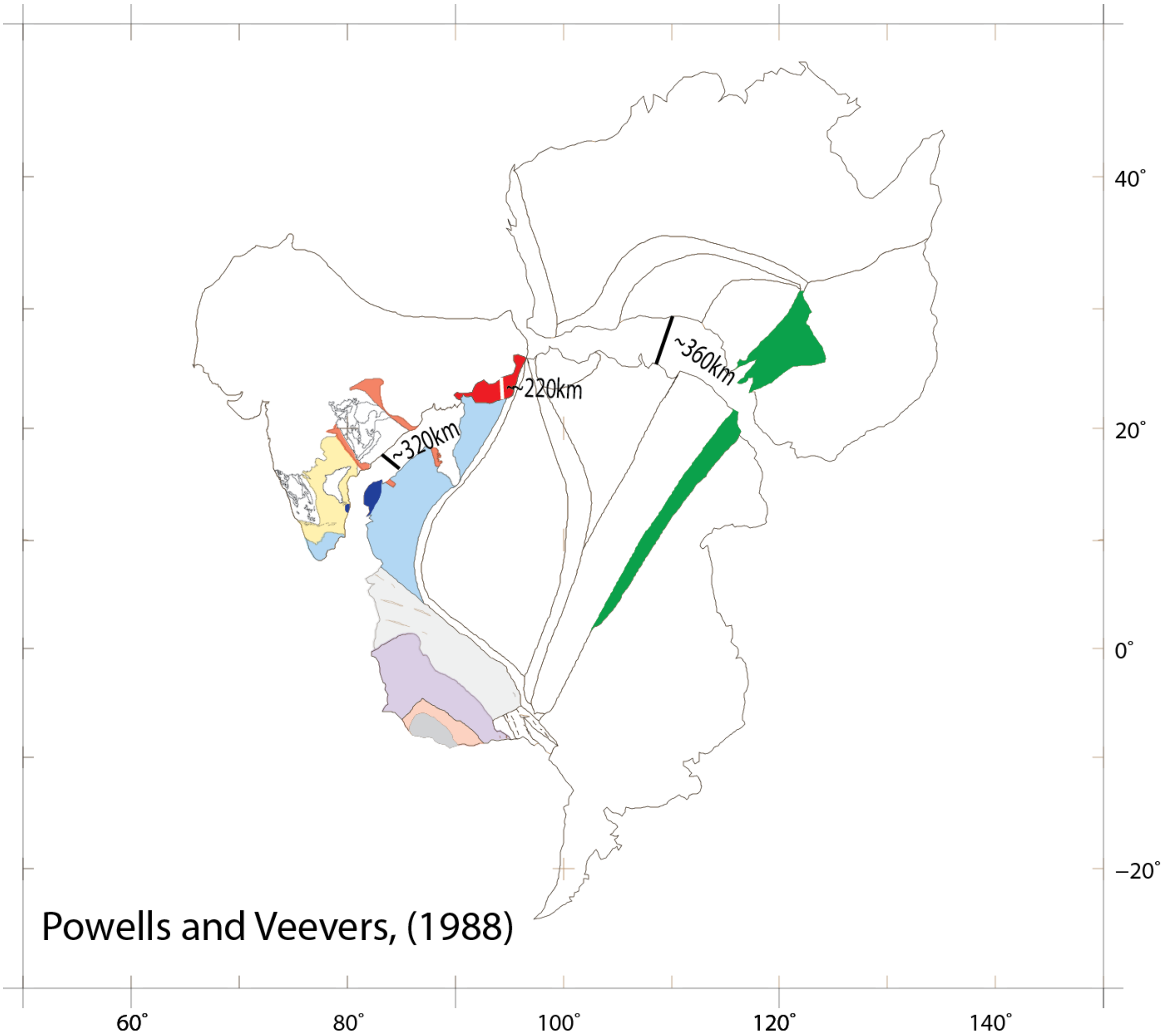

*Figure 2: **Reconstruction model of Powells and Veevers (1988). Mercator projection.***

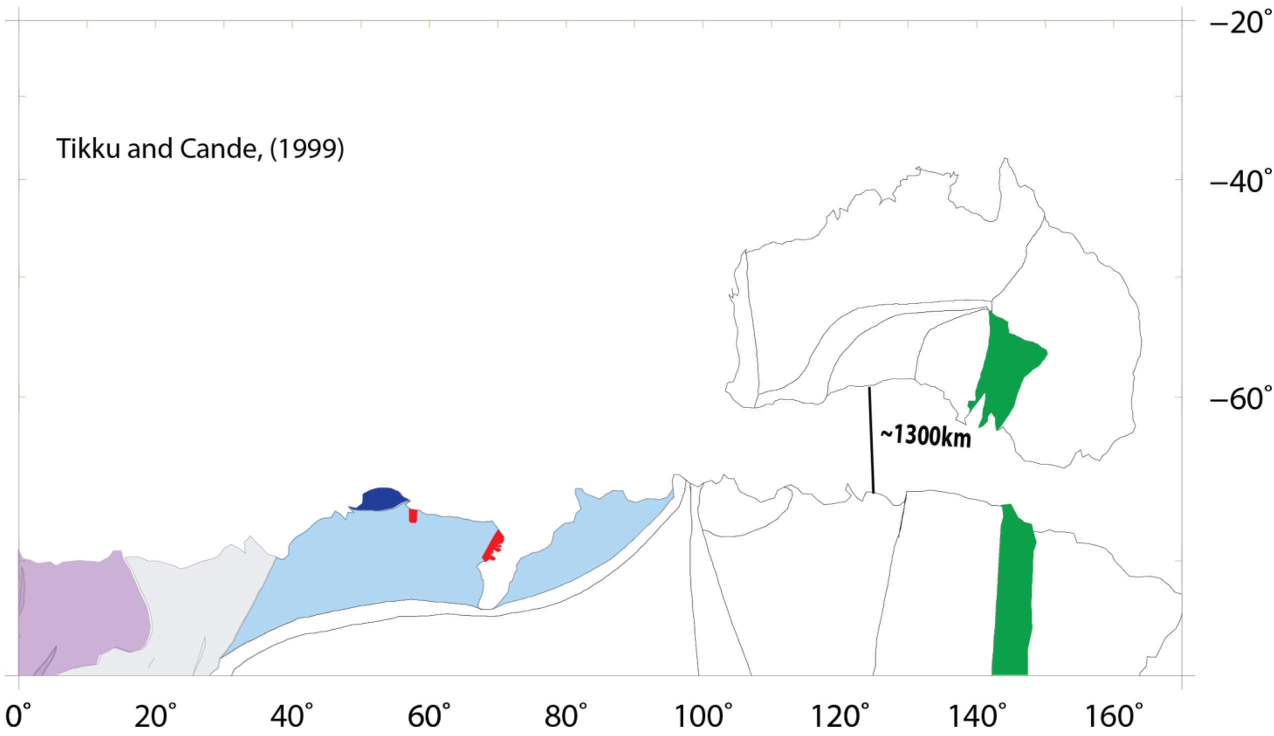

Figure 3: ***Reconstruction model of Tikku and Cande (1999). Mercator projection***

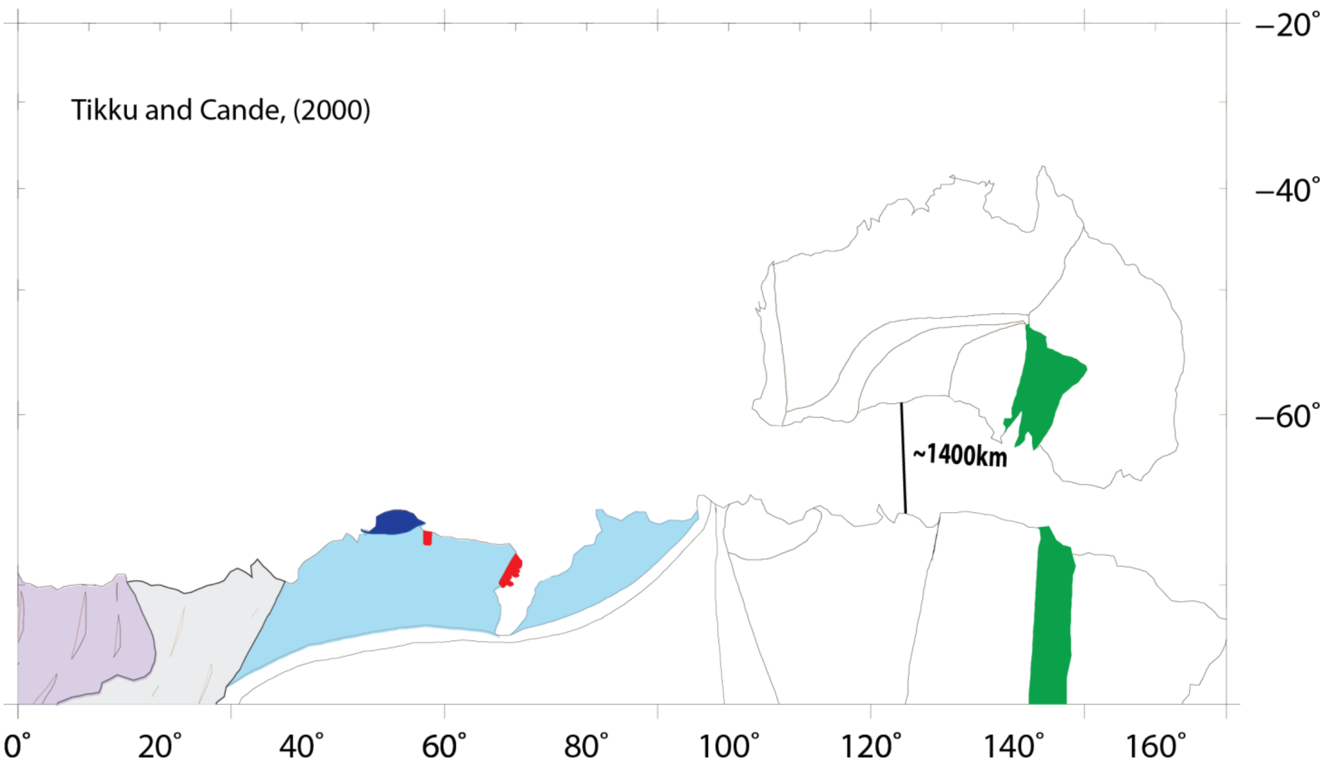

Figure 4: Reconstruction model of Tikku and Cande (2000). Mercator projection.

(a)

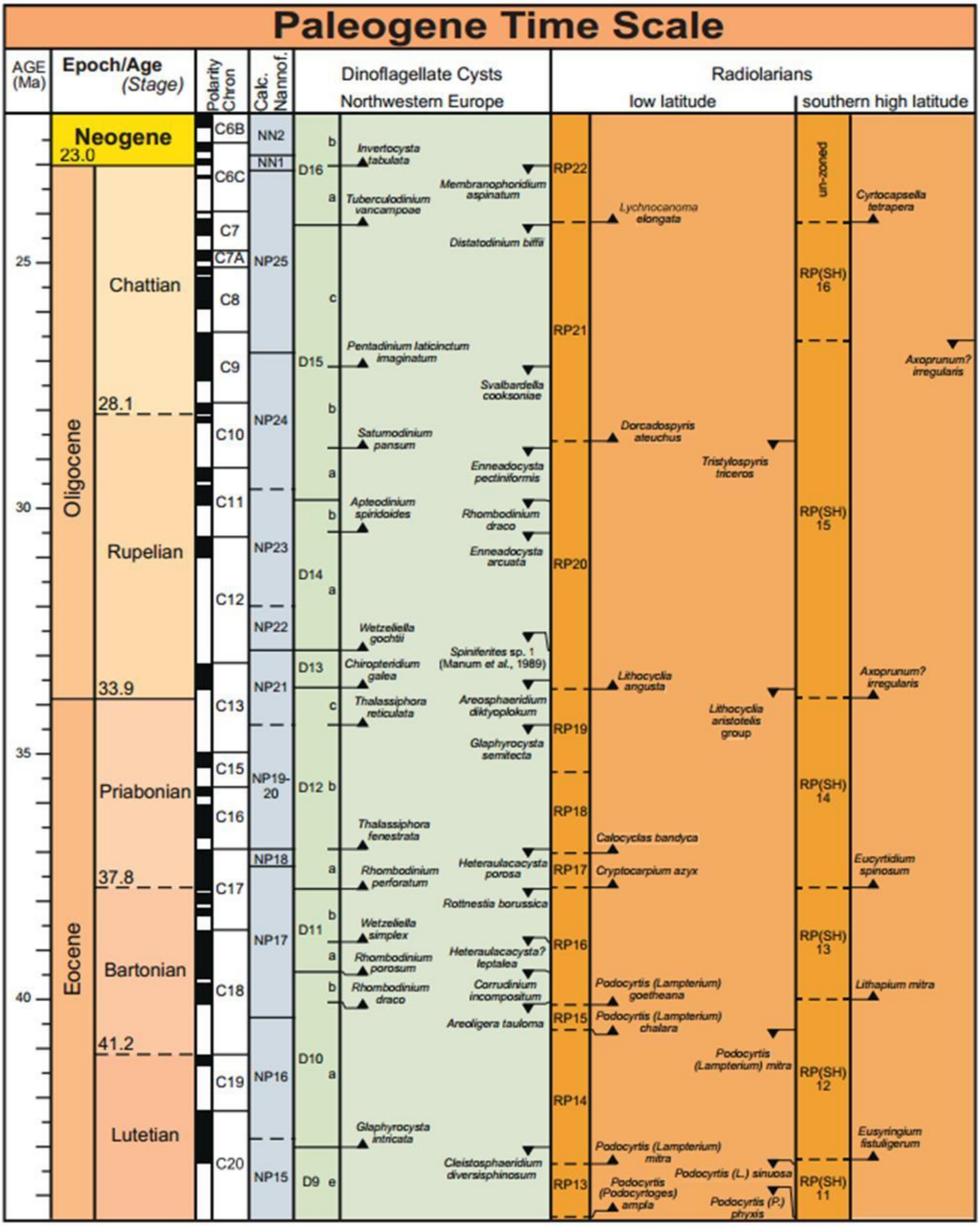

Paleogene Time Scale
AGE (Ma)
Epoch/Age (Stage)
Polarity Chron
Calc. Nannof.
Dinoflagellate Cysts Northwestern Europe
Radiolarians
low latitude
southern high latitude
Neogene
23.0
Oligocene
Chattian
28.1
Rupelian
33.9
Eocene
Priabonian
37.8
Bartonian
41.2
Lutetian
25
30
35
40
C6B
C6C
C7
C7A
C8
C9
C10
C11
C12
C13
C15
C16
C17
C18
C19
C20
NN2
NN1
NP25
NP24
NP23
NP22
NP21
NP19-20
NP18
NP17
NP16
NP15
D16
D15
D14
D13
D12
D11
D10
D9
Invertocysta tabulata
Membranophoridium aspinatum
Tuberculodinium vancampoae
Distatodinium biffii
Pentadinium laticinctum imaginatum
Svalbardella cooksoniae
Saturnodinium pansum
Enneadocysta pectiniformis
Apteodinium spiridoides
Rhombodinium draco
Enneadocysta arcuata
Wetzeliella gochtii
Spiniferites sp. 1 (Manum et al., 1989)
Chiropteridium galea
Areosphaeridium diktyoplokum
Thalassiphora reticulata
Glaphyrocysta semitecta
Thalassiphora fenestrata
Heteraulacacysta porosa
Rhombodinium perforatum
Rottnestia borussica
Wetzeliella simplex
Heteraulacacysta? leptalea
Rhombodinium porosum
Corrudinium incompositum
Rhombodinium draco
Areoligera tauloma
Glaphyrocysta intricata
Cleistosphaeridium diversisphinosum
RP22
RP21
RP20
RP19
RP18
RP17
RP16
RP15
RP14
RP13
Lychnocanoma elongata
Dorcadospyris ateuchus
Tristylospyris triceros
Lithocyclia angusta
Lithocyclia aristotelis group
Calocyclas bandyca
Cryptocarpium azyx
Podocyrtis (Lampterium) goetheana
Podocyrtis (Lampterium) chalara
Podocyrtis (Lampterium) mitra
Podocyrtis (Lampterium) mitra
Podocyrtis (L.) sinuosa
Podocyrtis (Podocyrtoges) ampla
Podocyrtis (P.) phyxis
un-zoned
RP(SH) 16
RP(SH) 15
RP(SH) 14
RP(SH) 13
RP(SH) 12
RP(SH) 11
Cyrtocapsella tetrapera
Axoprunum? irregularis
Axoprunum? irregularis
Eucyrtidium spinosum
Lithapium mitra
Eusyringium fistuligerum

(b)

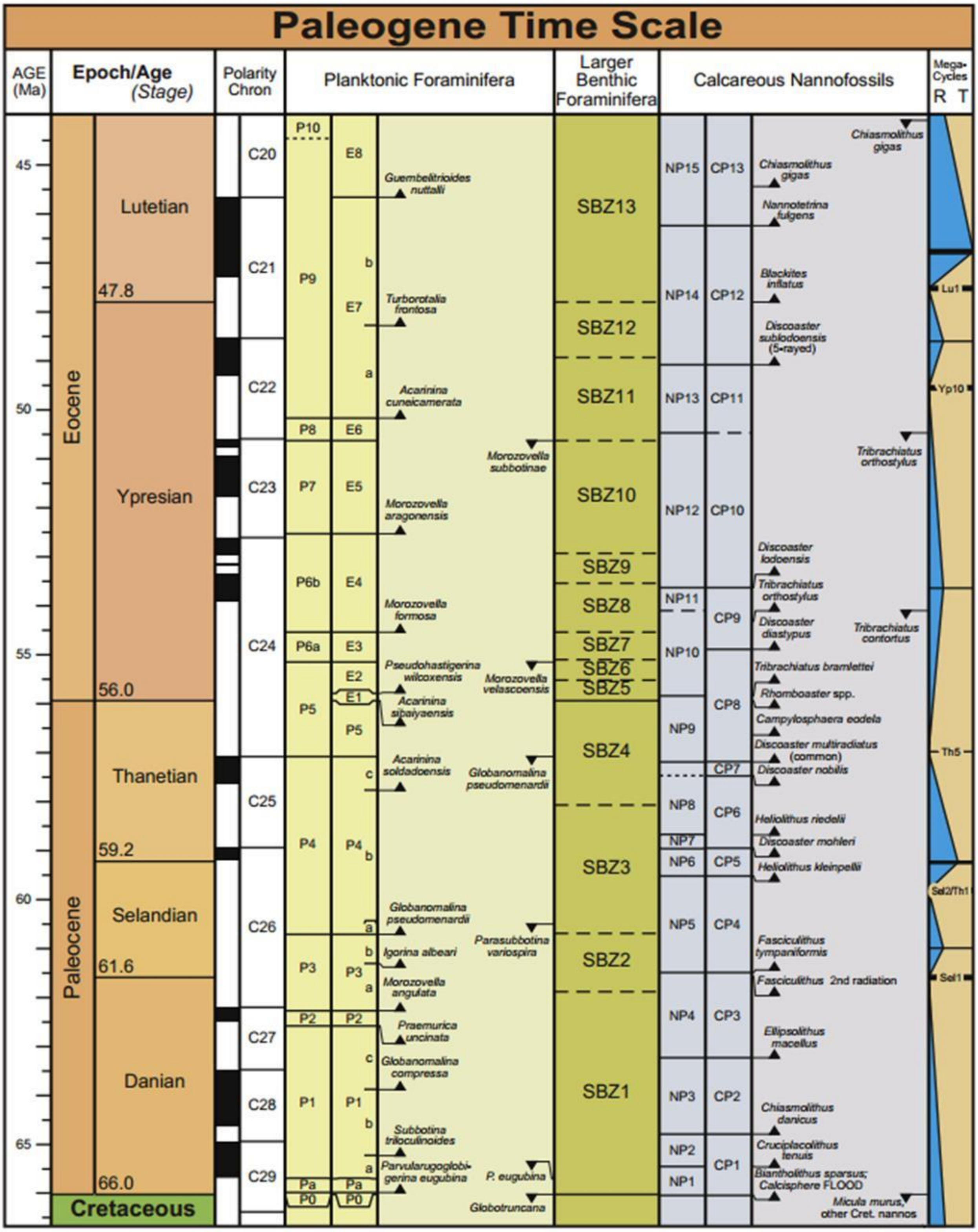

Paleogene Time Scale
AGE (Ma)
Epoch/Age (Stage)
Polarity Chron
Planktonic Foraminifera
Larger Benthic Foraminifera
Calcareous Nannofossils
Mega-Cycles R T
45
50
55
60
65
Eocene
Paleocene
Cretaceous
Lutetian
47.8
Ypresian
56.0
Thanetian
59.2
Selandian
61.6
Danian
66.0
C20
C21
C22
C23
C24
C25
C26
C27
C28
C29
P10
P9
P8
P7
P6b
P6a
P5
P4
P3
P2
P1
Pa
P0
E8
E7
E6
E5
E4
E3
E2
E1
Guembelitrioides nuttalli
Turborotalia frontosa
Acarinina cuneicamerata
Morozovella subbotinae
Morozovella aragonensis
Morozovella formosa
Pseudohastigerina wilcoxensis
Morozovella velascoensis
Acarinina sibaiyaensis
Acarinina soldadoensis
Globanomalina pseudomenardii
Parasubbotina variospira
Igorina albeari
Morozovella angulata
Praemurica uncinata
Globanomalina compressa
Subbotina triloculinoides
Parvularugoglobigerina eugubina
P. eugubina
Globotruncana
SBZ13
SBZ12
SBZ11
SBZ10
SBZ9
SBZ8
SBZ7
SBZ6
SBZ5
SBZ4
SBZ3
SBZ2
SBZ1
NP15
NP14
NP13
NP12
NP11
NP10
NP9
NP8
NP7
NP6
NP5
NP4
NP3
NP2
NP1
CP13
CP12
CP11
CP10
CP9
CP8
CP7
CP6
CP5
CP4
CP3
CP2
CP1
Chiasmolithus gigas
Nannotetrina fulgens
Blackites inflatus
Discoaster sublodoensis (5-rayed)
Tribrachiatus orthostylus
Discoaster lodoensis
Discoaster diastypus
Tribrachiatus contortus
Tribrachiatus bramlettei
Rhomboaster spp.
Campylosphaera eodela
Discoaster multiradiatus (common)
Discoaster nobilis
Heliolithus riedelii
Discoaster mohleri
Heliolithus kleinpellii
Fasciculithus tympaniformis
Fasciculithus 2nd radiation
Ellipsolithus macellus
Chiasmolithus danicus
Cruciplacolithus tenuis
Biantholithus sparsus; Calcisphere FLOOD
Micula murus, other Cret. nannos
Lu1
Yp10
Th5
Sel2/Th1
Sel1

(c)

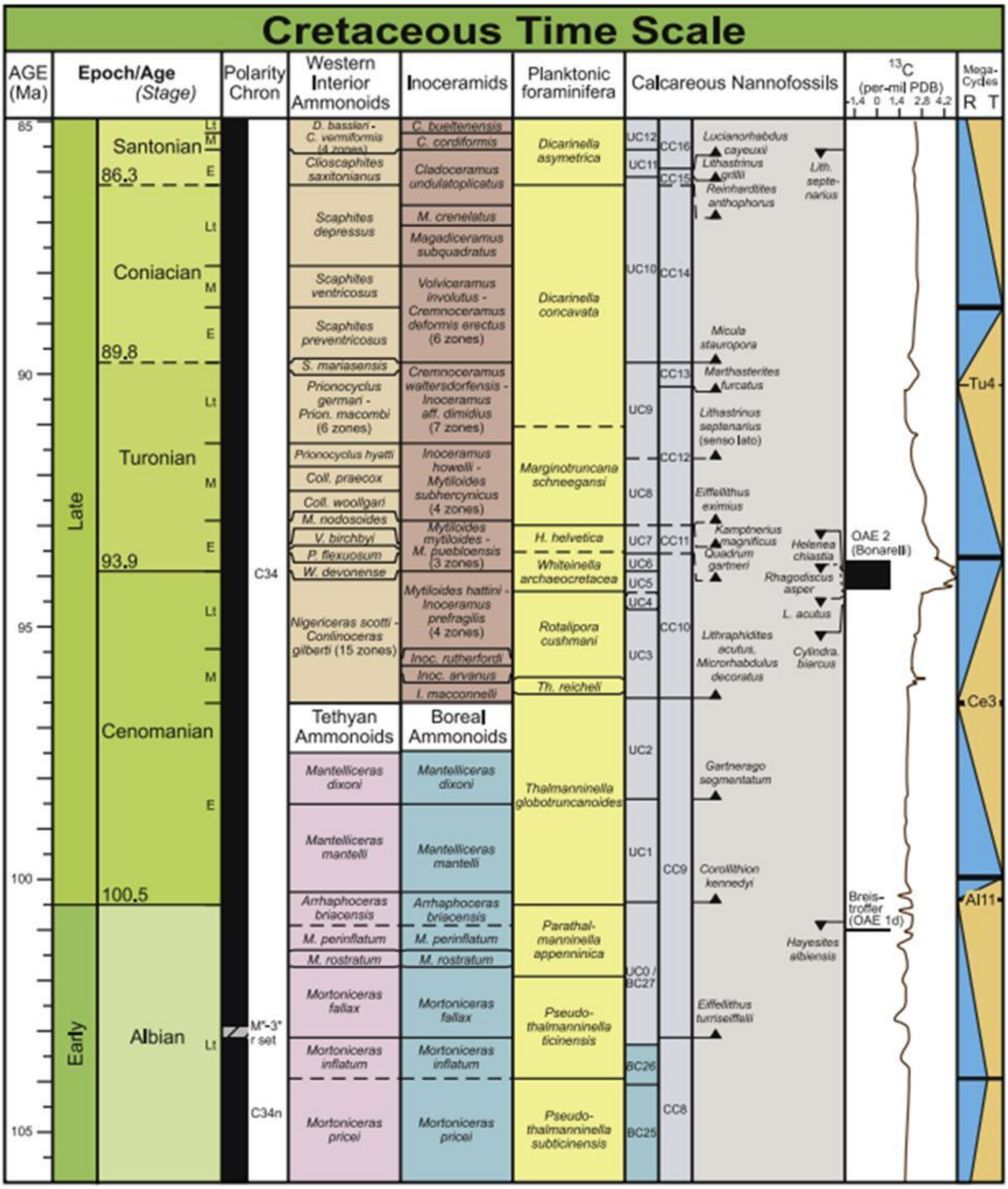

Cretaceous Time Scale
AGE (Ma)
Epoch/Age (Stage)
Polarity Chron
Western Interior Ammonoids
Inoceramids
Planktonic foraminifera
Calcareous Nannofossils
13C (per-mil PDB)
Mega-Cycles
R T
Late
Early
Santonian
86.3
Coniacian
89.8
Turonian
93.9
Cenomanian
100.5
Albian
C34
C34n
Tethyan Ammonoids
Boreal Ammonoids
OAE 2 (Bonarelli)
Breis-troffer (OAE 1d)
Tu4
Ce3
Al11

(d)

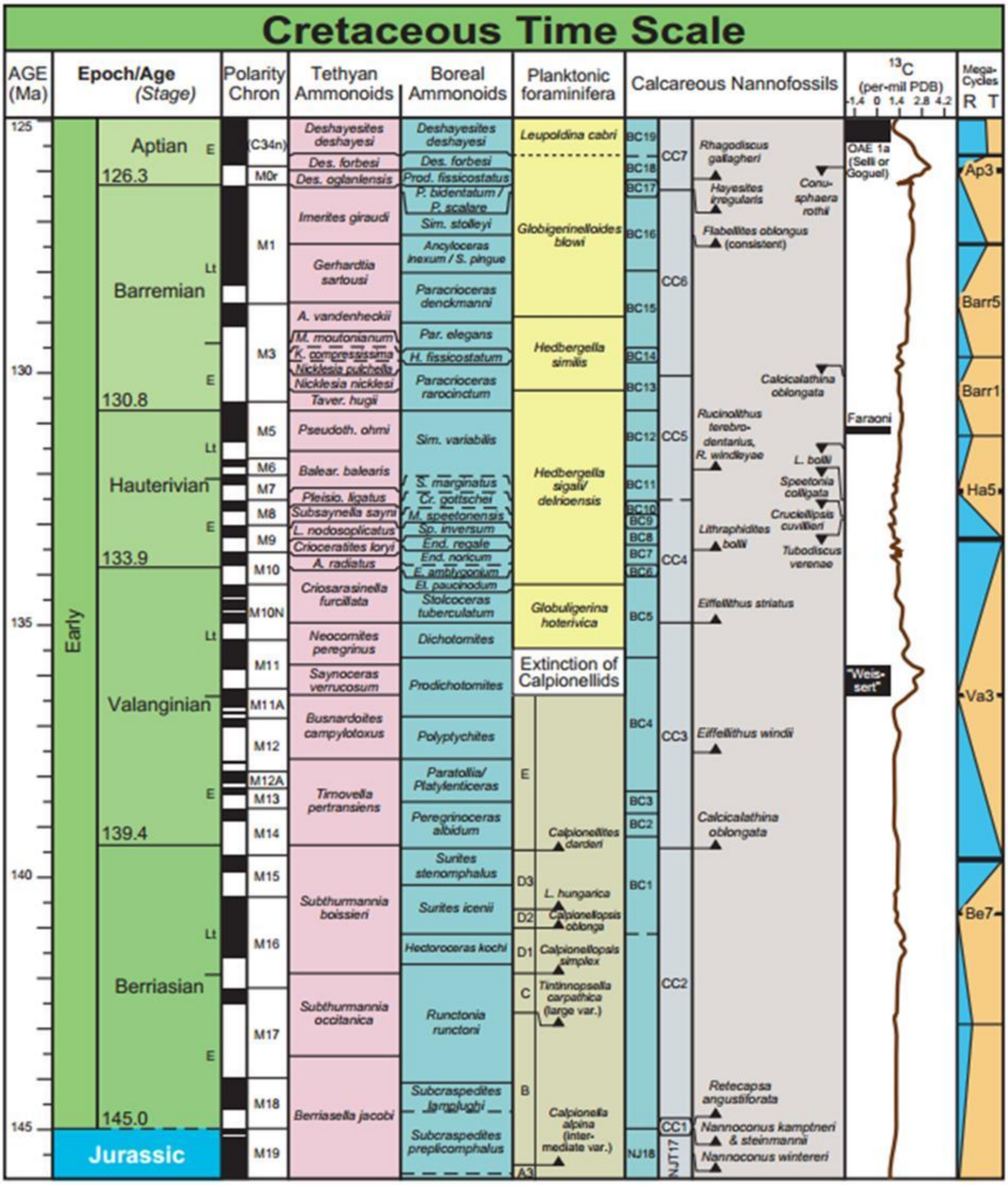

Cretaceous Time Scale
AGE (Ma)
Epoch/Age (Stage)
Polarity Chron
Tethyan Ammonoids
Boreal Ammonoids
Planktonic foraminifera
Calcareous Nannofossils
13C (per-mil PDB)
Mega-Cycles R T
125
130
135
140
145
Early
Aptian
126.3
Barremian
130.8
Hauterivian
133.9
Valanginian
139.4
Berriasian
145.0
Jurassic
(C34n)
M0r
M1
M3
M5
M6
M7
M8
M9
M10
M10N
M11
M11A
M12
M12A
M13
M14
M15
M16
M17
M18
M19
Deshayesites deshayesi
Des. forbesi
Des. oglanlensis
Imerites giraudi
Gerhardtia sartousi
A. vandenheckii
M. moutonianum
K. compressissima
Nicklesia pulchella
Nicklesia nicklesi
Taver. hugii
Pseudoth. ohmi
Balear. balearis
Pleisio. ligatus
Subsaynella sayni
L. nodosoplicatus
Crioceratites loryi
A. radiatus
Criosarasinella furcillata
Neocomites peregrinus
Saynoceras verrucosum
Busnardoites campylotoxus
Tirnovella pertransiens
Subthurmannia boissieri
Subthurmannia occitanica
Berriasella jacobi
Prod. fissicostatus
P. bidentatum / P. scalare
Sim. stolleyi
Ancyloceras inexum / S. pingue
Paracrioceras denckmanni
Par. elegans
H. fissicostatum
Paracrioceras rarocinctum
Sim. variabilis
S. marginatus
Cr. gottschei
M. speetonensis
Sp. inversum
End. regale
End. noricum
E. amblygonium
El. paucinodum
Stolcoceras tuberculatum
Dichotomites
Prodichotomites
Polyptychites
Paratollia/ Platylenticeras
Peregrinoceras albidum
Surites stenomphalus
Surites icenii
Hectoroceras kochi
Runctonia runctoni
Subcraspedites lamplughi
Subcraspedites preplicomphalus
Leupoldina cabri
Globigerinelloides blowi
Hedbergella similis
Hedbergella sigali/ delrioensis
Globuligerina hoterivica
Extinction of Calpionellids
E
D3
D2
D1
C
B
A3
Calpionellites darderi
L. hungarica
Calpionellopsis oblonga
Calpionellopsis simplex
Tintinnopsella carpathica (large var.)
Calpionella alpina (inter-mediate var.)
BC19
BC18
BC17
BC16
BC15
BC14
BC13
BC12
BC11
BC10
BC9
BC8
BC7
BC6
BC5
BC4
BC3
BC2
BC1
NJ18
CC7
CC6
CC5
CC4
CC3
CC2
CC1
NJT17
Rhagodiscus gallagheri
Hayesites irregularis
Conusphaera rothii
Flabellites oblongus (consistent)
Calcicalathina oblongata
Rucinolithus terebrodentarius, R. windleyae
L. bollii
Speetonia colligata
Cruciellipsis cuvillieri
Lithraphidites bollii
Tubodiscus verenae
Eiffellithus striatus
Eiffellithus windii
Retecapsa angustiforata
Nannoconus kamptneri & steinmannii
Nannoconus wintereri
OAE 1a (Selli or Goguel)
Faraoni
"Weissert"
Ap3
Barr5
Barr1
Ha5
Va3
Be7

(e)

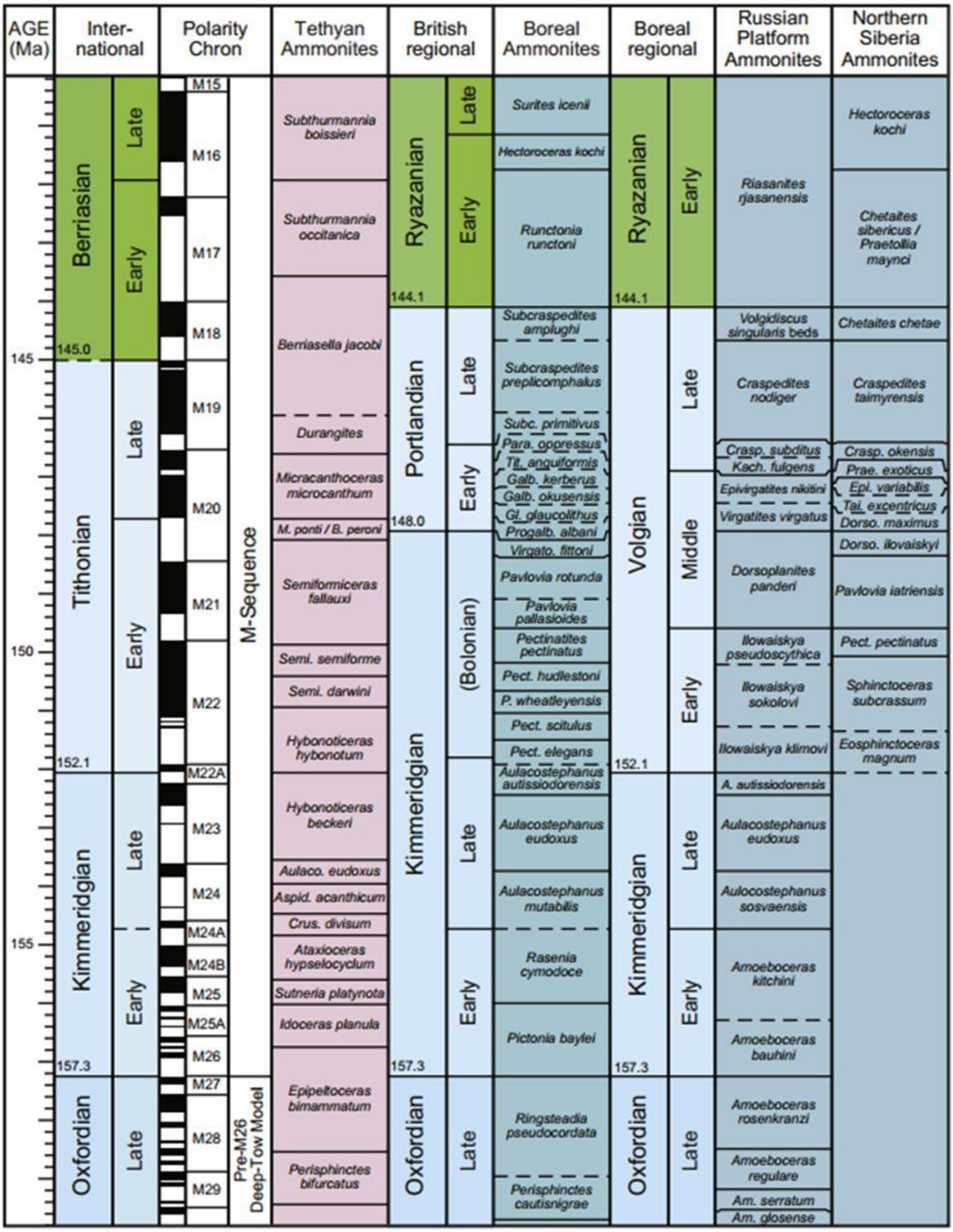
AGE (Ma)
International
Polarity Chron
Tethyan Ammonites
British regional
Boreal Ammonites
Boreal regional
Russian Platform Ammonites
Northern Siberia Ammonites
145
150
155
Berriasian
Late
Early
145.0
Tithonian
Late
Early
152.1
Kimmeridgian
Late
Early
157.3
Oxfordian
Late
M15
M16
M17
M18
M19
M20
M21
M22
M22A
M23
M24
M24A
M24B
M25
M25A
M26
M27
M28
M29
M-Sequence
Pre-M26 Deep-Tow Model
Subthurmannia boissieri
Subthurmannia occitanica
Berriasella jacobi
Durangites
Micracanthoceras microcanthum
M. ponti / B. peroni
Semiformiceras fallauxi
Semi. semiforme
Semi. darwini
Hybonoticeras hybonotum
Hybonoticeras beckeri
Aulaco. eudoxus
Aspid. acanthicum
Crus. divisum
Ataxioceras hypselocyclum
Sutneria platynota
Idoceras planula
Epipeltoceras bimammatum
Perisphinctes bifurcatus
Ryazanian
Late
Early
144.1
Portlandian
Late
Early
148.0
Kimmeridgian
(Bolonian)
Late
Early
157.3
Oxfordian
Late
Surites icenii
Hectoroceras kochi
Runctonia runctoni
Subcraspedites amplughi
Subcraspedites preplicomphalus
Subc. primitivus
Para. oppressus
Tit. anguiformis
Galb. kerberus
Galb. okusensis
Gl. glaucolithus
Progalb. albani
Virgato. fittoni
Pavlovia rotunda
Pavlovia pallasioides
Pectinatites pectinatus
Pect. hudlestoni
P. wheatleyensis
Pect. scitulus
Pect. elegans
Aulacostephanus autissiodorensis
Aulacostephanus eudoxus
Aulacostephanus mutabilis
Rasenia cymodoce
Pictonia baylei
Ringsteadia pseudocordata
Perisphinctes cautisnigrae
Ryazanian
Early
144.1
Volgian
Late
Middle
Early
152.1
Kimmeridgian
Late
Early
157.3
Oxfordian
Late
Riasanites rjasanensis
Volgidiscus singularis beds
Craspedites nodiger
Crasp. subditus
Kach. fulgens
Epivirgatites nikitini
Virgatites virgatus
Dorsoplanites panderi
Ilowaiskya pseudoscythica
Ilowaiskya sokolovi
Ilowaiskya klimovi
A. autissiodorensis
Aulacostephanus eudoxus
Aulocostephanus sosvaensis
Amoeboceras kitchini
Amoeboceras bauhini
Amoeboceras rosenkranzi
Amoeboceras regulare
Am. serratum
Am. glosense
Hectoroceras kochi
Chetaites sibericus / Praetollia maynci
Chetaites chetae
Craspedites taimyrensis
Crasp. okensis
Prae. exoticus
Epi. variabilis
Tai. excentricus
Dorso. maximus
Dorso. ilovaiskyi
Pavlovia iatriensis
Pect. pectinatus
Sphinctoceras subcrassum
Eosphinctoceras magnum

(f)

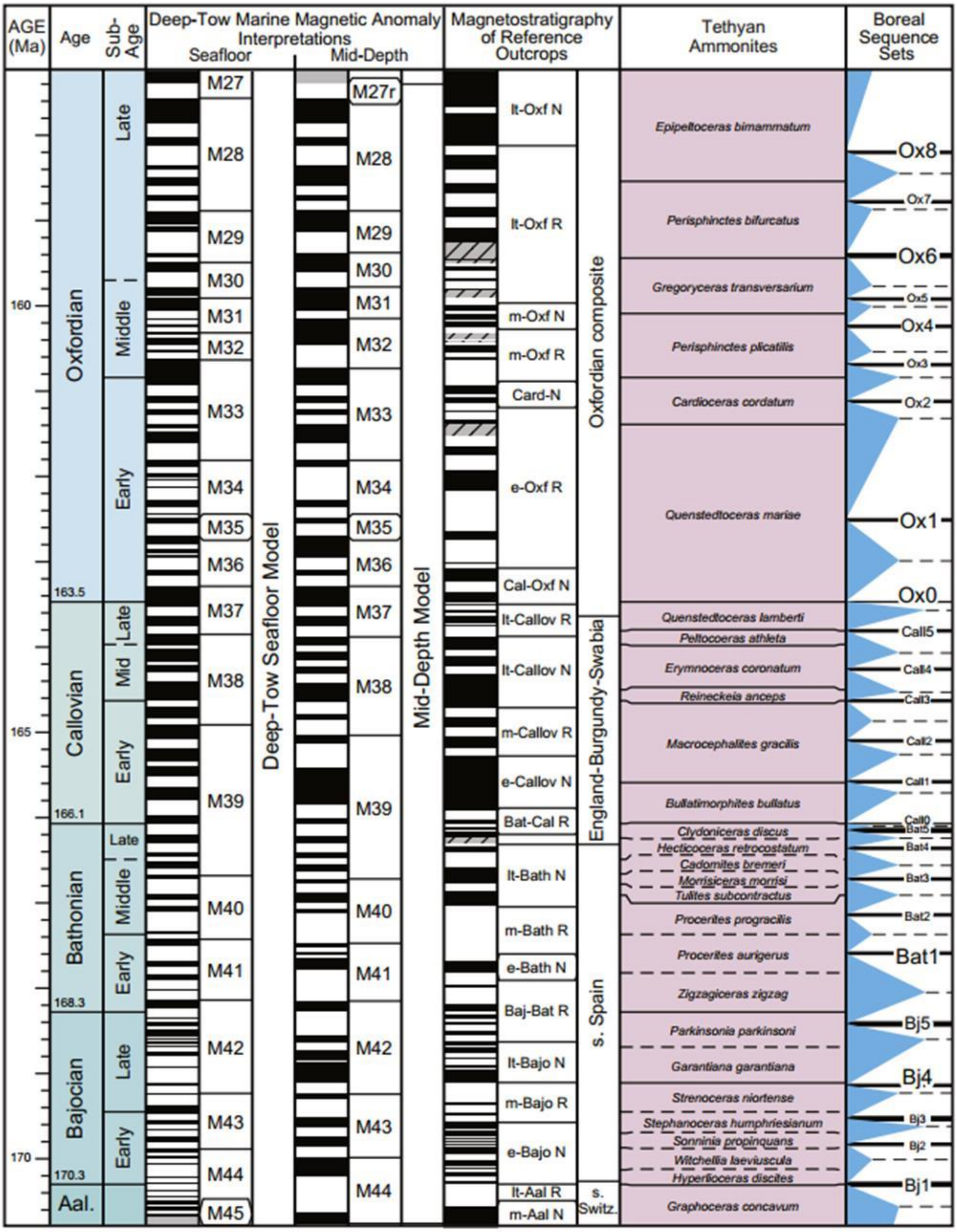

Figure 5: (a) and (b) Gradstein et al. (2012) Paleogene Time Scale. (c) and (d) Gradstein et al. (2012) Cretaceous Time Scale. (e) and (f) Jurssic Time Scale.